



Multi-hazard and risk informed system for Enhanced local and regional Disaster risk management

MEDiate

Deliverable D3.1

Individual and system-level physical vulnerability assessment methodologies for evaluating dynamic multi-hazard risk

Author(s):	Konstantinos Trevelopoulos, Pierre Gehl, Dina D'Ayala, Ahsana Parammal Vatterli, Kenneth Otárola, Carmine Galasso, Leandro Iannaccone, Roberto Gentile
Responsible Partner:	BRGM, UCL, IUSS
Version:	2.0
Date:	27.03.2024
Distribution level:	Public

DOCUMENT REVISION HISTORY

Version	Date	Comments
1.0	05.03.2024	Draft for internal review
2.0	28.03.2024	Revised version based on internal review

LIST OF PARTNERS

Participant	Name	Country
NOR	NORSAR	Norway
DEL	Deltares	Netherlands
IIASA	International Institute for Applied Systems Analysis	Austria
BRGM	Bureau de Recherches Géologiques et Minières	France
EUC	Fondazione Eucentre	Italy
IMO	Icelandic Meteorological Office	Iceland
IMT	Institut Mines-Telecom	France
UIce	University of Iceland	Iceland
R2M	R2M Solution	France
RINA-C	RINA Consulting	Italy
IUSS	Istituto Universitario di Studi Superiore Pavia	Italy
OSL	Oslo kommune	Norway
NICE	Metropole Nice Cote d'Azur	France
AUS	Austurbru	Iceland
UStr	University of Strathclyde	UK
UCL	University College London	UK
ARU	Anglia Ruskin University	UK
ECC	Essex County Council	UK

GLOSSARY

Acronym	Description
avgSA	Averaged Spectral Acceleration over a range of periods
EDP	Engineering Demand Parameter
GLM	Generalized Linear Model
IM	Intensity Measure
NLTHA	Non-Linear Time-History Analysis
PGA	Peak Ground Acceleration
PGD	Peak Ground Displacement
PGV	Peak Ground Velocity
SA(T)	Spectral Acceleration at period T

Document revision history	i
List of partners.....	i
Glossary	i
Index of figures.....	vii
Index of tables	xi
1 INTRODUCTION	1
2 LITERATURE REVIEW OF EXISTING VULNERABILITY AND FRAGILITY MODELS	3
2.1 General description of fragility and vulnerability models	3
2.2 Single-hazard vulnerability and fragility models for buildings.....	4
2.2.1 Earthquake.....	4
2.2.2 Flood.....	5
2.2.3 Mass movement (debris flows and slow-moving landslides).....	6
2.3 Vulnerability and fragility models for infrastructure networks.....	7
2.3.1 Fragility and vulnerability models for road network components.....	7
2.3.1.1 Bridges	7
2.3.1.2 Road segments	9
2.3.2 Fragility and vulnerability models for electric power network components.....	17
2.3.2.1 Earthquake	17
2.3.2.2 Flood	19
2.3.2.3 Wind.....	19
2.4 Multi-hazard fragility models	20
3 SELECTION OF PHYSICAL VULNERABILITY MODELS FOR THE TESTBEDS	25
3.1 Screening candidate models.....	25
3.2 Scoring fragility and vulnerability models for buildings	25
3.3 Selected fragility and vulnerability models for buildings in the testbeds	27
3.3.1 Oslo (Norway).....	28
3.3.2 Nice (France).....	29
3.3.3 Essex County (UK)	31
3.3.4 Mulathing (Iceland).....	32
4 DEVELOPMENT OF SPECIFIC FLOOD VULNERABILITY MODEL FOR NICE.....	34
4.1 Modelling framework.....	34
4.2 Calculation of economic loss	38
4.3 Conclusion	40
5 DEVELOPMENT OF SPECIFIC MULTI-HAZARD FRAGILITY MODELS	41
5.1 Modelling framework.....	41
5.1.1 General principle	41
5.1.2 Structural modelling	41

5.1.3	Applied external loadings.....	45
5.2	Multi-hazard fragility assessment of a building model for the CR_LFINF_CDM_11_HEX_2 building class.....	46
5.2.1	Seismic fragility of the intact model	46
5.2.2	Flood fragility of the intact model.....	48
5.2.3	State-dependent seismic fragility	51
5.2.4	Influence of hysteretic modelling assumptions	52
5.2.5	Influence of hazard type in the loading history	54
5.2.6	State-dependent flood fragility	55
5.3	Multi-hazard fragility assessment of a building model for the CR_LWAL_DUL_HEX_4 building class	61
5.3.1	Seismic fragility of the intact model	61
5.3.2	State-dependent seismic fragility	62
5.3.2.1	Initial damage state caused by earthquake	62
5.3.2.2	Initial damage state caused by flood	65
5.3.2.3	Initial damage state caused by earthquake or flood	68
5.3.3	Influence of the initial damage state and the type of hazard that caused it	71
5.3.4	Flood fragility of the intact model.....	73
5.3.5	State-dependent flood fragility	74
5.4	Discussion	77
6	TOWARDS MULTI-HAZARD LIFE-CYCLE CONSEQUENCE ANALYSIS OF DETERIORATING ENGINEERING SYSTEMS	78
6.1	An analytical approach: Markovian framework for multi-hazard life-cycle consequence analysis of deteriorating engineering systems	78
6.1.1	General framework and definitions	78
6.1.1.1	Interactions across hazards.....	79
6.1.2	Analytical formulation	81
6.1.2.1	Instantaneous deterioration transition matrix.....	82
6.1.2.2	Gradual deterioration transition matrix.....	84
6.1.2.3	Recovery transition matrix.....	85
6.1.3	Illustrative applications	86
6.1.3.1	Case study: deteriorating reinforced concrete building.....	86
6.1.3.2	Case study: road network with a deteriorating reinforced concrete bridge.....	91
6.2	A simulation-based approach: Life-cycle consequence analysis of reinforced-concrete buildings subjected to earthquake- and environment-induced damage accumulation	93
6.2.1	Methodology	93
6.2.1.1	Case-study building definition	93
6.2.1.2	Ground-motion sequence assembly	94
6.2.1.3	Corrosion deterioration modelling	94

6.2.1.4	Sequential cloud non-linear time-history analysis	95
6.2.2	Probabilistic seismic demand model	95
6.2.3	Collapse generalised logistic model	96
6.2.3.1	Time- and state-dependent fragility relationships	97
6.2.3.2	Time- and state-dependent vulnerability relationships	98
6.2.3.3	Stochastic event set assembly	99
6.2.3.4	Life-cycle consequence analysis	100
7	CONCLUSIONS	105
8	REFERENCES	107
9	APPENDIX I: SELECTED FRAGILITY AND VULNERABILITY MODELS	121
9.1	Seismic fragility models.....	121
9.1.1	Buildings	121
9.2	Flood vulnerability models	129
9.2.1	Buildings	129
9.2.2	Infrastructure	144
9.3	Debris flow fragility models	146
9.3.1	Buildings	146
9.4	Debris flow vulnerability models.....	152
9.4.1	Buildings	152
9.5	Landslide fragility models.....	157
9.5.1	Buildings	157
9.6	Wind fragility models	159
9.7	Ground settlement fragility models.....	170
9.7.1	Buildings	170
10	APPENDIX II: RANKING OF SELECTED FRAGILITY AND VULNERABILITY MODELS ..	175
10.1	Oslo Testbed	175
10.2	Nice Testbed	183
10.3	Essex Testbed.....	191
10.4	Mulathing Testbed	199

INDEX OF FIGURES

Figure 2-1: Examples of a) a fragility curve giving the probability of occurrence of a damage state equal or higher than damage state DS conditioned on the intensity measure [$P(DS IM)$] and b) a vulnerability curve (loss ratio as a direct function of IM).	3
Figure 2-2: Bridge category in HAZUS 5.1 according to scour potential (FEMA, 2022).	8
Figure 2-3: Seismic fragility curves for roads on slopes, from Kaynia (2013).	10
Figure 2-4: Seismic fragility curves for roads on embankments, from Kaynia (2013).	11
Figure 2-5: Seismic fragility curves for roads in cuts, from Kaynia (2013).	12
Figure 2-6: Identification of common failure modes for road segments exposed to flood hazard, from D'Ayala et al. (2015).	12
Figure 2-7: Safety criteria for the roadworthiness of passengers cars ($h_E = 0.3$ m) (Left) and emergency vehicles ($h_E = 0.6$ m) (Right), from Kramer et al. (2016). The angle α represents the direction of the water flow with respect to the orientation of the car.	13
Figure 2-8: Depth-disruption function, relating flood depth on a road with vehicle speed, developed by Pregnolato et al. (2017).	13
Figure 2-9: Road vulnerability model due to flood, proposed by Dunant (2019).	14
Figure 2-10: Identification of common failure modes for road segments exposed to ground failure hazard, from D'Ayala et al. (2015).	14
Figure 2-11: Fragility curves for urban and major roads exposed to ground failure, with permanent ground deformation as the intensity measure. Taken from HAZUS (NIBS, 2004).	15
Figure 2-12: Fragility curves for local roads (Left) and high-speed roads (Right) as a function of the volume of debris flow, taken from Winter et al. (2014) and Pitilakis et al. (2011).	16
Figure 2-13: Fragility curves for local roads (Left) and high-speed roads (Right) as a function of the volume of debris flow, taken from Winter et al. (2014) and Pitilakis et al. (2011).	16
Figure 2-14: Fragility curve for the failure of an electric substation, from Rasulo et al. (2004). Fragility parameters: $\alpha = 0.31$ g ; $\beta = 0.26$	17
Figure 2-15: Fragility curves for two types of electric substations, from Giovinazzi & King (2009).	18
Figure 2-16: Seismic fragility curves for single-phase 230 kV transformers; Source: Anagnos (1999).	18
Figure 2-17: Vulnerability curves for electric substations, from HAZUS flood model (FEMA, 2022).	19
Figure 2-18: Wind fragility curves for steel transmission towers in electric power networks as a function of the equivalent basic wind speed accounting for combined wind and rain loads (Fu et al., 2016) and the wind attack angle (β).	20
Figure 4-1: Data collection of buildings in the flood susceptible regions in the neighbourhood of River Paillon.	37
Figure 4-2: Estimated vulnerability indices distribution for the simulated building sample.	38
Figure 4-3: Depth-damage functions.	39
Figure 4-4: Cumulative replacement cost of masonry buildings for two flood scenarios.	39
Figure 5-1: Adopted scheme for the derivation of state-dependent fragility curves.	41
Figure 5-2: Geometry of the CR_LFINF_CDM_11_HEX_2 type building model.	43
Figure 5-3: Left: Capacity curve for the CR_LFINF_CDM_11_HEX_2 class building model (S_{du} is the ultimate spectral displacement); Right: Definition of damage states DS0-DS4.	43
Figure 5-4: Geometry of the CR_LFINF_CDL_HEX_4 type building model.	43
Figure 5-5: Left: Capacity curve for the CR_LWAL_CDN_HEX_4 class building model; Right: Definition of damage states.	44
Figure 5-6 Fragility curves for the intact CR_LFINF_CDM_11_HEX_2 Model 3.	47
Figure 5-7: Flood fragility models for the intact CR_LFINF_CDM_11_HEX_2 Models 1-4.	50
Figure 5-8: State-dependent seismic fragility curves for CR_LFINF_CDM_11_HEX_2 Model 3.	52
Figure 5-9: Ratio of the median of the state-dependent fragility curve ($A_{j,St.-Dep.}$) to the median of the undamaged building model (A_j) for the four model variants and for the three initial damage states.	53

Figure 5-10: State-dependent seismic fragility curves for CR_LFINF_CDM_11_HEX_2 Model 3, as a function of the type of hazard (EQ for earthquake, FL for flood) that has caused the initial damage state ($DS_{k,type}$).....	54
Figure 5-11: Flood fragility models for the CR_LFINF_CDM_11_HEX_2 Models 1-2 in $DS_{1,FL}$	56
Figure 5-12: Flood fragility model for the CR_LFINF_CDM_11_HEX_2 Models 3-4 in $DS_{1,FL}$	57
Figure 5-13: Flood fragility model for the CR_LFINF_CDM_11_HEX_2 Models 3-4 in $DS_{2,FL}$	58
Figure 5-14: Flood fragility models for the CR_LFINF_CDM_11_HEX_2 Models 1-2 in $DS_{3,FL}$	59
Figure 5-15 Flood fragility models for the CR_LFINF_CDM_11_HEX_2 Models 3-4 in $DS_{3,FL}$	60
Figure 5-16: Fragility curves for the intact CR_LWAL_CDN_HEX_4 type model.	61
Figure 5-17: Fragility curves for the CR_LWAL_CDN_HEX_4 type model in $DS_{1,EQ}$	62
Figure 5-18: Fragility curves for the CR_LWAL_CDN_HEX_4 type model in $DS_{2,EQ}$	63
Figure 5-19: Fragility curves for the CR_LWAL_CDN_HEX_4 type model in $DS_{3,EQ}$	64
Figure 5-20: Fragility curves for the CR_LWAL_CDN_HEX_4 type model in $DS_{1,FL}$	65
Figure 5-21: Fragility curves for the CR_LWAL_CDN_HEX_4 type model in $DS_{2,FL}$	66
Figure 5-22: Fragility curves (right) for the CR_LWAL_CDN_HEX_4 type model in $DS_{3,FL}$	67
Figure 5-23Fragility curves for the CR_LWAL_CDN_HEX_4 type model in $DS_{1,all}$	68
Figure 5-24: Fragility curves (right) for the CR_LWAL_CDN_HEX_4 type model in $DS_{2,all}$	69
Figure 5-25: Fragility curves (right) for the CR_LWAL_CDN_HEX_4 type model in $DS_{3,all}$	70
Figure 5-26: State-dependent seismic fragility curves for the CR_LWAL_CDN_HEX_4 type model.....	71
Figure 5-27: State-dependent seismic fragility curves for CR_LFINF_CDM_11_HEX_2 Model 3, as a function of the type of hazard (EQ for earthquake, FL for flood) that has caused the initial damage state ($DS_{k,type}$).....	72
Figure 5-28: Flood fragility models for the intact CR_LWAL_CDN_HEX_4 model.....	73
Figure 5-29: Flood fragility models for the CR_LWAL_CDN_HEX_4 model in $DS_{1,FL}$	74
Figure 5-30: Flood fragility models for the CR_LWAL_CDN_HEX_4 model in $DS_{2,FL}$	75
Figure 5-31: Flood fragility models for the CR_LWAL_CDN_HEX_4 model in $DS_{3,FL}$	76
Figure 6-1: Performance path due to multiple interacting hazard events during an engineering system's service life.....	78
Figure 6-2: Hazard and vulnerability modelling accounting for Level I and Level II interactions across multiple hazards.....	80
Figure 6-3: Adjusted performance path due to multiple interacting hazard events during a structural system's service life.	82
Figure 6-4: General transition matrix shapes for deterioration (i.e., TI and $TG, \delta t$) and recovery (i.e., $TR, \delta t$) processes.....	86
Figure 6-5: a) Earthquake hazard curves; b) flood hazard curves. θ : conditioning hazard event characteristics.	87
Figure 6-6: a) Normalised expected hazard-induced life-cycle cost of the building under instantaneous deterioration only; b) Normalised expected total life-cycle cost of the building under instantaneous and/or gradual deterioration.....	90
Figure 6-7: Normalised expected total life-cycle cost of the case-study building under instantaneous deterioration only and given various earthquake and flood rates of occurrence.	91
Figure 6-8. a) Transportation road network; b) expected life-cycle welfare loss of the original and upgraded bridge.....	93
Figure 6-9: Pushover capacity curves and DS thresholds definition (in θ terms) of the case-study building frame.....	95
Figure 6-10: Vector-valued PSDM of the case-study frame evaluated at $\psi = 0$ mm (response: magenta dots).	96
Figure 6-11: Vector-valued CGLM of the case-study frame evaluated at $\psi = 0$ mm (C: blue dots; NC: red dots).	97
Figure 6-12: Evolution of the fragility median values and dispersion for the case-study building frame as a function ψ	98

Figure 6-13: Evolution of the vulnerability relationships for the case-study building frame evaluated at $\psi = 0$ mm; 1.5 mm.....	99
Figure 6-14: Stochastic event set with mainshock-mainshock, mainshock-aftershock, aftershock-aftershock sequences (i.e., seismic sequences; the marker size is proportional to the magnitude of the seismic events).	100
Figure 6-15: Simulation-based approach to assess the life-cycle consequences of deteriorating engineering systems.....	101
Figure 6-16: Life-cycle consequence distribution given earthquake- and environment-induced damage accumulation.....	102
Figure 6-17: a) Life-cycle expected LR of the selected cases, as a function of time; b) relative variation (i.e., $1 - ELRLC, MS/ELRLC, [MS + AS + DE, MS + DE, MS + AS]$) between the life-cycle expected LR of the selected cases.....	103

INDEX OF TABLES

Table 2-1: Extract from a data file in Hazus 5.1 including the probability of bridge failure [columns named “damage_factor”] based on the scour potential [column “Scour Index”] (FEMA, 2022).....	9
Table 2-2: Fragility parameters (mean α and standard-deviation β) for roads on slopes, expressed as a function of PGA, for different values of yield coefficient k_y . Taken from Kaynia (2013).	9
Table 2-3: Fragility parameters (mean α and standard-deviation β) for roads on embankments, expressed as a function of PGA, for different heights and EC8 ground types. Taken from Kaynia (2013).	10
Table 2-4: Fragility parameters (mean α and standard-deviation β) for roads in cuts, expressed as a function of PGA, for different heights and EC8 ground types. Taken from Kaynia (2013).	11
Table 2-5: Fragility parameters (mean α and standard-deviation β) for urban and major roads exposed to ground failure, with permanent ground deformation as the intensity measure. Taken from HAZUS (NIBS, 2004). .	15
Table 2-6: Summary of some recent studies devoted to the development of multi-hazard fragility models (adapted from Gehl et al., 2019).	21
Table 2-7: Summary of damage scales for earthquake, flood/tsunami and wind, translated from Maiwald & Schwarz (2019).	24
Table 3-1: Fragility model scoring criteria (Gentile et al., 2022).	26
Table 3-2: Scoring for the selection of vulnerability models for residential buildings in the Oslo testbed. ...	28
Table 3-4: Scoring for the selection of fragility models for residential buildings in the Oslo testbed (the information in square brackets is to identify a model among others in the same publication).	29
Table 3-5: Scoring for the selection of vulnerability models for residential buildings in the Nice testbed. ...	30
Table 3-6: Scoring for the selection of fragility models for residential buildings in the Nice testbed (the information in square brackets is to identify a model among others in the same publication).	30
Table 3-7: Scoring for the selection of vulnerability models for residential buildings in the Essex testbed. ...	31
Table 3-8: Scoring for the selection of fragility models for residential buildings in the Essex testbed.	32
Table 3-9 Scoring for the selection of physical vulnerability and fragility models for buildings vulnerable to wind in the Essex testbed.	32
Table 3-10: Scoring for the selection of vulnerability models for residential buildings in the Mulathing testbed.	33
Table 3-11: Scoring for the selection of fragility models for residential buildings in the Mulathing testbed.	33
Table 4-1: Parameters for the PARNASSUS v.3 approach.	36
Table 5-1: Simplified distribution of RC building types in Nice municipality, according to the ESRM20 exposure model (Crowley et al., 2021a).	42
Table 5-2: Parametric definition of the damage state thresholds used in this study as a function of S_{dy} and S_{du} (i.e, the yield and ultimate spectral displacement) the according to Martins & Silva (2021).	44
Table 5-3: Definition of the four models with respect to their hysteretic material parameters, as defined in OpenSees. The parameter “pinchY” is the pinching factor for stress during reloading (value of 1.0 implies no pinching). The parameter “damage1” is the damage factor due to ductility (value of 0.0 implies no strength degradation). The parameter “damage2” is the damage factor due to energy (value of 0.0 implies no strength degradation).	45
Table 5-4 Best-fit approximation for the drag coefficient (C_d) in ASCE 7-16 (from Baiguera et al., 2022). .	45
Table 5-5: Coefficients of the generalized linear model for the intact CR_LFINF_CDM_11_HEX_2 Model 3.	47
Table 5-6: Fragility parameters for the intact CR_LFINF_CDM_11_HEX_2 models, along with the fragility values provided for the two corresponding ESRM20 models.	48
Table 5-7: Coefficients of the generalized linear model for the intact CR_LFINF_CDM_11_HEX_2 Models 1-4.	50
Table 5-8: Threshold coefficients for the intact CR_LFINF_CDM_11_HEX_2 Models 1-4.	50
Table 5-9: State-dependent fragility parameters for CR_LFINF_CDM_11_HEX_2 Model 3.	51
Table 5-10: State-dependent fragility parameters for CR_LFINF_CDM_11_HEX_2 Model 3, in the cases where the initial state is induced by a seismic loading ($DS_{k,EQ}$) or by a flood loading ($DS_{k,FL}$).	54

Table 5-11: Coefficients of the generalized linear model for the CR_LFINF_CDM_11_HEX_2 Models 1-2 in DS _{1,FL} .	56
Table 5-12: Coefficients of the generalized linear model for the CR_LFINF_CDM_11_HEX_2 Models 3-4 in DS _{1,FL} .	57
Table 5-13: Coefficients of the generalized linear model for the CR_LFINF_CDM_11_HEX_2 Models 3-4 in DS _{2,FL} .	58
Table 5-14: Coefficients of the generalized linear model for the CR_LFINF_CDM_11_HEX_2 Models 1-2 in DS _{3,FL} .	59
Table 5-15: Coefficients of the generalized linear model for the CR_LFINF_CDM_11_HEX_2 Models 3-4 in DS _{3,FL} .	60
Table 5-16: Coefficients of the generalized linear model for the intact CR_LWAL_CDN_HEX_4 type model.	61
Table 5-17: Parameters of lognormal fragility curves for the intact CR_LWAL_CDN_HEX_4 as a function of the PGA (g).	61
Table 5-18: Coefficients of the generalized linear model for the intact CR_LWAL_CDN_HEX_4 type model in DS _{1,EQ} .	62
Table 5-19: Parameters of lognormal fragility curves for the intact CR_LWAL_CDN_HEX_4 type model in DS _{1,EQ} as a function of the PGA (g).	62
Table 5-20: Coefficients of the generalized linear model for the intact CR_LWAL_CDN_HEX_4 type model in DS _{2,EQ} .	63
Table 5-21: Parameters of lognormal fragility curves for the intact CR_LWAL_CDN_HEX_4 type model in DS _{2,EQ} as a function of the PGA (g).	63
Table 5-22: Coefficients of the generalized linear model for the intact CR_LWAL_CDN_HEX_4 type model in DS _{3,EQ} .	64
Table 5-23: Parameters of lognormal fragility curves for the intact CR_LWAL_CDN_HEX_4 type model in DS _{3,EQ} as a function of the PGA (g).	64
Table 5-24: Coefficients of the generalized linear model for the intact CR_LWAL_CDN_HEX_4 type model in DS _{1,FL} .	65
Table 5-25: Parameters of lognormal fragility curves for the intact CR_LWAL_CDN_HEX_4 type model in DS _{1,FL} as a function of the PGA (g).	65
Table 5-26: Coefficients of the generalized linear model for the intact CR_LWAL_CDN_HEX_4 type model in DS _{2,FL} .	66
Table 5-27: Parameters of lognormal fragility curves for the intact CR_LWAL_CDN_HEX_4 type model in DS _{2,FL} as a function of the PGA (g).	66
Table 5-28: Coefficients of the generalized linear model for the intact CR_LWAL_CDN_HEX_4 type model in DS _{3,FL} .	67
Table 5-29: Parameters of lognormal fragility curves for the intact CR_LWAL_CDN_HEX_4 type model in DS _{3,FL} as a function of the PGA (g).	67
Table 5-30: Coefficients of the generalized linear model for the intact CR_LWAL_CDN_HEX_4 type model in DS _{1,all} .	68
Table 5-31: Parameters of lognormal fragility curves for the intact CR_LWAL_CDN_HEX_4 type model in DS _{1,all} as a function of the PGA (g).	68
Table 5-32: Coefficients of the generalized linear model for the intact CR_LWAL_CDN_HEX_4 type model in DS _{2,all} .	69
Table 5-33: Parameters of lognormal fragility curves for the intact CR_LWAL_CDN_HEX_4 type model in DS _{2,all} as a function of the PGA (g).	69
Table 5-34: Coefficients of the generalized linear model for the intact CR_LWAL_CDN_HEX_4 type model in DS _{3,all} .	70
Table 5-35: Parameters of lognormal fragility curves for the intact CR_LWAL_CDN_HEX_4 type model in DS _{3,all} as a function of the PGA (g).	70
Table 5-36: Coefficients of the generalized linear model for the intact CR_LWAL_CDN_HEX_4 model.	73

Table 5-37: Coefficients of the generalized linear model for the CR_LWAL_CDN_HEX_4 model in DS _{1,FL} .	74
Table 5-38: Coefficients of the generalized linear model for the CR_LWAL_CDN_HEX_4 model in DS _{2,FL} .	75
Table 5-39: Coefficients of the generalized linear model for the CR_LWAL_CDN_HEX_4 model in DS _{3,FL} .	76
Table 6-1: Instantaneous deterioration transition probability matrix (TI). The non-bold values correspond to the TI only due to earthquake events, and the bold values correspond to the TI due to earthquake and flood events.	89
Table 6-2: Gradual deterioration transition probability matrix (TG, δt). This transition matrix is only affected by earthquake events and is constant given the assumed linear time-dependent corrosion level curve.	89
Table 6-3: Recovery transition probability matrix (TR, δt). The non-bold values correspond to the TR, δt only due to earthquake events, and the bold values correspond to the TR, δt due to earthquake and flood events.	89
Table 6-4: Instantaneous deterioration transition probability matrix (TI).	92
Table 6-5: Gradual deterioration transition probability matrix (TG, δt).	92
Table 6-6: Recovery transition probability matrix (TR, δt).	92

1 INTRODUCTION

Within the MEDIATE project, the development of the risk-informed decision support system requires the implementation of reliable and accurate models that are able to assess the physical vulnerability of a wide range of assets (i.e., buildings, components of critical infrastructure) exposed to multiple hazards. To this end, in this report, we review and we present physical vulnerability models – consisting of vulnerability and fragility functions – for buildings, road networks, and electric power networks for a series of natural hazards, with a focus on the project’s testbeds. We also develop new functions based on simulations using high-fidelity structural models. The physical vulnerability models in this report are intended for the multi-hazard risk analyses and the subsequent development of the decision support system, which are undertaken in other tasks of the MEDIATE project. The present work has benefited from the identification of relevant hazard types (WP2) and exposed assets (WP4) in each of the testbeds, which results in a focus on flood and ground failure hazards, applied to built areas, road networks and electric power networks. Earthquake hazard is also considered, due to the existence of various models and datasets available at European level, which allow for testbed applications without additional efforts.

This report is organised around the following elements:

- Identification and general review of existing vulnerability and fragility models (or repositories of models) for various types of hazards (e.g., flood, mass movement, wind, earthquake, and tsunami);
- Selection and ranking of models relevant for each of the four testbeds present in MEDIATE;
- Modelling tasks focused on the Nice testbed:
 - Empirical development of flood vulnerability curves for masonry buildings, by applying and adapting the PARNASSUS approach (D’Ayala et al., 2020);
 - Analytical development of state-dependent fragility models for reinforced-concrete buildings, accounting for combinations of flood and earthquake loading;
- Application of a Markovian framework for the multi-hazard life-cycle consequence analysis of deteriorating engineering systems.

Chapter 2 conducts a literature review of existing physical vulnerability and fragility models, applied to buildings and components of road networks and electric power networks. This chapter is divided in two main parts, i.e. (i) the review of existing models and repositories for single-hazard loadings, such as flood, mass movement, earthquake and tsunami, and (ii) the identification of literature references that have developed models for cumulative or joint hazard loadings, allowing the combination of multiple hazards for a multi-hazard risk analysis framework.

Chapter 3 includes the screening, scoring, and selection of vulnerability and fragility models for the testbeds and for the different elements exposed to the considered hazards. Selected models concern buildings, bridges, road segments, and components of electric power networks such as transmission towers. The collected physical vulnerability models are being scored based on the criteria proposed by Gentile et al. (2022) in order to select the most useful model for each exposed element-hazard-testbed combination. One of the scoring criteria is the relevance with respect to the geographical area, in order to account for the specific context of each testbed. Models are selected for each testbed and for multiple hazards, however without considering cumulated or joint hazard loadings.

In the light of the findings of Chapters 2 and 3 regarding existing models, the next two chapters focus on modelling tasks, where distinct methods to address identified shortcomings are proposed: (i) accounting for local specificities of the building stock in the development of vulnerability functions (application to flood hazard, in Chapter 4), and (ii) deriving damage state-dependent fragility functions in the case of combined hazard loadings (application to flood and earthquake hazards, in Chapter 5).

In Chapter 4, we present an application of the PARNASSUS vulnerability index approach (D'Ayala et al., 2020), where the flood vulnerability of masonry buildings is characterized. This approach is applied in the case of flood susceptible areas in the project's testbed of Nice, France. In this approach, the relative vulnerability of an individual building is determined based on a number of parameters concerning the building itself and its surroundings. In the case study presented here, the parameters are characterized as discrete or continuous distributions based on a virtual data collection from a sample of buildings using free and publicly available geographical information resources. The collected data are then used to estimate the vulnerability of a simulated building population representative of the region's masonry building stock.

In Chapter 5, we use high-fidelity physics-based models of reinforced-concrete building classes that are common in the Nice testbed, in order to develop new analytical fragility models in the case of cumulative hazard loadings. The structural models are designed and used in simulations with sequential loadings representing earthquake and/or flood actions. Seismic fragility curves are developed for the undamaged structural models, while state-based seismic fragility curves are developed for the building models with an existing damage state caused by earthquake, or by flood, or by earthquake or flood. The same procedure is applied in the case of flood fragility curves.

While many existing computational risk modelling frameworks for natural hazards independently analyse and aggregate the expected consequences of distinct hazard events; it has been shown that multiple, often interacting, hazard events can lead to expected consequences greater than the sum of those given by the individual ones (De Angeli et al., 2022). Moreover, most available frameworks assume that assets sustaining structural/non-structural damage or functional impairment are either instantaneously repaired or do not receive any repair actions after a hazard event (e.g., Fereshtehnejad & Shafieezadeh, 2018). This prevents the accurate quantification of the consequences, as such frameworks do not account for dynamic changes in the asset's performance over time. Therefore, a novel framework, based on state-dependent fragility models, is proposed in Chapter 6. A Markovian framework for multi-hazard life-cycle consequence analysis of engineering systems (e.g., buildings and infrastructure components) is presented in the first part (Section 6.1), while an end-to-end computational framework for simulation-based life-cycle consequence analysis of reinforced-concrete buildings is proposed in the second part (Section 6.2). In both parts of this chapter, the variation of the vulnerability of engineering systems is modelled over the course of time, which allows the estimation of consequences because of a major event based on the vulnerability at the time of the event, as opposed to typical risk analyses where the vulnerability is time-independent.

The first part of Chapter 6 presents a novel Markovian framework for multi-hazard life-cycle consequence analysis of deteriorating engineering systems (e.g., buildings, infrastructure components), which separates the modelling of hazard events and the impact of those events on an engineering system. This framework allows for assessing the consequences of progressive enhancements in the condition of an engineering system resulting from repair activities and integrates uncertainties linked to the repair durations associated with diverse limit states (i.e., performance level). The proposed framework is demonstrated using an archetype case-study reinforced-concrete moment-resisting frame, and a real, symmetric, double-span, box-girder, seat-type bridge; part of a simplified transportation road network.

The second part of Chapter 6 proposes an end-to-end computational framework for simulation-based life-cycle consequence analysis of reinforced-concrete buildings subjected to earthquake- and environment-induced damage accumulation. The outcomes from the developed framework (e.g., time- and state-dependent fragility, vulnerability relationships, and expected life-cycle consequences) can be utilised for assessing a building's seismic structural performance at a certain point in time or in a life-cycle consequence analysis; for a single-building or a portfolio of buildings. The proposed framework is demonstrated by analysing an archetype case-study reinforced-concrete moment-resisting frame.

2 LITERATURE REVIEW OF EXISTING VULNERABILITY AND FRAGILITY MODELS

The present section proposes a non-exhaustive review of available vulnerability and fragility models for the range of hazards considered in the MEDiate project, by distinguishing single-hazard models from models that account for multiple hazard loadings. Following a general description of the adopted definitions of vulnerability and fragility models, the section proceeds by highlighting various helpful compendia of models that may be relevant for the exposed assets in the MEDiate testbeds, i.e. buildings and infrastructure components (road networks and electric power networks). Finally, the section ends with a summary of existing models that account for multiple hazard loadings, revealing a relative scarcity of such studies.

2.1 General description of fragility and vulnerability models

Before discussing various available models for the different hazard loadings, a distinction has to be made between fragility and vulnerability models (see Figure 2-1):

- *Fragility functions* are probabilistic models that provide the probability of reaching or exceeding a given damage state (DS) as a function of an intensity measure (IM) representing the hazard loading. The most common form of fragility models is a lognormal cumulative distribution function, characterised by a mean and standard deviation (i.e. fragility parameters). When more than one damage states are used, the fragility curves may give the probabilities of exceedance of the Engineering Demand Parameter (EDP) defining the damage state thresholds, or the probability of damage states equal or higher than a specific damage state. Other types of fragility models also exist, e.g., fragility surfaces, which are functions of two IMs instead of one, in order to represent the hazard loading with more accuracy. Another distinction is usually made between empirical (e.g., damage probability matrices, vulnerability index approach), synthetic (e.g., capacity spectrum-based approaches, dynamic analyses) and expert elicitation-based methods, when deriving fragility models.
- *Vulnerability functions* are deterministic models that provide directly a measure of consequence (e.g., most commonly the loss ratio of the exposed asset) as a function of an IM. Vulnerability curves are usually empirically fitted from data collected from past events (i.e., identification of incurred losses vs levels of hazard intensity). An alternative consists in combining fragility functions with consequence functions (e.g., functions providing loss ratios for each damage state) in order to assemble the vulnerability function.

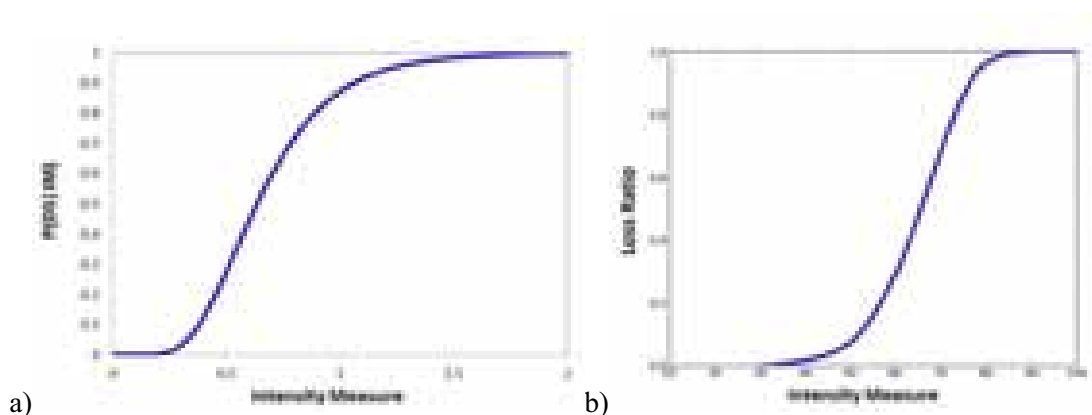


Figure 2-1: Examples of a) a fragility curve giving the probability of occurrence of a damage state equal or higher than damage state DS conditioned on the intensity measure [$P(DS|IM)$] and b) a vulnerability curve (loss ratio as a direct function of IM).

2.2 Single-hazard vulnerability and fragility models for buildings

Single-hazard fragility models consist of a set of fragility functions that correspond to a single external loading (e.g., inertia forces generated by an earthquake ground motion, lateral loading on a structure cause by water flooding, etc.), which may be represented by one or more intensity measures (IMs).

2.2.1 Earthquake

Seismic fragility curves have been the object of an extensive body of research work for the past decades (Calvi et al., 2006).

While it is not the aim of this report to provide an extensive account of available models, the following references and projects have inventoried a large amount of earthquake fragility functions for buildings and they are considered here due to the relevance for European building classes:

- Within the European project SYNER-G (2009-2013), a compendium of fragility curves for reinforced concrete (Crowley et al., 2011a) and masonry (Crowley et al., 2011b) buildings has been assembled. This database is stored and accessible in a fragility function manager tool (Silva et al., 2014).
- The vulnerability database of the GEM Foundation (Yepes-Estrada et al., 2016 – <https://platform.openquake.org/vulnerability/list>) is an online platform that can be used to store, select and analyse fragility functions, vulnerability models, damage-to-loss models and pushover/capacity curves. It contains data from the Global Earthquake Model Physical Vulnerability Guidelines (<https://www.ucl.ac.uk/epicentre/resources/gem-vulnerability-databases>) (2010-2013) (D'Ayala et al 2014, Rossetto et al., 2014, Porter et al., 2014), as well as the aforementioned fragility functions collected within the European project SYNER-G.
- The European project SERA (2017-2020) has established the SERA.REVIEW database, containing hundreds of capacity, fragility and vulnerability curves for common buildings in Europe (Romao et al., 2019a, 2019b). Through statistical treatment and post-processing, this database has served as a basis for the development of fragility and vulnerability models for the European Seismic Risk Model (ESRM20; Crowley et al., 2021a).

All of the aforementioned databases of vulnerability and fragility models have been harmonized to some extent in order to comply with the GEM taxonomy of buildings (Brzev et al., 2013; Silva et al., 2018), which contains collapsable attributes that are relevant to the seismic performance of different construction types. This taxonomy has also been applied to the European building exposure model (Crowley et al., 2020a, 2020b), which is used as input to the European Seismic Risk Model.

European empirical fragility functions commonly use the EMS-98 damage scale (Grünthal, 1998), which contains 5 damage states, from Grade 1 ('Negligible to slight damage') to Grade 5 ('Destruction'). However, the HAZUS damage scale (FEMA, 2020), with 4 damage states from 'Slight' to 'Collapse', is also used by some models. Finally, a few models are based on custom damage scales with a varying number of damage scales, which would require some degree of harmonization when estimating losses from the physical damage states. A guide to correlate damage states from different scales is proposed by Hill and Rossetto (2008). For analytical vulnerability functions, damage levels are usually correlated to drift and to specific damage modes for the structure of interest (D'Ayala et al. 2014).

Most IMs used in seismic fragility curves are Peak Ground Acceleration (PGA), Peak Ground Velocity (PGV), spectral acceleration (SA), spectral displacement (DS) and macroseismic intensity. Some of these IMs have been found to be able to convey the most information possible from the ground-motion time histories.

According to Luco & Cornell (2007), adequate IMs should be both *efficient* (i.e., ability of an IM to induce a low dispersion in the distribution of the structural response) and *sufficient* (i.e., ability of an IM to “carry” the characteristics of the earthquake that has generated the ground motion). Another essential criterion to consider is the *computability* or *hazard compatibility* (Hariri-Ardebili & Saouma, 2016), which checks whether the IM may be computed accurately with current ground-motion models to ensure the link between the fragility function and the hazard assessment. For this reason, most of the fragility models generated for the European Seismic Risk Model (ESRM20) use PGA and SA (at periods 0.3, 0.6 and 1.0s) as IMs, since these ground-motion parameters correspond to standard outcomes of ShakeMap® services (Wald et al., 2022).

Experience has shown that finding a scalar IM that fulfils all the aforementioned criteria is usually not feasible. Therefore, a few studies have introduced vector-valued IMs (i.e., use of two or more IMs as input to the fragility function), in order to reduce the dispersion induced by the record-to-record variability. Such fragility surfaces have been developed for an eight-story RC building (Seyedi et al., 2010) and a masonry buildings (Gehl et al., 2013), using for instance the spectral accelerations at the periods of the first two vibration modes as a vector-valued IM. Modica & Stafford (2014) have also searched for the most efficient vector-valued IMs, with respect to a series of European low- and mid-rise reinforced concrete frames. They have found that the most efficient vector corresponds to a combination of SA and a spectral shape parameter. Seismic fragility surfaces have also been applied to other types of structures, such as RC bridges (Li et al., 2014) or industrial equipment (Cai et al., 2018a, 2018b).

2.2.2 Flood

Two approaches are common in flood vulnerability assessment: the physical approach and the empirical approach (Balica et al., 2013). Physical approaches use hydrological models to estimate the flood hazard and compute economic consequences for a particular event or area on the basis of a damage index relating a measure of intensity of the flood to the associated economic loss. Parametric or empirical approaches use a set of quantitative or qualitative indicators to rate the vulnerability of a building or area, with no particular reference to the hazard intensity. Current flood risk assessment studies use either an empirical approach, relying on post-event damage data collection to determine vulnerability functions, or synthetic approaches, whereby the vulnerability functions are based on expert opinion. Most current IMs are flood depth and flow velocity, which are either used as single IMs or combined together. Galasso et al. (2021) provide an overview of existing empirical and expert opinion based approaches. It includes an extensive compendium of fragility and vulnerability models, a set of criteria for evaluating the usefulness of such models, as well as a model taxonomy compatible with the GEM exposure taxonomy (Silva et al., 2020) and the GED4ALL multi-hazard exposure taxonomy by Dabbeek & Silva (2020).

One of the most detailed vulnerability models is the one by Schwarz & Maiwald (2007), addressing the physical vulnerability of masonry and reinforced concrete buildings. These models were developed using data from the 2002 Elbe River flood (Germany); the damage scale was developed specifically to characterize flood damage in reinforced concrete and masonry buildings, using the same framework as the already existing EMS'98, developed for seismic hazard. Although damage modes are substantially different, the two scales are supposed to have commensurate damage levels, and hence in theory applicable in multi-hazard risk analysis.

Empirical methods are basin or catchment specific (Merz et al., 2010) and hence of limited transferability and applicability to other locations without substantial calibration. The “Global flood depth-damage model” released by the European Commission’s Joint Research Centre (Huizinga et al., 2017), which consists of large-scale (pan-European level) models. The usefulness of these models lies in the fact that they cover a wide range of elements such as residential, commercial, and industrial buildings, and transport infrastructures.

The PARNASSUS project was funded by the UK research councils in 2010, to investigate the vulnerability of historic city centres in England to flooding, following the summers floods of 2007. The PARNASSUS v.1 procedure, based on a vulnerability index approach, can determine the relative vulnerability of individual

buildings, considering the building and its immediate curtilage as the system exposed to the flood hazard. The vulnerability index is obtained by identifying a number of parameters considered all equally critical to the response of the system, ranging from its characteristics to its surrounding conditions. The PARNASSUS v.1 version was applied to three city centres in UK, York, Winchester and Tewkesbury (Stephenson and D'Ayala, 2014). Later it was adapted to determine the vulnerability of specific classes of buildings, such as churches, for an application in the Philippines for multi-hazard risk assessment (D'Ayala et al., 2016). PARNASSUS v.3, developed for a study of the urban centre of Kuala Lumpur, Malaysia, incorporates a damage loss function, derived considering a large number of existing vulnerability models available in literature, to provide a complete approach for flood risk assessment applicable at multiple scale, from the single building to a whole district (D'Ayala et al 2020). A new economic loss model is developed to quantify the flood risk in terms of replacement cost, taking into account both specific vulnerability and a normalized depth–damage ratio function. The findings provide multiscale flood-resistant strategies for the protection of individual residential buildings.

In parallel to vulnerability models, there are much less available studies related to flood fragility models. However, it is worth noting the recent work by Nofal et al. (2020) and Nofal & van de Lindt (2020), who have derived flood fragility curves and surfaces from numerical analyses, with flood depth and flood duration as IMs.

2.2.3 Mass movement (debris flows and slow-moving landslides)

Luo et al. (2023) have proposed a state of the art on the vulnerability of buildings to landslides, which categorizes the physical vulnerability models into the following categories, based on the approach used to create each model:

- Experience-based vulnerability models;
- Indicator-based vulnerability models;
- Data-driven vulnerability models;
- Mechanism-based vulnerability models.

The models in the above categories concern the debris flow hazard, while the state-of-the-art review by Luo et al. (2023) also includes vulnerability models in the case of slow-moving landslides, which – technically – may be considered as models for a different hazard.

An example of an experience-based model for the vulnerability to landslides is a model for Central Italy by Cardinali et al. (2002), which is based on a qualitative description of the intensity of the hazard (e.g., low / medium / high ranges of intensity). Although this type of model is easy to use, it suffers from significant epistemic uncertainties with respect to the characterization of the intensity of the hazard as well as the relationship between consequences and hazard intensity.

Indicator-based models are based on a set of variables, whose value is determined based on a set of characteristics of the elements exposed to the landslide hazard. The indicator-based model by Silva & Pereira (2014) is developed for a municipality in North Portugal, which includes indicators related to the construction material, the number of storeys, and how well the building has been preserved. Although characteristics such as the construction material may be established with little uncertainty, there may be misclassification errors with respect to variables depending on qualitative criteria, as in the case of the preservation status of the building. Moreover, in Silva & Pereira (2014), the values assigned to the indicators of the building characteristics have been defined from expert judgement, as it is often the case in indicator-based models. Even though this physical vulnerability model does not allow quantitative risk assessment, it can be useful in the context of decision support for risk reduction.

Data-driven driven vulnerability models are developed based on damage observations from past events. These models often have a sigmoid functional form relating an intensity measure of the landslide loads and the ratio of loss (e.g., Papathoma-Köhle et al., 2015), as is the case with earthquake vulnerability curves.

The mechanism-based vulnerability models are the equivalent of synthetic earthquake fragility curves based on numerical models, which can simulate the mechanical behaviour and response of buildings. However, there is a lack of models covering a wide range of building classes, such as the set of fragility curves in the European Seismic Risk Model (ESMR20, Crowley et al., 2021), which would enable a risk analysis on the urban scale.

Luo et al. (2023) also reviewed several damage scales that have been used to estimate landslide impact: most of them present 5 damage degrees, usually ranging from non-structural damage (damage to windows and doors, cracks on non-bearing walls) to heavy structural damage (especially in columns) and collapse of the buildings (with sometimes a translation or rotation of the structure). According to their evaluation, these scales for damage caused by landslides lack the level of precision that is present in the seismic damage scale proposed by HAZUS (FEMA, 2020). Nevertheless, they do not make any recommendation about whether or how the damage scale in FEMA (2020) could be used to classify damage by landslides.

2.3 Vulnerability and fragility models for infrastructure networks

2.3.1 Fragility and vulnerability models for road network components

This section proposes a set of available fragility and vulnerability models for road network components. Several models are presented, depending on the type of components (bridge or road segment) and the type of hazard (earthquake, flood or ground failure).

2.3.1.1 Bridges

This section presents a few sources related to fragility and vulnerability models for road bridges exposed to earthquake, mass movement and flood hazards.

2.3.1.1.1 Earthquake

Within the FP7 SYNER-G project, the work by Crowley et al. (2011c) had led to the collection, review and harmonization of seismic fragility curves for road bridges. To this end, a taxonomy of bridge types has been proposed, which is based on similar principles to the GEM taxonomy for buildings (i.e., modular, detailed, collapsible and expandable). The main bridge characteristics used in the taxonomy are the following:

- Material;
- Type of superstructure;
- Deck structural system;
- Pier to deck connection;
- Type of pier to superstructure connection;
- Type of pier section;
- Spans;
- Type of connection to the abutments;
- Bridge configuration;
- Level of seismic design.

A specific tool, the bridge fragility function manager (<https://www.vce.at/SYNER-G/files/downloads.html>), has been developed in order to store and compare fragility functions, with the ability to harmonize related intensity measures, limit states and bridge typologies. Around 370 fragility models are made available in the database by Crowley et al. (2011c).

Within the H2020 TURNkey project, the review by Tiganescu et al. (2021) has studied around 40 references, based on the derivation method used and the bridges typologies covered. This review covers mostly either single/multi-span continuous or simply supported steel/RC deck bridges, although a few fragility models of masonry arch bridges are also mentioned (Pelà et al., 2009; Zampieri et al., 2016; Tecchio et al., 2016; Morandi

et al., 2019). It is worth noting that models related to masonry arch bridges are limited to Italian examples and they are based on non-linear kinematic analyses.

Borzi et al. (2015) developed a tool for automatic calculation of seismic fragility curves for roadway bridges. This tool generates a finite element model based on a set of bridge characteristics and performs the fragility analysis. The validation of this automatic procedure was done using data from approximately 17,000 bridges in Italy. This tool could be adapted for use in the case of this project's testbeds, and the automatically generated building models could be used to develop bridge fragility models for hazards other than earthquake.

To the best of our knowledge, in the testbeds of this project, there is one railway bridge at the limits of the metropolitan area of Nice. The review by Tiganescu et al. (2021) for the H2020 TURNkey project also includes seismic fragility curves for railway bridges, and they have proposed the fragility models in a report produced by the FP7 SYNER-G project (European Commission. Joint Research Centre, 2013). This report also includes seismic fragility curves for roadway bridges.

2.3.1.1.2 Flood

HAZUS 5.1 (FEMA, 2022) includes models for bridge failure due to scour caused by flood, which are function of the type of bridge, and whether the bridge is scour critical. The scour potential and the classification of the bridges is done based on the descriptions in Figure 2-2. Based on the scour potential and whether the bridge is single-span or continuous-span, the probability of failure is given by a table, an extract of which is given in Table 2-1. The probability of the bridge being functional is the complementary of the failure probability. Note that the probabilities proposed by Table 2-1 are independent of the pier height.

Scour Index Category	Description	Scour Analysis Status
0	Bridge identified as structurally sufficient. Bridge is closed to traffic.	Not Analyzed
1	Bridge is scour critical, field review indicates that failure of piers, abutments is imminent. Bridge is closed to traffic.	Analyzed
2	Bridge is scour critical, field review indicates that extensive scour has occurred at bridge foundations.	Analyzed
3	Bridge is scour critical, bridge foundations determined to be unstable for assumed or calculated scour conditions.	Analyzed
4	Bridge foundation is determined to be stable for assumed or calculated scour conditions, field review indicates action is required to protect exposed foundations.	Not Analyzed
5	Bridge foundation is determined to be stable for assumed or calculated scour condition.	Not Analyzed
6	Scour calculation/evaluation has not been made.	Not Analyzed
7	Countermeasures have been installed to mitigate an existing problem with scour and to reduce the risk of bridge failure during a flood event.	Not Analyzed
8	Bridge foundations determined to be stable for the assumed or calculated scour condition.	Not Analyzed
9	Bridge foundations (including piers on dry land well above flood water elevations).	Not Analyzed
10	Bridge over "hard" waters that has not been evaluated for scour but considered low risk.	Not Analyzed
11	Bridge with "unknown" foundation that has not been evaluated for scour.	Analyzed / Treated as category 11.
12	Bridge not over waterway.	Not Analyzed

Figure 2-2: Bridge category in HAZUS 5.1 according to scour potential (FEMA, 2022).

Table 2-1: Extract from a data file in Hazus 5.1 including the probability of bridge failure [columns named “damage_factor”] based on the scour potential [column “Scour Index”] (FEMA, 2022).

Return period [years]		100	500	1000
Depth [m]		0.32	1.95	5.15
Scour Index	Description	damage_factor	damage_factor	damage_factor
ID_U	Single Span	0.050	0.100	0.150
ID_2	Single Span	0.020	0.040	0.060
ID_3	Single Span	0.010	0.020	0.030
ID_U	Continuous Span	0.013	0.025	0.038
ID_2	Continuous Span	0.005	0.010	0.015
ID_3	Continuous Span	0.003	0.005	0.008
ID_1	Single Span	0.050	0.100	0.150
ID_1	Continuous Span	0.013	0.025	0.038

2.3.1.2 Road segments

This section details selected fragility and vulnerability models for road segments exposed to earthquake, flood and ground failure hazards.

2.3.1.2.1 Earthquake

In the case of earthquake hazard, it is assumed that wave propagation effects on the road surface are not significant and that most damages result from induced permanent ground deformation, which may be assimilated to ground failure phenomena. However, roads on slopes, in cuts (trenches) or on embankments may be damaged due to the failure of the surrounding relief. Within the FP7 SYNER-G project, fragility models for roads in such configuration have been proposed by Kaynia (2013). In the case of roads on slopes, fragility curves are expressed as a function of PGA, and they are available for various values of the yield coefficient k_y of the surrounding slope (see Table 2-2 and Figure 2-3).

Table 2-2: Fragility parameters (mean α and standard-deviation β) for roads on slopes, expressed as a function of PGA, for different values of yield coefficient k_y . Taken from Kaynia (2013).

Damage states	$k_y = 0.05$		$k_y = 0.10$		$k_y = 0.20$		$k_y = 0.30$	
	α [g]	β	α [g]	β	α [g]	β	α [g]	β
Minor	0.14	0.40	0.25	0.35	0.45	0.35	0.64	0.30
Moderate	0.22	0.40	0.40	0.35	0.71	0.35	1.00	0.30
Extensive/Complete	0.37	0.40	0.64	0.35	1.11	0.35	1.55	0.30

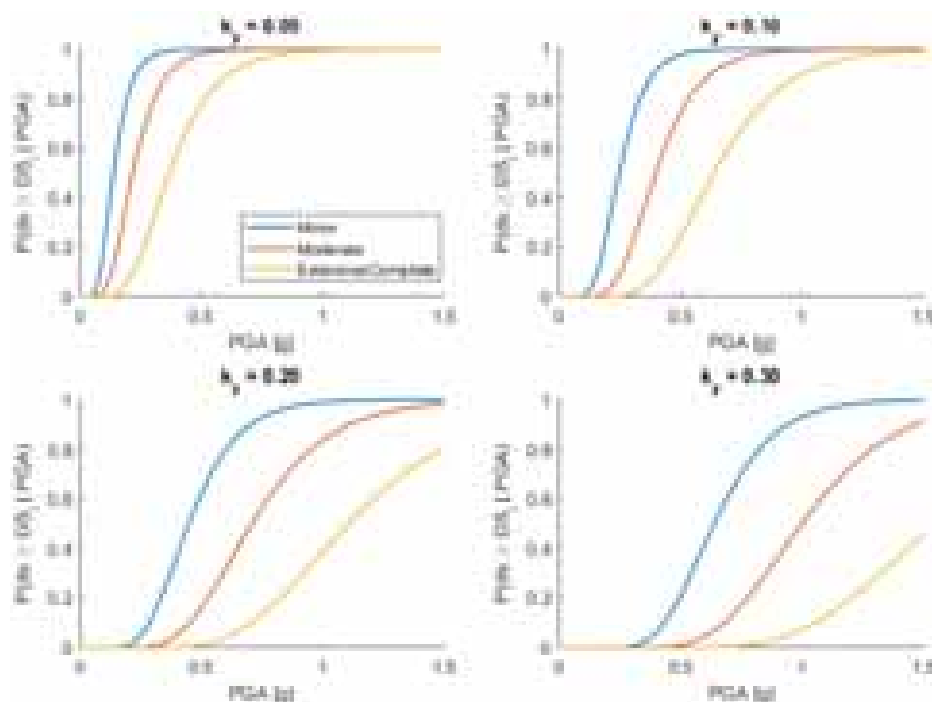


Figure 2-3: Seismic fragility curves for roads on slopes, from Kaynia (2013).

In the case of roads on embankments, fragility curves are expressed as a function of PGA, and they are available for various embankment heights and for EC8 soil types C and D (see Table 2-3 and Figure 2-4).

Table 2-3: Fragility parameters (mean α and standard-deviation β) for roads on embankments, expressed as a function of PGA, for different heights and EC8 ground types. Taken from Kaynia (2013).

Damage states	Ground type C				Ground type D			
	$h = 2 \text{ m}$		$h = 4 \text{ m}$		$h = 2 \text{ m}$		$h = 4 \text{ m}$	
	α [g]	β	α [g]	β	α [g]	β	α [g]	β
Minor	0.65	1.00	0.51	0.90	0.47	0.90	0.31	0.70
Moderate	1.04	1.00	0.88	0.90	0.66	0.90	0.48	0.70
Extensive/Complete	1.57	1.00	1.42	0.90	0.89	0.90	0.72	0.70

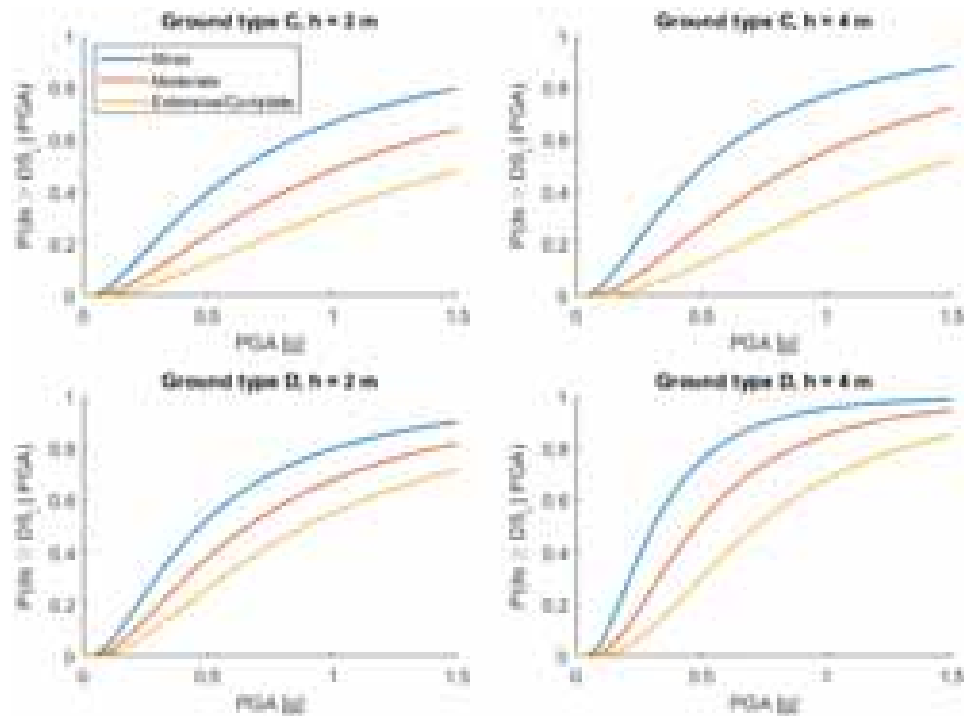


Figure 2-4: Seismic fragility curves for roads on embankments, from Kaynia (2013).

In the case of roads in cuts, fragility curves are expressed as a function of PGA, and they are available for various embankment heights and for EC8 soil types C and D (see Table 2-4 and Figure 2-5).

Table 2-4: Fragility parameters (mean α and standard-deviation β) for roads in cuts, expressed as a function of PGA, for different heights and EC8 ground types. Taken from Kaynia (2013).

Damage states	Ground type C		Ground type D			
	$h = 6 \text{ m}$		$h = 4 \text{ m}$		$h = 6 \text{ m}$	
	$\alpha \text{ [g]}$	β	$\alpha \text{ [g]}$	β	$\alpha \text{ [g]}$	β
Minor	0.59	1.00	0.44	1.00	0.38	1.00
Moderate	1.09	1.00	0.92	1.00	0.77	1.00
Extensive/Complete	1.90	1.00	1.77	1.00	1.46	1.00

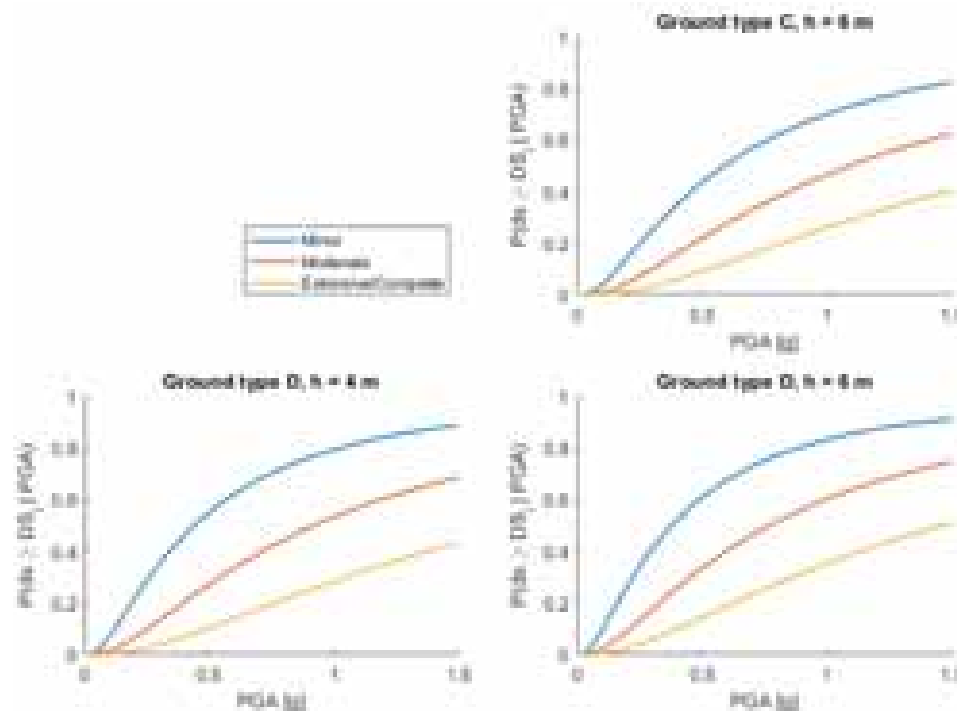


Figure 2-5: Seismic fragility curves for roads in cuts, from Kaynia (2013).

2.3.1.2.2 Flood

The inventory of potential failure modes affecting road segments in the case of flood hazard is taken from the work by D'Ayala et al. (2015) in the FP7 INFRARISK Project, as detailed in Figure 2-6. It is then possible to distinguish between two main types of effects, i.e. the deterioration of the paved surfaces (i.e., requiring clean up or rehabilitation) and the disruption of traffic (i.e., road impassable due to water depth or flow).



Figure 2-6: Identification of common failure modes for road segments exposed to flood hazard, from D'Ayala et al. (2015).

Kramer et al. (2016) have conducted experiments using model cars and a water flume, in order to estimate the roadworthiness of passenger cars and emergency vehicles with various conditions of water depth, flow velocity and flow angle. The roadworthiness is represented by a total head variable, which is expressed as follows:

$$h_E = h_n + \frac{v_n^2}{2g} \quad (3-1)$$

where h_n is the water depth, v_n the flow velocity and g the gravitational constant. Therefore, the effect of flood hazard on vehicles is represented in Figure 2-7, as a function of water depth and flow velocity, using different safety criteria for different types of vehicles.

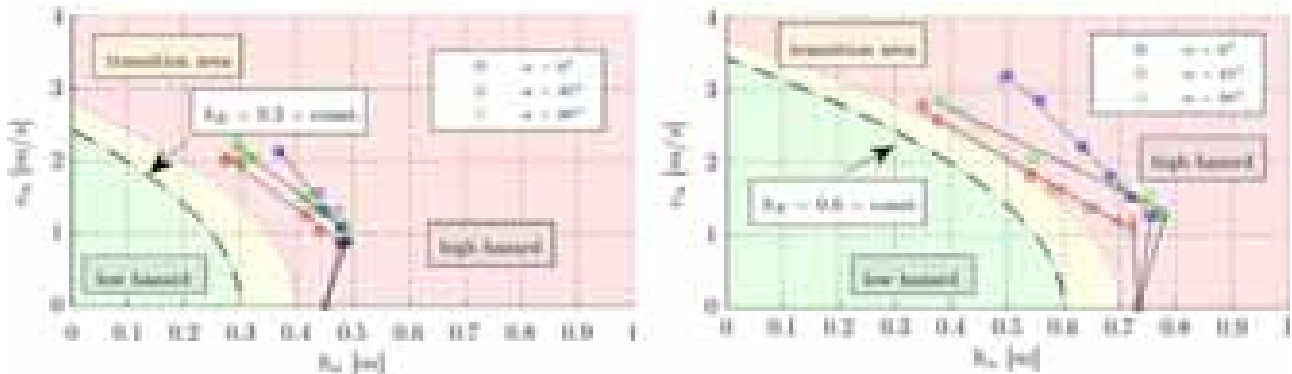


Figure 2-7: Safety criteria for the roadworthiness of passengers cars ($h_E = 0.3$ m) (Left) and emergency vehicles ($h_E = 0.6$ m) (Right), from Kramer et al. (2016). The angle α represents the direction of the water flow with respect to the orientation of the car.

Alternatively, Pregnotato et al. (2017) have proposed a depth-disruption function, by exploiting various sources of data, such as experimental studies, safety literature, experts' opinion or videos. This function, represented in Figure 2-8, describes the evolution of vehicle speed as a function of water depth. Information about speed reduction due to the intensity of rainfall and about the potential flotation of parked cars is also provided. It is worth noting that the water depth values leading to impassable conditions (i.e., zero speed) are around 0.3 m, which are in line with the safety criteria proposed by Kramer et al. (2016).

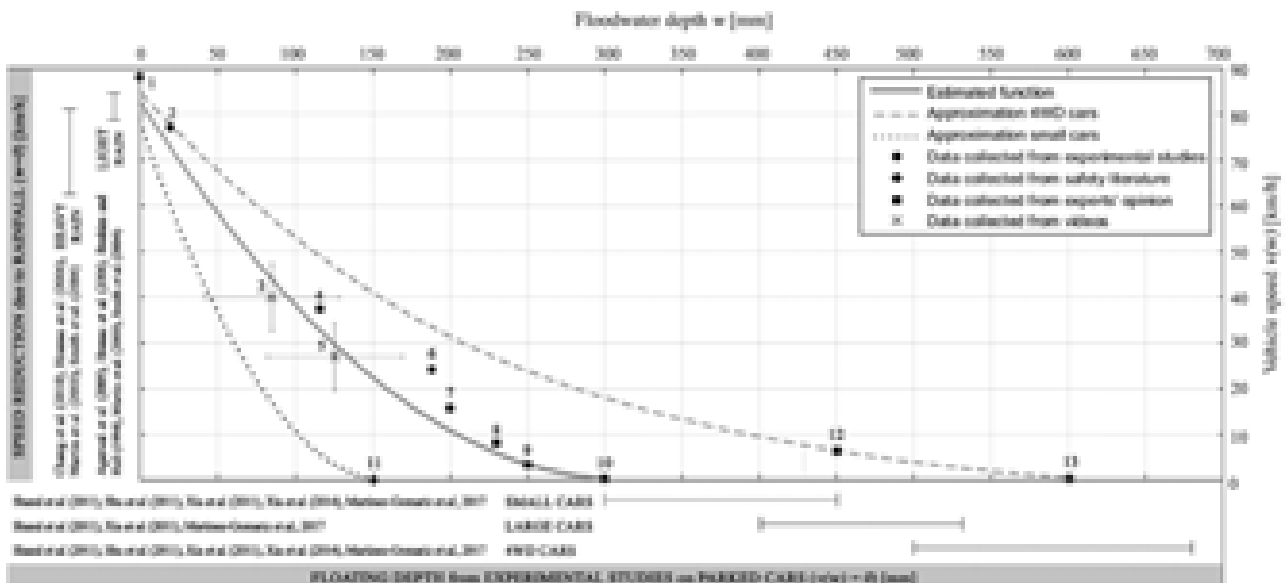


Figure 2-8: Depth-disruption function, relating flood depth on a road with vehicle speed, developed by Pregnotato et al. (2017).

A line graph showing the relationship between Water Depth (m) on the x-axis and Damage Ratio on the y-axis. The x-axis ranges from 0 to 5 with major grid lines every 1 unit. The y-axis ranges from 0.0 to 1.0 with major grid lines every 0.2 units. A blue curve starts at (0, 0.0) and increases monotonically, passing through approximately (1, 0.01), (2, 0.05), (3, 0.1), (4, 0.2), and ending at (5, 0.5).

Water Depth (m)	Damage Ratio
0	0.00
1	0.01
2	0.05
3	0.10
4	0.20
5	0.50

The inventory of potential failure modes affecting road segments in the case of ground failure hazard is taken

The diagram illustrates the relationship between Soil Conditions, Specific System Mechanisms, and Damage Components for various types of foundation settlement.

Soil Conditions	Specific System Mechanisms	Damage Components
Shallow Foundations	Uniform Settlement	Uniform rates of settlement at the top of piles only, minor cracks on the surface of the wall Deep structures of embankment backing with flow, medium cracks on the surface of the wall Surface subsiding of embankment
	Differential Settlement	Uniform rates of settlement at the top of piles only, minor cracks on the surface of the wall Deep structures of embankment backing with flow, medium cracks on the surface of the wall Surface subsiding of embankment
Deep Foundations	Uniform Settlement	Uniform rates of settlement at the top of piles only, minor cracks on the surface of the wall Deep structures of embankment backing with flow, medium cracks on the surface of the wall Surface subsiding of embankment
	Differential Settlement	Uniform rates of settlement at the top of piles only, minor cracks on the surface of the wall Deep structures of embankment backing with flow, medium cracks on the surface of the wall Surface subsiding of embankment
Shallow Foundations	Uniform Settlement	Uniform rates of settlement at the top of piles only, minor cracks on the surface of the wall Deep structures of embankment backing with flow, medium cracks on the surface of the wall Surface subsiding of embankment
	Differential Settlement	Uniform rates of settlement at the top of piles only, minor cracks on the surface of the wall Deep structures of embankment backing with flow, medium cracks on the surface of the wall Surface subsiding of embankment
Deep Foundations	Uniform Settlement	Uniform rates of settlement at the top of piles only, minor cracks on the surface of the wall Deep structures of embankment backing with flow, medium cracks on the surface of the wall Surface subsiding of embankment
	Differential Settlement	Uniform rates of settlement at the top of piles only, minor cracks on the surface of the wall Deep structures of embankment backing with flow, medium cracks on the surface of the wall Surface subsiding of embankment

Regarding road pavement exposed to ground failure, the review by Argyroudis & Kaynia (2014) has advocated the use of the fragility curves developed by the HAZUS methodology (NIBS, 2004), which are based on expert judgment. These curves use the permanent ground deformation as intensity measure and they are presented in Figure 2-11 for the following damage states: “minor” (road open), “moderate” (road partially open) and “extensive/complete” (road closed). Corresponding fragility parameters are detailed in Table 2-5.

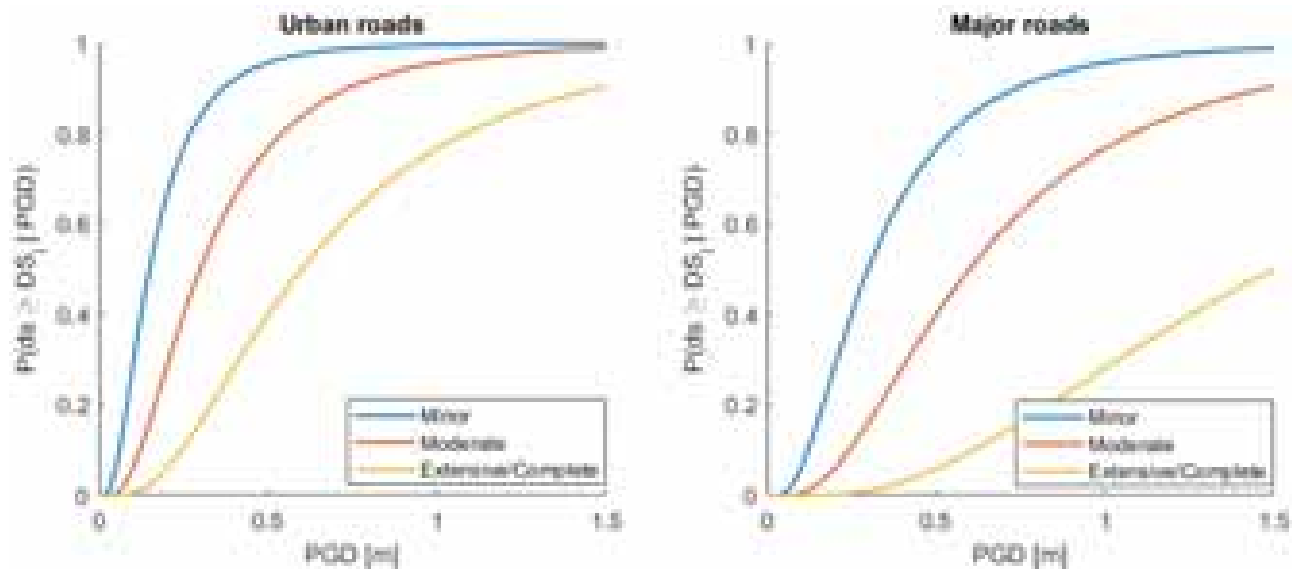


Figure 2-11: Fragility curves for urban and major roads exposed to ground failure, with permanent ground deformation as the intensity measure. Taken from HAZUS (NIBS, 2004).

Table 2-5: Fragility parameters (mean α and standard-deviation β) for urban and major roads exposed to ground failure, with permanent ground deformation as the intensity measure. Taken from HAZUS (NIBS, 2004).

Typology	Damage states	α [m]	β
2 traffic lanes (urban roads)	Minor	0.15	0.70
	Moderate	0.30	0.70
	Extensive/Complete	0.60	0.70
≥ 4 traffic lanes (major roads)	Minor	0.30	0.70
	Moderate	0.60	0.70
	Extensive/Complete	1.50	0.70

Within the SAFELAND project (Pitilakis et al., 2011), Winter et al. (2014) have used experts' opinion to propose fragility curves for roads exposed to fast moving landslides (i.e., debris flow), where the selected intensity measure is the volume of the debris flow. These curves are represented in Figure 2-12, for the damage states “limited damage” (no significant impact on the passage of vehicles), “serious damage” (complete blockage of carriageway) and “destroyed” (blockage and damage to the road itself).

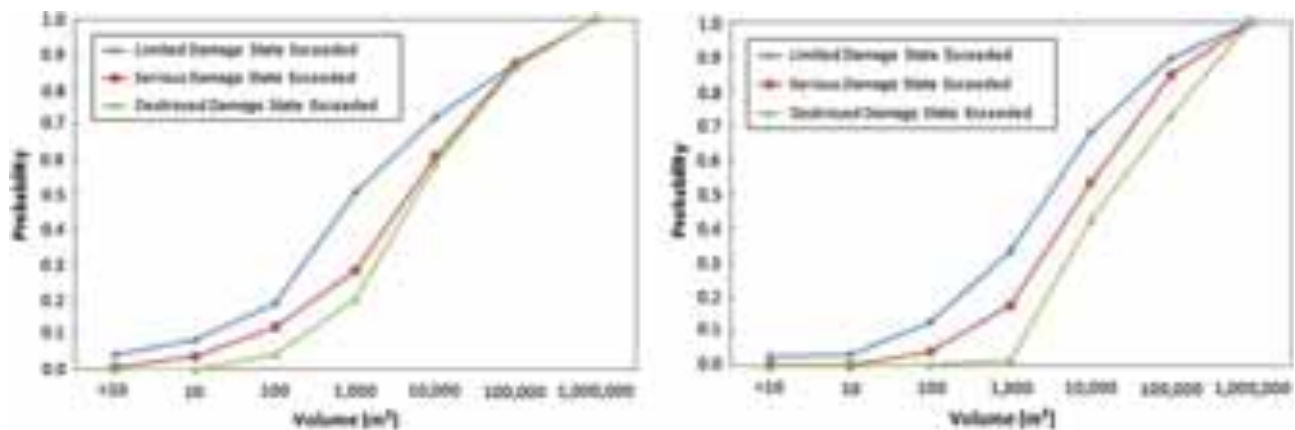


Figure 2-12: Fragility curves for local roads (Left) and high-speed roads (Right) as a function of the volume of debris flow, taken from Winter et al. (2014) and Pitilakis et al. (2011).

Also in the SAFELAND project, Pitilakis et al. (2011) have investigated the reliability of road protection galleries with respect to rock falls. Based on some analytical computations, the developed fragility functions express the probability of destroying the roof of the protection gallery, as a function of rock impact velocity and rock mass. In Figure 2-13, some examples of such fragility functions are presented, for various configurations of thicknesses for the concrete slab and cushion layer.

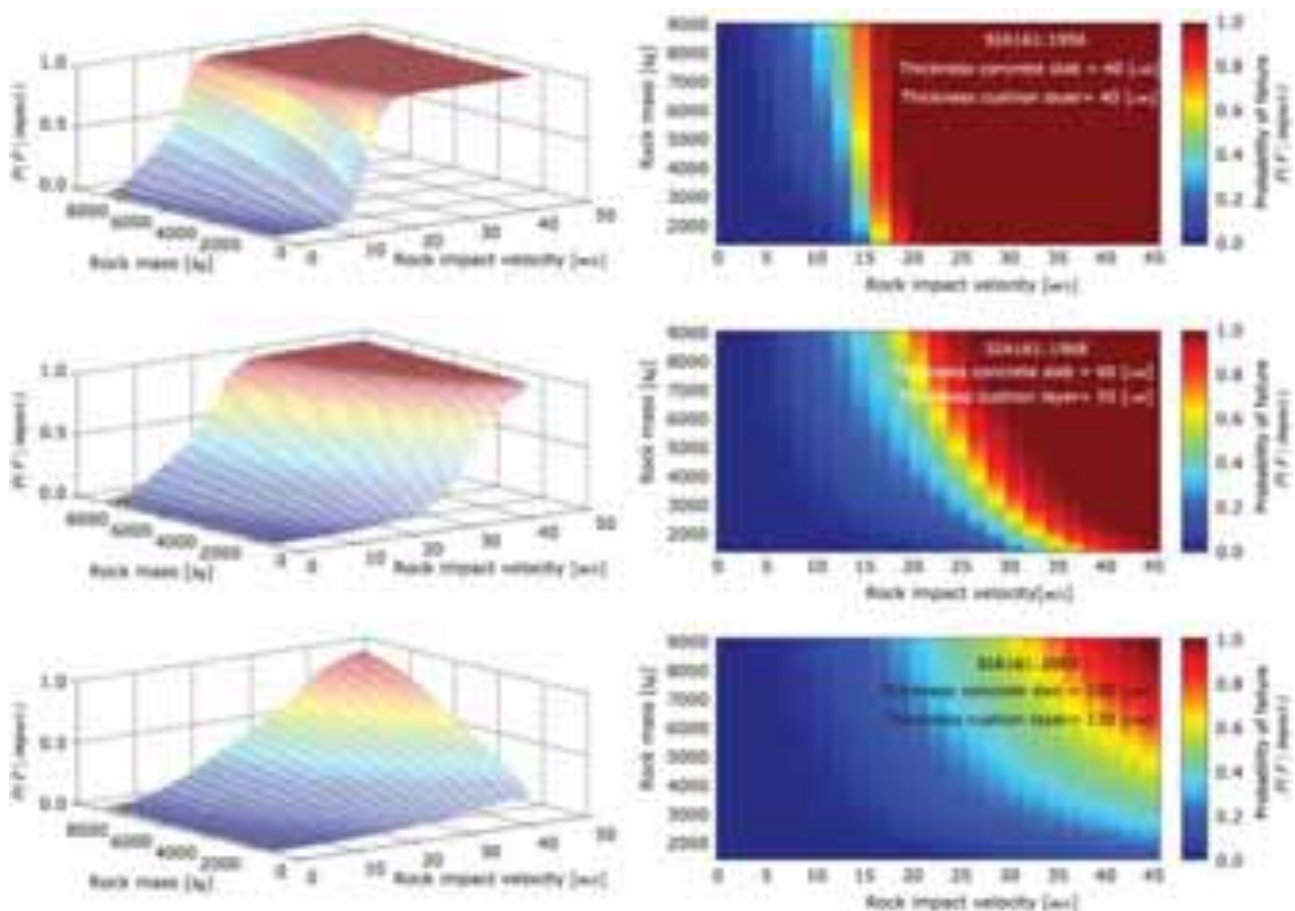


Figure 2-13: Fragility curves for local roads (Left) and high-speed roads (Right) as a function of the volume of debris flow, taken from Winter et al. (2014) and Pitilakis et al. (2011).

2.3.2 Fragility and vulnerability models for electric power network components

This section proposes a set of available fragility and vulnerability models for electric power network components. Regarding earthquake and flood, hazards, electric substations have been found to be the most susceptible. Transmission lines have been found to be mostly susceptible to wind hazard. No reference has been retrieved regarding the vulnerability to mass movement (i.e., a binary model may be assumed, with complete damage when the component is in the landslide area).

2.3.2.1 Earthquake

Within the FP7 SYNER-G project, the review by Pinto et al. (2010) of seismic fragility curves for electric power network components has identified several models related to substations. Among these, two models are proposed here, due to their relative recency or their focus on European typologies.

Rasulo et al. (2004) have proposed a fragility curve expressing the failure of a typical Italian substation, as a function of PGA. The substation fragility curve is derived from the substation equipment by identifying the minimal cut-sets that are necessary to interrupt the electric flow, and by combining the corresponding component fragilities for a system in series. The corresponding fragility curve is presented in Figure 2-14.

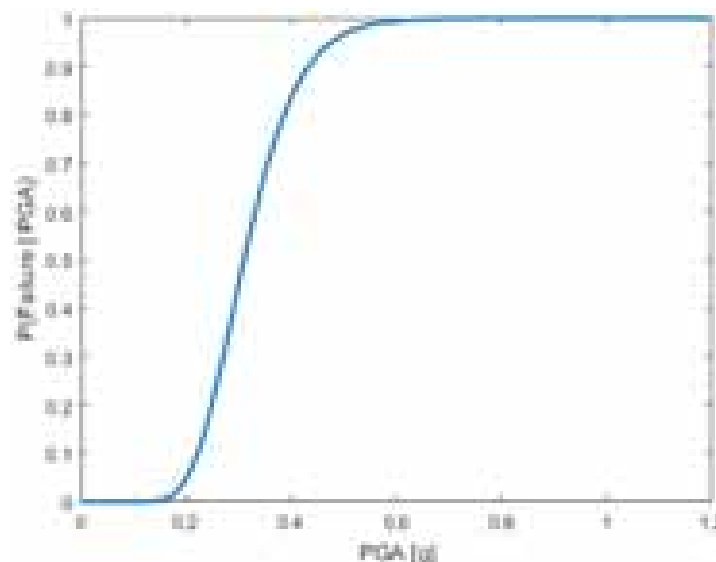


Figure 2-14: Fragility curve for the failure of an electric substation, from Rasulo et al. (2004). Fragility parameters: $\alpha = 0.31 \text{ g}$; $\beta = 0.26$.

Alternatively, Giovinazzi & King (2009) have derived fragility functions for substations as well, by reusing the HAZUS model (FEMA, 2020) and by combining it with expert judgment models and empirical models based on statistical treatment of past damage data. Fragility curves are expressed as a function for PGA and they cover four damage states (Slight/Minor, Moderate, Extensive, Complete). They are available for two types of substations, namely with anchored/seismically-designed components or with unanchored/standard components, as shown in Figure 2-15.

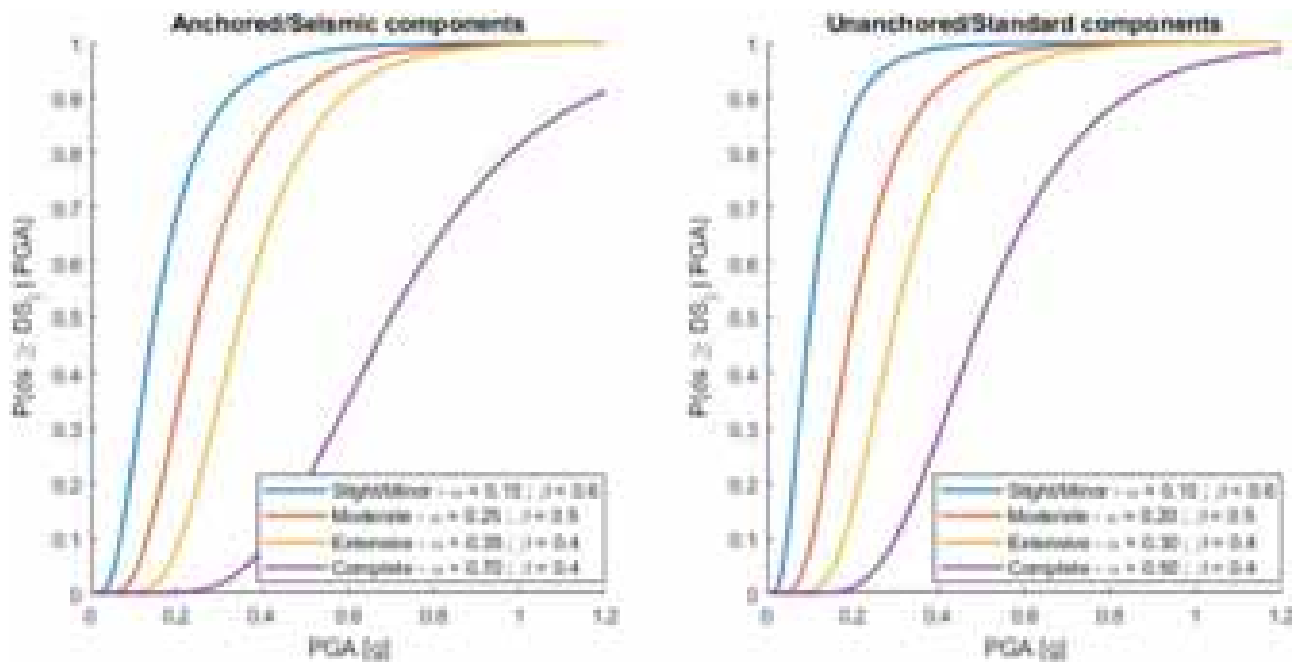


Figure 2-15: Fragility curves for two types of electric substations, from Giovinazzi & King (2009).

Anagnos (1999) developed a database of damage observations in electric substations caused by 12 earthquakes in California and produced empirical seismic fragility curves for electric substation equipment (e.g. Figure 2-16). The fragility curves are non-parametric functions of the peak horizontal acceleration and correspond to different modes of failure of equipment in a substation (e.g. transformer overturn, anchorage failure, etc.).

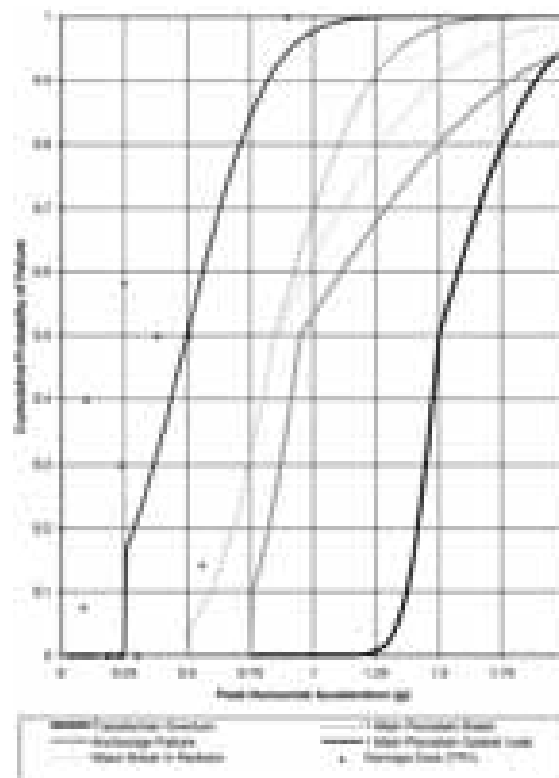


Figure 2-16: Seismic fragility curves for single-phase 230 kV transformers; Source: Anagnos (1999).

2.3.2.2 Flood

Regarding the impact of floods, components such as substations appear to be the most exposed, compared to overhead or buried lines. However, apart from data in the HAZUS flood model (FEMA, 2022), no relevant model has been found in the literature. Therefore, it is proposed to use the HAZUS vulnerability curve, which expresses the percent of damage as a function of flood depth, as shown in Figure 2-17. Although various types of substations are considered in HAZUS (low-, medium- or high-voltage), the vulnerability curve applies to all types. Apart from the damage ratio, HAZUS also proposes a functionality threshold depth, at 4 feet (~1.2 m).

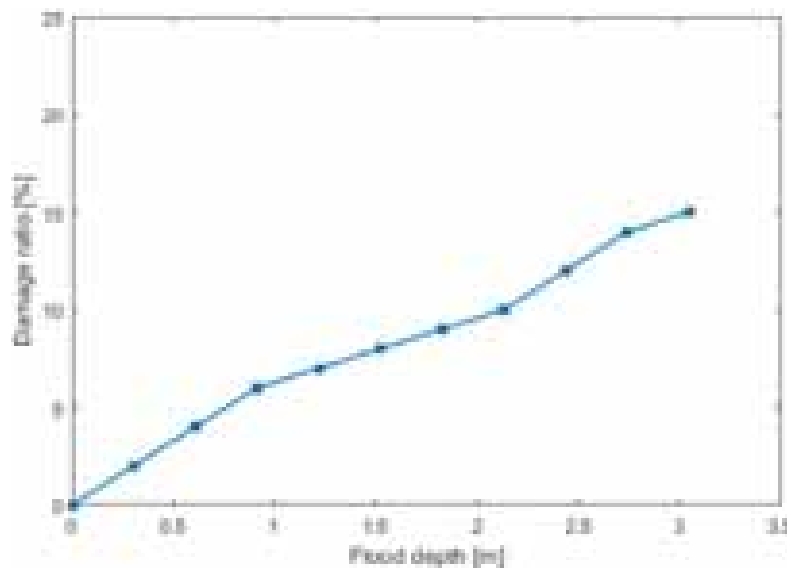


Figure 2-17: Vulnerability curves for electric substations, from HAZUS flood model (FEMA, 2022).

2.3.2.3 Wind

Steel transmission towers are components of electric power networks, which are vulnerable to wind. Fu et al. (2016) produced synthetic fragility curves for transmission towers (500 kV) as a function of the equivalent basic wind speed, which accounts for the combined loads from wind and rain (Figure 2-18). Moreover, their fragility curves are also a function of the wind attack angle. Raj et al. (2022) produced an empirical fragility curve for transmission towers in India for one damage state, i.e. functionality disruption, and they compared this fragility model to other models, which are also a function of the 3-sec gust speed.

Watson (2018) used fragility curves in HAZUS for substations under hurricane wind.

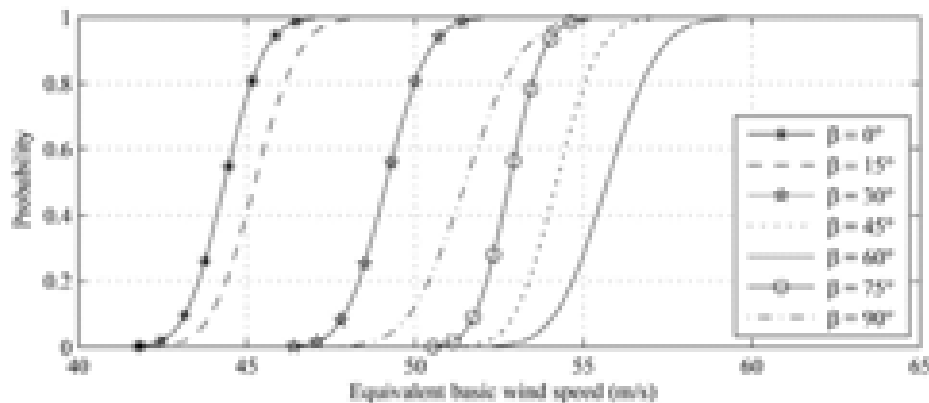


Figure 2-18: Wind fragility curves for steel transmission towers in electric power networks as a function of the equivalent basic wind speed accounting for combined wind and rain loads (Fu et al., 2016) and the wind attack angle (β).

2.4 Multi-hazard fragility models

Accurate multi-hazard risk assessment implies the integration of multi-hazard interactions at the impact or consequence level (e.g., Marzocchi et al., 2012; Selva, 2013; Gehl, 2017), which makes the development of multi-hazard fragility models necessary. In recent years, a growing number of research studies have proposed multi-hazard frameworks that strive to account for the wide range of possible interactions between multiple hazard types (Gill & Malamud, 2014; Bruneau et al., 2017; Drakes & Tate, 2022; De Angeli et al., 2022).

According to the review by Gentile et al. (2022) of physical impact models for multi-hazard risk assessment, the classification proposed by Zaghi et al. (2016) is adapted to study of multi-hazard fragility models, since it relies on two types of interactions:

- i) Level-I Interactions, representing natural interactions of hazards independent of the presence of physical components;
- ii) Level-II Interactions, representing interactions through the effects of hazards on a given site, component or infrastructure.

The latter type of interactions is of most interest here, since it focuses on the impact on physical components, whatever the type or origin of the multiple hazard combinations (e.g., concurrent, successive, triggered, independent, etc.). What matters is the alteration of the physical or functional properties of an asset (e.g., fragility/vulnerability curve) due to cumulative damage. For this reason, multi-hazard fragility also includes repeated instances of the same hazard, such as earthquake sequences or compound flooding (Gentile et al., 2022).

However, the development of multi-hazard models remains relatively limited, with respect to the wide range of possible multi-hazard combinations and the variety of exposed assets to consider. This technical gap may be explained by several factors, such as differences in the scientific maturity between the various hazard assessment fields (Douglas, 2007), the need to integrate different physical phenomena in the structural modelling step, and the lack of harmonised damage scales between various hazard loading mechanisms. A brief review of existing multi-hazard fragility models is proposed in Table 2-6, which is based on earlier work by Gehl et al. (2019) and updated with recent references.

Table 2-6: Summary of some recent studies devoted to the development of multi-hazard fragility models (adapted from Gehl et al., 2019).

Reference	Hazard(s)	Exposed element(s)	Intensity measure(s)	Main features
D'Ayala, Copping and Wang (2006)	Earthquake, flood, windstorm, lightening	Historic buildings components	Macroseismic intensity, depth of water, wind speed, isochrone maps	Conceptual model to compare relevance of hazard to risk of damage
Lee & Rosowsky (2006)	earthquake, snow	wood frame building	PGA, snow load on rooftop	numerical simulations, parametric fragility (different snow loads)
Kafali (2008)	wind, wave effects	offshore platform	wind speed over sea surface, wind angle	analytical solution, crossing theory for system fragility, linear oscillator approximation
Zuccaro et al. (2008)	explosive volcanic eruption (earthquake, ash-fall, pyroclastic flow)	residential buildings	macroseismic intensity, ash load, dynamic pressure	empirical / expert-based vulnerability functions, updated Damage Probability Matrices, sequence of events
Asprone et al. (2010)	blast, earthquake	RC building	load factor, SA(T)	numerical simulations, independent fragility curves, aggregated annual collapse probabilities
Chiodi et al. (2011)	earthquake, wind	steel hangar structure	SA(T), wind speed	methodological framework, hazard-independent fragility
Alipour & Shafei (2012)	earthquake, riverine flood (scour)	RC bridge	PGA, scour depth (from flow discharge and flow depth)	numerical simulations, parametric fragility (different scour conditions)
Li & van de Lindt (2012)	wind, flood earthquake, snow	residential buildings	wind speed, water depth, SA(T), snow load	hazard-independent fragility curves, harmonized losses
Pita et al. (2012)	rainfall, wind (hurricane)	residential buildings	wind speed, rain rate	numerical simulations, building component damage curves due to wind (roof, gable, windows, doors), damages curves due to water ingress
Prasad & Banerjee (2013)	earthquake, riverine flood (scour)	RC bridge	PGA, scour depth (from flow discharge and flow depth)	numerical simulations, parametric fragility (different scour conditions)
Kameshwar & Padgett (2014)	earthquake, storm surge (hurricane)	highway bridges	PGA, surge, water depth	numerical simulations, multivariate GLM, hazard-independent fragility, risk comparison
Ribeiro et al. (2014)	earthquake (aftershocks)	steel structure	SA(T) for mainshock and aftershock	numerical simulations, back-to-back NLTHAs, conditional probability of failure during aftershock given mainshock, robustness index
Charvet et al. (2015)	tsunami, debris impact	wood / masonry / RC / steel buildings	water depth, flow velocity, impact	empirical fragility (data from 2011 Great East Japan tsunami), multivariate GLM
Yilmaz (2015)	earthquake, riverine flood (scour)	highway bridges	PGA, occurrence of characteristic flood event	numerical simulations, component- and system-level fragility
Bodda et al. (2016)	earthquake, flood	flood defence structure (gravity dam)	PGA, water depth	numerical simulations, modelling of seepage through foundation, fragility surface

Reference	Hazard(s)	Exposed element(s)	Intensity measure(s)	Main features
Cavalieri et al. (2016)	earthquake, flood (rainfall)	storm water system	PGV, PGD, flow discharge	numerical simulations (OOFIMS), effects of earthquake damage on the subsequent flood hazard
Gehl & D'Ayala (2016)	earthquake, riverine flood	RC bridge	PGA, flow discharge	numerical simulations, system reliability
D'Ayala et al (2016)	Earthquake, flood, wind	Historic masonry and timber buildings	PGA, Flood depth, wind speed.	Simplified numerical simulation of critical components
Song et al. (2016)	earthquake (aftershocks)	steel building	SA(T) for mainshock and aftershock	numerical simulations, back-to-back NLTHAs, aggregation of mainshock-aftershock losses
Reed et al. (2016)	wind, inundation, rainfall height	electric power deliver lifeline	rainfall, wind speed, inundation depth	system-level logistic fragility surface
De Risi et al. (2017a)	tsunami	wood / masonry / RC / steel buildings	water depth, flow velocity	empirical fragility (data from 2011 Great East Japan tsunami), multivariate GLM
Goda & De Risi (2018)	earthquake, tsunami	residential buildings	PGV, water depth	empirical fragility, hazard-independent fragility, aggregation of losses
Tyagunov et al. (2018)	earthquake (liquefaction), riverine flood	fluvial dike	PGA, water depth	numerical simulations, computation of liquefaction potential , fragility surface
Venanzi et al. (2018)	earthquake, wind	tall building	SA(T), wind speed	numerical simulations, hazard-independent fragility curves, aggregated annual losses
Petrone et al. (2020)	earthquake, tsunami	5-storey moment-resisting reinforced concrete frame	hydrodynamic lateral force	numerical simulations, back-to-back NLTHAs, effect of earthquake damage on subsequent tsunami fragility
Gentile & Galasso (2020)	earthquake mainshock, aftershock	reinforced concrete frame buildings	avgSA, hysteretic energy	numerical simulations, back-to-back NLTHAs, probabilistic seismic demand surface model
Argyroudis & Mitoulis (2021)	flood, earthquake	reinforced concrete bridges	scour depth, ratio of scour over foundation depth, PGA	numerical simulations, back-to-back NLTHAs, single-IM fragility curves, fragility surfaces
Parammal Vatteri et al. (2022)	Earthquake, repeated flooding	Confined masonry	PGA, flood depth	Advanced numerical simulations Bayesian approach to system failure assessment
Chen et al. (2022)	earthquake (aftershocks)	tall pier reinforced concrete bridges	mainshock PGV, aftershock PGV	numerical simulations, back-to-back NLTHAs, fragility surface
Crawford et al. (2022)	repeated floods	single- and multifamily residential buildings	inundation depth	field data, empirical flood fragilities
Gómez Zapata et al. (2023)	any hazard; in the application: tsunami	buildings (building portfolios)	any intensity measure; in the application: tsunami inundation depth	analytical framework, single-hazard state-dependent fragility functions, effect of earthquake damage on subsequent tsunami fragility

Most of the above models may be associated to one of the two following categories of modelling structures:

- *State-dependent fragility curves*, which are conditioned on the damage state of the element in addition to the hazard intensity measure. The initial damage state relates to a previous hazard event and it conditions the response of the exposed asset when subjected to a subsequent hazard loading. They constitute multi-hazard physical vulnerability models for successive hazards, which may be of the same type (e.g., an earthquake followed by another earthquake or even independent events (e.g., flood followed by an earthquake). The modelization of the accumulation of seismic damage using a Markov chain has been proposed by Iervolino et al. (2015). The applications, which employ a Markovian modelling scheme (e.g., Shokrabadi & Burton, 2018; Trevisopoulou et al., 2020; Trevisopoulou & Guéguen, 2016) use state-dependent fragility models to calculate the transition matrices for the shock deterioration, which are used in the Markov chain. An example of derivation of state-dependent fragility curves is proposed in Section 5, while Section 6 introduces a Markovian framework where such models may be applied.
- *Vector-valued fragility functions* (or fragility surfaces), which express the probability of reaching or exceeding a damage state given two or more hazard loadings. Such models are especially useful to represent the combined effect of correlated or co-occurring hazards (e.g., fragility surface for wind and rainfall due to a storm event, Reed et al., 2016). However, they may also be used in the context of successive hazards, where one IM represents the first hazard loading, and the other IM the subsequent event: as a result, the outcome of the fragility surfaces expresses the probability of damage due to the whole sequence of successive events (e.g., fragility surface for seismic mainshock and aftershock, Chen et al., 2022).

Although the above multi-hazard models constitute relevant solutions to represent the combined effect of multiple hazard loadings, a pending issue concerns the definition or application of damage scales that may be harmonised across various hazard types. Korswagen et al. (2019) proposed a methodology for defining a damage scale, which could be used to characterize damage due to building actions by multiple hazards. They based their methodology on the selection of metrics and indicators of damage, which can describe the damage caused by the considered hazards. The challenges in the proposed methodology include selecting metrics so that the damage scales are mutually exclusive and collectively exhaustive, as well as the fact that the selected metrics may not reflect the different failure mechanisms because of the differences between the actions by the different hazards.

Maiwald & Schwarz (2019) proposed a unified damage classification system, which includes damage scales for flooding and tsunami impact, and wind. Moreover, for each damage scale, it includes descriptions of the damage at each damage grade, while the damage grades of the damage scales for the different hazards have been harmonized to each other and to the damage grades in the EMS-98. This harmonization of the damage grades across hazards allows comparing damage caused by different hazards, and facilitates cumulative damage assessment. A summary of the harmonised damage scales is presented in , while the description of each specific damage degree is detailed in Maiwald & Schwarz (2019).

Table 2-7: Summary of damage scales for earthquake, flood/tsunami and wind, translated from Maiwald & Schwarz (2019).

Damage state	Earthquake	Flood / Tsunami	Wind	Damage		Safety of life and limb
				Structural	Non-structural	
D0	X	-	X	None	None	Guaranteed
D1	X	X	X	None	Light	
D2	X	X	X	Light	Moderate	
D3	X	X	X	Moderate	Heavy	
D4	X	X	X	Heavy	Very heavy	Critical
D5	X	X	X	Very heavy	Very heavy	Not guaranteed
D6	-	X	X	Complete	Complete	Not guaranteed

Gómez Zapata et al. (2023) developed a procedure for converting typical single-hazard fragility curves to state-dependent fragility curves to account for cumulative damage. This procedure has been developed as an alternative to the development of new synthetic or empirical state-dependent fragility curves. They applied this procedure in scenario-based multi-risk assessment in the case of an earthquake in Lima (Peru) followed by a tsunami. To overcome the difficulties due to the differences between damage scales for different hazards, they introduced “inter-scheme compatibility matrices”, which account probabilistically for the correspondences between damage scales.

3 SELECTION OF PHYSICAL VULNERABILITY MODELS FOR THE TESTBEDS

In order to select the models that will be subsequently used to account for the physical vulnerability of the exposed elements, we apply a procedure involving screening candidate models, scoring the models that passed the screening, and selecting the models, which could be used in the subsequent multi-hazard risk analyses. This procedure is based on the work by Gentile et al. (2022) and Galasso et al. (2021), which developed a set of criteria and a scoring procedure for physical vulnerability models. The applied procedure includes a phase of screening during which, amongst the published and accessible models, the models which could be used are being selected, and a phase where the models are evaluated on a set of criteria and assigned the corresponding score. The types of exposed elements (engineering assets) for which physical vulnerability models are selected are buildings. As opposed to buildings, there is no ranking system yet for infrastructure components such as bridges, road segments, electric substations or electrical power transmission towers. Therefore, the selection of physical vulnerability models for infrastructure components should simply be based on the review of existing models carried out in Section 2.

Models are selected for various types of hazards: earthquake, flood, debris flow (i.e., impact of the landslide runoff on the exposed asset) and landslide / ground settlement (i.e., ground failure beneath the exposed asset). Although earthquakes are not included in the multi-hazard testbed scenarios that have been eventually considered in WP2, they are still considered here as a potentially relevant single hazard that could be readily integrated to the subsequent risk assessment, thanks to European initiatives such as the ESRM20.

3.1 Screening candidate models

The types of models that are evaluated in this report are fragility and vulnerability models (Figure 2-1). Depending on the state of the art, one or the other, or both fragility and vulnerability models may be available for a class of exposed element for a specific hazard. In the cases that a suitable damage to loss model exists, it is possible to calculate the vulnerability curve using the damage to loss model and the corresponding fragility curves.

The criteria for the screening are the correspondence of the models with the class of the exposed element, and the hazard, for which a model had been developed. The classes of the exposed elements are categories of engineering assets (e.g. buildings), which have common characteristics and vulnerability to one or more hazards. The physical vulnerability models are selected for such classes rather than for specific exposed elements. For hazards where existing models are rather scarce (e.g., flood, landslide), most of the models available in the literature (to the best of our knowledge) have been selected, while prioritising models that may be readily exploited in the subsequent parts of the project (i.e., risk assessment in WP3 and WP4). Regarding earthquake hazard, due to the large number of available fragility models, only a handful of models have been selected: priority has been given to models from extensive and consistent studies (Crowley et al., 2021) or from robust derivation approaches. Some of the latter models may correspond to the right asset class but not to the correct geographical of the testbeds: they are still ranked, since the criteria by Gentile et al. (2022) will be able to apply a score penalty during the evaluation. The details of the selected models are summarized in Appendix I.

3.2 Scoring fragility and vulnerability models for buildings

The scoring of the models that passed the screening phase is employed to rank the models based on a set of criteria with respect to their relevance and usefulness in the context of the project. The fragility models are scored using the list of criteria proposed by Gentile et al. (2022) (Table 3-1). For each criterion, there are three possible qualitative scores: high, medium, and low, which are assigned using as guidelines the corresponding descriptions in Table 3-1. The descriptions for assigning a score for the introduced criteria for the user-specific requirements are original and aim to leave little ambiguity during the scoring. Once all models are given a

high/medium/low score for all considered criteria, the qualitative scores are subsequently recoded to the numerical values, i.e. 3 for high, 2 for medium, and 1 for low, and the total score was calculated as the sum of the individual scores normalized on the scale 0-100. It is possible to assign weights to each criterion to emphasize some criteria, but this has not been done here. The models are scored per testbed and asset category.

The following subsections provide a summary of the final score obtained by the selected vulnerability and fragility models in each of the testbed, while a detailed breakdown of the ranking is provided in Appendix II of the present report.

Table 3-1: Fragility model scoring criteria (Gentile et al., 2022).

Criterion: Attribute	Score	Description
<i>Relevance:</i> Geographical area	High	Model defined for the required city (e.g., Kathmandu)
	Med	Model defined for the required country (e.g., Nepal)
	Low	Model defined for the required region (e.g., South Asia)
<i>Relevance:</i> Asset characteristics	High	Model matching structural detailing, geometry, and materials parameters appropriate for the asset class
	Med	Geometry and materials parameters appropriate for the asset class, structural details inappropriate or unavailable
	Low	Materials params. appropriate for the asset class, geometry and structural details inappropriate or unavailable
<i>Relevance:</i> IM	High	Adopted IM(s) clearly sufficient/efficient for the required application
	Med	-
	Low	Adopted IM(s) clearly not sufficient/efficient for the required application
<i>Statistical refinement:</i> Uncertainties	High	Appropriate assumptions. Goodness of fit demonstrated. Aleatory (and possibly epistemic) unc. considered
	Med	Appropriate assumptions. Inappropriate aleatory unc. considered
	Low	Inappropriate assumptions (e.g., unsound statistical distributions)
<i>Statistical refinement:</i> First principles	High	Physically sound models (e.g., fragility curves for different DSs not crossing; reasonable maximum)
	Med	Minor first-principle issues (e.g., fragility curves for different DSs cross outside required IM range)
	Low	Relationships not physically sound (e.g., fragility curves for different DSs cross)
<i>Model quality (emp.):</i> Impact observations	High	Damage scales/impact measures clearly defined. Negligible non-sampling errors
	Med	Damage scales/impact measures clearly defined. Non-sampling errors treated with unchecked assumptions
	Low	Damage scales/impact measures ambiguously defined (e.g., two assessors may assign different DSs for the same situation). Non-sampling errors not reduced
<i>Model quality (emp.):</i> IM observations	High	IM data directly measured or estimated accurately. IM data predicted-vs-true error investigated
	Med	-
	Low	IM data directly measured or estimated inaccurately. IM data predicted-vs-true error not investigated
<i>Model quality (emp.):</i> Constrained asset class	High	Empirical dataset filtered using asset class definition according to GED4ALL, or with similar attributes

Criterion: Attribute	Score	Description
	Med	Asset class defined as per “High”, but some aggregated attributes (e.g., different heights considered together)
	Low	Asset class defined with less than 4 attributes
<i>Model quality (emp.):</i> Data quantity	High	Continuous functions: more than 200 observations; min 10 IM bins; min 20 observations per IM bin Discrete functions: more than 200 observations; min 20 observations per IM bin
	Med	Continuous functions: between 20 and 200 observations; between 5 and 10 IM bins; min 10 observations per IM bin. Discrete functions: min 10 observations per IM bin
	Low	Continuous functions: less than 20 observations; less than 5 IM bins Discrete functions: less than 20 observations
<i>Model quality (synt.):</i> Fidelity to mechanics	High	State-of-the-art. All relevant damage mechanisms/impact sources considered. Sound parameter characterisation
	Med	Minor simplifications of relevant mechanics (e.g., less-relevant damage mechanisms/impact sources neglected). Sound parameter characterisation
	Low	Major simplifications of relevant mechanics (e.g., fundamental damage mechanisms/impact sources neglected). Unsound parameter characterisation (e.g., excessive strength assumed for a key structural member)
<i>Model quality (synt.):</i> Aggregation level	High	Calibrated using component-by-component analysis. Each component modelled explicitly
	Med	Calibrated using subcomponent analysis (e.g., aggregating components at the same building storey)
	Low	Asset-level model. Aggregating all sources of damage or impact

3.3 Selected fragility and vulnerability models for buildings in the testbeds

This section concerns the selection of physical vulnerability models for buildings, while sections 2.3.1 and 2.3.2 concern road network and electric power network components, respectively. The aforementioned scoring and ranking procedure is applied to the four testbeds in order to identify appropriate vulnerability and fragility models, depending on a given combination of building classes and hazard types. For homogenisation purposes, the European exposure model for ESRM20 (Crowley et al., 2021a) is used to extract distributions of building types at the location of each testbed, and the most common building types are considered. In some cases where detailed local exposure datasets are available (i.e., Oslo and Nice testbeds), these local exposure datasets are preferred over the European exposure model. The corresponding vulnerability and fragility models are detailed in Appendix I. Sections 3.3.1 - 3.3.4 present tables that include physical vulnerability models for each testbed and building class for which the application of the procedure by Gentile et al. (2022) led to the highest scores.

The ESRM20 exposure dataset is compatible with the GED4ALL multi-hazard taxonomy. This taxonomy has resulted from the expansion of an existing taxonomy focused on earthquake risk, which explains the focus on seismic-specific attributes such as lateral load resisting systems or ductility levels. The GED4ALL taxonomy is also able to consider information such as the number of storeys below ground, roof shape, and roof material, which is relevant to hazards such as flood and wind. However, in the case of this project’s testbeds, such attributes are not available. Also, it has been found that currently available fragility and vulnerability models for hazards other than earthquakes are usually based on somewhat generic attributes, mostly limited to the structural type or the height of the building. Therefore, the taxonomy strings in the ESRM20 exposure dataset

is currently sufficient to associate and to rank fragility and vulnerability models, pending the on-going creation of the multi-hazard exposure models by other tasks in the project.

3.3.1 Oslo (Norway)

For this testbed, the hazards considered for the physical vulnerability model selection are flood, landslide / debris flow, landslide / ground settlement. In the screening process (see Section 3.1), we chose models for these hazards for the most common building classes in the testbed.

The following building classes are found to be the most common in the Oslo testbed (the percentage of the class in the testbed's ESRM20 residential exposure model is in square brackets):

- W_LFM_DUL_LOW: wood frame, low ductility, low rise [83.5 %];
- CR_LFM_DUL_MID: RC frame, low ductility, mid-rise [4.3 %];
- MUR_LWAL_DNO_MID: unreinforced masonry, non-ductile, mid-rise [4.0 %];
- CR_LFM_DUL_LOW: RC frame, low ductility, low rise [2.9 %].

The scores for candidate vulnerability and fragility models are detailed in Table 3-2 and Table 3-3, respectively. The detailed breakdown of the scores for the physical vulnerability models is given in Annex II (Section 10).

Table 3-2: Scoring for the selection of vulnerability models for residential buildings in the Oslo testbed.

Model	Score (0-100)			
	W_LFM_DUL_LOW	CR_LFM_DUL_MID	MUR_LWAL_DNO_MID	CR_LFM_DUL_LOW
<i>Flood</i>				
Huizinga et al. (2017)	44	44	44	44
Apel et al. (2004)	26	26	26	26
Buechele et al. (2006)	37	37	37	37
Gersonius et al. (2008)	37	37	37	37
PARNASSUS v3 (D'Ayala et al., 2020)	-	-	70	-
<i>Landslide / Debris Flow</i>				
Papathoma-Köhle et al. (2012)	56	56	56	56
Papathoma-Köhle et al. (2015)	56	56	56	56
Calvo & Salvi (2009)	-	70	-	70
Fuchs et al. (2007)	-	-	56	-

Table 3-3: Scoring for the selection of fragility models for residential buildings in the Oslo testbed (the information in square brackets is to identify a model among others in the same publication).

Model	Score (0-100)			
	W LFM DUL LOW	CR LFM DUL MID	MUR LWAL DNO MID	CR LFM DUL LOW
<i>Earthquake</i>				
Crowley et al. (2021)	67	67	67	67
Manfredi et al. (2023)	-	63	-	63
Jeon et al. (2015)	-	63	-	63
Kappos (2013)	-	59	59	59
<i>Landslide / Ground Settlement</i>				
Negulescu & Foerster (2010)	-	70	-	70
Peduto et al. (2017)	44	44	44	44
Miano et al. (2022) [Number of storeys: 2; IM: Deflection ratio]	-	60	-	63
Miano et al. (2022) [Number of storeys: 5; IM: Deflection ratio]	-	63	-	60
Peduto et al. (2019) [Shallow foundations; IM: Rotation]	52	-	52	-

3.3.2 Nice (France)

For this testbed, the principal hazards considered for the the physical vulnerability model selection are flood, landslide / debris flow, landslide / ground settlement, and earthquakes. In the screening process (see Section 3.1), we chose models for these hazards for the most common building classes in the testbed.

The following building classes are found to be the most common in the Nice testbed (the percentage of the class in the testbed's exposure model is in square brackets):

- MUR_LWAL_CDN_LOW: unreinforced masonry, pre-code, low rise [25.9 %];
- MUR_LWAL_CDN_MID: unreinforced masonry, pre-code, mid-rise [21.1 %];
- CR_LWAL_DUL_MID: RC bearing wall, pre-code, mid-rise [11.8 %];
- MUR_LWAL_CDN_HIG: unreinforced masonry, pre-code, high-rise [9.7 %];
- MCF_LWAL_MID: confined masonry, mid-rise [8.4 %].

The scores for candidate vulnerability and fragility models are detailed in Table 3-4 and Table 3-5, respectively.

Table 3-4: Scoring for the selection of vulnerability models for residential buildings in the Nice testbed.

Model	Score (0-100)				
	MUR_LWAL_C DN_LOW	MUR_LWAL_C DN_MID	CR_LWAL_DUL _MID	MUR_LWAL_C DN_HIG	MCF_LWAL_MI D
<i>Flood</i>					
Huizinga et al. (2017)	44	44	44	44	44
Apel et al. (2004)	26	26	26	26	26
Buechele et al. (2006)	37	37	37	37	37
Gersonius et al. (2008)	37	37	37	37	37
PARNASSUS v3 (D'Ayala et al., 2020)*	78	78	-	78	78
<i>Landslide / Debris Flow</i>					
Papathoma-Köhle et al. (2012)	56	56	56	56	56
Papathoma-Köhle et al. (2015)	56	56	56	56	56
Cavo & Salvi (2009)	-	-	60	-	-
Fuchs et al. (2007)	56	56	-	56	56

* Model specifically adapted to the Nice testbed (Section 4)

Table 3-5: Scoring for the selection of fragility models for residential buildings in the Nice testbed (the information in square brackets is to identify a model among others in the same publication).

Model	Score (0-100)				
	MUR_LWAL_CDN _LOW	MUR_LWAL_CDN _MID	CR_LWAL_DUL _MID	MUR_LWAL_CDN _HIG	MCF_LWAL_MID
<i>Earthquake</i>					
Crowley et al. (2021)	67	67	67	67	67
Manfredi et al. (2023)	-	-	63	-	-
Jeon et al. (2015)	-	-	63	-	-
Kappos (2013)	59	59	59	59	59
<i>Landslide / Ground Settlement</i>					
Negulescu & Foerster (2010)	-	-	70	-	-
Peduto et al. (2017)	44	44	44	44	44
Miano et al. (2022) [Number of storeys: 2; IM: Deflection ratio]	-	-	60	-	-
Miano et al. (2022) [Number of storeys: 5; IM: Deflection ratio]	-	-	63	-	-
Peduto et al. (2019) [Shallow foundations; IM: Rotation]	52	52	-	52	52

3.3.3 Essex County (UK)

For this testbed, the principal hazards considered for the physical vulnerability model selection are flood, and wind. Additionally, the model selection is also carried out for the following hazards: landslide / debris flow, landslide / ground settlement, and earthquakes. In the screening process (see Section 3.1), we chose models for these hazards for the most common building classes in the testbed.

The following building classes are found to be the most common in the Essex testbed (the percentage of the class in the testbed's ESRM20 residential exposure model is in square brackets):

- MUR_CL_LWAL_CDN_LOW: unreinforced masonry (clay bricks), pre-code, mid-rise [63.9 %];
- CR_LFINF_CDN_MID: RC infilled frame, pre-code, mid-rise [31.5 %];
- W_LPB_CDL_LOW: wood post and beam, low code, low rise[4.6 %].

Moreover, based on additional information from local end-users, the following type of building is found in Castle Point district, Canvey Island (Town):

- CR_LFM_CDN_LOW: RC frame, pre-code, low-rise.

The scores for candidate vulnerability and fragility models are detailed in Table 3-6 and Table 3-7, respectively.

Table 3-6: Scoring for the selection of vulnerability models for residential buildings in the Essex testbed.

Model	Score (0-100)			
	MUR_CL_LWAL_CDN_LOW	CR_LFINF_CDN_MID	W_LPB_CDL_LOW	CR_LFM_CDN_LOW
<i>Flood</i>				
Huizinga et al. (2017)	44	44	44	44
Apel et al. (2004)	26	26	26	26
Buechele et al. (2006)	37	37	37	37
Gersonius et al. (2008)	37	37	37	37
PARNASSUS v3 (D'Ayala et al., 2020)**	74	-	-	-
<i>Landslide / Debris Flow</i>				
Papathoma-Köhle et al. (2012)	56	56	56	56
Papathoma-Köhle et al. (2015)	56	56	56	56
Cavo & Salvi (2009)	-	70	-	70
Fuchs et al. (2007)	56	-	-	-

** Model specifically adapted to the Essex testbed (Section 4)

Table 3-7: Scoring for the selection of fragility models for residential buildings in the Essex testbed.

Model	Score (0-100)			
	MUR CL LWAL CDN LOW	CR LFINF CDN MID	W LPB CDL LOW	CR LFM CDN LOW
<i>Earthquake</i>				
Crowley et al. (2021)	67	67	67	67
Manfredi et al. (2023)	-	63	-	63
Jeon et al. (2015)	-	63	-	63
Kappos (2013)	59	59	59	59
<i>Landslide / Ground Settlement</i>				
Negulescu & Foerster (2010)	-	70	-	70
Peduto et al. (2017)	44	44	44	44
Miano et al. (2022) [Number of storeys: 2; IM: Deflection ratio]	-	60	-	63
Miano et al. (2022) [Number of storeys: 5; IM: Deflection ratio]	-	63	-	60
Peduto et al. (2019) [Shallow foundations; IM: Rotation]	52	-	-	-

Table 3-8 Scoring for the selection of physical vulnerability and fragility models for buildings vulnerable to wind in the Essex testbed.

Model	Score (0-100)	Score (0-100)
	W LPB CDL LOW	S LFM CDL MID
<i>Wind</i>		
Abdelhady et al. (2022) [fragility]	67	-
Elingwood et al. (2004) [fragility]	63	-
Stewart et al. (2016) [vulnerability curve]	-	70

3.3.4 Mulathing (Iceland)

For this testbed, the principal hazards considered for the physical vulnerability model selection are flood, landslide / debris flow, landslide / ground settlement. Additionally, the model selection is also carried out as an exercise for earthquake hazard. In the screening process (see Section 3.1), we chose models for these hazards for the most common building classes in the testbed.

The following building classes are found to be the most common in the Mulathing testbed (the percentage of the class in the testbed's ESRM20 exposure model is in square brackets):

- CR_LWAL_CDL_LOW: RC bearing wall, low code, low rise [32.7 %];
- W_LWAL_LOW: wood bearing wall, low rise [28.2 %];
- CR_LWAL_CDN_LOW: RC bearing wall, pre-code, low rise [18.2 %];
- CR_LDUAL_CDH_LOW: RC dual frame-wall, high code, low rise [11.7 %].

The scores for candidate vulnerability and fragility models are detailed in Table 3-9 and Table 3-10, respectively.

Table 3-9: Scoring for the selection of vulnerability models for residential buildings in the Mulathing testbed.

Model	Score (0-100)			
	CR LWAL CDL LOW	W LWAL LOW	CR LWAL CDN LOW	CR LDUAL CDH LOW
<i>Flood</i>				
Huizinga et al. (2017)	44	44	44	44
Apel et al. (2004)	26	26	26	26
Buechele et al. (2006)	37	37	37	37
Gersonius et al. (2008)	37	37	37	37
PARNASSUS v3 (D'Ayala et al., 2020)	-	-	-	-
<i>Landslide / Debris Flow</i>				
Papathoma-Köhle et al. (2012)	56	56	56	56
Papathoma-Köhle et al. (2015)	56	56	56	56
Cavo & Salvi (2009)	70	-	70	70
Fuchs et al. (2007)	-	-	-	-

Table 3-10: Scoring for the selection of fragility models for residential buildings in the Mulathing testbed.

Model	Score (0-100)			
	CR LWAL CDL LOW	W LWAL LOW	CR LWAL CDN LOW	CR LDUAL CDH LOW
<i>Earthquake</i>				
Crowley et al. (2021)	67	67	67	67
Manfredi et al. (2023)	63	-	63	63
Jeon et al. (2015)	63	-	63	63
Kappos (2013)	59	-	59	59
<i>Landslide / Ground Settlement</i>				
Negulescu & Foerster (2010)	70	-	70	70
Peduto et al. (2017)	44	44	44	44
Miano et al. (2022) [Number of storeys: 2; IM: Deflection ratio]	63	-	63	63
Miano et al. (2022) [Number of storeys: 5; IM: Deflection ratio]	60	-	60	60
Peduto et al. (2019) [Shallow foundations; IM: Rotation]	-	-	-	-

4 DEVELOPMENT OF SPECIFIC FLOOD VULNERABILITY MODEL FOR NICE

This section presents a specific study to characterise the flood vulnerability of residential masonry buildings in the municipality of Nice, as a way of illustrating how this approach could be implemented in a given location, depending on the availability of time and resources. This can lead to more relevant vulnerability models compared to generic flood vulnerability models such as the ones identified in this report for the four test beds. This approach determines the relative vulnerability of individual buildings based on a number of parameters concerning the building and the surroundings. In this specific case, the parameters are characterized as discrete or continuous distributions based on a virtual data collection from a sample of buildings using open-source map resources such as Google Street View Maps® and Open Street Maps®, and the vulnerability is estimated for a simulated building population representative of the region's masonry building stock. It is acknowledged that this mode of data collection has limitations in characterising the parameters accurately, as compared to a field data collection, however, the following sections illustrate the process and its applicability on a sample set of masonry buildings.

4.1 Modelling framework

In the present study, the PARNASSUS v.3 procedure, based on a vulnerability index approach, is applied to determine the relative vulnerability of individual buildings. The building and its immediate curtilage are here defined as the system exposed to the flood hazard. Therefore, the vulnerability index is obtained by identifying a number of parameters which are considered all equally critical to the response of the system. More details of this approach, its development and previous versions are discussed in section 2.2.2 and the cited references (Stephenson and D'Ayala, 2014; D'Ayala et al., 2016).

The flooding vulnerability of an individual building is estimated as the summation of vulnerability rating for thirteen parameters according to the PARNASSUS v.3 approach (D'Ayala et al., 2020). A full list of these parameters and their ratings are listed in Table 4-1. Number of storeys, footprint and perimeter indicate the volume of the building, its contents and the bearing pressure on the ground. This has implications for soil failure and subsidence following floods, which could write off the building, hence outweighing the lower proportion of exposure of the total volume of the building, usually assumed for multi-storey buildings, particularly relevant for the long-term flooding scenarios, and in areas nearby the river course with soft clays. Other descriptors such as height of the plinth, doors and windows, and the possibility of raised ground floors allow the estimation of vulnerability to water breach. Finally, building fabrics, materials and building condition provide a measure of the permeability of the building construction and its likelihood to deteriorate when exposed to water. External parameters such as a classification of drainage systems in the immediate setting of the buildings, sloping of the ground and permeability of the surface surrounding the building and of any local flood prevention measures are also included as vulnerability indicators. This information can be directly surveyed on-site where possible or gathered from virtual surveys, as performed in this study, in order to determine the extent of local vulnerability.

A range of two to five attributes is defined for each parameter as shown in Table 4-1, based on a logical derivation of the maximum possible number of states for each parameter. These are assigned a vulnerability rating (VR) on a linear scale from 10 to 100, depending on their minimal or maximum contribution towards flood vulnerability, and recognising that any system would be vulnerable, even though minimally. For instance, the parameter “drainage system” has three possible outcomes: “good”, “poor” and “no”, so that the numerical rating among these three outcomes can be assigned as 10, 55 and 100, to represent the increase in vulnerability (D'Ayala et al., 2020).

Flood susceptible areas within the Nice municipality for a 100-year return period flood are identified from the maps provided by (IPSEAU, 1999) as shown in Figure 4 1, neighbouring the Paillon River. These maps constitute the basis for the flood risk regulation plans (PPR – Plan de Prévention des Risques) currently active

in the Nice area¹, pending the development of more recent maps. Due to their date of publication, these flood estimates do not account for climate change; hence, they might need updating for future applications. Considering the lack of specific information on buildings, a virtual survey is carried out on a sample of buildings in the localities highlighted in Figure 4-1, using Google Street View® maps to identify the attributes and their distribution. This of course has inherent limitation as some of the attributes are easier to identify from the Street View than others, while for some such as presence of basement, for instance, there might be some uncertainty. Moreover, the buildings are mostly visible only from the elevation on the street, while layout of openings and other details on other elevation might affect the vulnerability of the building.

The virtual survey is carried out for 50 masonry buildings in the regions identified. It is seen in Chapter 3 that unreinforced masonry buildings, of various rise, constitute 55% of Nice's building stock and confined masonry accounts for a further 8%. Therefore, the results on vulnerability obtained with this approach can be quite representative, also considering that concrete structures have a lower vulnerability rating. The PARNASSUS v.3 procedure is conceptually applicable to concrete buildings as well, as per the material parameter's attributes in Table 4-1.

The distribution characteristics of the 13 flood vulnerability parameters for the Nice's sample are identified as shown in Table 4-1 (6th column). All the continuous variables are assumed to be normally distributed with mean and standard deviation as indicated in the table. Similarly, the likelihood of the occurrence of the attributes of the discrete variables are also identified from the virtual survey. These distributions are used to simulate parameter attributes for a population of 500 buildings. A set of parameter attributes corresponding to each simulated building translates to a set of vulnerability ratings (VR) as indicated in Table 4-1 (4th column), summation of which gives the vulnerability index (VI) of the building (Eq. 4-1):

$$VI_i = \sum_j VR_{ij} \quad (4-1)$$

where i is the building ID, ranging from 1 to 500 in this case, and j is the parameter under consideration, ranging from 1 to 13 in this analysis.

VI values computed for the simulated population of 500 buildings are found to range from 540 to 1030. The VIs is normalised with their mean value (Eq. 4-2) to obtain a relative indicator of the vulnerability as seen in Figure 4-2a, alongside a lognormal fit to the normalised VI data. Histogram and cumulative frequency of the normalised vulnerability index of the sample are obtained as shown in Figure 4-2.

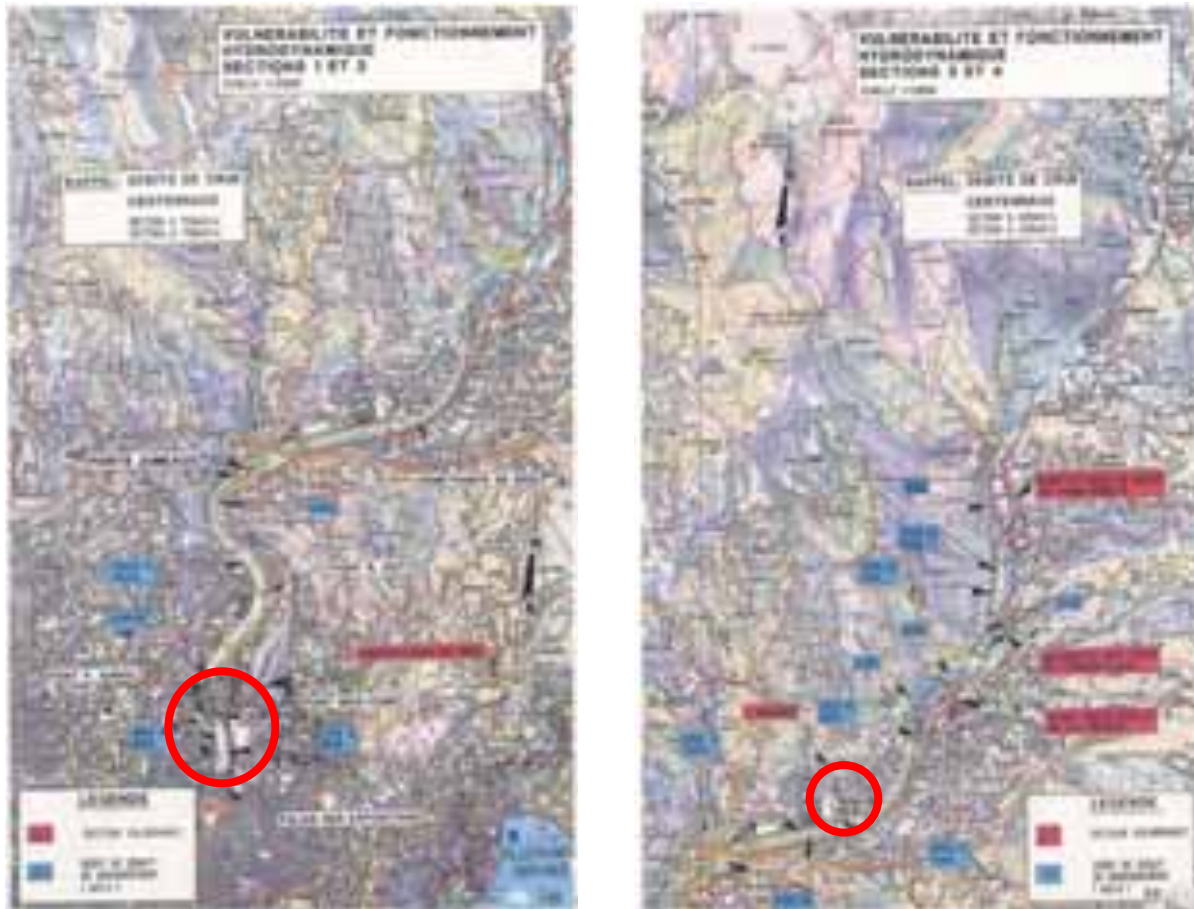
$$nVI_i = \frac{VI_i}{(VI_{i_{max}} + VI_{i_{min}})/2} \quad (4-2)$$

In Figure 4-1, the cumulative and lognormal distribution obtained for the simulated sample for Nice are compared with two curves obtained with the same method by on site survey for samples of buildings in Tewkesbury and Bristol, two cities in the UK, characterised by a high proportion of historic masonry buildings. The Nice sample accordingly shows a lower mean vulnerability value and less dispersion consistent with a more homogeneous sample of 20th Century masonry construction.

¹ <https://www.alpes-maritimes.gouv.fr/Actions-de-l-Etat/Environnement-risques-naturels-et-technologiques/Les-risques-naturels-et-technologiques/Les-plans-de-prevention-des-risques-PPR-approuves-et-l-Information-acquereurs-locataires-IAL/NICE/2-PPR-APPROUVES-cliquez-ici>

Table 4-1: Parameters for the PARNASSUS v.3 approach.

No	Vulnerability Parameter	Attributes	Vulnerability Rating	Distribution type	Probabilities/distribution parameters of the vulnerability parameters
1	No of storeys	1	10	Discrete	0.09
		2	40		0.57
		3	70		0.27
		>4	100		0.07
2	Footprint area (Sq m)	< 50	10	Continuous	Mean= 117.37, SD=57.50, Min=35.75, Max=300.00
		[50, 100)	32.5		
		[100, 150)	55		
		[150, 200)	77.5		
3	Roof height (m)	<3	10	Discrete	Defined as a function of number of storeys
		(3,6)	40		
		(6,10)	70		
		>10	100		
4	Ground floor raised?	No	10	Discrete	0.84
		Yes	100		0.16
5	Drainage	No	100	Discrete	0.27
		Poor	55		0.73
		Good	10		0.00
6	Flood prevention	No	100	Discrete	0.91
		Yes	10		0.09
7	Building condition	Poor	100	Discrete	0.18
		Good	55		0.70
		Excellent	10		0.11
8	External perimeter (m)	<30	10	Continuous	Mean= 43.38, SD=11.28, Min=24.00, Max=72.37
		[30,45)	55		
		>45	100		
9a	Surface condition Vegetation	No	100	Discrete	0.70
		Poor	55		0.27
		Good	10		0.02
b	inclination	Down	100	Discrete	0.20
		No	55		0.66
		Up	10		0.14
c	Permeability	No	100	Discrete	0.93
		Poor	55		0.05
		Good	10		0.02
10a	Building fabric frame material	Timber	100	Discrete	0.00
		Masonry	55		1.00
		Concrete	10		0.00
b	wall material	Timber	100	Discrete	0.00
		Masonry	55		1.00
		Concrete	10		0.00
11	Height of door (from plinth in m)	0	100	Continuous	Mean= 0.12, SD=0.16, Min=0.00, Max=1.0
		≤0.1	70		
		(0.1,0.5]	40		
		>0.5	10		
12	Height of window (from plinth in m)	0	100	Continuous	Mean= 0.42, SD=0.32, Min=0.00, Max=1.20
		≤0.5	70		
		(0.5,1]	40		
		>1	10		
13	Height of plinth (from road in m)	≤ -1	100	Continuous	Mean= 0.19, SD=0.38, Min= -0.50, Max=1
		(-1,0]	70		
		(0,1]	40		
		>1	10		



a) Flood susceptible areas in Nice municipality (IPSEAU, 1999)

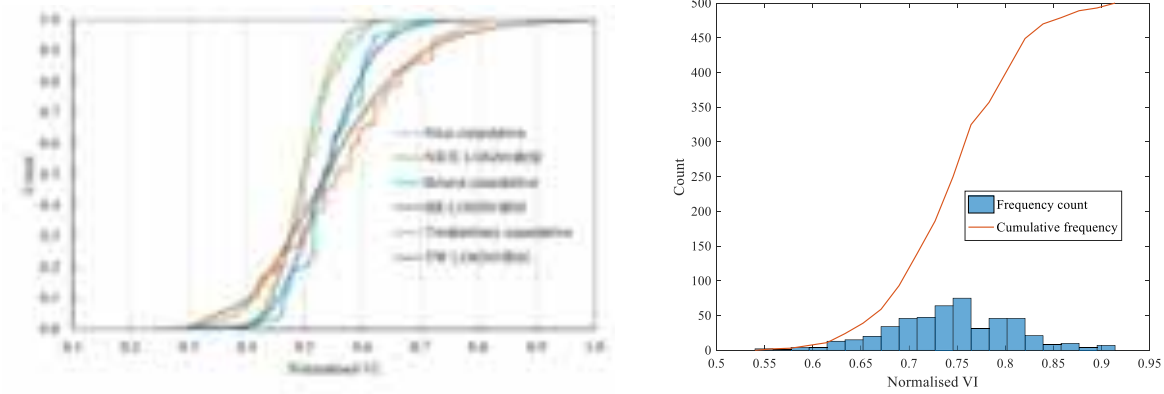


b) Sample of masonry buildings, 2 storeys with door threshold at the level of the street or below



c) 3 and 4 storeys building with commercial units and basement (Google Street View, 2024)

Figure 4-1: Data collection of buildings in the flood susceptible regions in the neighbourhood of River Paillon.



a) Total VI (normalised) and lognormal fit to the cumulative function for Nice compared to curves obtained for samples in Bristol, UK, and Tweekesbury, UK.

b) Distribution of normalised VI and cumulative frequency count

Figure 4-2: Estimated vulnerability indices distribution for the simulated building sample.

4.2 Calculation of economic loss

The VI of individual buildings are used to estimate the economic losses from a flood event, considering the physical damage to the buildings and the cost of the contents. Economic losses from physical damage is computed as:

$$E(i) = C(i) \cdot D(h_i) \cdot FVR(VI_i) \cdot A_{Ti} \quad (4-3)$$

where i indicates the building identifier and C , D , FVR and A_T are the construction cost per unit area of building, the damage factor, the vulnerability factor and the surface area of the building directly affected by the flood, respectively. A brief description of these factors are given below, while the detailed formulation is available in D'Ayala et al. (2020).

Building cost is the total of the replacement cost of the building and of the content:

$$C(i) = C_B(i) + C_c(i) \quad (4-4)$$

where $C_B(i)$ is a function of the basic construction cost, a value factor to indicate the perceived value of the building which depends on the building condition and a value factor to indicate the historic and cultural value of the building. The first value factor is taken as 0.4, 0.7 and 1 for poor, good and excellent building conditions, while the latter is considered equal to one for ordinary residential buildings assessed in this study.

The content cost $C_c(i)$ is taken as a factor of the basic construction cost and the building condition ranging from 15% to 60% from poor to excellent condition.

The damage factor is estimated from the depth-damage function (D'Ayala et al. 2020) presented in -Figure 4-3a, corresponding to the water depth at the building location. The mean curve in this model compares to the Huizinga et al. (2017) model, selected as an applicable flood damage function in Chapter 3, as shown in Figure 4-3b. For a given flood scenario, in the absence of further information, the inundation depth in the locality under study is assumed to be a constant and water depth at the building location is calculated as the difference between inundation depth and the height of plinth from road surface (parameter 13) which could be positive or negative.

The vulnerability factor FVR is the VI of each building normalised with respect to the median VI of the sample. The area affected is taken as the plan area of the building, assuming the inundation depth is not more than 3m, i.e. only affecting the first storey content and the basement if present.

Considering a uniform inundation depth of 0.5m and 1.0m for the 500 simulated buildings, the cumulative economic losses computed are presented in Figure 4-4. At the specified inundation depth of a scenario, the actual water depth at the building location varies depending on the relative height between the base of the building and the ground or the road surface. Accordingly, the economic losses from building damage and content damage corresponding to actual water depth at each building location are computed, and summed up to get the cumulative economic loss for both the inundation scenarios of 0.5m and 1.0m. The flood hazard mapping as per IPSEAU (1999) indicates zones of flood inundation up to 0.5m and 1.0 m corresponding to a 100 year return period event. The damage function considered in the study (D'Ayala et al. (2020)) is comparable to the selected damage function (Huizinga et al. (2017)) at these flood depths as seen in Figure 4-3b. It can be seen that water depth at the location of some buildings which have basement floors can exceed the inundation depth. The replacement cost of masonry buildings per square meter is taken as 1543.75 Euros, according to the ESRM20 (2021) exposure model. It can be observed that as the water depth doubles, the total replacement cost also approximately doubles.

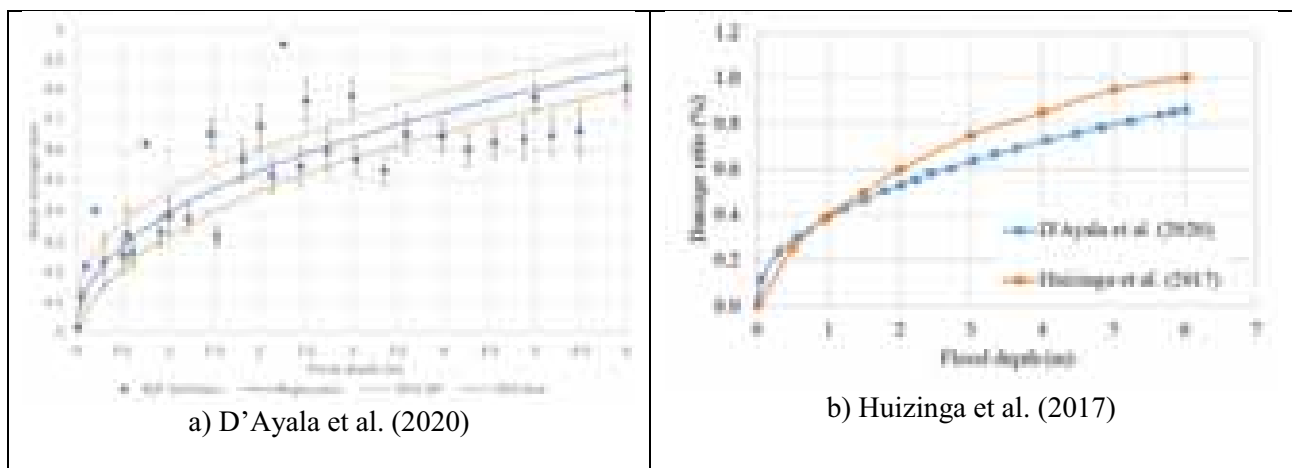


Figure 4-3: Depth-damage functions.

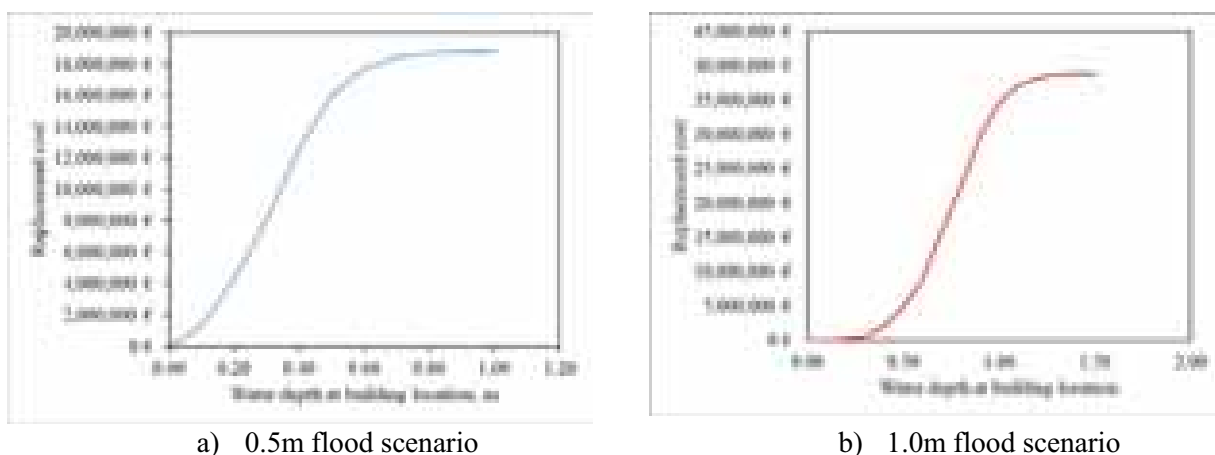


Figure 4-4: Cumulative replacement cost of masonry buildings for two flood scenarios with pre-defined inundation depths. Note that actual water depth at the building location depends on the plinth level of the building with respect to the road.

The accuracy of the results could be further improved by:

- Field data collection and characterisation of flood vulnerability parameters of buildings, instead of a simulated set of buildings
- Incorporating actual flood hazard models of the region with the digital elevation of the terrain, to compute the actual water depth at building locations, instead of uniform inundation depth as assumed in this study.

4.3 Conclusion

This section illustrates the PARNASSUS v.3 approach for generating site-specific flood vulnerability functions based on local building information, for the municipality of Nice. Considering the feasibility of virtual data collection and simulation-based vulnerability estimation, it is adaptable and scalable to other test beds in the future. The results of the analysis shall however be treated under the limitations and improvement options as mentioned in this section.

5 DEVELOPMENT OF SPECIFIC MULTI-HAZARD FRAGILITY MODELS

The present section introduces an approach to derive so-called state-dependent fragility models, which are able to quantify the probability to reach a given damage state for a given hazard level, for a given initial state of the exposed engineering asset (i.e., a building potentially damaged by a previous loading, whether it is due to the same hazard type or a different one). Therefore, this framework enables the treatment of various multi-hazard interactions, such as the case of triggered hazards or successive hazards that are potentially unrelated. It may also be applied to sequences of same hazards events, such as mainshock-aftershock earthquake sequences, in order to account for the effects of damage accumulation. For demonstration purposes, the proposed approach is applied to the fragility assessment of RC buildings representative of the Nice testbed, exposed to independent flood and earthquake events.

5.1 Modelling framework

5.1.1 General principle

State-dependent fragility curves are numerically derived by subjecting structural models of a RC building to a chain of successive loadings. In the simulations, the models are subjected to loading time-histories that include four steps, as schematized in Figure 5-1.

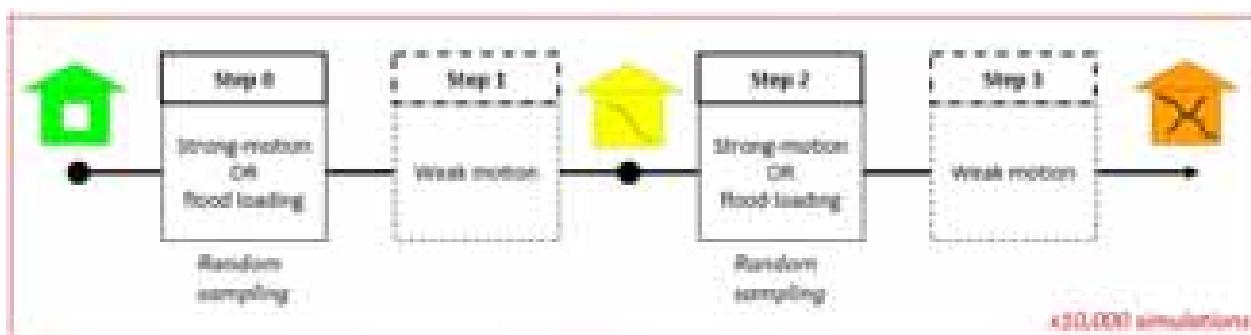


Figure 5-1: Adopted scheme for the derivation of state-dependent fragility curves.

During the first and third steps (or Steps 0 and 2, respectively), the potentially damaging hazard loads are applied to the building models. The type of hazard loads may be a strong ground motion or flood loads, and the type of loads is randomly chosen for Steps 0 and 2 in each simulation. During the second and fourth step (Steps 1 and 3), a weak ground motion of a very low intensity ($PGA < 10^{-3} g$) is applied at the base of the building model. Steps 1 and 3 allow the dissipation of any strong vibration of the building model in Steps 0 and 2, while the weak ground motion may assist the identification of the dynamic characteristics of the building model as well as its damage state.

5.1.2 Structural modelling

The approach is applied to existing RC buildings in the city center of Nice (France), which is exposed to an average seismicity level (i.e. the highest level in mainland France) according to the French seismic zonation. This area is also at risk of recurring floods near the Var and Paillon rivers. The distribution of the building stock has been obtained from the exposure model (Crowley et al., 2021a) of the European Seismic Risk Model 2020 (ESRM20, Crowley et al., 2021b). Using simplified classes of the GEM taxonomy (Brzev et al., 2013), the distribution of RC buildings in Nice is detailed in Table 5-1.

Table 5-1: Simplified distribution of RC building types in Nice municipality, according to the ESRM20 exposure model (Crowley et al., 2021a).

Macro Taxonomy	Class	Percentage of total number of buildings	Percentage of number of RC buildings
Concrete frame with infill panels, low rise, low/moderate code	CR_LFINF_CDM_LOW	9.8	30.3
Concrete frame with infill panels, mid rise, pre code	CR_LFINF_CDL_MID	6.0	18.6
Concrete frame, mid rise, low/moderate code	CR_LFINF_DUM_MID	0.1	0.2
Concrete frame, high rise, pre code	CR_LFM_CDL_HIGH	1.5	4.8
Concrete wall, low rise, pre code	CR_LWAL_DUL_LOW	1.0	3.0
Concrete wall, mid rise, low/moderate code	CR_LWAL_DUM_MID	2.4	7.5
Concrete wall, mid rise, pre code	CR_LWAL_DUL_MID	11.6	35.6

The response of the building models to the earthquake and flood loads is modeled using OpenSeesPy (Zhu et al., 2018). All building models are two-dimensional. Although simplified 2D archetype models are unable to account for effects related to irregularities such as torsion, it has been shown that they can be used to make an effective estimation of losses of real 3D structures (Kappos et al., 2006). Three types of analysis are used: fiber, modal and non-linear time-history analyses. The fiber analyses are employed to calibrate bilinear moment-curvature hysteretic models, which are used in the context of distributed plasticity modelling. Pinching in the moment-curvature loops is used only for the structural walls with a factor of 0.3 assuming a strong pinching effect. In the fiber analyses, reinforcement steel is modeled using the Steel02 material in OpenSeesPy. The strength degradation of confined concrete is modeled using the material Concrete02 in OpenSeesPy. The infill walls are modeled with double struts as in Karapetrou et al. (2016) with a compressive strength of 3.2 MPa and an elastic modulus of 3.2 GPa. The inelastic behavior of the struts is modeled using the hysteretic material in OpenSees. Modal analyses are used to compute the fundamental period of the models in their undamaged states. In the total mass of each model, the mass corresponding to structural elements, infill walls, live and dead loads of the slab floors are included. Since a hysteretic law with stiffness degradation is used for bending behavior in the dynamic analyses, which models stiffness degradation after yield, the stiffness of the elements is taken into account equal to a fraction of the un-cracked stiffness, which fits the moment-curvature results of the fiber analysis. The simulations consider P-Delta effects caused by second-order moments, fully fixed base nodes, and floors as rigid diaphragms.

Two building models from the building classes CR_LFINF_CDM_11_HEX_2 and CR_LWAL_CDN_HEX_4 are considered representative of the building classes CR_LFINF_CDM_11_LOW and CR_LWAL_CDN_MID, respectively, and are taken as examples for the remainder of the study, due to their significant part in the distribution of existing RC buildings (see Table 5-1).

The design of the CR_LFINF_CDM_11_HEX_2 building model (Figure 5-2) with respect to the seismic loads is done based on the taxonomy string, i.e., using modern limit state design, for lateral resistance for seismic loads with a coefficient of 0.11, and without capacity design. The corresponding capacity curve is shown in Figure 5-3 Left, along with two capacity curves extracted from the ESRM20 vulnerability model (Romao et al., 2021), for similar building classes (i.e., CR_LINF_CDL_10_H2 and CR_LINF_CDM_10_H2). The modelled capacity curve presents lower initial stiffness, however it has a higher yielding point. Approximately 20% of the yield spectral acceleration is due to the presence of the infill walls. The ultimate displacement is selected so that the available ductility is equal to 2.25, which is proposed by HAZUS (FEMA, 2020) for low-rise reinforced concrete buildings with infills.

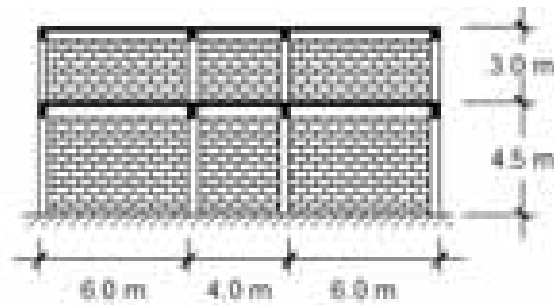


Figure 5-2: Geometry of the CR_LFINF_CDM_11_HEX_2 type building model.

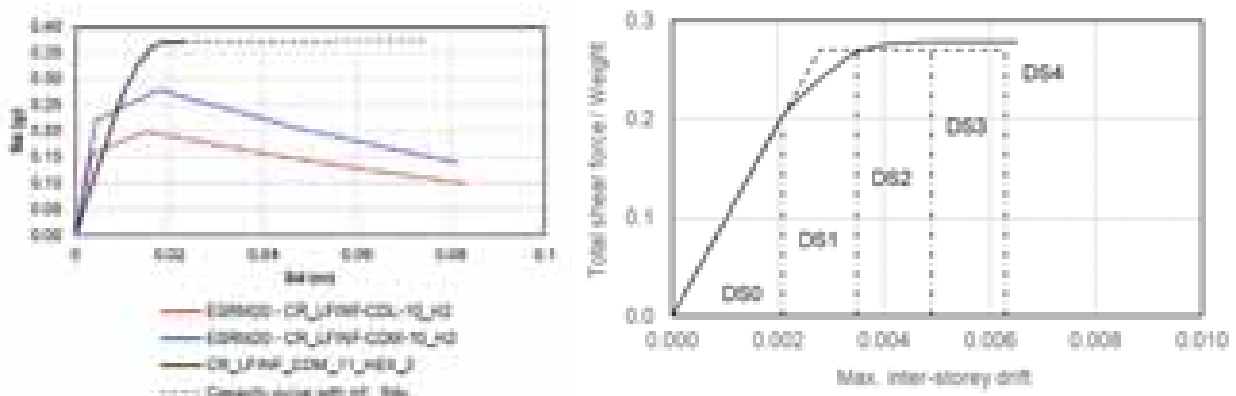


Figure 5-3: Left: Capacity curve for the CR_LFINF_CDM_11_HEX_2 class building model (S_{du} is the ultimate spectral displacement); Right: Definition of damage states DS0-DS4.

Regarding the CR_LWAL_DUL_HEX_4 building model (Figure 5-4), the ultimate displacement is selected so that the available ductility is equal to 3.0, which is higher than the value (2.50) proposed by HAZUS (FEMA, 2020) for mid-rise reinforced concrete buildings with shear walls. Nevertheless, the ultimate displacement is lower than the ultimate displacements of the capacity curves in the ESRM20 for the building types CR_LWAL_DUL_H4 and CR_LDUAL_DUL_H4 (Figure 5-5, left), which are the closest building types in ESRM20 to the studied CR_LWAL_DUL_HEX_4 building type.

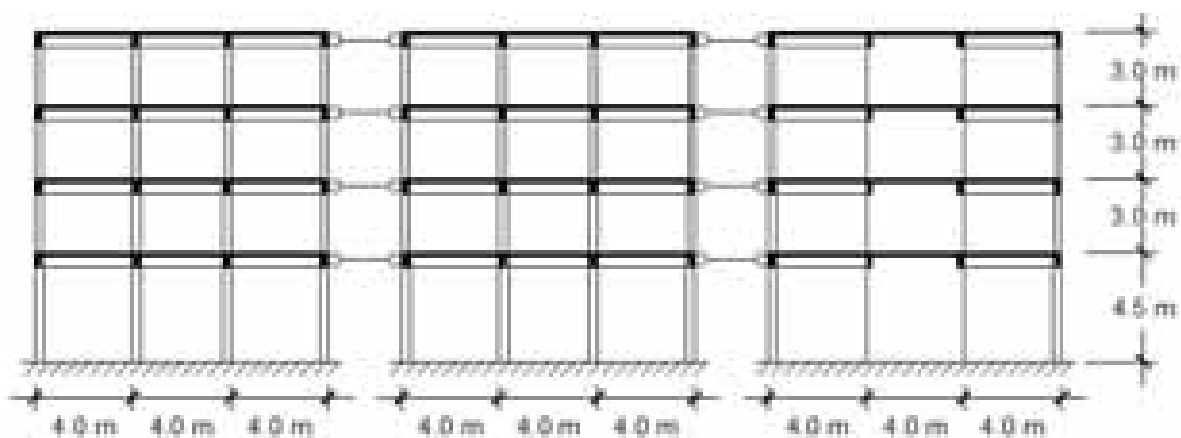


Figure 5-4: Geometry of the CR_LFINF_CDL_HEX_4 type building model.

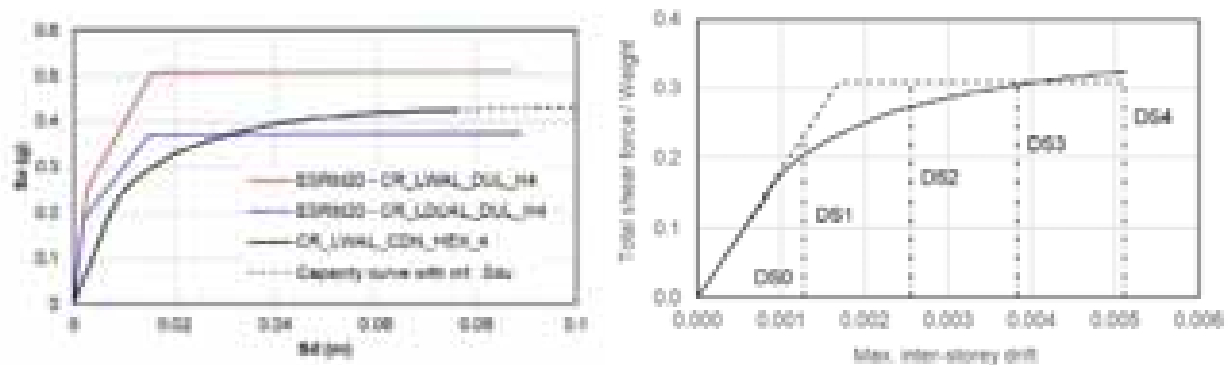


Figure 5-5: Left: Capacity curve for the CR_LWAL_CDN_HEX_4 class building model; Right: Definition of damage states.

We define the thresholds of the damage states by adapting the procedure and the damage scale in Martins and Silva (2021). The damage scale includes the undamaged state (DS0) in addition to the following damage states: slight (DS1), moderate (DS2), extensive (DS3), and complete (DS4) combined structural and non-structural damage. Their procedure uses the pushover capacity curve in terms of spectral displacement and spectral acceleration to define the damage state thresholds in terms of spectral displacement. An ultimate ductility ratio $S_{du} / S_{dy} = 2.25$ is chosen as a reasonable assumption, where S_{dy} and S_{du} are the yield and ultimate spectral displacement. The ductility ratio indicates the ability of the structure to absorb the energy of the seismic excitation in the form of inelastic deformations, i.e., structural damage. Here, we are using the maximum inter-storey drift (θ) as the Engineering Demand Parameter (EDP); therefore, we use the pushover capacity curve in terms of θ and total shear force-to-weight ratio (e.g., see Figure 5-3 Right). The parametric definition of the damage state thresholds used in this study is given in Table 5-2.

Table 5-2: Parametric definition of the damage state thresholds used in this study as a function of S_{dy} and S_{du} (i.e, the yield and ultimate spectral displacement) the according to Martins & Silva (2021).

Damage state description	Threshold
DS0: no structural damage (implied)	-
DS1: slight structural damage	$0.75 \cdot S_{dy}$
DS2: moderate structural damage	$0.50 \cdot S_{dy} + 0.33 \cdot S_{du}$
DS3: extensive structural damage	$0.25 \cdot S_{dy} + 0.67 \cdot S_{du}$
DS4: complete structural damage	S_{du}

Finally, four variants of the CR_LFINF_CDM_11_HEX_2 model are considered, depending on various assumptions of the hysteretic behavior during cyclic loadings. The objective is to investigate the effects of these modelling assumptions on the evolution of the state-dependent fragility curves. The description of the four models in detailed in Table 5-3.

Table 5-3: Definition of the four models with respect to their hysteretic material parameters, as defined in OpenSees. The parameter “pinchY” is the pinching factor for stress during reloading (value of 1.0 implies no pinching). The parameter “damage1” is the damage factor due to ductility (value of 0.0 implies no strength degradation). The parameter “damage2” is the damage factor due to energy (value of 0.0 implies no strength degradation).

Model	<i>pinchY</i>	<i>damage1</i>	<i>damage2</i>	Description
1	1.0	0.0	0.0	no pinching; no strength degradation
2	0.5	0.0	0.0	pinching; no strength degradation
3	0.5	0.1	0.0	pinching; strength degradation related to damage due to ductility only
4	0.5	0.1	0.1	pinching; strength degradation related to damage due to both ductility and in-cycle energy dissipation

5.1.3 Applied external loadings

The strong ground motion is applied as a time-history of displacements of the nodes at the base of the building model. The time-history of a ground motion is randomly selected among the horizontal components of 294 three-dimensional records in a dataset selected from the Engineering Strong Motion Database (Luzi et al., 2016; Lanzano et al., 2022). The criteria used to create this dataset are the following: a minimum earthquake magnitude of 6.0, a maximum epicentral distance of 30 km, and a PGA of 1 cm/s² ($\approx 10^{-3}$ g).

The flood loads are horizontal loads applied to the exterior columns on one side of the building models, and include the hydrostatic pressure, and the hydrodynamic pressure. Based on Baiguera et al. (2022), the hydrodynamic force (Eq. 5-1) is assumed to be uniformly distributed over the surface of the building façade below the inundation depth.

$$F = \frac{1}{2} \rho_w \cdot k_s \cdot C_d \cdot C_{cx} \cdot B \cdot (h \cdot u^2) \quad (5-1)$$

Where ρ_w is the density of water, $k_s = 1.1$ is the fluid density factor accounting for suspended solids and small objects, C_d is the drag coefficient (Table 5-4), $C_{cx} = 0.7$ the proportion closure coefficient, B is the building width in the direction perpendicular to the flow, h the inundation depth, and u the flow velocity.

Table 5-4 Best-fit approximation for the drag coefficient (C_d) in ASCE 7-16 (from Baiguera et al., 2022).

Building width to water height ratio (B / h)	Best-fit approximation
0-12	$C_d = 1.25$
12-16	$C_d = 0.01525 \cdot B/H + 1.1$
16-36	$C_d = 0.01 \cdot B/H + 1.14$
36-60	$C_d = 0.010417 \cdot B/H + 1.125$
60-100	$C_d = 0.00125 \cdot B/H + 1.675$
100-120	$C_d = 0.01 \cdot B/H + 0.8$
>120	$C_d = 2.0$

The flood loads are discretized and applied as 5 forces over the length of each column on one outer edge of the building model.

5.2 Multi-hazard fragility assessment of a building model for the CR_LFINF_CDM_11_HEX_2 building class

5.2.1 Seismic fragility of the intact model

The simulation scheme presented in Section 5.1.1 is applied, with 10,000 stochastic realizations of the Step 0 – Step 3 loading chains. In order to evaluate the seismic fragility of the model in its intact state (i.e., without any prior loadings), the outcomes of the simulations right after Step 0 are taken, and only if the Step 0 simulations consist of seismic time-history loadings. Due to the fact that the occurrence of an earthquake or flood loading in Step 0 is random, equally likely and independent, approximately 5,000 earthquake loadings are applied in Step 0. Each of these loadings uses as an excitation at the base of the building models one of the horizontal components of the ground motions in the selected dataset (see Section 5.1.3). With this dataset, fragility curves for the four damage states are derived, using PGA as Intensity Measure (IM). Although other intensity measures may be more efficient, especially the spectral acceleration at the first eigenperiod of the building, we chose to use the PGA as IM. This choice is made based on the fact that the first eigenperiod of the building is increased as the level of damage increases, and the range of the first eigenperiod for an existing damage state is apriori unknown. Therefore, we consider that the spectral acceleration at the first eigenperiod of the undamaged building model may be less efficient than the PGA. If estimations or a model for the first eigenperiod of the building model conditioned on the damage state were available, it would be preferable to use them to select a more efficient IM. Fragility parameters are estimated with an ordinal Generalized Linear Modelling (GLM) procedure, using probit (Φ^{-1}) as the link function. As a result, the functional form of a fragility curve, expressing the probability of exceeding a damage state DS_i given PGA, is defined as follows:

$$P(DS \geq DS_j | IM) = \Phi \left(\frac{\ln IM - \ln A_j}{\beta} \right) \quad (5-2)$$

Where A_j and β are the fragility parameters (median and standard deviation) and Φ is the standard normal cumulative distribution function. The ordinal regression applied here (Eq. 5-3) prevents successive fragility curves from crossing each other, since it forces a unique standard deviation for all four damage states. Results are presented in Table 5-6, and they are compared with the fragility parameters provided by ESRM20 for the two similar building classes.

$$\begin{aligned} P(DS_i \geq DS_j | IM_i) &= 1 - P(Y_i \leq j) \\ \text{with } P(Y_i \leq j) &= \Phi(a_j - b \cdot \ln IM_i) = \sum_{j=1}^j \pi_{ij}, \quad j = 1, \dots, J-1 \\ \text{with } \sum_{j=1}^J \pi_{ij} &= 1 \end{aligned} \quad (5-3)$$

Where a_j and b are the model coefficients, i the index of the i -th observation, $k = 0-4$ is the index of the damage state, $j = k+1$ is the index of the ordinal category, $J = \max(j)$ (e.g. for 4 damage states and one implied state for no damage, $k = 0-4$, $J = 5$), Y_i is the ordinal category for the i -th observation, π_{ij} is the probability of ordinal category j for the i -th observation.

The fragility model resulting from the regression may be expressed using Eq. 5-4.

$$\begin{aligned} P(DS \geq DS_j | IM) &= 1 - \Phi(a_j - b \cdot \ln IM) = \\ &= 1 - \Phi \left(b \cdot \left(\frac{a_j}{b} - \ln IM \right) \right) \end{aligned}$$

$$P(DS \geq DS_j | IM) = \Phi \left(\frac{\ln IM - \ln A_j}{\beta_{dem}} \right)$$

with $A_j = \exp \left(\frac{a_j}{b} \right)$, $\beta_{dem} = \frac{1}{b}$ (5-4)

Where A_j are the medians, and β_{dem} is the dispersion resulting from the ordinal regression. This dispersion is calculated based on the responses of the building model in the simulations. The dispersion of the final model results by adding two additional components (Eq. 5-5).

$$\beta = \sqrt{\beta_{dem}^2 + \beta_{thr}^2 + \beta_{cap}^2} \quad (5-5)$$

Where β_{thr} and β_{cap} the components with respect to the uncertainty in the damage state threshold, and the uncertainty in structural capacity, respectively. Based on FEMA (2022), the value for β_{thr} is taken equal to equal to 0.4, and the value for β_{cap} is taken equal to 0.30 for pre-code buildings and 0.25 for code buildings.

The seismic fragility curves for the intact CR_LFINF_CDM_11_HEX_2 Model 3 are shown in Figure 5-6, and the parameters of the generalized linear model in Table 5-16. The parameters of the fragility curves for the CR_LFINF_CDM_11_HEX_2 Models 1-4 are compared in Table 5-6 to the parameters for two similar building classes in ESRM20.

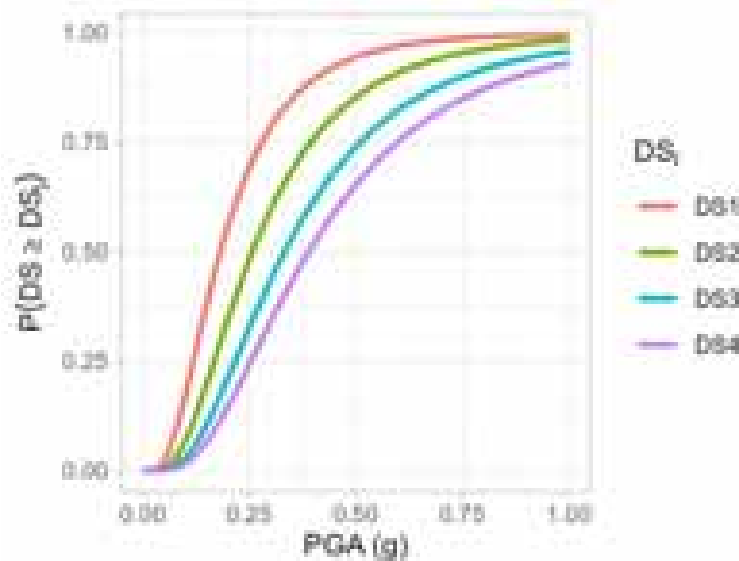


Figure 5-6 Fragility curves for the intact CR_LFINF_CDM_11_HEX_2 Model 3.

Table 5-5: Coefficients of the generalized linear model for the intact CR_LFINF_CDM_11_HEX_2 Model 3.

Parameter	Estimate
b	2.3589
a_1	-4.0212
a_2	-3.2024
a_3	-2.5961
a_4	-2.2228

Table 5-6: Fragility parameters for the intact CR_LFINF_CDM_11_HEX_2 models, along with the fragility values provided for the two corresponding ESRM20 models.

Model	A_1	A_2	A_3	A_4	β
CR_LFINF_CDM_11_HEX_2 – Model 1	0.240	0.356	0.451	0.541	0.55
CR_LFINF_CDM_11_HEX_2 – Model 2	0.233	0.332	0.414	0.516	0.57
CR_LFINF_CDM_11_HEX_2 – Model 3	0.182	0.257	0.333	0.390	0.63
CR_LFINF_CDM_11_HEX_2 – Model 4	0.182	0.257	0.333	0.390	0.63
CR_LINF-CDL-10_H2 (ESRM20)	0.354	0.491	0.639	0.781	1.21
CR_LINF-CDM-10_H2 (ESRM20)	0.403	0.569	0.745	0.912	1.10

In Table 5-6, the two ESRM20 models have higher fragility medians than the CR_LFINF_CDM_11_HEX_2 models, which may be explained by the fact that they have a larger ultimate displacement. Moreover, they also have much larger standard deviations: in our simulations, the uncertainties accounted for are the record-the-record variability, the damage state threshold definition, and modelling uncertainty. Adding other components of variability, such as intra-class building variability, would result in more comparable β values.

When comparing the four CR_LFINF_CDM_11_HEX_2 models with each other, it appears that pinching and especially strength degradation result in lower fragility medians for Models 2 to 4 than Model 1, which only accounts for stiffness degradation. Model 3 and 4 have the same fragility parameters because the dynamic analyses have yielded almost identical EDP values, which results in negligible difference when performing the ordinal GLM regression. This observation shows that the parameter “damage2” for strength degradation (see Table 5-3) has little influence on the simulation outcomes, at least in the case of an intact model.

5.2.2 Flood fragility of the intact model

The flood fragility models are functions of two intensity measures, i.e., the inundation depth and the flow velocity. The inundation depth and the flow velocity are randomly sampled for each flood loading step in the simulations from uniform distributions ($U[0,20]$ m, $U[0,10]$ m/s, respectively). The fragility functions are modelled as surfaces whose parameters are calculated based on an ordinal GLM regression (Eq. 5-6). The fragility functions for all damage states are calculated simultaneously so that the resulting surfaces are mutually exclusive and collectively exhaustive (i.e., they do not intersect).

$$\begin{aligned}
 P(DS_i \geq DS_j | IM_{1i}, IM_{2i}) &= 1 - P(Y_i \leq j) \\
 \text{with } P(Y_i \leq j) &= \Phi(a_j - b_1 \cdot \ln IM_{1i} - b_2 \cdot \ln IM_{2i}) = \sum_{j=1}^j \pi_{ij}, \quad j = 1, \dots, J-1 \\
 \text{with } \sum_{j=1}^J \pi_{ij} &= 1
 \end{aligned} \tag{5-6}$$

Where a_j , b_1 , and b_2 are the generalized linear model coefficients, i the index of the i -th observation, IM_{1i} and IM_{2i} are the values of the two intensity measures, $k = 0-4$ is the index of the damage state, $j = k+1$ is the index of the ordinal category, $J = \max(j)$ (e.g. for 4 damage states and one implied state for no damage, $k = 0-4$, $J = 5$), Y_i is the ordinal category for the i -th observation, π_{ij} is the probability of ordinal category j for the i -th observation.

The fragility surface may be expressed as the fragility curve of a composite IM using Eq. 5-7.

$$P(DS \geq DS_j | IM_1, IM_2) = 1 - \Phi(a_j - b_1 \cdot \ln IM_1 - b_2 \cdot \ln IM_2) =$$

$$\begin{aligned}
 &= 1 - \Phi \left((b_1 + b_2) \left(\frac{a_j}{b_1 + b_2} - \frac{b_1}{b_1 + b_2} \cdot \ln IM_1 - \frac{b_2}{b_1 + b_2} \cdot \ln IM_2 \right) \right) = \\
 &= 1 - \Phi \left((b_1 + b_2) \left(\frac{a_j}{b_1 + b_2} - \ln \left(IM_1^{\frac{b_1}{b_1+b_2}} \cdot IM_2^{\frac{b_2}{b_1+b_2}} \right) \right) \right)
 \end{aligned}$$

$$\begin{aligned}
 P(DS \geq DS_j | IM_c) &= \Phi \left(\frac{\ln IM_c - \ln A_{cj}}{\beta_c} \right) \\
 \text{with } A_{cj} &= \exp \left(\frac{a_j}{b_1+b_2} \right), \quad IM_c = IM_1^{\frac{b_1}{b_1+b_2}} \cdot IM_2^{\frac{b_2}{b_1+b_2}}, \quad \beta_c = \frac{1}{b_1+b_2}
 \end{aligned} \tag{5-7}$$

Where A_{cj} , β_c , and IM_c are the composite medians, the composite dispersion, and the composite intensity measure, respectively.

The total dispersion of the fragility model is calculated based on the responses of the building model in the simulations. The dispersion of the final model results by adding to β_c two components (Eq. 5-8).

$$\beta = \sqrt{\beta_c^2 + \beta_{thr}^2 + \beta_{cap}^2} \tag{5-8}$$

Where β_{thr} and β_{cap} the components with respect to the uncertainty in the damage state threshold, and the uncertainty in structural capacity, respectively. The values for β_{thr} and β_{cap} are taken equal to equal to 0.4, and 0.25, respectively, based on FEMA (2020). To calculate the coefficients of the model with a composite dispersion equal to β (estimate for total variability) and to preserve the medians of the fragility model, all coefficients (a_j , b_1 , b_2) are multiplied by a factor equal to β/β_c .

In the rest of this section, the visualizations of the fragility surfaces for flood may be found as well as tables containing the model parameters.

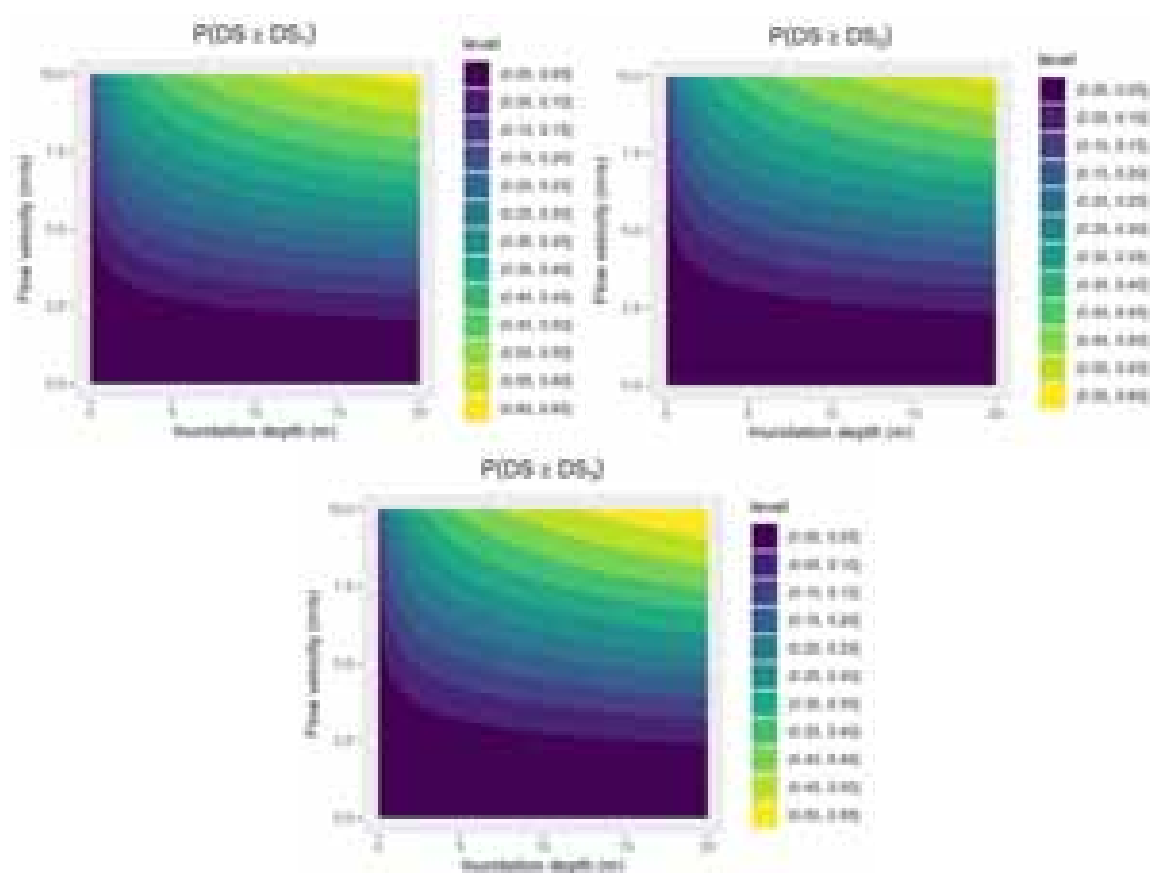


Figure 5-7: Flood fragility models for the intact CR_LFINF_CDM_11_HEX_2 Models 1-4.

Table 5-7: Coefficients of the generalized linear model for the intact CR_LFINF_CDM_11_HEX_2 Models 1-4.

Parameter	Estimate	Estimate for total variability
b_1	27.968	0.358
b_2	137.450	1.761

Table 5-8: Threshold coefficients for the intact CR_LFINF_CDM_11_HEX_2 Models 1-4.

Parameter	Estimate	Estimate for total variability
a_1	366.92	4.702
a_2	382.84	4.906
a_3	386.43	4.952

5.2.3 State-dependent seismic fragility

A similar procedure is applied when deriving state-dependent fragility curves: in this case, outcomes of Step 2 are examined, only for Step 2 simulations consisting of seismic time-history loadings. Given that seismic fragility curves are functions of a single IM, comparisons of fragility curves for different initial damage states are more intuitive than comparisons of fragility surfaces. Therefore the analysis in this section is limited to just earthquake loading in Step 2. Outcomes of Step 0 are used to determine the initial state of the model. Since the initial state of the model may be incurred by either seismic or flood loadings (i.e., depending on what type of simulation was randomly selected during Step 0), it is necessary to check whether the type of prior loading influences the state-dependent fragility curves or if the knowledge of the initial state has an effect on the fragility curves, or if the seismic fragility curves in this study are agnostic of the type of hazard that caused the initial damage state. In the latter case, such state-dependent fragility curves would satisfy the Markov assumption and would constitute a powerful tool to assess the evolution of structural vulnerability throughout the lifetime of the studied building.

The parameters of the state-dependent fragility curves, $P(DS \geq DS_j | IM, DS_{k,all})$, with DS_i representing the damage state to exceed in the current step and $DS_{k,all}$ the initial damage state whatever the type of prior loading, are estimated using ordinal GLM regression and they are detailed in Table 5-9, using Model 3 as an example. The corresponding fragility curves are plotted in Figure 5-8.

Table 5-9: State-dependent fragility parameters for CR_LFINF_CDM_11_HEX_2 Model 3.

Initial state $DS_{k,all}$	A_1	A_2	A_3	A_4	β_{dem}	β
$DS_{0,all}$	0.182	0.257	0.333	0.390	0.42	0.63
$DS_{1,all}$	-	0.205	0.258	0.301	0.45	0.65
$DS_{2,all}$	-	-	0.201	0.257	0.67	0.82
$DS_{3,all}$	-	-	-	0.034	1.02	1.12

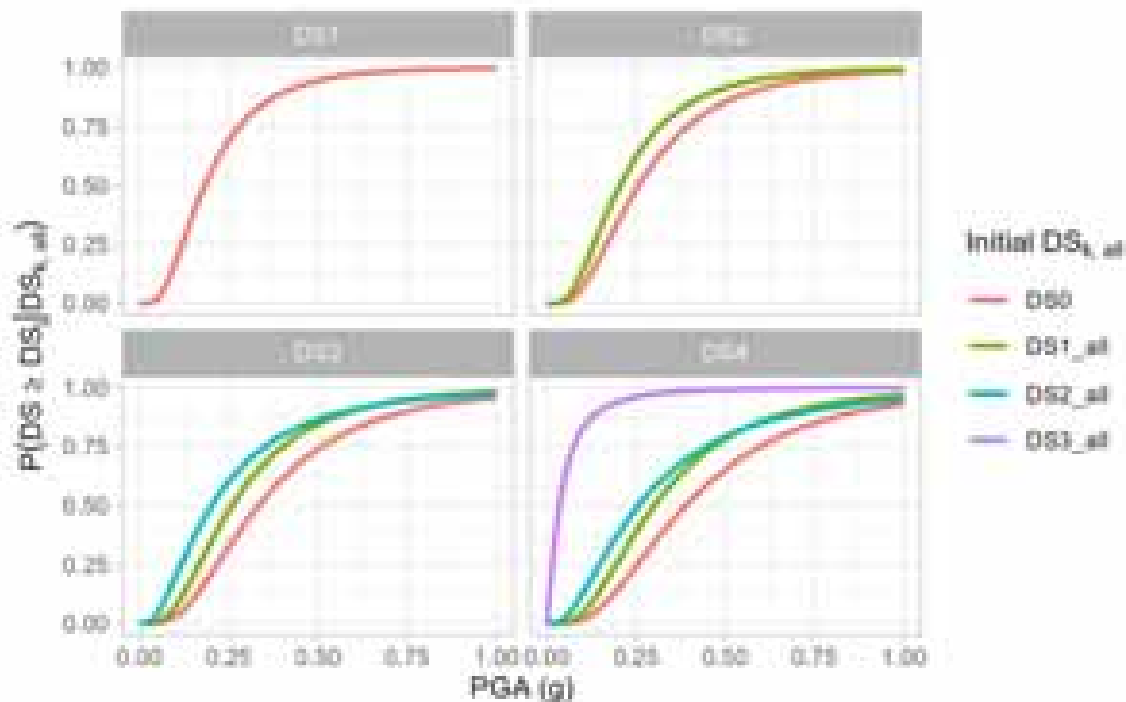


Figure 5-8: State-dependent seismic fragility curves for CR_LFINF_CDM_11_HEX_2 Model 3.

As expected, the median fragility parameter decreases as the initial damage state increases. This is especially the case when comparing the fragility parameters between initial DS_0 and the rest, and also between initial $DS_{3,all}$ and the rest. The differences between initial $DS_{1,all}$ and initial $DS_{2,all}$ in Figure 5-8 are much less significant, with even some overlap between the curves at larger intensities. This may be due to the proximity between DS_1 and DS_2 in terms of ductility; both damage states being close to the yielding point of the capacity curve (see Figure 5-3).

There is also a sharp increase of the standard deviation parameter β , which may explain the overlap between the curves for initial damage states $DS_{1,all}$ and $DS_{2,all}$, which is an expected effect. If the building is damaged, it is expected that the uncertainty will increase in term of expected building performance for new load conditions. For higher initial damage states, an increase in the standard deviation is due to the existence of a larger population of models with possibly different local damage configurations belonging to the same initial state, which creates more variability in the fragility model. However, another reason might be the elongation of the fundamental period of the models as damage states increase, so that PGA might become a less efficient IM.

5.2.4 Influence of hysteretic modelling assumptions

Similarly to the study of Model 3 in the previous sub-section, state-dependent fragility curves are also derived for the other models (Model 1 to 4, as described in Table 5-3). In order to compare all models, the evolution of the state-dependent fragility medians, normalized by their respective intact-state values (see Table 5-6), is plotted as bar diagrams in Figure 5-9.

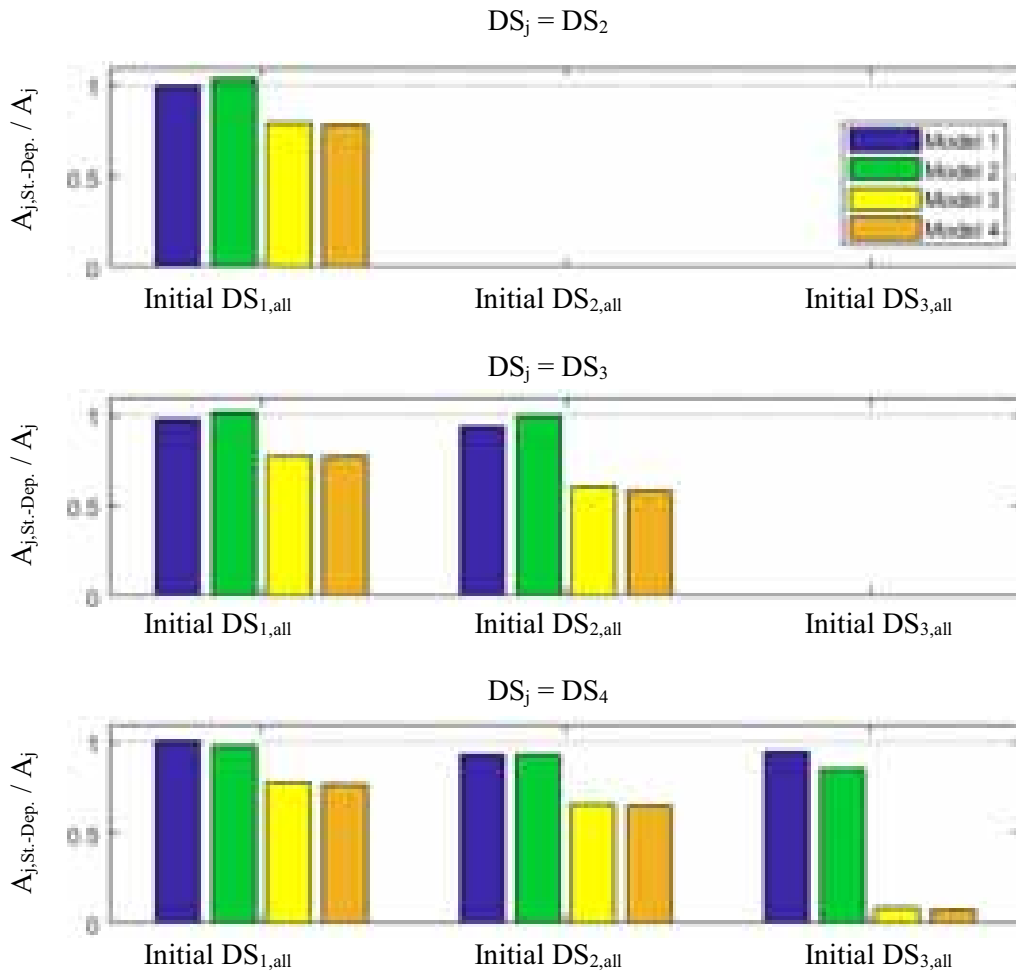


Figure 5-9: Ratio of the median of the state-dependent fragility curve ($A_{j,St.-Dep.}$) to the median of the undamaged building model (A_j) for the four model variants and for the three initial damage states.

Values should be below 1 in order to reproduce an increase of the vulnerability of previously damaged structures. Moreover, as the initial damage DS_j increases, the ratio values should decrease (i.e., from left to right in bar plots). Such behavior is indeed observed for Models 3 and 4; it is also found that differences between these two variants are not significant, which means that the strength degradation due to in-cycle energy dissipation (i.e., hysteretic parameter “damage2” in Table 5-3) has little influence in the present case.

On the other hand, Models 1 and 2 that are based on stiffness degradation demonstrate similar evolutions, and their median ratios remain very close to 1. As a result, it may be concluded that accounting for strength degradation in the hysteretic behavior is necessary in order to properly model the effects of damage accumulation. Only in the case of damage state DS_4 (i.e., fragility curves for complete damage), it may be observed that the median ratios for Models 1 and 2 given DS_2 or DS_3 initial damage state drop consistently below 1, although at a much lower rate than the other models. In the bottom plot of Figure 5-9, the effect of pinching in the hysteretic behavior starts also to become more noticeable. Note that in the cases, where the ratios exceed 1.0, the fragilities remain practically unchanged, while the increase of the median is the result of the uncertainty in the estimation of the median itself.

5.2.5 Influence of hazard type in the loading history

Similar state-dependent fragility curves are also derived by distinguishing now the type of hazard loading simulated in Step 0. The results are presented in Table 5-10 and Figure 5-10, where the fragility parameters are different depending on whether the initial damage state has been induced by an earthquake ($DS_{k,EQ}$) or by a flood ($DS_{k,FL}$). The focus here is on Model 3, since it has been shown in the above discussion that Models 3 and 4 yield very similar results, and that Models 1 and 2 are not able to properly account for the effects of damage accumulation.

Table 5-10: State-dependent fragility parameters for CR_LFINF_CDM_11_HEX_2 Model 3, in the cases where the initial state is induced by a seismic loading ($DS_{k,EQ}$) or by a flood loading ($DS_{k,FL}$).

Initial state DS_j	A_1	A_2	A_3	A_4	β_{dem}	β
DS_0	0.182	0.257	0.333	0.390	0.42	0.63
$DS_{1,EQ}$	-	0.203	0.241	0.284	0.49	0.68
$DS_{1,FL}$	-	0.210	0.311	0.357	0.39	0.61
$DS_{2,EQ}$	-	-	0.186	0.240	0.67	0.82
$DS_{2,FL}$	-	-	0.325	0.375	0.42	0.63
$DS_{3,EQ}$	-	-	-	0.033	1.03	1.13
$DS_{3,FL}$	-	-	-	0.097	0.94	1.05

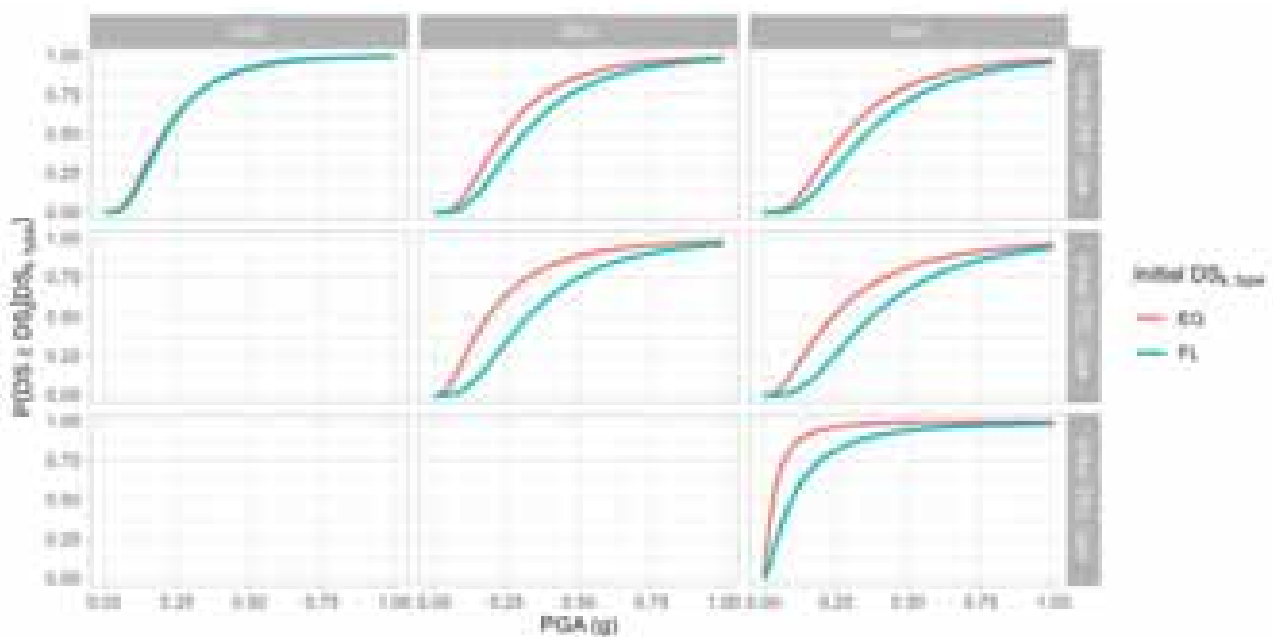


Figure 5-10: State-dependent seismic fragility curves for CR_LFINF_CDM_11_HEX_2 Model 3, as a function of the type of hazard (EQ for earthquake, FL for flood) that has caused the initial damage state ($DS_{k,type}$).

Fragility curves for the damage state DS_2 are very close to each other, showing little difference whether the initial state DS_1 has been caused by seismic or flood loading. However, for initial damage states DS_2 and DS_3 (i.e., middle and lower row of Figure 5-10), much larger differences start to appear; and the state-dependent fragility curves based on flood loading in the first step have a smaller decrease of their median value as the initial damage state gets higher.

Possible reasons for this observation include the absence of cyclic loading in the flood load in Step 0 (as opposed to the seismic load), as well as the potential differences in the local damage distribution between the two types of loading. The latter point would require further investigations, such as the identification of the locations of the damaged structural elements or the creation of specific mechanisms such as soft-story, etc. Such work would then support the creation of a more precise damage scale, in order to account for the types of damage that may be specific to each loading type.

5.2.6 State-dependent flood fragility

This section includes the state-dependent flood fragility models for the Models 1-4 of the CR_LFINF_CDM_11_HEX_2 type building class. The fragility models are surfaces, i.e., functions of two intensity measures: the inundation depth (m) and the flow velocity (m/s). Moreover, the fragility models are conditioned on the existing damage state caused by flood in the first loading step. For all considered existing damage states (DS1 to DS3), the employed calculation procedure returned values only for the fragility surface for the probability of exceeding the highest damage state (DS4). This is coherent with the observation by Petrone et al. (2020), who calculated synthetic tsunami fragility curves for a reinforced concrete building model. In their simulations, the building model transitioned from the existing damage state to the highest damage state, in the cases that the tsunami loading exceeded its structural strength. In the case of the Models 1-2 with an existing damage state DS2, there were no responses in damage states 3 and 4, i.e., the calculated maximum interstory drifts were below the threshold of DS3, therefore the calculation of the fragility model parameters was not possible.

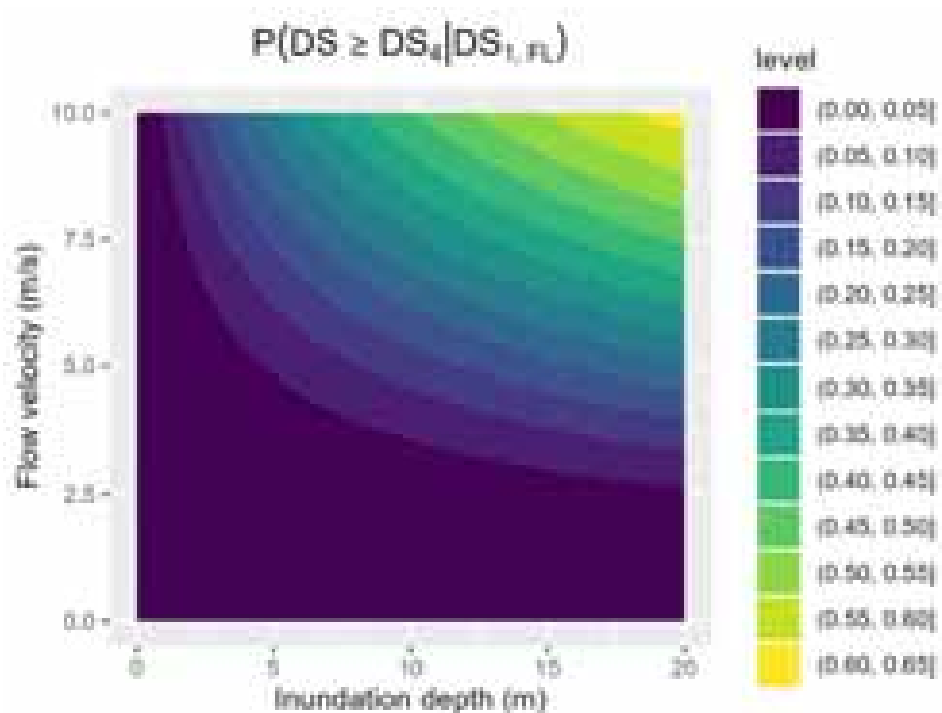


Figure 5-11: Flood fragility models for the CR_LFINF_CDM_11_HEX_2 Models 1-2 in $DS_{1,FL}$.

Table 5-11: Coefficients of the generalized linear model for the CR_LFINF_CDM_11_HEX_2 Models 1-2 in $DS_{1,FL}$.

Parameter	Estimate	Estimate for total variability
b_1	83.64	0.648
b_2	190.09	1.472
a_d	1647.4	5.014

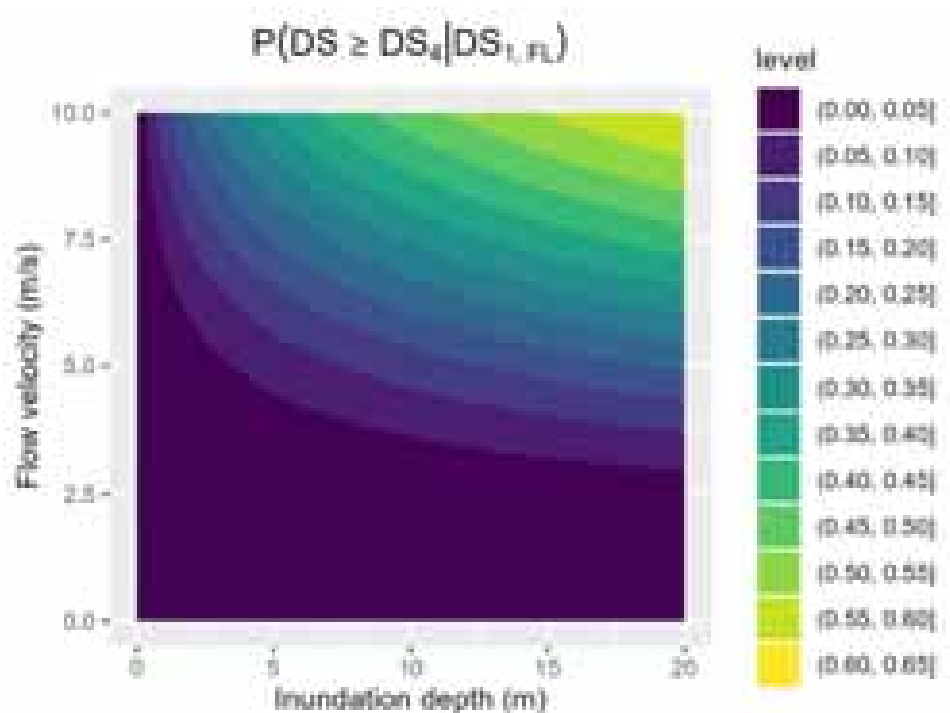


Figure 5-12: Flood fragility model for the CR_LFINF_CDM_11_HEX_2 Models 3-4 in $DS_{1,FL}$.

Table 5-12: Coefficients of the generalized linear model for the CR_LFINF_CDM_11_HEX_2 Models 3-4 in $DS_{1,FL}$.

Parameter	Estimate	Estimate for total variability
b_1	1.908	0.472
b_2	6.400	1.582
a_4	19.357	4.786

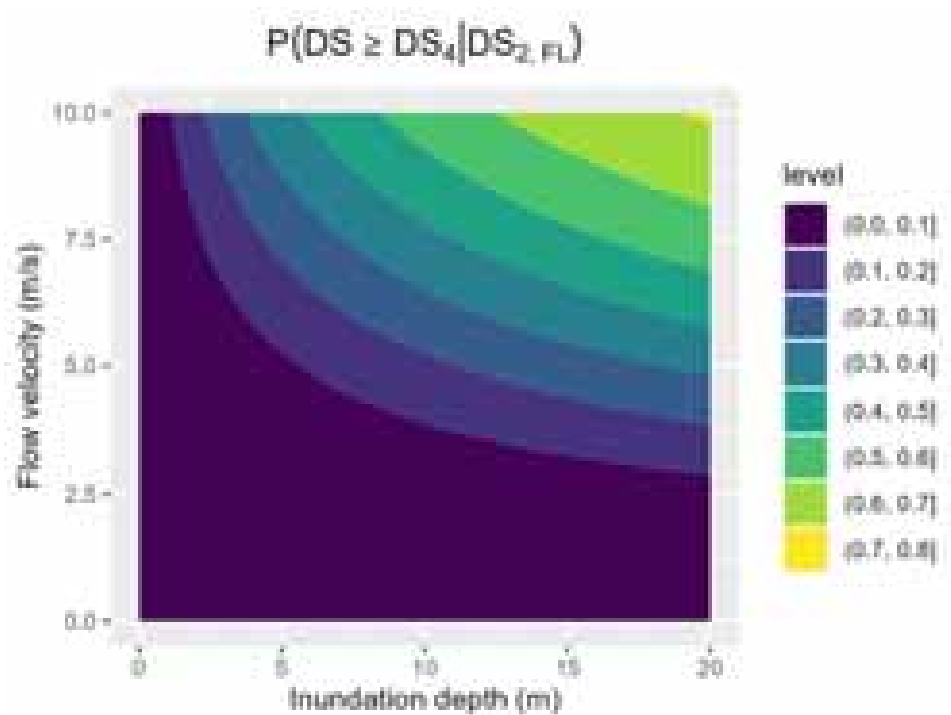


Figure 5-13: Flood fragility model for the CR_LFINF_CDM_11_HEX_2 Models 3-4 in $DS_{2,FL}$.

Table 5-13: Coefficients of the generalized linear model for the CR_LFINF_CDM_11_HEX_2 Models 3-4 in $DS_{2,FL}$.

Parameter	Estimate	Estimate for total variability
b_1	19.89	0.642
b_2	45.78	1.477
a_4	147.8	4.767

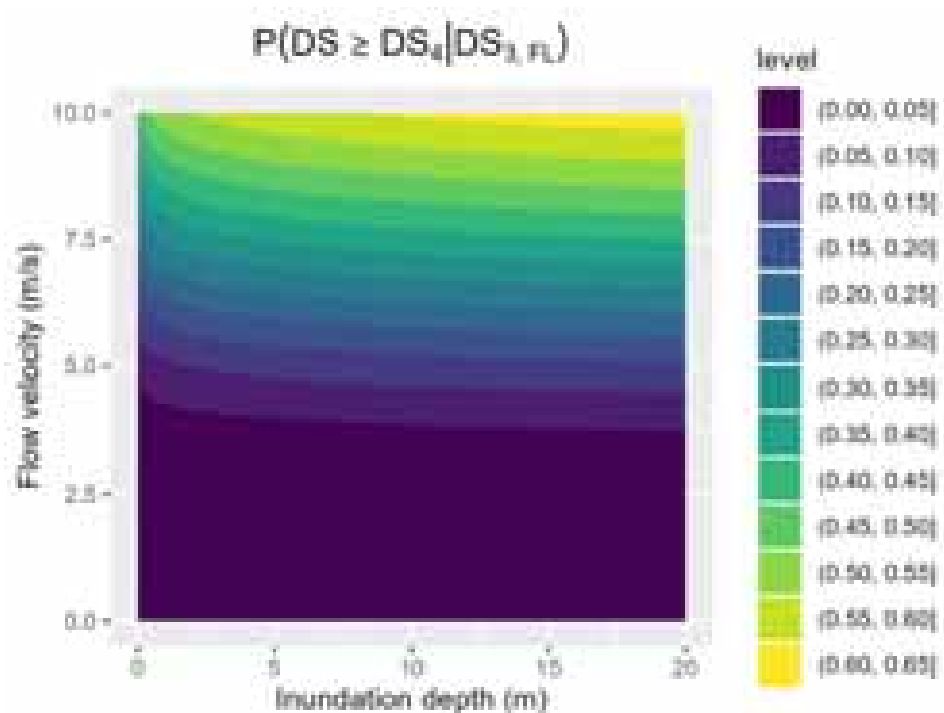


Figure 5-14: Flood fragility models for the CR_LFINF_CDM_11_HEX_2 Models 1-2 in $DS_{3,FL}$.

Table 5-14: Coefficients of the generalized linear model for the CR_LFINF_CDM_11_HEX_2 Models 1-2 in $DS_{3,FL}$.

Parameter	Estimate	Estimate for total variability
b_1	2.205	0.088
b_2	50.916	2.030
a_4	115.5	4.608

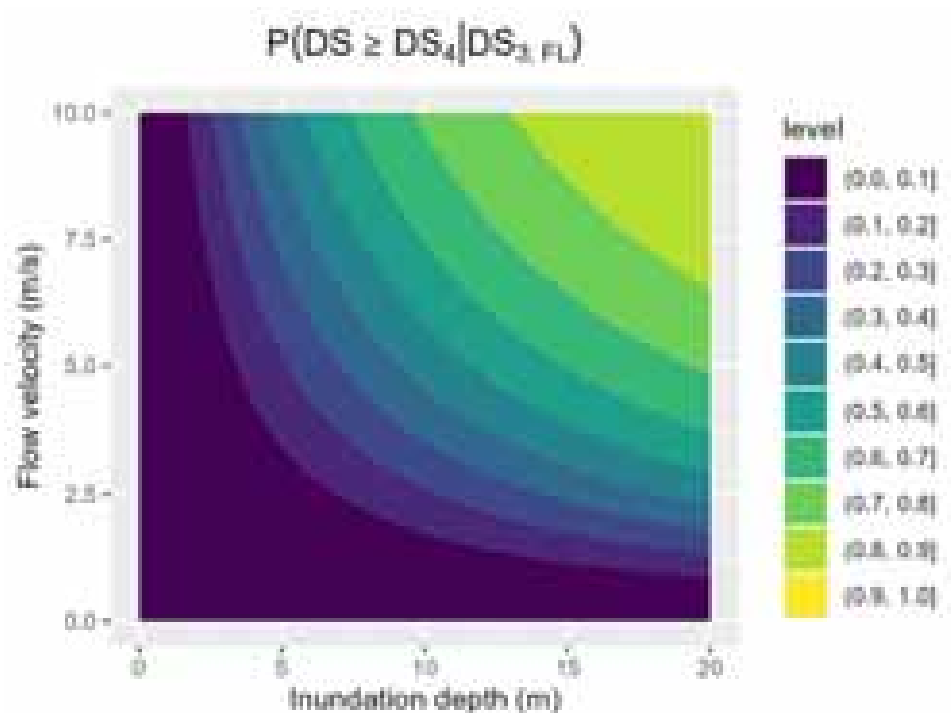


Figure 5-15 Flood fragility models for the CR_LFINF_CDM_11_HEX_2 Models 3-4 in $DS_{3,FL}$.

Table 5-15: Coefficients of the generalized linear model for the CR_LFINF_CDM_11_HEX_2 Models 3-4 in $DS_{3,FL}$.

Parameter	Estimate	Estimate for total variability
b_1	9.447	1.051
b_2	9.498	1.056
a_4	38.53	4.285

5.3 Multi-hazard fragility assessment of a building model for the CR_LWAL_DUL_HEX_4 building class

This section includes the multi-hazard fragility models for the CR_LWAL_DUL_HEX_4 type building class. The fragility models in this section include seismic fragility curves, and flood fragility surfaces. Both the fragility curves and the fragility surfaces concern the intact building model as well as the building model with an existing damage state. In the latter case, the models are state-dependent fragilities, conditioned on an initial (or existing) damage state. The state-dependent seismic fragilities are separated in three groups depending on the hazard that has caused the existing damage state: (1) earthquake, (2) flood, and (3) earthquake or flood.

5.3.1 Seismic fragility of the intact model

The approach for the calculation of the parameters of the fragility curves is exactly the same as that described in Section 5.2. The seismic fragility curves for the intact CR_LWAL_CDN_HEX_4 type building model are given in Figure 5-16 in addition to the cloud of data used to calculate the fragilities. The parameters of the generalized linear model and the parameters of the fragility curves are given in Table 5-16 - Table 5-17.

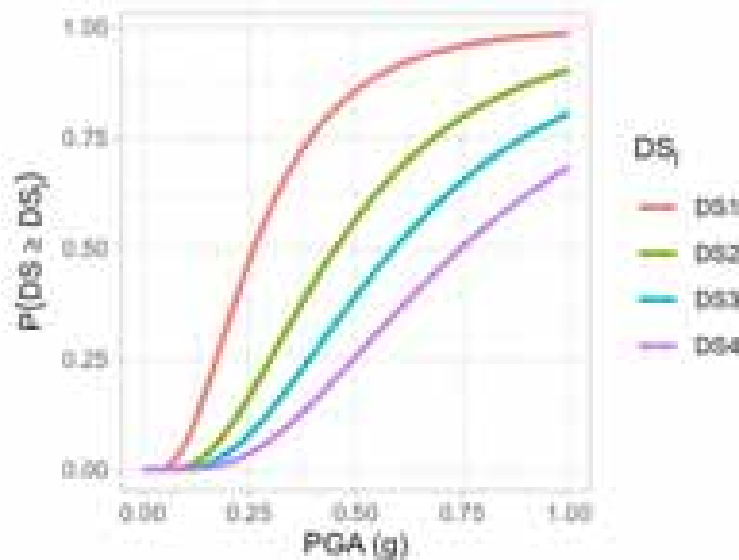


Figure 5-16: Fragility curves for the intact CR_LWAL_CDN_HEX_4 type model.

Table 5-16: Coefficients of the generalized linear model for the intact CR_LWAL_CDN_HEX_4 type model.

Parameter	Estimate
b	27.968
a_1	-3.8514
a_2	-2.2734
a_3	-1.5084
a_4	-0.8366

Table 5-17: Parameters of lognormal fragility curves for the intact CR_LWAL_CDN_HEX_4 as a function of the PGA (g).

A_1	A_2	A_3	A_4	β_{dem}	β
0.261	0.452	0.591	0.747	0.348	0.587

5.3.2 State-dependent seismic fragility

5.3.2.1 Initial damage state caused by earthquake

The state-dependent seismic fragility curves for the CR_LWAL_CDN_HEX_4 type building models with an existing damage state caused by earthquake are presented in Figure 5-17 - Figure 5-19 in addition to the cloud of data used to calculate the fragility parameters. The figures containing the cloud of maximum inter-story drifts as a function of the PGA also include regression models. These models are used only for visualization purposes and they are not used to calculate the fragility curves. The parameters of the generalized linear model and the parameters of the fragility curves are given in Table 5-18 - Table 5-23.

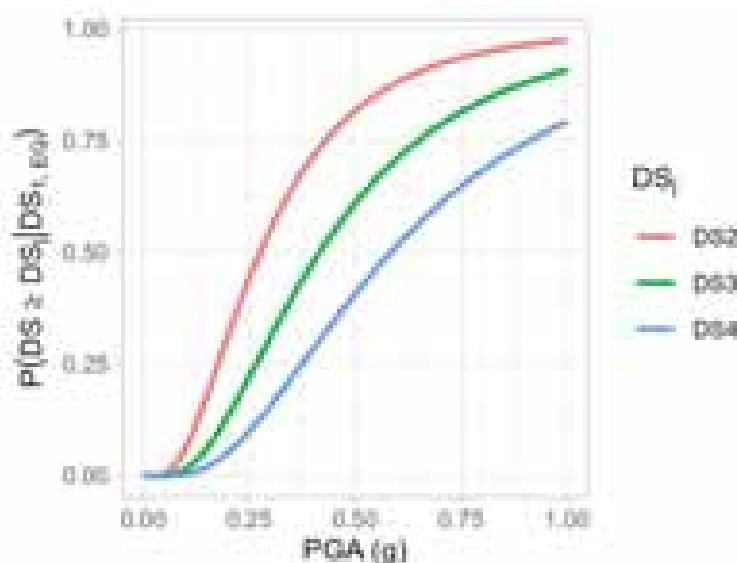


Figure 5-17: Fragility curves for the CR_LWAL_CDN_HEX_4 type model in $DS_{1,EQ}$.

Table 5-18: Coefficients of the generalized linear model for the intact CR_LWAL_CDN_HEX_4 type model in $DS_{1,EQ}$.

Parameter	Estimate
b	2.323
a_2	-2.9928
a_3	-2.0358
a_4	-1.2474

Table 5-19: Parameters of lognormal fragility curves for the intact CR_LWAL_CDN_HEX_4 type model in $DS_{1,EQ}$ as a function of the PGA (g).

A_2	A_3	A_4	β_{dem}	β
0.276	0.416	0.584	0.431	0.639

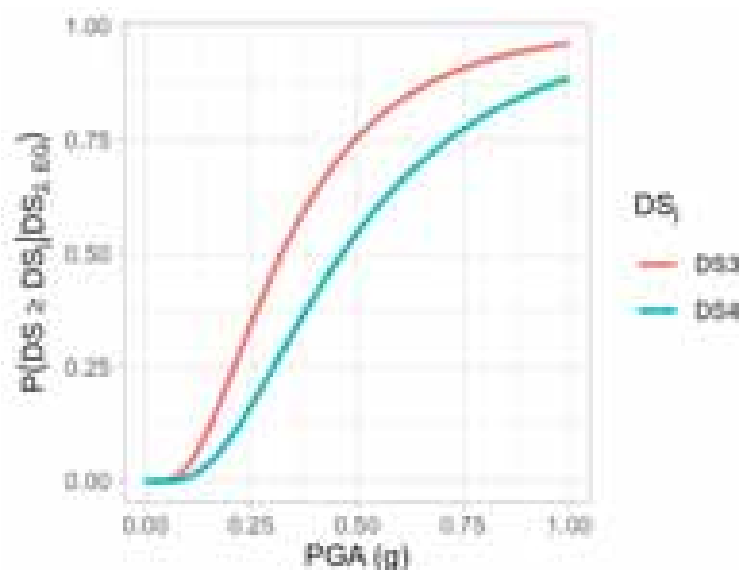


Figure 5-18: Fragility curves for the CR_LWAL_CDN_HEX_4 type model in $DS_{2,EQ}$.

Table 5-20: Coefficients of the generalized linear model for the intact CR_LWAL_CDN_HEX_4 type model in $DS_{2,EQ}$.

Parameter	Estimate
b	2.5340
a_3	-2.8715
a_4	-1.9435

Table 5-21: Parameters of lognormal fragility curves for the intact CR_LWAL_CDN_HEX_4 type model in $DS_{2,EQ}$ as a function of the PGA (g).

A_3	A_4	β_{dem}	β
0.322	0.464	0.394	0.615

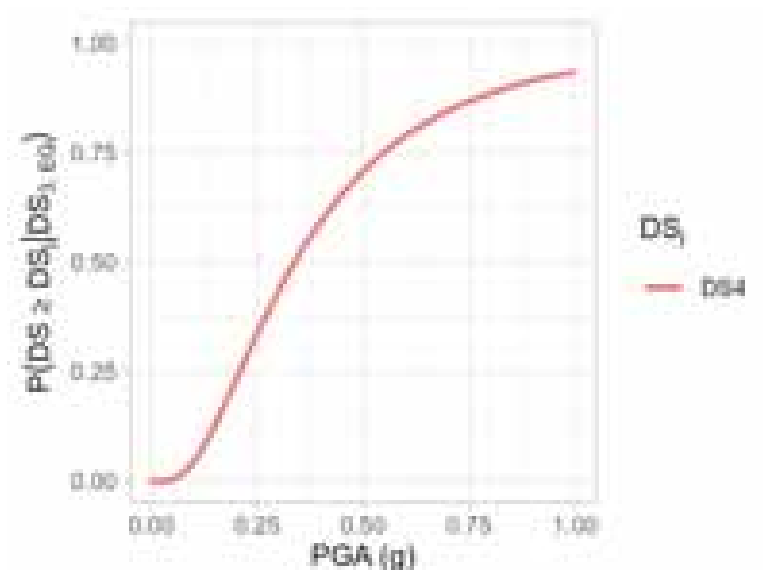


Figure 5-19: Fragility curves for the CR_LWAL_CDN_HEX_4 type model in $DS_{3,EQ}$.

Table 5-22: Coefficients of the generalized linear model for the intact CR_LWAL_CDN_HEX_4 type model in $DS_{3,EQ}$.

Parameter	Estimate
b	1.961
a_4	-2.1256

Table 5-23: Parameters of lognormal fragility curves for the intact CR_LWAL_CDN_HEX_4 type model in $DS_{3,EQ}$ as a function of the PGA (g).

A_4	β_{dem}	β
0.338	0.510	0.695

5.3.2.2 Initial damage state caused by flood

The state-dependent seismic fragility curves for the CR_LWAL_CDN_HEX_4 type building models with an existing damage state caused by flood are presented in Figure 5-20 - Figure 5-22 in addition to the cloud of data used to calculate the fragilities. The figures containing the cloud of maximum inter-story drifts as a function of the PGA also include regression models. These models are used only for visualization purposes and they are not used to calculate the fragility curves. The parameters of the generalized linear model and the parameters of the fragility curves are given in Table 5-24 - Table 5-29.

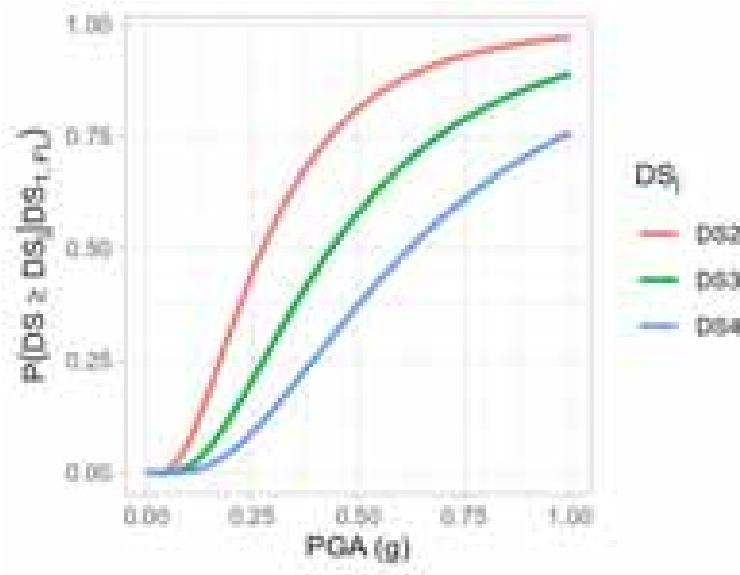


Figure 5-20: Fragility curves for the CR_LWAL_CDN_HEX_4 type model in $DS_{1,FL}$.

Table 5-24: Coefficients of the generalized linear model for the intact CR_LWAL_CDN_HEX_4 type model in $DS_{1,FL}$.

Parameter	Estimate
b	2.1917
a_2	-2.8308
a_3	-1.8181
a_4	-1.0429

Table 5-25: Parameters of lognormal fragility curves for the intact CR_LWAL_CDN_HEX_4 type model in $DS_{1,FL}$ as a function of the PGA (g).

A_2	A_3	A_4	β_{dem}	β
0.275	0.436	0.621	0.456	0.677

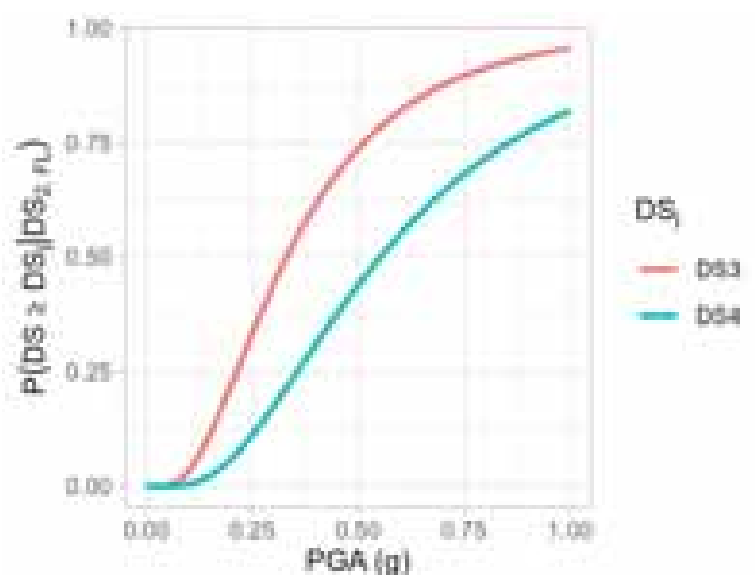


Figure 5-21: Fragility curves for the CR_LWAL_CDN_HEX_4 type model in DS_{2,FL}.

Table 5-26: Coefficients of the generalized linear model for the intact CR_LWAL_CDN_HEX_4 type model in DS_{2,FL}.

Parameter	Estimate
b	2.4171
a_3	-2.6728
a_4	-1.4335

Table 5-27: Parameters of lognormal fragility curves for the intact CR_LWAL_CDN_HEX_4 type model in DS_{2,FL} as a function of the PGA (g).

A_3	A_4	β_{dem}	β
0.331	0.553	0.414	0.627

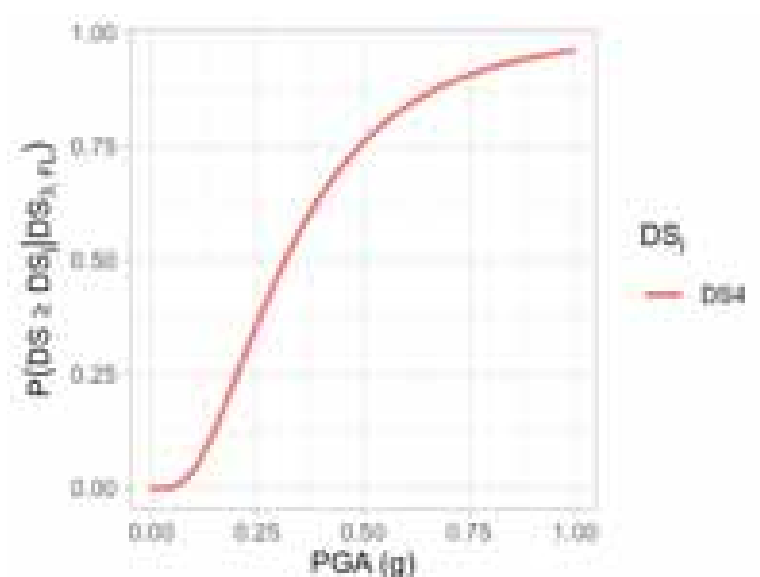


Figure 5-22: Fragility curves (right) for the CR_LWAL_CDN_HEX_4 type model in $DS_{3,FL}$.

Table 5-28: Coefficients of the generalized linear model for the intact CR_LWAL_CDN_HEX_4 type model in $DS_{3,FL}$.

Parameter	Estimate
b	2.3754
a_4	-2.738

Table 5-29: Parameters of lognormal fragility curves for the intact CR_LWAL_CDN_HEX_4 type model in $DS_{3,FL}$ as a function of the PGA (g).

A_4	β_{dem}	β
0.316	0.421	0.632

5.3.2.3 Initial damage state caused by earthquake or flood

The state-dependent seismic fragility curves for the CR_LWAL_CDN_HEX_4 type building models with an existing damage state without distinguishing the hazard that caused it (caused by earthquake or flood) are presented in Figure 5-23 - Figure 5-25 in addition to the cloud of data used to calculate the fragilities. The figures containing the cloud of maximum inter-story drifts as a function of the PGA also include regression models. These models are used only for visualization purposes and they are not used to calculate the fragility curves. The parameters of the generalized linear model and the parameters of the fragility curves are given in Table 5-30 - Table 5-35.

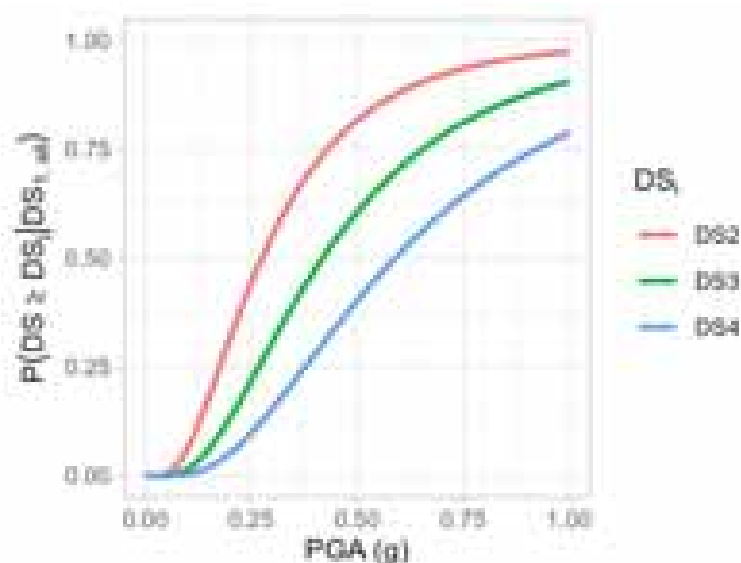


Figure 5-23Fragility curves for the CR_LWAL_CDN_HEX_4 type model in DS_{1,all}.

Table 5-30: Coefficients of the generalized linear model for the intact CR_LWAL_CDN_HEX_4 type model in DS_{1,all}.

Parameter	Estimate
b	2.2993
a_2	-2.9658
a_3	-1.9999
a_4	-1.2135

Table 5-31: Parameters of lognormal fragility curves for the intact CR_LWAL_CDN_HEX_4 type model in DS_{1,all} as a function of the PGA (g).

A_2	A_3	A_4	β_{dem}	β
0.275	0.419	0.590	0.435	0.662

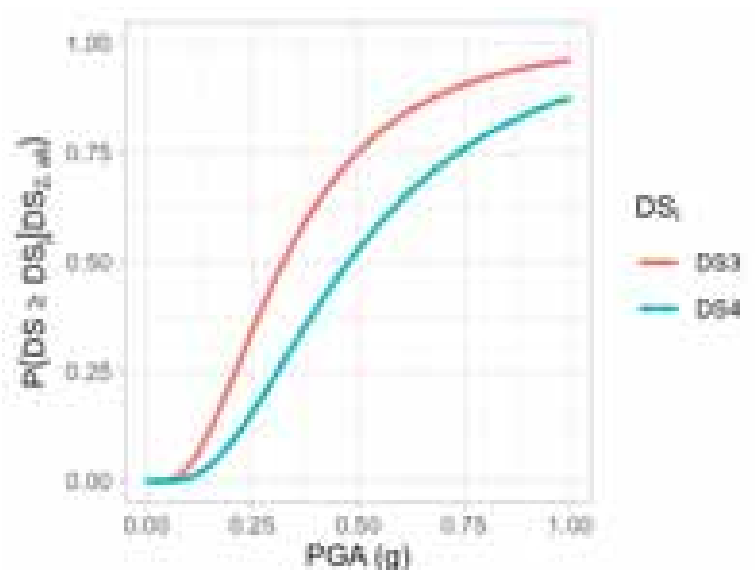


Figure 5-24: Fragility curves (right) for the CR_LWAL_CDN_HEX_4 type model in $DS_{2,all}$.

Table 5-32: Coefficients of the generalized linear model for the intact CR_LWAL_CDN_HEX_4 type model in $DS_{2,all}$.

Parameter	Estimate
b	2.5104
a_3	-2.8320
a_4	-1.8561

Table 5-33: Parameters of lognormal fragility curves for the intact CR_LWAL_CDN_HEX_4 type model in $DS_{2,all}$ as a function of the PGA (g).

A_3	A_4	β_{dem}	β
0.324	0.447	0.398	0.639

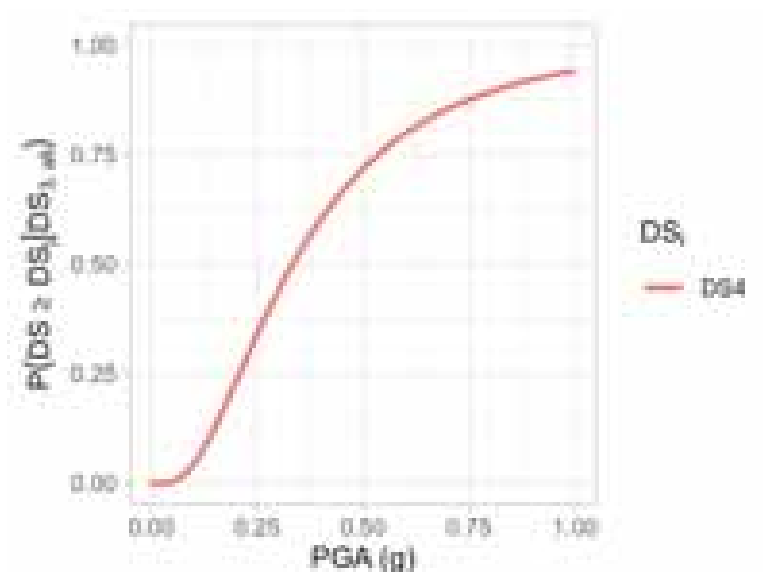


Figure 5-25: Fragility curves (right) for the CR_LWAL_CDN_HEX_4 type model in $DS_{3,all}$.

Table 5-34: Coefficients of the generalized linear model for the intact CR_LWAL_CDN_HEX_4 type model in $DS_{3,all}$.

Parameter	Estimate
b	2.0426
a_4	-2.2421

Table 5-35: Parameters of lognormal fragility curves for the intact CR_LWAL_CDN_HEX_4 type model in $DS_{3,all}$ as a function of the PGA (g).

A_4	β_{dem}	β
0.334	0.490	0.700

5.3.3 Influence of the initial damage state and the type of hazard that caused it

In this section we compare the seismic state-dependent fragility curves for the CR_LWAL_CDN_HEX_4 type model to highlight the effect of the existing damage state, as well as the effect of the type of hazard (earthquake or flood), that caused it. The comparisons are made in the same manner as the comparison for the CR_LFINF_CDM_11_HEX_2 in Sections 5.2.3 and 5.2.5. Figure 5-26 shows the fragility curves for damage states DS_1 - DS_4 (in four separate facets) as a function of the initial damage state ($DS_{k,all}$), which has been caused by earthquake or flood. Figure 5-26 also includes the fragility curves of the undamaged building model (initial damage state DS_0), and shows that the fragilities are significantly affected by the existing damage state. This is mostly pronounced in the case of the fragility curve for damage state DS_4 , whose median is reduced over 50 % for an existing damage state $DS_{3,all}$ in comparison to the undamaged building model.

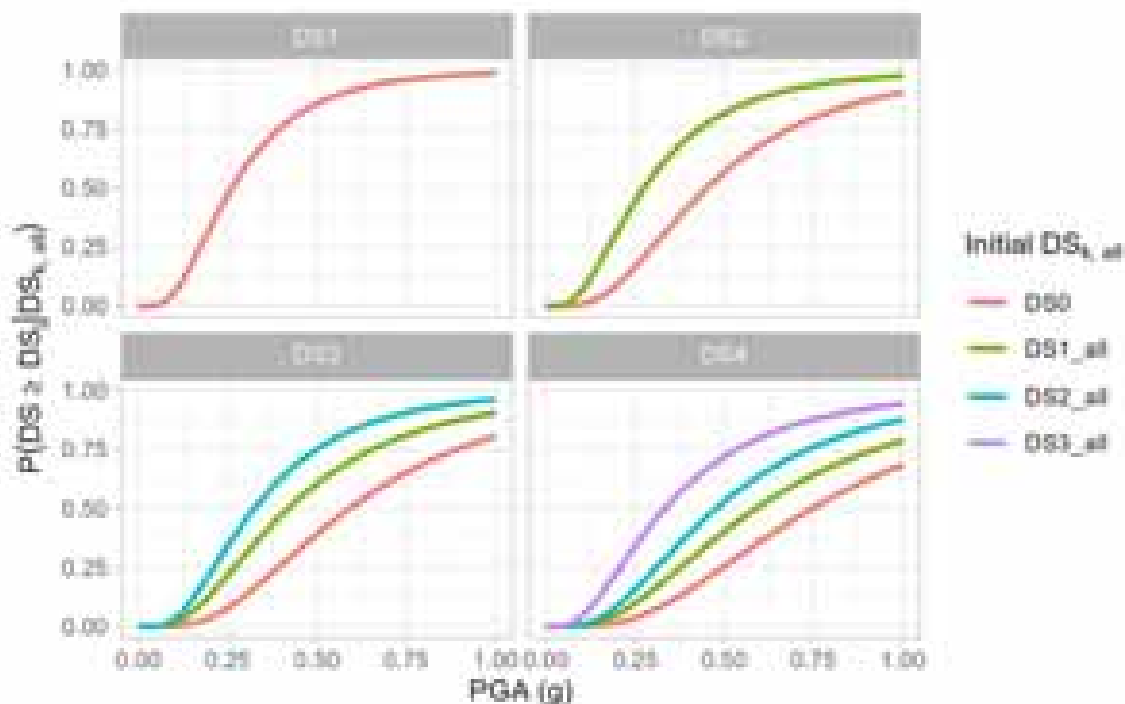


Figure 5-26: State-dependent seismic fragility curves for the CR_LWAL_CDN_HEX_4 type model.

Figure 5-27 shows the state-dependent fragility curves for the CR_LWAL_CDN_HEX_4 model for damage states DS_2 – DS_4 as a function of the initial damage state ($DS_{1,type}$ – $DS_{3,type}$) and the type of hazard that has caused it (EQ for earthquake, FL for flood). In contrast to the case of the CR_LFINF_CDM_11_HEX_2 Model 3, the type of hazard appears to have a minor if any effect on the state-dependent fragility curves calculated for the CR_LWAL_CDN_HEX_4 type model. This is attributed to the fact that strength degradation has not been modelled in the case of the CR_LWAL_CDN_HEX_4 model (as in the case of CR_LFINF_CDM_11_HEX_2 Models 1-2).

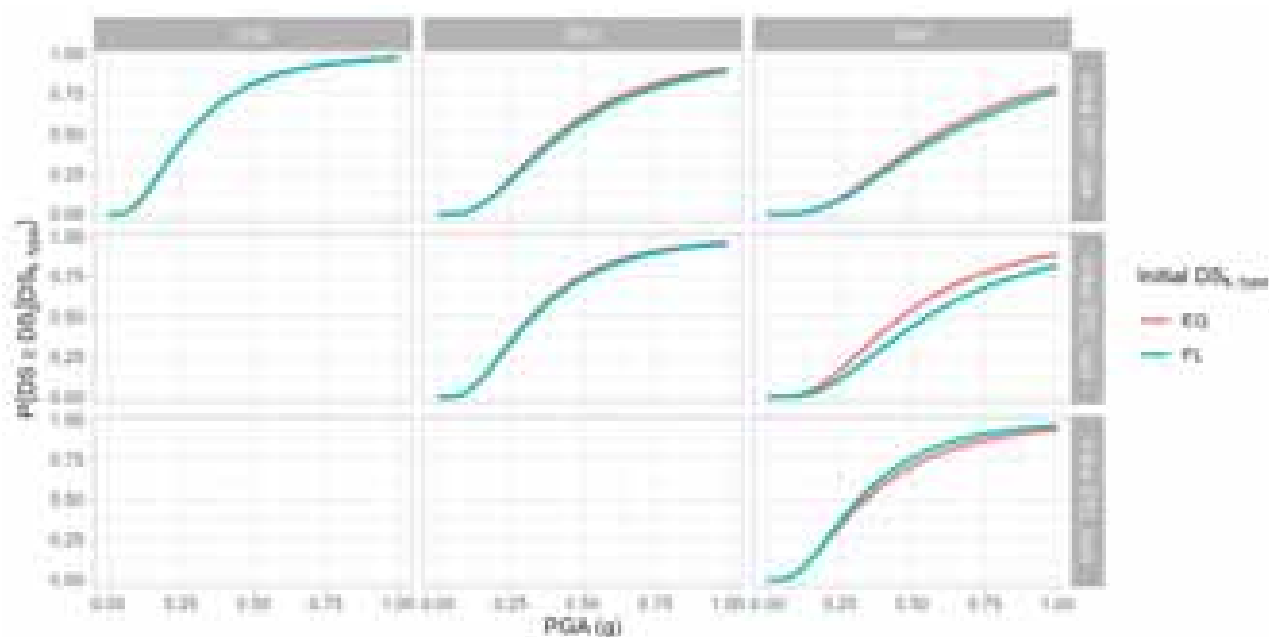


Figure 5-27: State-dependent seismic fragility curves for CR_LFINF_CDM_11_HEX_2 Model 3, as a function of the type of hazard (EQ for earthquake, FL for flood) that has caused the initial damage state (DSk,type).

5.3.4 Flood fragility of the intact model

The flood fragility surfaces for the intact CR_LWAL_CDN_HEX_4 type building model are given in Figure 5-28. The parameters of the fragility model are given in Table 5-36.

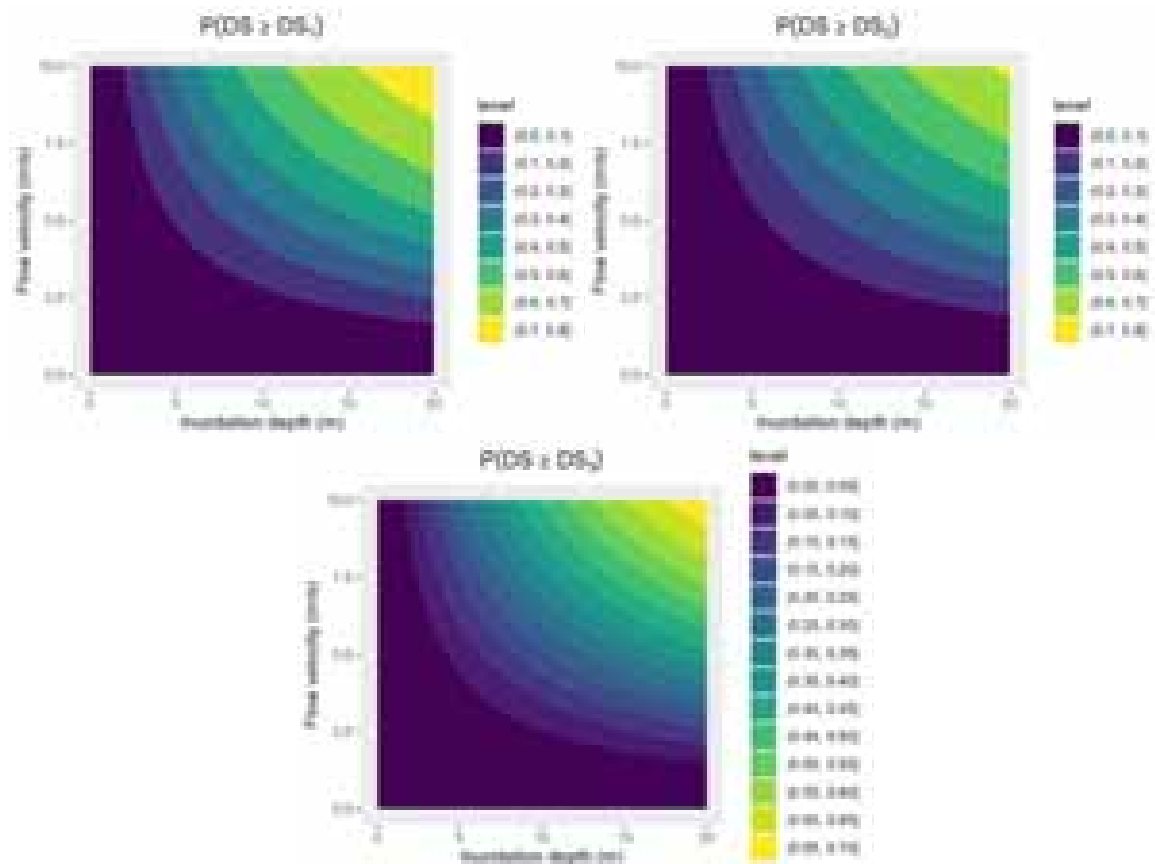


Figure 5-28: Flood fragility models for the intact CR_LWAL_CDN_HEX_4 model.

Table 5-36: Coefficients of the generalized linear model for the intact CR_LWAL_CDN_HEX_4 model.

Parameter	Estimate	Estimate for total variability
b_1	17.5430	0.866
b_2	22.9142	1.131
a_1	90.277	4.457
a_2	93.704	4.627
a_3	95.218	4.701

5.3.5 State-dependent flood fragility

The state-dependent flood fragility surfaces for the CR_LWAL_CDN_HEX_4 type building models with an existing damage state caused by flood are presented in Figure 5-29 - Figure 5-31. The parameters of the the fragility models are given in Table 5-37 - Table 5-39.

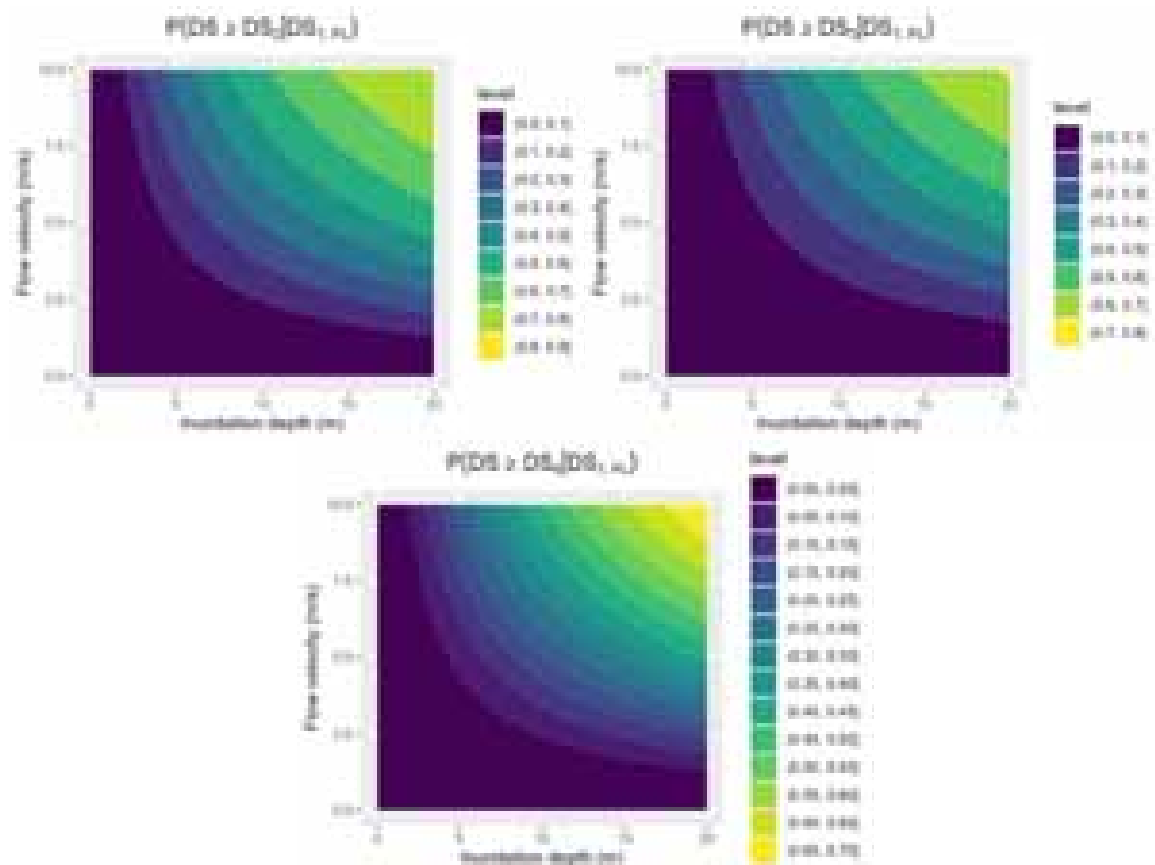


Figure 5-29: Flood fragility models for the CR_LWAL_CDN_HEX_4 model in DS_{1,FL}.

Table 5-37: Coefficients of the generalized linear model for the CR_LWAL_CDN_HEX_4 model in DS_{1,FL}.

Parameter	Estimate	Estimate for total variability
b_1	6.350	0.925
b_2	7.236	1.054
a_2	29.802	4.341
a_3	31.822	4.635
a_4	2.140	4.681

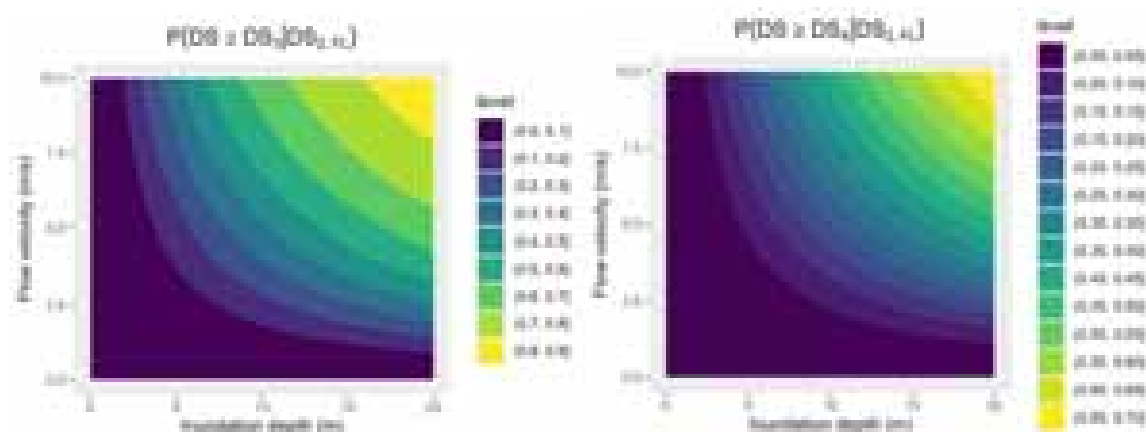


Figure 5-30: Flood fragility models for the CR_LWAL_CDN_HEX_4 model in DS_{2,FL}.

Table 5-38: Coefficients of the generalized linear model for the CR_LWAL_CDN_HEX_4 model in DS_{2,FL}.

Parameter	Estimate	Estimate for total variability
b_1	8.212	1.008
b_2	7.963	0.977
a_3	34.15	4.191
a_4	38.73	4.753

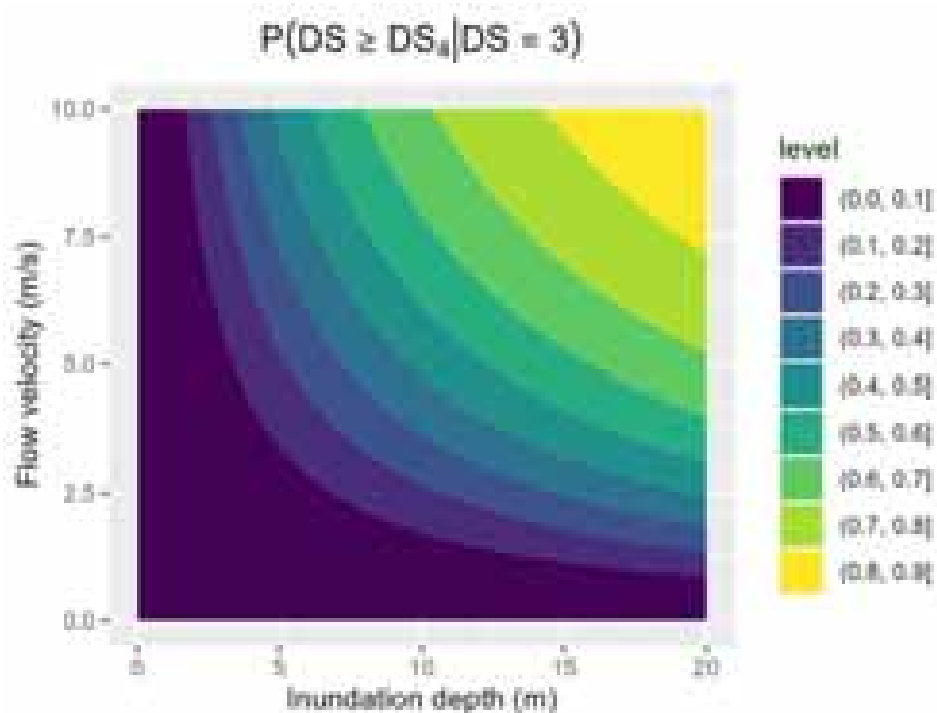


Figure 5-31: Flood fragility models for the CR_LWAL_CDN_HEX_4 model in $DS_{3,FL}$.

Table 5-39: Coefficients of the generalized linear model for the CR_LWAL_CDN_HEX_4 model in $DS_{3,FL}$.

Parameter	Estimate	Estimate for total variability
b_1	144.2	0.992
b_2	146.5	1.008
a_4	598	4.114

5.4 Discussion

Based on the results with respect to the state-dependent fragility curves for the two studied reinforced-concrete building models, it is worth discussing two subjects: the effect of strength degradation on state-dependent fragility curves, and the number of realizations of the building models in the damage states based on the adopted modelling scheme.

The four CR_LFINF_CDM_11_HEX_2 type building models used in this study differ with respect to the parameters for the pinching in the moment-curvature response of the structural elements, and with respect to the parameters for the strength degradation. The two models, where strength degradation is modelled, lead to state-dependent fragility curves, which are affected by the type of hazard that has caused the existing damage state. This is not observed in the calculated fragility curves for the models, where strength degradation is not modelled. This is also observed in the case of the CR_LWAL_CDN_HEX_4 type model that has no strength degradation. This observation should be further investigated, and if it is proven that it may be generalized, it may have implications with respect to time-variable fragility modelling based on Markovian approaches. In specific, the transition matrices in a Markov chain would have to include a number of columns (and rows) equal to the number of damage states multiplied by the types of hazards, plus one for the undamaged state. This would be different from calculations using transition matrices assuming a number of columns equal to the number of damage states, which is based on the assumption that state-dependent fragilities depend on the existing damage state but are agnostic to the hazard that caused it.

As far as the number of realizations of the building model in the damage states in the multi-step modelling scheme is concerned, we note that, in some cases, it was small, which made it impossible to calculate the parameters of the fragility curves. One reason for this is the fact that the seismic excitations were selected randomly from a dataset of ground motions extracted from the Engineering Strong Motion Database (Luzi et al., 2020) using the following criteria: Magnitude ≥ 6.0 , PGA ≥ 1.0 cm/s², epicentral distance ≤ 30.0 km. Although the dataset includes ground motions capable of leading the models to all damage states, most ground motions in the dataset are of low intensity. Another reason is the shape of the capacity curve in the case of the CR_LFINF_CDM_11_HEX_2, which flattens out after the yield point. In this case we observe transitions from the existing damage state, caused by the loading in the first step, directly to the highest damage state. This phenomenon has also been observed by Petrone et al. (2020). This phenomenon is not observed in the case of the CR_LWAL_CDN_HEX_4 type model, whose capacity curve remains sloped after yield. In such cases, the hardening could be artificially increased in the moment-curvature laws for the structural elements of the models in order to introduce some hardening in the capacity curve of the building model. Nevertheless, this could introduce a bias in the fragilities and would require further investigation.

6 TOWARDS MULTI-HAZARD LIFE-CYCLE CONSEQUENCE ANALYSIS OF DETERIORATING ENGINEERING SYSTEMS

In its first part, this section proposes a Markovian framework for multi-hazard life-cycle consequence (LCCon) analysis of deteriorating engineering systems (e.g., buildings and infrastructure components) that builds upon classical hypotheses for performance-based engineering, separating the modelling of hazard events and the impact that those events impose on an engineering system. The framework leverages the Markovian assumption, which assumes the memoryless property (or Markov property) of a stochastic process (e.g., Bonamente, 2017) – i.e., the future state of the process depends only on its current state and not on any of its past states – to adequately model structural/non-structural damage (or damage-accumulation) and/or functional impairment (e.g., Iervolino et al., 2016). This allows, in turn, modelling of a system's dynamic performance (deterioration and/or recovery) in the aftermath of multiple interacting hazard events and their associated consequences, as well as the interplay between a system's performance deterioration and recovery (**Erreur ! Source du renvoi introuvable.**).

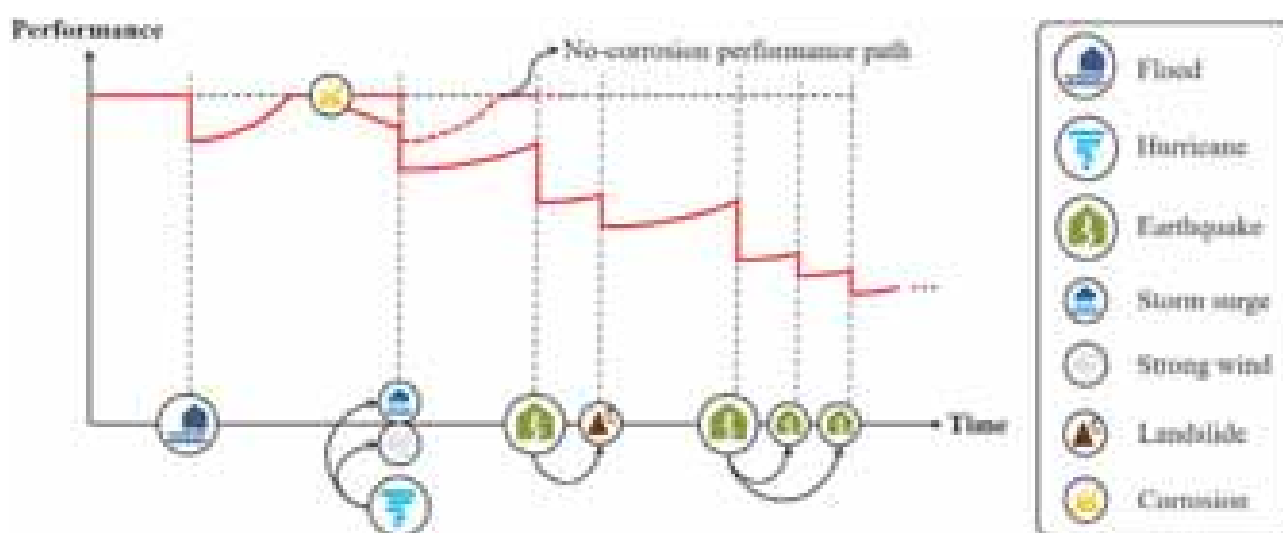


Figure 6-1: Performance path due to multiple interacting hazard events during an engineering system's service life.

In its second part, this section proposes an end-to-end computational framework for simulation-based life-cycle consequence analysis of reinforced-concrete (RC) buildings subjected to earthquake- and environment-induced damage accumulation: i.e., the analysis of seismically pre-damaged buildings (e.g., multiple mainshocks or seismic sequences in the form of mainshock-aftershock and aftershock-aftershock sequences) under chloride-induced corrosion attacks.

6.1 An analytical approach: Markovian framework for multi-hazard life-cycle consequence analysis of deteriorating engineering systems

6.1.1 General framework and definitions

In the proposed framework, the evolution of an engineering system's performance over time is modelled as a discrete-time, discrete-state Markov process (i.e., the system performance jumps between discrete states in fixed time intervals; e.g., Iervolino et al., 2016). Specifically, the system's performance domain is partitioned into mutually exclusive and collectively exhaustive performance levels or limit states (LSs). Such LSs should be represented using a single consistent scale valid for different hazard types since specific hazard events can cause distinct modes of performance decline to a system (e.g., earthquake- and flood-related events can induce distinct damage mechanisms). Different scales for the LSs may be needed when analysing multiple consequence metrics (e.g., repair and disruption costs). For instance, to calculate the disruption cost after a

hazard event, a valid (hazard-agnostic) scale could be defined based on its implications for post-hazard-event functionality and recovery. In such a case, the system could be classified as fully functional with insignificant damage, functional with damage triggering inspection, occupiable with functionality loss, unoccupiable but repairable, and irreparable (e.g., Burton et al., 2016).

The Markovian assumption is used to compute the probability of a system being in any LS at any given time during its service life. Both instantaneous deterioration processes (e.g., hazard events) and gradual deterioration processes (e.g., environment-induced corrosion) cause transitions between LSs. The transition probabilities refer to the probabilities that after one event (or after a specific time has elapsed) the system is in the m -th LS, given that it was in the n -th LS (for $n < m$). They are derived employing state-dependent fragility relationships (defining the probability of exceeding an LS given a hazard intensity measure, IM, and given a lower LS achieved during a preceding event; e.g., Otárola et al., 2022b) and hazard curves/surfaces (defining the annual rate of exceeding a hazard IM). The transition probabilities due to a recovery process between LSs refer to the probabilities that after a given time interval, the system is in the n -th LS, given that it was in the m -th LS (for $n < m$). They are derived, for instance, employing state-dependent recovery relationships (defining the probability of exceeding the recovery time for a LS given a higher LS achieved during a preceding event; e.g., Badal & Tesfamariam, 2023).

The transition matrices (i.e., the stochastic square matrices used to describe the LS transitions) are assembled by collecting each (n,m) transition probability between LSs. The transition matrices can be used in closed-form formulations to obtain the probability mass function (PMF) for the LSs at any time during the life cycle. The resulting expected LCCon estimates are then obtained by combining the LSs' PMF with suitable deterministic/probabilistic system-level consequence models through the total probability theorem (e.g., Aljawhari et al., 2023). The formulation builds upon classical hypotheses for performance-based engineering, separating the modelling of hazard events and the impact that those events impose on an engineering system. As such, two modelling stages can be identified (adapted from Zaghi et al., 2016): 1) hazard modelling, considering interactions through the nature of the hazards (Level I interactions; i.e., the interactions that are independent of the presence of a physical asset; e.g., a landslide triggered by an earthquake event); 2) vulnerability modelling, considering the interactions resulting from the impact of the hazards on a physical asset, regardless of the interactions through the nature of the hazards (Level II interactions; e.g., damage accumulation due to earthquake-induced ground-motion sequences).

6.1.1.1 Interactions across hazards

It is well-established that natural hazards can interact due to interdependencies in hazard frequencies and characteristics or the triggering or intensifying/diminishing effect of one hazard type upon another (e.g., Iannacone et al., 2023). These interactions are classified as *Level I interactions*. For example, earthquakes can trigger landslides or tsunamis. Similarly, hurricanes can cause storm surges and floods, inducing subsequent erosion and coastal inundation. Furthermore, natural hazards can interact through their impacts (effects) on physical assets regardless of the interactions between the hazards. These interactions are classified as *Level II interactions*. For instance, a severe earthquake event can damage critical infrastructure such as bridges and water networks, leading to cascading effects such as road/water network closures and resulting in human casualties and/or diseases. Moreover, a sequence of earthquakes can lead to the accumulation of (physical) damage within a system, thereby magnifying the potential consequences of each individual event. Figure 6-2 shows a schematic representation of the identified interactions.

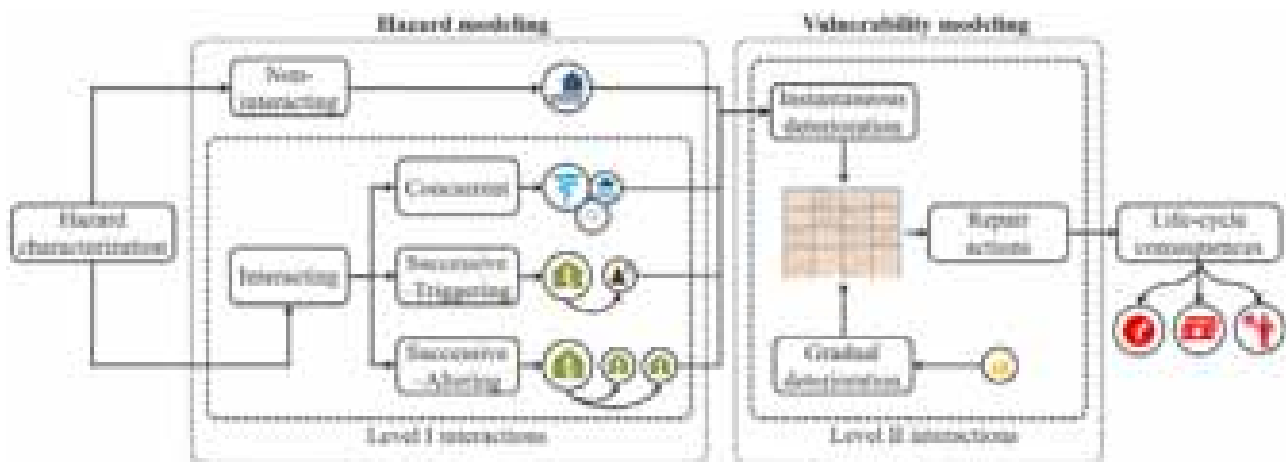


Figure 6-2: Hazard and vulnerability modelling accounting for Level I and Level II interactions across multiple hazards.

6.1.1.1.1 Level I interactions (through the nature of hazards)

Level I (i.e., occurrence) interactions occur inherently due to the nature of the hazards, independently of the presence of physical assets. In the hazard modelling stage, hazard types/events can be subclassified for probabilistic modelling purposes in:

- *Non-interacting*: independent hazard types/events whose occurrence/severity is not affected by the simultaneous or preceding occurrence of other hazard types/events (e.g., earthquakes and hurricanes; i.e., hazard types/events with no causal relationships);
- *Interacting*: dependent hazard types/events whose occurrence/severity can be attributed to the simultaneous or preceding occurrence of other hazard types/events (e.g., landslides induced by an earthquake; i.e., hazard types/events having causal relationships). Interacting hazard types/events can be additionally subdivided into (Iannacone et al., 2023):
 1. *Concurrent*: Hazard types/events that co-occur or have a significant joint probability of occurrence in an interval of time and in a spatial location (e.g., heavy rain, storm surge, sea waves, and strong wind that co-occur during a hurricane);
 2. *Successive*: Hazard types/events having a causal relationship between a primary and secondary type(s)/event(s); these causal relationships depend on the hazard types/events involved, and two broad categories can be further identified:
 - a) *Successive – Triggering*: a secondary hazard type/event is immediately triggered after the occurrence of a primary hazard type/event;
 - b) *Successive – Altering*: the rate of occurrence of a secondary hazard type/event increases following the occurrence of a primary hazard type/event.

The classifications considered in this study only account for the temporal dependencies across hazards, and the spatial dimension and its implications (regarding hazard interactions) are disregarded. However, the inclusion of spatial dependencies is envisioned for future applications.

6.1.1.1.2 Level II interactions (through the impacts of hazards)

Level II (i.e., consequence) interactions occur through impacts/consequences on physical assets (e.g., described by LSs) given multiple hazard types/events. In the vulnerability modelling stage, hazard types/events can also be subclassified for probabilistic modelling purposes into those causing 1) *instantaneous* performance deterioration (shocks occurring at a point in time, e.g., earthquake-induced ground motions); 2) *gradual* performance deterioration (ageing and/or deteriorating mechanisms over time; e.g., environment-induced steel rebars' corrosion). The effects of such deterioration processes can be exacerbated due to dynamic changes in

the structural/non-structural components' fragility (e.g., damage accumulation) and/or the cumulative failure of these components, causing cascading consequences. In contrast, a system's performance can be recovered (i.e., improved from the current state) due to possible repair actions executed between hazard types/events. Specific repair actions are taken following the occurrence of events causing instantaneous deterioration and may differ across events (e.g., repair actions following an earthquake differ from repair actions following a flood). This study does not consider repair actions taken to reduce the effects of gradual deterioration. Nonetheless, it is possible to alter this assumption as needed (e.g., Tao et al., 2021).

6.1.2 Analytical formulation

This section presents the analytical formulation for estimating the expected life-cycle consequences of an engineering system subject to multiple hazards. The formulation adopts a top-down perspective, initiating with the description of a general probabilistic modelling approach to assess the LCCon and concluding with a set of probabilistic modelling approaches to computing the necessary transition matrices given the various interaction definitions above. The expected LCCon is estimated as the sum of the expected consequences in N_t fixed time intervals of length δt during a system's service life t_{LC} , where $N_t = t_{LC}/\delta t$. By selecting a sufficiently small δt such that only one primary hazard event is likely within each interval (i.e., for $v_T \delta t \ll 1$) and guaranteeing that the related secondary event(s) (when applicable) can occur within this interval (e.g., months), the expected LCCon estimates can be computed as,

$$E[Con] = \sum_{m=1}^{N_t} E[Con|LS] P(LS)_{m\delta t}^T \quad (1)$$

In Equation (1), $E[Con|LS]$ is a vector of expected consequences associated with each LS (e.g., system-level consequence models; e.g., Aljawhari et al., 2023), and $P(LS)_{m\delta t}$ is the $1 \times N_{LS}$ probability mass function (PMF) of the system's performance LSs at time $m\delta t$ (after m time steps of length δt) for a total of N_{LS} LSs, computed as (adapted from Iervolino et al., 2016),

$$P(LS)_{m\delta t} = P(LS)_0 \prod_{n=1}^m [v_T T_I T_{G,\delta t} T_{R,\delta t} + (1 - v_T) T_{G,\delta t} T_{R,\delta t}] \quad (2)$$

In Equation (2), $P(LS)_0$ is the $1 \times N_{LS}$ PMF of the system's performance LSs at initial conditions, v_T is the combined (i.e., total) rate of occurrence of independent hazard types (i.e., individual hazard types with no Level I interactions) and/or hazard clusters (i.e., a primary hazard type/event inducing secondary hazard types/events) impacting an engineering system, relying on the assumption that independent hazard types and hazard clusters follow competing homogeneous Poisson processes, obtained as,

$$v_T = \sum_{h=1}^{N_h} v_h \quad (3)$$

In Equation (3), v_h ($h = 1, \dots, N_h$) is the rate of occurrence of the h -th primary hazard type for a total of N_h independent hazard types and/or hazard clusters. In Equation (2), the $N_{LS} \times N_{LS}$ transition probability matrices T_I , $T_{G,\delta t}$, and $T_{R,\delta t}$ are associated with instantaneous deterioration, gradual deterioration, and repair actions occurring in a time step of length δt , respectively. The use of a consistent scale (for LSs) ensures that the definition of these matrices is meaningful. The matrix T_I is obtained combining the matrices, T_{I_h} (i.e., the transition probability matrices due to the occurrence of the h -th independent hazard type or hazard cluster), as,

$$T_I = \sum_{h=1}^{N_h} \frac{v_h}{v_T} T_{I_h} \quad (4)$$

The matrix $T_{G,\delta t}$ is obtained from gradual deterioration models (e.g., Duracrete, 2000) after the deterioration process initiation time (t_i ; assuming a constant gradual deterioration rate at each time step of length δt). It is

worth mentioning that before the t_i , there is no gradual deterioration in the engineering system. The matrix $T_{R,\delta t}$ is obtained (analogously to the matrix T_I) combining the matrices, $T_{R,\delta t,h}$ (i.e., transition probability matrices due to the recovery actions expected to be taken after the occurrence of the h -th independent hazard type or hazard cluster in a time step of length δt), as,

$$T_{R,\delta t} = \sum_{h=1}^{N_h} \frac{v_h}{v_T} T_{R,\delta t,h} \quad (5)$$

The rationale behind Equation (3) to (5) is that clusters of interacting hazard events exhibit the same rate of occurrence as the primary hazard type (e.g., Iervolino et al., 2020). For example, in scenarios involving mainshock-aftershock sequences or mainshock-landslide sequences, the mainshock event is considered a primary hazard event, and the subsequent event(s) can be conceptualised as clusters that plausibly follow the same rate of occurrence as the mainshock. Given this context, the performance path presented in **Erreur ! Source du renvoi introuvable.** can be thus simplified, as shown in Figure 6-3, since, in essence, the decreases in performance as a consequence of individual hazard events within a cluster may be conceptualised as an aggregate decrease attributed to the entirety of such a cluster, provided that no repair actions occur between events. This assumption is reasonable since planning, approving, and executing recovery measures is usually unfeasible within the time span between hazards within the same cluster (e.g., Molina Hutt et al., 2022). However, this assumption can be relaxed (e.g., Iervolino & Giorgio, 2022).

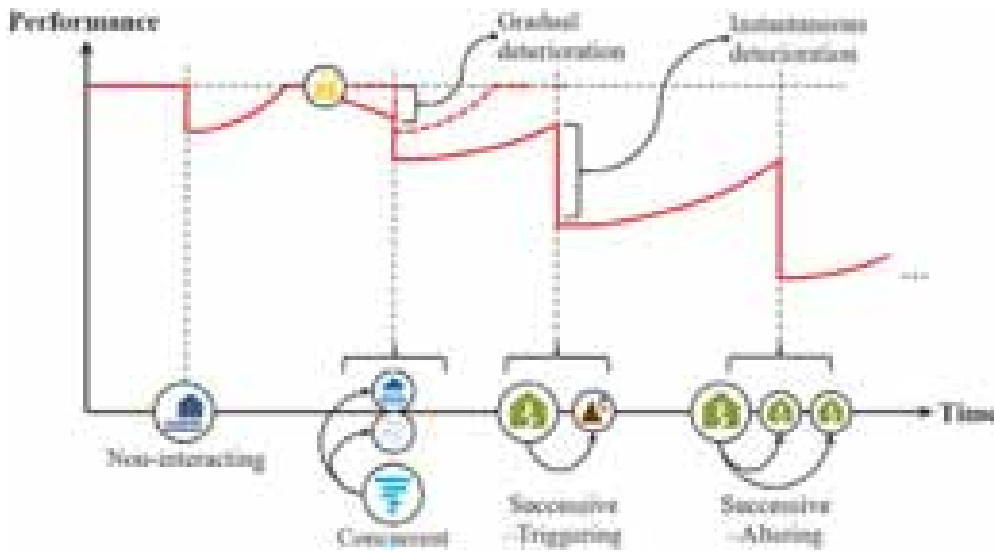


Figure 6-3: Adjusted performance path due to multiple interacting hazard events during a structural system's service life.

6.1.2.1 Instantaneous deterioration transition matrix

The instantaneous deterioration transition matrix (i.e., T_I) only has diagonal and upper-triangular entries corresponding to the probabilities of transitioning from a given LS to a higher LS (i.e., a transition between progressively worse LSs) or staying at the same LS after a hazard event. It is obtained from the transition matrix of the individual hazard types T_{I_h} (i.e., related to independent hazards or hazard clusters following the no-repair assumption made before). In this section, the methods to assemble T_{I_h} are detailed for four cases, according to the Level I interaction definitions:

1. hazard type h is a non-interacting hazard, not affecting the occurrence of other hazard events (e.g., mainshock followed by a non-interacting flood event);

2. hazard type h induces the simultaneous occurrence of other multiple concurrent hazard events (e.g., storm surge, heavy rain, and strong wind that follow a hurricane);
3. hazard type h is the primary hazard type of a series of successive hazard events with a triggering interaction (e.g., mainshock followed by a landslide);
4. hazard type h is the primary hazard type of a series of successive hazard events with an altering interaction (e.g., mainshock followed by an aftershock).

It is worth recalling that, as presented in Figure 6-2, Level II interactions can always occur, independently of the nature of Level I interactions. Thus, cascading consequences can be expected for any of the specified cases (i.e., 1-4), even between two independent hazard types, if they occur close in time (e.g., within a short time interval) and space. In the following, equations accounting for interactions between two hazards are shown. However, such equations can generally be adapted for cases including more than two distinct hazard types. Also, the equations refer to a single intensity measure associated with each hazard type. However, in general, multiple intensity measures may be possible (e.g., Otárola et al., 2023).

6.1.2.1.1 Non-interacting hazards

If hazard type h does not interact with any other hazard types through their nature or, in other words, at Level I, the (n, m) entry of the matrix \mathbf{T}_{I_h} is obtained by total probability theorem as,

$$\mathbf{T}_{I_h}(n, m) = \int_{-\infty}^{\infty} P(LS_m | LS_n, IM) f_{IM}(im) dim \quad (6)$$

In Equation (6), $f_{IM}(im)$ is the probability density function (PDF) of the hazard's intensity measure, which can be obtained from probabilistic hazard analysis as in current performance-based engineering practice and $P(LS_m | LS_n, IM)$ is the probability that a system in the n -th LS transitions to the m -th LS after a hazard event of intensity IM , which can be obtained using state-dependent fragility relationships (e.g., Otárola et al., 2022b). The methods to obtain the state-dependent fragility relationships depend on the level II (i.e., consequence) interactions between the consecutive hazards. In general, two distinct cases can be identified based on the damage process: 1) cumulative: the hazard events cause structural/non-structural damage accumulation in the respective components and $P(LS_m | LS_n, IM)$ should be modelled analytically, accounting for the likely physical interactions (e.g., seismic sequences acting concurrently with corrosion deterioration; e.g., Otárola et al., 2022a); 2) non-cumulative: the hazard events do not cause structural/non-structural damage accumulation in the component and $P(LS_m | LS_n, IM)$ correspond to $P(LS_m | LS_0, IM)$ (e.g., flood-flood sequences causing the increasing, yet independent, failure of non-structural components; e.g., Nofal & van de Lindt, 2020).

6.1.2.1.2 Concurrent hazards

If h -th hazard type induces the simultaneous occurrence of two other concurrent hazard events (i.e., the hazards co-occur at a certain point in time and space), the joint PDF of the intensity measures of the associated hazard events, $f_{IM_1, IM_2}(im_1, im_2)$, can be obtained from vector-valued probabilistic hazard analysis (e.g., by multivariate Normal distributions or Copulas; e.g., Lan et al., 2022). The probability that a system in the n -th LS transitions to the m -th LS after the concurrent hazard events with intensities IM_1 and IM_2 , $P(LS_m | LS_n, IM_1, IM_2)$, is computed using state-dependent fragility surfaces, similarly obtained as in Section 6.1.2.1.1. The (n, m) entry of the matrix \mathbf{T}_{I_h} is obtained as,

$$\mathbf{T}_{I_h}(n, m) = \int_{-\infty}^{\infty} \int_{-\infty}^{\infty} P(LS_m | LS_n, IM_1, IM_2) f_{IM_1, IM_2}(im_1, im_2) dim_1 dim_2 \quad (7)$$

6.1.2.1.3 Successive – Triggering hazard

If h -th hazard type is the primary hazard of a successive triggering interaction, the PDF of the secondary hazard's intensity measure given the primary hazard's intensity measure, $f_{IM_2 | IM_1}(im_2 | im_1)$, can be obtained

from probabilistic hazard analysis that accounts for the probability of triggering a secondary event given the primary one (e.g., Gasparini & Garcia, 2014). The probability that a system in the n -th LS transitions to the m -th LS after a primary event of intensity IM_1 and a secondary one of intensity IM_2 , $P(LS_m|LS_n, IM_1, IM_2)$, is obtained using state-dependent fragility surfaces, similarly obtained as in Section 6.1.2.1.1. The (n, m) entry of the matrix \mathbf{T}_{I_h} can be obtained as,

$$\mathbf{T}_{I_h}(n, m) = \int_{-\infty}^{\infty} \int_{-\infty}^{\infty} P(LS_m|LS_n, IM_1, IM_2) f_{IM_2|IM_1}(im_2|im_1) f_{IM_1}(im_1) dim_1 dim_2 \quad (8)$$

6.1.2.1.4 Successive – Altering hazard

If h -th hazard type is the primary hazard of a successive altering interaction having a $1 \times k$ vector of event characteristics ($\boldsymbol{\theta}$), the transition matrix related to the primary hazard $\mathbf{T}_{I_{h1}}$ can be conditioned on $\boldsymbol{\theta}$ (i.e., $\mathbf{T}_{I_{h1}|\boldsymbol{\theta}}$; computed similarly to Section 6.1.2.1.1, yet conditioning on $\boldsymbol{\theta}$). A conditional rate of occurrence is then used for the secondary hazards (i.e., a time-dependent occurrence model; e.g., Iannacone et al., 2023) to obtain: 1) the PDF of the secondary hazard events given $\boldsymbol{\theta}$, $f_{IM_2|\boldsymbol{\theta}}(im_2|\boldsymbol{\theta})$; and 2) the expected number of secondary hazard events caused by the primary hazard in δt , $E[N_{h2|\boldsymbol{\theta}}(0, \delta t)]$. The (n, m) entry of the transition matrix of a single instance of the secondary hazard $\mathbf{T}_{I_{h2}|\boldsymbol{\theta}}$ is obtained as,

$$\mathbf{T}_{I_{h2}|\boldsymbol{\theta}}(n, m) = \int_{-\infty}^{\infty} P(LS_m|LS_n, IM_2) f_{IM_2|\boldsymbol{\theta}}(im_2|\boldsymbol{\theta}) dim_2 \quad (9)$$

In Equation (9), $P(LS_m|LS_n, IM_2)$ is similarly calculated as in Section 6.1.2.1.1. The transition matrix for the entire sequence of events (i.e., a cluster composed of a primary hazard event and subsequent secondary hazard events) is obtained through the total probability theorem integrating over the possible range of $\boldsymbol{\theta}$ as in Equation (10), which is a k -fold integral where $f(\boldsymbol{\theta})$ is the PDF of each of the k -th event characteristic.

$$\mathbf{T}_{I_h} = \int_{\boldsymbol{\theta}} \left\{ \mathbf{T}_{I_{h1}|\boldsymbol{\theta}} \left(\mathbf{T}_{I_{h2}|\boldsymbol{\theta}} \right)^{E[N_{h2|\boldsymbol{\theta}}(0, \delta t)]} \right\} f(\boldsymbol{\theta}) d\boldsymbol{\theta} \quad (10)$$

6.1.2.2 Gradual deterioration transition matrix

Before the initiation time (i.e., t_i) of the gradual deterioration, there is no transition between LSs. Thereby, the gradual-type deterioration transition matrix (i.e., $\mathbf{T}_{G, \delta t}$) is numerically equal to the identity matrix ($\mathbf{T}_{G, \delta t} = \mathbf{I}$). After t_i , the system starts transitioning from a given LS to a higher LS (i.e., a transition between progressively worse LSs) or staying at the same LS, and $\mathbf{T}_{G, \delta t}$ becomes an upper-triangular matrix whose entries correspond to the probability of transitioning during δt , valid for $t > t_i$. Several probabilistic models can be used to model a system's gradual deterioration (e.g., Duracrete, 2000) and, thus, to obtain the (n, m) entry of the matrix $\mathbf{T}_{G, \delta t}$. In the described procedure, gradual deterioration is treated for modelling purposes as the impact of small shocks, and in general, the (n, m) entry of the matrix $\mathbf{T}_{G, \delta t}$ is obtained as,

$$\mathbf{T}_{G, \delta t}(n, m) = \begin{cases} P(LS_m|LS_n, t) & \text{if } n < m \\ 1 - \sum_{k=1}^{N_{LS}} \mathbf{T}_{G, \delta t}(n, k) & \text{if } n = m \\ 0 & \text{if } n > m \end{cases} \quad (11)$$

The matrix $\mathbf{T}_{G, \delta t}$ can be directly estimated from a \mathbf{T}_{I+G} transition probability matrix defined as a function of instantaneous and gradual deterioration processes simultaneously (i.e., assembled using time- and state-dependent fragility relationships; e.g., Otárola, Iannacone, et al., 2023b) by simply dividing the $\mathbf{T}_{I+G, (0, t+\delta t)}$ over $\mathbf{T}_{I+G, (0, t)}$ matrix, between time t and $t + \delta t$ (given $t > t_i$). Specifically, for each δt , a \mathbf{T}_{I+G} transition

matrix can be assembled considering instantaneous and gradual deterioration (i.e., such a matrix is not stationary); therefore, describing a non-homogeneous Markov process. If the ratio between $\mathbf{T}_{I+G,(0,t+\delta t)}$ over $\mathbf{T}_{I+G,(0,t)}$ is taken as mentioned above, the resultant matrix corresponds to the one associated with gradual deterioration (i.e., $\mathbf{T}_{G,\delta t}$), as a function of time (i.e., the matrix is also not stationary). This study utilises this approach, and it can be expressed as,

$$\mathbf{T}_{G,\delta t}(n, m) = \mathbf{T}_{I+G,(0,t+\delta t)}(\mathbf{T}_{I+G,(0,t)})^{-1} \quad (12)$$

6.1.2.3 Recovery transition matrix

The repair recovery transition matrix (i.e., $\mathbf{T}_{R,\delta t}$) only has diagonal and lower-triangular entries relating to the probabilities of transitioning from a given LS to a lower LS (i.e., a transition between progressively better LSs) or staying in the same LS as the structural system recovers with time. The repair actions are modelled through a Poisson process. The daily rate of occurrence of an event where the system is recovered from a worse LS to a better LS is assumed as the inverse of the difference between the mean repair times for each LS, $t_{rep}(n, m)$. This time difference does not necessarily correspond to the mean repair times associated with transitioning between state-dependent LSs; however, this is the simplest approximation to a potential recovery path between the LSs. The values of $t_{rep}(n, m)$ are only defined for $n > m$, and they can be found in the literature (e.g., Burton et al., 2016). The (n, m) entry of the matrix $\mathbf{T}_{R,\delta t}$ is obtained as,

$$\mathbf{T}_{R,\delta t}(n, m) = \begin{cases} P(LS_m|LS_n, \delta t) & \text{if } n > m \\ 1 - \sum_{k=1}^{N_{LS}} \mathbf{T}_{R,\delta t}(n, k) & \text{if } n = m \\ 0 & \text{if } n < m \end{cases} \quad (13)$$

The δt must be expressed in the same units than $t_{rep}(n, m)$. It is worth noting that several recovery models are available in the literature (e.g., Badal & Tesfamariam, 2023), and they are applicable in this framework with reasonable adjustments in Equation (13) (i.e., modifying $P(LS_m|LS_n, \delta t)$, as appropriate to account for the particularities of such recovery models). In Equation (13), $P(LS_m|LS_n, \delta t)$ is the probability of being in a LS_m given the δt (or Δt_j when applicable) and a prior LS . In Equation (13), $P(LS_m|LS_n, \delta t)$ is the probability of being in a LS_m given the δt (or Δt_j when applicable) and a prior LS , computed as in Equation (14), corresponding to the subtraction of two exponential cumulative density functions, as,

$$P(LS_m|LS_n, \delta t) = e^{-\left[\frac{1}{t_{rep}(n,m+1)}\delta t\right]} - e^{-\left[\frac{1}{t_{rep}(n,m)}\delta t\right]} \quad (14)$$

Figure 6-4 displays the general appearance of the three transition matrices (i.e., \mathbf{T}_I and $\mathbf{T}_{G,\delta t}$ as deterioration processes, and $\mathbf{T}_{R,\delta t}$ as a recovery process) used in this study.

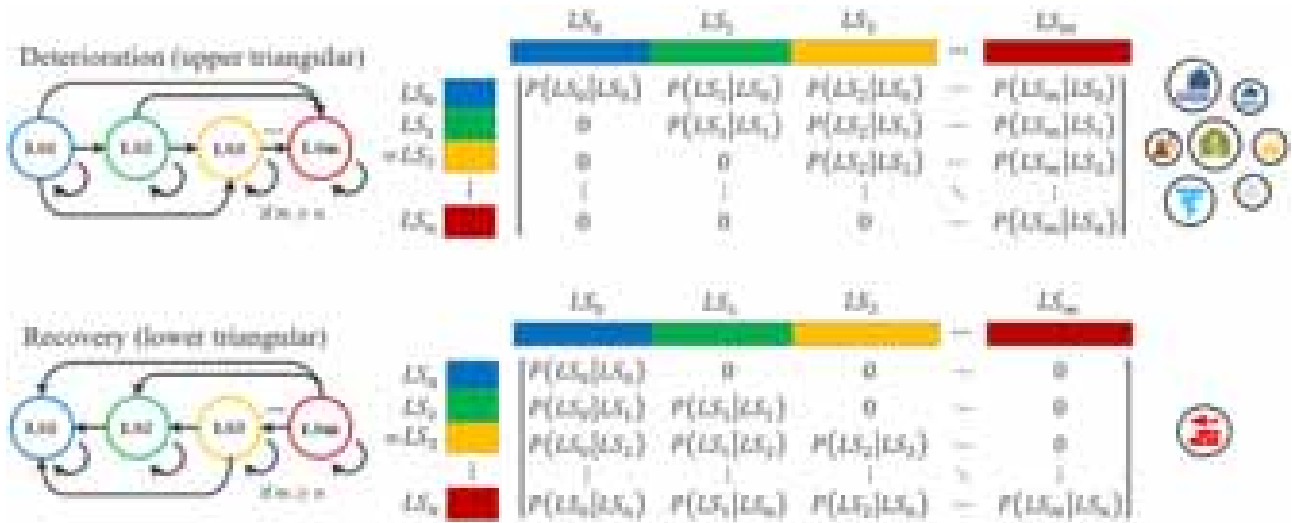


Figure 6-4: General transition matrix shapes for deterioration (i.e., T_I and $T_{G,\delta t}$) and recovery (i.e., $T_{R,\delta t}$) processes.

6.1.3 Illustrative applications

6.1.3.1 Case study: deteriorating reinforced concrete building

The proposed framework is demonstrated using an archetype four-story, four-bay, moment-resisting reinforced concrete building assumed representative of a “Colleges/Universities” occupancy class (Federal Emergency Management Agency (FEMA), 2020), with a replacement cost equal to €900/m² (Cardone & Perrone, 2017). Such a building represents a typical vulnerability class in Southern Europe. It is characterised by a total height equal to 13.5 m (i.e., a first story of 4.5 m and upper stories of 3.0 m) and a total width in both horizontal directions equal to 18.0 m (i.e., bay spans of 4.5 m). It comprises beams and columns with 30x50 cm cross sections, designed and detailed according to the Eurocode 8 Part 3 seismic provisions for high ductility class structures (Eurocode 8, 2005), as detailed in Otárola, Iannacone, et al., 2023b. The inventory of the non-structural components is assumed to be the same on each occupiable floor (i.e., excluding the building rooftop), adapted from Shahnazaryan et al., 2021 (for this particular case study).

The building is assumed to undergo earthquake-induced ground motions and flood inundations while experiencing environment-induced corrosion in marine splash exposure. Various rates of occurrence are evaluated to ascertain the impact of, for instance, frequent/rare and intense events on the LCCon estimates. Specifically, the earthquake rates of occurrence (v_E) are: 1) 0.05; 2) 0.20; 3) 0.35 per year, while the flood rates of occurrence (v_F) are: 1) 0.50; 2) 1.00; 3) 1.50 per year. Given this assumption, this application should be considered ideal and illustrative rather than representative of any specific setting and location. The assumed (dummy, yet realistic; e.g., Otárola et al., 2023) hazard curves for earthquakes (using average spectral acceleration, $avgSA$, as IM) and floods (using the height of the water, H_W , as IM; i.e., low flow velocities) can be seen in Figure 6-5a and b, respectively. The utilised averaged 95th percentile corrosion level curve is obtained from Duracrete, 2000, using the corresponding (i.e., introduced) corrosion-penetration model.

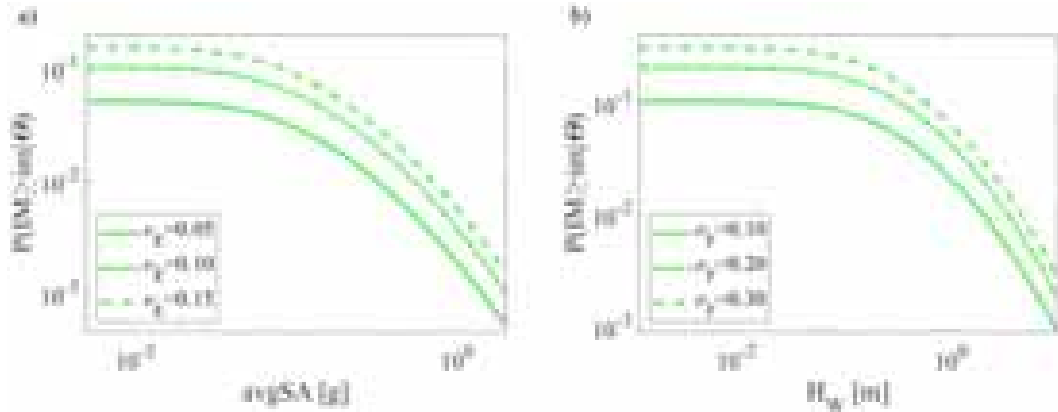


Figure 6-5: a) Earthquake hazard curves; b) flood hazard curves. θ : conditioning hazard event characteristics.

The expected LCCon's are expressed in terms of the total life-cycle cost of the engineering system ($E[C_T]$), considering a nominal service life of 50 years. Such an estimate can be subdivided into three constituent parts:

1. construction cost (C_0);
2. maintenance cost (C_M);
3. expected hazard-induced cost ($E[C]$)

While the costs associated with points (1-2) are deterministic, the estimation of $E[C]$ requires the LCCon analysis of the engineering system (i.e., $E[C] = E[Con]$ from Equation (1)). To streamline its calculation, this metric is further subdivided into two elements, as follows:

- a) expected hazard-induced direct cost ($E[C_D]$), quantified in terms of the repair/replacement expenses of damaged structural/nonstructural components due to potential hazard events;
- b) expected hazard-induced indirect cost ($E[C_I]$), quantified in terms of rental and disruption expenses (additional indirect costs like the income loss are omitted for brevity).

Firstly, to calculate $E[C_D]$, five performance LSs are adopted in terms of the observable structural/non-structural damage (often referred to as damage states, DSs), defined as (e.g., Otárola et al., 2023):

- null damage (LS_0);
- slight damage (LS_1);
- moderate damage (LS_2);
- severe damage (LS_3);
- complete damage (LS_4).

The structural-related direct repair cost is exclusively linked to earthquake-induced damage since this study assumes that flood events exclusively impact non-structural components (e.g., the system is protected against scour through short-pile foundations and the flood flow velocity is negligible). The earthquake state-dependent fragility relationships used to assemble the instantaneous deterioration transition matrix, T_I , and the gradual deterioration matrix, $T_{G,\delta t}$, are those developed in Otárola, Iannacone, et al., 2023b. The consequence model

related to earthquake-induced structural damage corresponds to that shown in the HAZUS Earthquake Model Technical Manual (HAZUS-MH 5.1, 2022a); $E[C_D|LS] = [0, 0.002, 0.011, 0.055, 0.11]C_0$. The state-dependent recovery relationships used to assemble the recovery transition matrix, $T_{R,\delta t}$, are derived using the expected recovery times from the HAZUS Earthquake Model Technical Manual (HAZUS-MH 5.1, 2022a) (i.e., 10, 45, 180, and 360 days for LS_1, LS_2, LS_3, LS_4 , respectively).

The state-dependent fragility relationships in Otárola, Iannacone, et al., 2023b are also used to assess non-structural damage and associated costs. The consequence model for non-structural damage is computed using an adaptation of the simulation-based approach by Aljawhari et al., 2023, corresponding to $E[C_D|LS] = [0, 0.18, 0.36, 0.48, 0.89]C_0$. The state-dependent recovery-from-earthquake relationships are derived using the expected recovery times from HAZUS Earthquake Model Technical Manual (HAZUS-MH 5.1, 2022a) (i.e., 10, 45, 180, and 360 days for LS_1, LS_2, LS_3, LS_4 , respectively). The flood state-dependent fragility relationships are derived modelling damage severity ensuring consistent consequences (maintaining a consistent scale) using the approach in Nofal et al., 2020 (i.e., $E[C_D|LS] = [0, 0.18, 0.36, 0.48, 0.89]C_0$ for both earthquakes and floods). The state-dependent recovery-from-flood relationships are derived using the expected recovery times from HAZUS Flood Model Technical Manual (HAZUS-MH 5.1, 2022b) (i.e., 10, 45, 180, and 240 days for LS_1, LS_2, LS_3, LS_4 , respectively). The damage from consecutive flood events is assumed to be equivalent to the damage caused by a single flood event with the same final inundation depth.

To calculate $E[C_I]$, five performance LSs are adopted in terms of the corresponding implications for post-hazard-event functionality and recovery (often referred to as functionality states, FSs), defined as:

- fully functional with insignificant damage (LS_0);
- functional with damage triggering inspection (LS_1);
- occupiable with functionality loss (LS_2);
- unoccupiable but repairable (LS_3);
- irreparable (LS_4).

The indirect relocation and disruption costs are associated with the LSs where the building is tagged unoccupiable (i.e., LS_3 and LS_4). As such, the consequence model for such costs is calculated using the equation from the HAZUS Earthquake Model Technical Manual (HAZUS-MH 5.1, 2022a); in other words,

$$E[C_I|LS] = \begin{cases} 0, & \text{for } LS_0, LS_1, LS_2 \\ FA[(1 - \%OO)DC + \%OO(DC + RC \cdot RT)], & \text{for } LS_3, LS_4 \end{cases} \quad (15)$$

In Equation (15), for “Colleges/Universities” occupancy class, FA is the occupied floor area (1296 m²), $\%OO$ is the percent owner occupied (0.90), DC is the disruption cost (€13.09/m²), RC is the rental cost (€0.62/day/m²), and RT is the expected recovery time from the HAZUS Earthquake Model Technical Manual (HAZUS-MH 5.1, 2022a) (i.e., 10, 45, 180, and 360 days for LS_1, LS_2, LS_3, LS_4 , respectively). The resulting consequence model is equal to $E[C_I|LS] = [0, 0, 0, 0.10, 0.19]C_0$. A transition matrix for such new scale is obtained from the state-dependent fragility relationships for earthquakes, given that a mapping is established between the two scales. This mapping can be performed one-to-one between DSs and FSs for earthquakes (i.e., $DS_1 \rightarrow FS_1$; $DS_4 \rightarrow FS_4$; e.g., Badal & Tesfamariam, 2023). The impact of floods on $E[C_I]$ is negligible, and it is not included in the analysis because floods alone, causing only non-structural damage, cannot cause a transition to LS_2, LS_3 , and LS_4 from lower limit states. Table 6-1 to Table 6-3 show the values of the assembled T_I (with $v_E = 0.05$ and $v_F = 0.10$), $T_{G,\delta t}$, and $T_{R,\delta t}$ transition matrices, with δt expressed in months.

As mentioned, the expected total life-cycle cost can be computed as,

$$E[C_T] = C_0 + C_{M,NPV} + E[C]_{NPV} \quad (16)$$

In Equation (16), both C_M and $E[C]$ have been actualised at the time of construction (Net Present Value, NPV). Namely, $C_{M,NPV}$ is estimated as follows (e.g., Jalayer et al., 2011),

$$C_{M,NPV} = \sum_{m=1}^{N_t} \frac{1}{(1 + \alpha)^{m\delta t}} C_M \quad (17)$$

Table 6-1: Instantaneous deterioration transition probability matrix (T_I). The non-bold values correspond to the T_I only due to earthquake events, and the bold values correspond to the T_I due to earthquake and flood events.

LSs	LS_0	LS_1	LS_2	LS_3	LS_4
LS_0	0.6957/ 0.7356	0.1178/ 0.1856	0.0834/ 0.0391	0.0566/ 0.0235	0.0465/ 0.0161
LS_1	0	0.7646/ 0.9049	0.1245/ 0.0528	0.0642/ 0.0261	0.0468/ 0.0162
LS_2	0	0	0.8665/ 0.9502	0.0851/ 0.0330	0.0485/ 0.0167
LS_3	0	0	0	0.9446/ 0.9809	0.0554/ 0.0191
LS_4	0	0	0	0	1

Table 6-2: Gradual deterioration transition probability matrix ($T_{G,\delta t}$). This transition matrix is only affected by earthquake events and is constant given the assumed linear time-dependent corrosion level curve.

LSs	LS_0	LS_1	LS_2	LS_3	LS_4
LS_0	0.9999	0.0000	0.0000	0.0000	0.0001
LS_1	0	0.9999	0.0000	0.0000	0.0001
LS_2	0	0	0.9999	0.0000	0.0001
LS_3	0	0	0	0.9998	0.0002
LS_4	0	0	0	0	1

Table 6-3: Recovery transition probability matrix ($T_{R,\delta t}$). The non-bold values correspond to the $T_{R,\delta t}$ only due to earthquake events, and the bold values correspond to the $T_{R,\delta t}$ due to earthquake and flood events.

LSs	LS_0	LS_1	LS_2	LS_3	LS_4
LS_0	1	0	0	0	0
LS_1	0.4636/ 0.4636	0.5364/ 0.5364	0	0	0
LS_2	0.3331/ 0.3331	0.4138/ 0.4139	0.2531/ 0.2531	0	0
LS_3	0.0736/ 0.0485	0.0796/ 0.0529	0.1084/ 0.0739	0.7384/ 0.8247	0
LS_4	0.0800/ 0.1050	0.0821/ 0.1089	0.0908/ 0.1253	0.1535/ 0.3135	0.5935/ 0.3473

In Equation (17), $C_M = 0.01 C_0$, α is the discount factor, illustratively assumed to be 0.05. $E[C]_{NPV}$ is obtained as the summation of $E[C_D]_{NPV}$ and $E[C_I]_{NPV}$, estimated as per Equations (18) and (19). The $P(\mathbf{LS})_{m\delta t,D}$ and $P(\mathbf{LS})_{m\delta t,I}$ are PMFs of the system's performance LSs for direct and indirect consequences computed with the respective transition matrices.

$$E[C_D]_{NPV} = \sum_{m=1}^{N_t} \frac{1}{(1 + \alpha)^{m\delta t}} E[C_D | \mathbf{LS}] P(\mathbf{LS})_{m\delta t,D}^T \quad (18)$$

$$E[C_I]_{NPV} = \sum_{m=1}^{N_t} \frac{1}{(1 + \alpha)^{m\delta t}} E[C_I | \mathbf{LS}] P(\mathbf{LS})_{m\delta t,I}^T \quad (19)$$

Figure 6-6a shows the expected hazard-induced life-cycle cost normalised with the cost of construction (i.e., $E[C]/C_0$), starting in pristine conditions (i.e., $P(\mathbf{LS})_0 = [1, 0, 0, 0, 0]$) and using $v_E = 0.05$ and $v_F = 0.10$. The results are disaggregated based on the hazards causing the costs. It can be noticed that the consequences are strongly dominated by the costs associated with the replacement/repair of the non-structural components. In fact, at 50 years, such costs are 20.71% higher than the costs associated with the replacement/repair of the structural components. Moreover, the indirect costs are 12.48% higher than the costs associated with the replacement/repair of the structural components. This indicates that the structural integrity of the case-study building is robust and well-protected against the various hazards it may face. As expected, given the modelling assumptions, it is noticed that the flood structural-related direct cost and flood indirect cost equals zero. Figure 6-6b shows the $E[C_T]/C_0$ including/excluding gradual deterioration, also starting in pristine conditions (i.e., $P(\mathbf{LS})_0 = [1, 0, 0, 0, 0]$) and with $v_E = 0.05$ and $v_F = 0.10$. Specifically, this estimate is shown for four cases:

1. the system is subjected to earthquake and flood events and corrosion deterioration (EQ+FL, Ins+Gra);
2. the system is subjected to earthquake and flood events without corrosion deterioration (EQ+FL, Ins);
3. the system is subjected to earthquake events and corrosion deterioration (EQ, Ins+Gra);
4. the system is subjected to earthquake events without corrosion deterioration (EQ, Ins).

It is clear that flood events, while primarily affecting low-performance LSs, can still yield substantial consequences, confirming the importance of adopting protection measures for non-structural components. Furthermore, it is also evident that corrosion-induced deterioration introduces significant variations in the outcomes, emphasizing that the impact of such a gradual deterioration process should not be overlooked in engineering contexts. The differences between the consequences of including/excluding gradual deterioration are about 4.14% at 50 years. Figure 6-7 presents a sensitivity analysis of the v_E and v_F parameters, to investigate the effects of frequent/rare and intense events on the LCC estimates. As expected, for higher rates of occurrence, the consequences increase accordingly. Nevertheless, no particular/uncommon trends are observed. It is evident that frequent floods can yield higher consequences, particularly those associated with direct non-structural damage. Nevertheless, it is essential to note that even though rare earthquakes occur less frequently, they have the potential to inflict far more devastating consequences than those stemming from frequent floods. This holds when both cases maintain the same probability distribution of IMs. The unique characteristics of each hazard type will determine the extent of their impact.

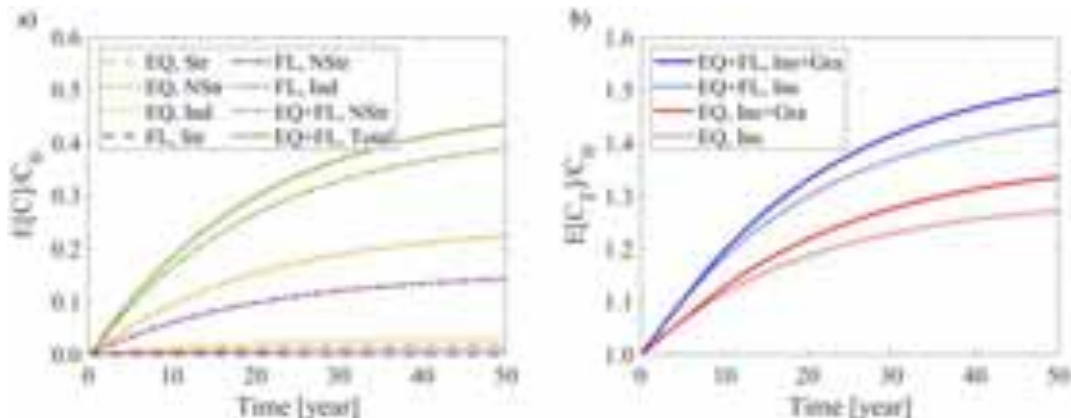


Figure 6-6: a) Normalised expected hazard-induced life-cycle cost of the building under instantaneous deterioration only; b) Normalised expected total life-cycle cost of the building under instantaneous and/or gradual deterioration.

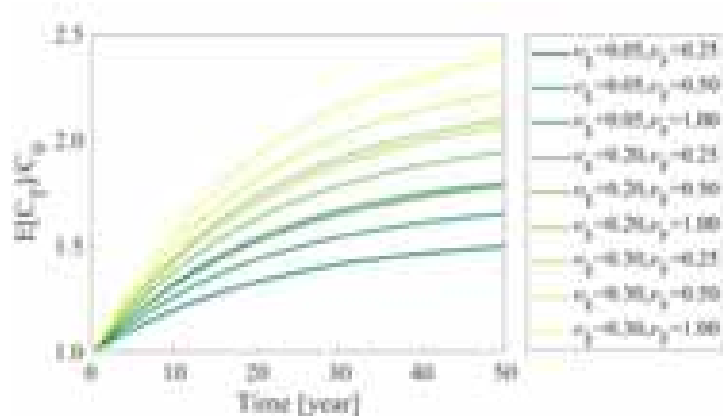


Figure 6-7: Normalised expected total life-cycle cost of the case-study building under instantaneous deterioration only and given various earthquake and flood rates of occurrence.

6.1.3.2 Case study: road network with a deteriorating reinforced concrete bridge

The proposed framework is also demonstrated using a real, symmetric, double-span, box-girder, seat-type bridge; part of a simplified transportation road network. Such a bridge represents a typical vulnerability class used worldwide (e.g., Otárola et al., 2022b) having a high-code design level (e.g., Caltrans, 2019). The bridge is characterised by deck width: 23 m; number of spans: 2; span lengths: 45.7 m; number of columns: 2; columns radius: 0.85 m; columns height: 6.70 m; and it is assumed to be subjected to earthquake-induced ground motions while experiencing environmentally induced corrosion in a marine splash exposure (e.g., Otárola, Iannacone, et al., 2023b). The earthquake rate of occurrence is assumed to be $v_E = 0.05/\text{year}$, and the corresponding assumed hazard curve for earthquakes (using average spectral acceleration, $avgSA$, as IM) can be seen in Figure 6-5a. The adopted averaged 95th percentile corrosion level curve is also adapted from Duracrete, 2000 and its corresponding corrosion-penetration model.

Structural DSs are used to describe the bridge's performance level (i.e., $LS = DS$ in the framework equations) since a unique hazard type inducing instantaneous deterioration is investigated, as in common performance-based engineering practice. In total, five DSs are adopted, corresponding to null (DS_0), slight (DS_1), moderate (DS_2), extensive (DS_3), and complete (DS_4) structural damage (e.g., Otárola et al., 2022b). The state-dependent fragility relationships developed by Otárola et al., 2022b are used to assemble \mathbf{T}_I and the expected repair times from Dehghani et al., 2021 are used to derive state-dependent recovery relationships to assemble $\mathbf{T}_{R,\delta t}$ (i.e., 35, 91, 174, and 339 days for DS_1 , DS_2 , DS_3 , DS_4 , respectively). The values for $\mathbf{T}_{G,\delta t}$ are from the $\mathbf{T}_{I+G,(0,t+\delta t)}$ and $\mathbf{T}_{I+G,(0,t)}$ matrices, as explained already using the averaged 95th percentile corrosion level curve. The different matrices follow the general shape of the transition matrices shown in Figure 6-4, and δt is expressed in months. Table 6-4 to Table 6-6 present the values of the assembled \mathbf{T}_I , $\mathbf{T}_{G,\delta t}$, and $\mathbf{T}_{R,\delta t}$ transition matrices to facilitate the reproducibility of the results attained.

The expected LCCon is estimated in terms of expected welfare loss ($E[\Delta W]$; i.e., a measure of the impact of road network disruption on the commuters' welfare; Silva-Lopez et al., 2022) and considering 75 years as the bridge's service life (i.e., Equation (1) now provides $E[\Delta W] = E[Con]$). A welfare-loss consequence model is developed, associating each DS to a restrictive action that causes an increase in the travel time of the members of the community, namely: 1) DS_0 : no restrictions; 2) DS_1 : speed restrictions; 3) DS_2 : one lane open only; 4) DS_3 : one lane open only and speed restrictions; 5) DS_4 : closure (e.g., Otárola, Iannacone, et al., 2023a). The consequence estimates are obtained from analysing the road network's performance given a restrictive action (Figure 6-8a). The outcome of such analyses is the aggregated travel time of the commuters, T_C , from where the difference in the travel time is obtained as $\Delta T_C = T_C - T_{C,0}$, where $T_{C,0}$ is the travel time

in the “no restrictions” case. To compute ΔT_C , a graph-based approach based on the shortest-path algorithm is implemented (e.g., Dijkstra, 1959). In this regard, the road network is idealised as a directed graph (the travels are assumed to be directed to a unique destination, i.e., node 4). A demand of 500, 500, and 1000 vehicles/h is assumed to originate from nodes 1, 2, and 3, respectively. The links are assumed to be at full capacity with no congestion in the “no restriction” case (i.e., vehicles move at the free flow speed); the free flow speed is assumed as 40, 80, 40, and 80 km/h for the two-lane links 1-2, 1-3, 2-4, and 3-4, respectively. A speed restriction is assumed to reduce the free flow speed to 75% of the original value. A lane closure is assumed to reduce the capacity of the link to the value C^* , causing congestion and changing the aggregated travel time associated with the link, as follows:

$$T_C^* = \frac{C^*}{D} T_{C,0} \quad (20)$$

Table 6-4: Instantaneous deterioration transition probability matrix (T_I).

DSs	DS_0	DS_1	DS_2	DS_3	DS_4
DS_0	0.67348	0.22252	0.08253	0.00968	0.01179
DS_1	0	0.89615	0.08238	0.00946	0.01201
DS_2	0	0	0.96991	0.01626	0.01384
DS_3	0	0	0	0.97980	0.02020
DS_4	0	0	0	0	1

Table 6-5: Gradual deterioration transition probability matrix ($T_{G,\delta t}$).

DSs	DS_0	DS_1	DS_2	DS_3	DS_4
DS_0	0.99946	0.00037	0.00014	0.00002	0.00002
DS_1	0	0.99983	0.00014	0.00002	0.00002
DS_2	0	0	0.99995	0.00003	0.00002
DS_3	0	0	0	0.99997	0.00003
DS_4	0	0	0	0	1

Table 6-6: Recovery transition probability matrix ($T_{R,\delta t}$).

DSs	DS_0	DS_1	DS_2	DS_3	DS_4
DS_0	1	0	0	0	0
DS_1	0.30203	0.69797	0	0	0
DS_2	0.12243	0.21804	0.65952	0	0
DS_3	0.07456	0.10094	0.19271	0.63178	0
DS_4	0.08582	0.09509	0.11564	0.16835	0.53510

In this case study, $C^* = C_0/2$ is assumed, where C_0 is the capacity of the link in the “no restriction” case. No reduction in the demand is assumed between cases. The ΔT_C metric is then used to estimate the welfare loss (ΔW) as in Equation (21), using the same parameters presented in Silva-Lopez et al., 2022, where y is the commuter’s wage rate, assumed to be 17.8 USD/h (the use of such parameters guarantees that the use of Equation (21) is meaningful in this illustrative application; yet, those parameters can vary for other scenarios). Thereby, the consequence model $E[\Delta W|DS] = [0, 52.26, 156.79, 261.32, 522.63]$ is proposed in utils/h. It is worth recalling that utils are utility units, a measure of satisfaction or happiness derived from consuming goods or services. In this case, those associated with commuting time.

$$\Delta W = \frac{1}{2y^{0.26}} \Delta T_C \quad (21)$$

Figure 6-8b shows the expected life-cycle welfare loss for the case-study road network for the bridge starting in pristine conditions (i.e., $P(\mathbf{DS})_0 = [1, 0, 0, 0, 0]$) obtained with the proposed framework. It is apparent that the corrosion-induced deterioration effects can be significant for a bridge whose structural redundancy is limited. Additionally, the expected life-cycle welfare loss of the same bridge upgraded with FRP (i.e., to increase the lateral-resisting system structural capacity; e.g., Dehghani et al., 2021) at $t = 10$ years is presented. Although no explicit structural analysis is conducted, the upgrade is assumed to decrease the fragility median values by a maximum additional of 85% while the dispersion remains constant (e.g., Dehghani et al., 2021). As expected, an enhancement in the bridge's seismic lateral resisting system can significantly reduce its LCC estimates by 17.58%, as also observed in Figure 6-8b. This confirms the flexibility and efficiency of the proposed framework; such improvements can be analysed at any point in time and utilised to showcase the value and/or significance of risk management and adaptation pathways, even when analysing utility networks. This exercise, even if simplified, highlights the framework's potential implementation, and more research is warranted for its further application in complex infrastructure networks, given several hazards and consequence metrics.

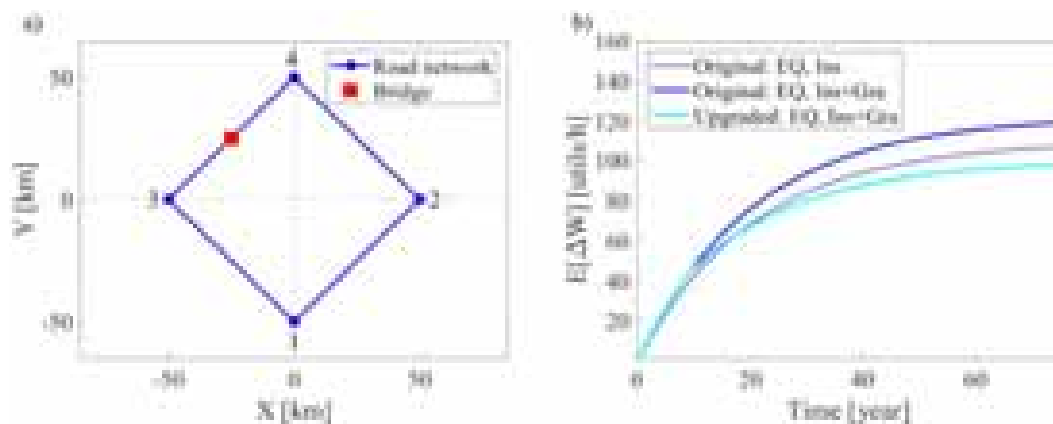


Figure 6-8. a) Transportation road network; b) expected life-cycle welfare loss of the original and upgraded bridge

6.2 A simulation-based approach: Life-cycle consequence analysis of reinforced-concrete buildings subjected to earthquake- and environment-induced damage accumulation

6.2.1 Methodology

6.2.1.1 Case-study building definition

The proposed framework is demonstrated by analysing an archetype case-study RC moment-resisting frame, representing a typical building class in Southern Europe (e.g., Otárola et al., 2023). The frame is characterised by a total height equal to 13.5 m (i.e., a first story of 4.5 m and upper stories of 3.0 m) and a total length equal to 18.0 m (i.e., bay spans of 4.5 m). It includes beams and columns with 30x50 cm cross sections, designed and detailed according to Eurocode 8 Part 3 (e.g., Eurocode 8, 2005) seismic provisions for high ductility class structures. The RC's mechanical properties are selected based on the average of those in the Italian context. The frame's structural response is simulated using a computational finite element model developed in OpenSeesPy. Specific details regarding the case study (e.g., nonlinear modelling procedure implemented) can be found in Otárola, Iannacone, et al., 2023b. It is worth noting that the building represents a modern structure characterised by a special-code design level that might experience steel-rebar corrosion in the future. However, the proposed framework and its implementing methods/models are general and can be applied to any system.

6.2.1.2 Ground-motion sequence assembly

The ground-motion record pairs (representing generic ground-motion sequences, GM1-GM2) are selected using the simulated annealing method (i.e., dual annealing; with the same assumptions as Iacoletti et al., 2023) with average spectral accelerations ($avgSA_{GM1}$ and $avgSA_{GM2}$) nearly following a discrete uniform distribution covering a wide range of values of interest, being consistent with the adopted nonlinear analysis procedure (i.e., cloud-based analysis). The distinct $avgSAs$ (i.e., the adopted IM) are herein calculated using the following spectral acceleration ordinates: $0.2T_1$; $\min[1.5T_2, (T_1+T_2)/2]$; T_1 ; $1.5T_1$; $2.0T_1$ (e.g., Kazantzi & Vamvatsikos, 2015). Specifically, pairs of unscaled GM1 and GM2 records are obtained from a candidate ground-motion database (e.g., NGA-West2 database; e.g., Ancheta et al., 2014) and corresponding scaling factors are defined. For each set of scaled GM1 and GM2 records, a discrete two-dimensional distribution with several bins along the $avgSA_{GM1}$ and $avgSA_{GM2}$ axes is computed (up to a maximum value, $avgSA_{max}$), ensuring these distributions uniformly cover the required range of $avgSA_{GM1}$ and $avgSA_{GM2}$. Specific details regarding this ground-motion record pair selection procedure can be found in Iacoletti et al., 2023.

6.2.1.3 Corrosion deterioration modelling

In the proposed formulation, the impact of uniform and pitting corrosion (e.g., Stewart, 2004) is reflected in the change of various materials' mechanical properties of the structure, namely the steel rebars' cross-sectional area, strength, strains, buckling behaviour, and cyclic deterioration, as well as the concrete cover's and the confined concrete core's strength and strains. Specific details on how to model the impact of corrosion on each of those mechanical properties are presented in Otárola et al., 2022b. The DuraCrete chloride-penetration model (Duracrete, 2000) is employed to obtain realisations of the rate of corrosion (r_c) over time with plain Monte-Carlo sampling. To streamline the simulation of the r_c , a hurdle model is fitted to the N_r total r_c realisations. Hurdle models consist of two components – the first quantifying the probability of attaining a value equal to zero, and the second modelling the probability of the non-zero values (e.g., Cragg, 1971), as per Equation (22). In such an equation, $P(R_c = 0|t)$ is the probability that $r_c = 0$ at time t , and $f_{R_c \neq 0}(r_c|t)$ is a truncated (specifically at $r_c = 0$) probability distribution function modelling the probability of $r_c > 0$ at time t . The truncated Extreme Value – Type I is selected using the Akaike Information Criterion (Akaike, 1974).

$$\begin{cases} P(R_c = 0|t) = \frac{\sum_{r=1}^{N_r} \mathbf{1}_{\{r_c(t)_r=0\}}}{N_r} \\ f_{R_c}(r_c|R_c > 0, t) = f_{R_c \neq 0}(r_c|t) \end{cases} \quad (22)$$

The structural corrosion deterioration level can be measured through a corrosion deterioration parameter (ψ) that can be directly related to the r_c . The adopted ψ corresponds to the steel-rebar diameter loss due to uniform corrosion (non-adjusted for pitting corrosion effects), measured in mm. Such a parameter is obtained as two times the r_c , corresponding to two times the corrosion penetration in the utilised corrosion penetration model. The non-adjusted steel-rebar area loss due to uniform corrosion can be obtained directly using ψ , by simply estimating the area change given the deterioration process. The adjusted steel-rebar area loss due to pitting corrosion can be obtained by multiplying the non-adjusted steel-rebar area loss due to uniform corrosion by the median “area pitting coefficient” obtained from the probabilistic log-normal model introduced in Kashani et al., 2013. In total, ten equally-spaced values for ψ are considered, ranging from $\psi = 0.0$ mm (i.e., pristine conditions) up to $\psi = 1.5$ mm (i.e., a realistic value of ψ at the end of typical buildings' service life; e.g., Du, Clark, et al., 2005; Du, Clark, et al., 2005). For each ψ selected, a single computational finite element model is constructed, facilitating the analysis of the building frame's response across corrosion deterioration levels.

The damage severity in the building is assessed through damage states (DSs). The DS thresholds are defined in terms of the maximum inter-storey drift ratio (θ) obtained by a pushover analysis, according to structure-specific DS descriptions for slight (DS1), moderate (DS2), extensive (DS3), and complete damage (DS4), where DS0 indicates no damage. Specifically, the DS1 threshold is associated with the global yielding strength of the system. At this point, concrete is assumed to be at the onset of visible cracking. The DS2 threshold is

associated with reaching the ultimate strain in the extreme fibres of the columns' concrete cover. At this stage (i.e., spalling strain), potential plastic hinges form due to slippage of the lap-splices (e.g., Hwang et al., 2001; Priestley et al., 1996). The DS3 threshold is associated with the global ultimate strength of the system. At this stage, the system is assumed to have reached its maximum structural capacity and started strain softening. The DS4 threshold is expected to be between DS3 and collapse thresholds. Therefore, this study uses the geometric mean of the two (i.e., DS3 and collapse) as the DS4 threshold (e.g., Ghosh & Sood, 2016). Collapse (i.e., C) is associated either with the attainment of the ultimate strain at the extreme fibres of the columns' core concrete (i.e., compression strain at which transverse column ties start to fracture; e.g., Mander et al., 1988; Paulay & Priestly, 1992), the attainment the fracture strain at the most stressed columns' longitudinal steel rebar, or the attainment of a conventional θ threshold equal to 10%. Figure 6-9 illustrates the obtained pushover capacity curves (i.e., curves of the base-shear coefficient, C_V vs maximum inter-storey drift ratio, θ) and the defined structure-specific DS thresholds for various values of the ψ .

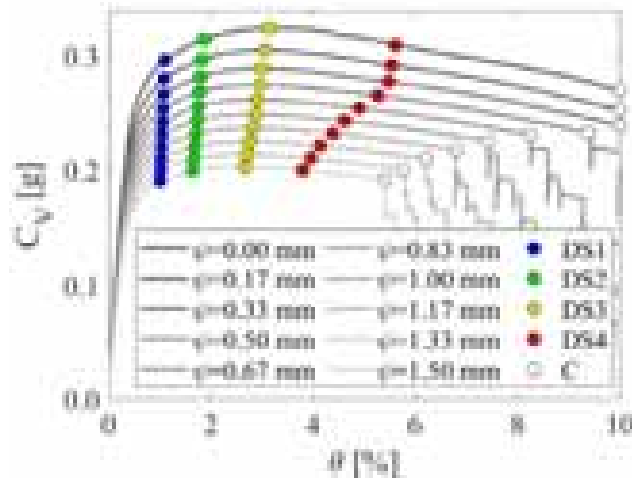


Figure 6-9: Pushover capacity curves and DS thresholds definition (in θ terms) of the case-study building frame.

6.2.1.4 Sequential cloud non-linear time-history analysis

Sequential cloud-based NLTHAs are conducted using the selected ground-motion sequences (i.e., pairs). Padding consisting of zeros is inserted between the first and second record and at the end of the second record, with a length equivalent to $30T_1$. This allows the building computational finite-element models to attain its steady-state response in both the ground motions of the sequence, which is essential when dealing with cumulative-based engineering demand parameters (EDPs; e.g., Otárola et al., 2023, 2023). From the time history of the structural response, the maximum inter-storey drift (i.e., θ) is obtained for GM1, while the dissipated hysteretic energy (E_H) is obtained for both ground motions within the sequence (i.e., the proportion of the dissipated hysteretic energy achieved during GM1 and GM2; i.e., $E_{H,GM1}$ and $E_{H,GM2}$, respectively). The above analysis is repeated for each value of ψ to capture the effect of deterioration. A vector-valued PSDM and CGLM (i.e., models conditioned on a vector of parameters) are calibrated using the sequential cloud-based NLTHA-related results for the different values of ψ , as shown in the following subsections.

6.2.2 Probabilistic seismic demand model

The developed vector-valued PSDM relates the total dissipated hysteretic energy (E_H) during a seismic sequence to a maximum inter-storey drift induced by GM1 (θ_{GM1}), an *avgSA* related to GM2 (IM_{GM2}), and a ψ induced by corrosion (e.g., Otárola et al., 2022b). The E_H is adopted as the main EDP as it is a cumulative measure that monotonically increases (or stays constant) with the length of the applied seismic excitation. To ensure the physics of this problem are satisfied, a seven-parameter (i.e., $a_0, b_0, c_0, d_0, e_0, f_0, m_0$) functional

form is adopted, as shown in Equations (23) and (24), ensuring that: 1) $E_{H,GM1GM2}$ during the sequence is monotonic with respect to θ_{GM1} and IM_{GM2} ; 2) for any given value of IM_{GM2} , $E_{H,GM2}$ is monotonically decreasing with respect to θ_{GM1} . The associated standard deviation, $\sigma_{ln(E_H)}$, of the PSDM is computed as the root-mean-squared error. Figure 6-10 shows a fitted median PSDM for the case-study building frame in pristine conditions, as well as the computed fragility median values (i.e., the coloured circles) for the diverse defined DSs. The sequential steps to fit the PSDM functional form are as follows (adapted from Gentile & Galasso, 2021):

1. The $\widehat{E_{H,GM1}} = a_0 \theta_{GM1}^{b_0} (1 + \psi)^{c_0}$ relationship is fitted using the data corresponding to GM1 through nonlinear least-squares regression in the log-log space, obtaining the parameters a_0 , b_0 , and c_0 .
2. The $\widehat{E_{H,GM1}} = d_0 IM_{GM1}^{e_0} (1 + \psi)^{f_0}$ relationship is fitted using the data corresponding to GM1 through nonlinear least-squares regression in the log-log space, obtaining the parameters d_0 , e_0 , and f_0 .
3. The $\widehat{E_{H,GM2}} = d_0 (1 - m_0 \theta_{GM1}) IM_{GM2}^{e_0} (1 + \psi)^{f_0}$ is fitted using the data corresponding to GM1 and GM2 through nonlinear least-squares regression in log-log space, obtaining the parameter m_0 .

$$\widehat{E_H} = \widehat{E_{H,GM1}} + \widehat{E_{H,GM2}} = a_0 \theta_{GM1}^{b_0} (1 + \psi)^{c_0} + d IM_{GM2}^{e_0} (1 + \psi)^{f_0} \quad (23)$$

$$d = d_0 (1 - m_0 \theta_{GM1}) \quad (24)$$

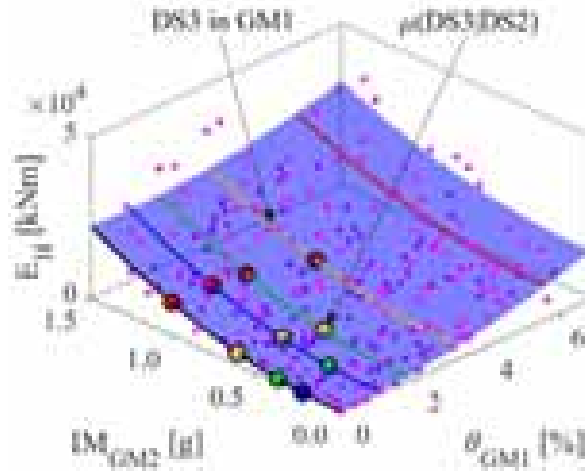


Figure 6-10: Vector-valued PSDM of the case-study frame evaluated at $\psi = 0$ mm (response: magenta dots).

6.2.3 Collapse generalised logistic model

The developed vector-valued CGLM to estimate the probability of collapse (i.e., C), $P(C|DS_{GM1}, IM_{GM2}, \psi)$, also relates E_H to θ_{GM1} , IM_{GM2} , and ψ . The model is calibrated using the generalised logistic function formulation (e.g., Richards, 1959), following the same assumptions as the PSDM to maintain consistency with the relevant physics of the problem. A six-parameter (i.e., α_0 , α_1 , α_2 , β_0 , β_1 , and β_2) functional form is adopted, as shown in Equations (25). The sequential steps to fit the CGLM functional form are summarised as follows (adapted from Iacoletti et al. Iacoletti et al., 2023):

1. The $P(C|DS_{GM1}, IM_{GM2} = 0, \psi) = \frac{1}{1 + e^{-[\alpha_0 + \alpha_1 \ln(\theta_{GM1}) + \alpha_2 \psi]}}$ – an univariate logistic regression model – is calibrated using the collapse data corresponding to GM1 through multiple logistic regression, obtaining the parameters α_0 , α_1 and α_2 .

2. The $P(C|DS_{GM1} = 0, IM_{GM2}, \psi) = \frac{1}{1+e^{-[\beta_0+\beta_1 \ln(IM_{GM1})+\beta_2 \psi]}}$ – an univariate logistic regression model – is calibrated using the collapse data corresponding to GM1 through multiple logistic regression, obtaining the parameters β_0 , β_1 and β_2 .

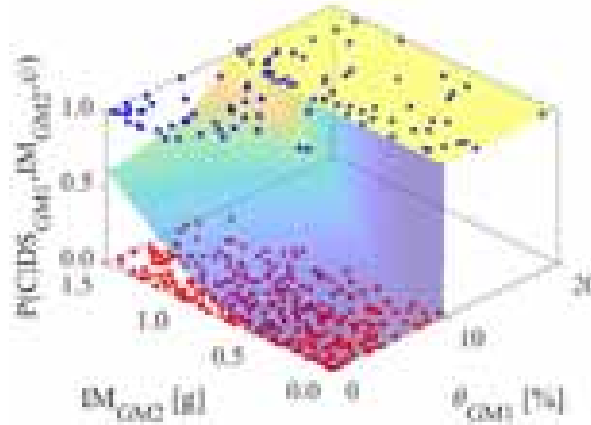


Figure 6-11: Vector-valued CGLM of the case-study frame evaluated at $\psi = 0$ mm (C: blue dots; NC: red dots).

In such equations, $\overline{\theta_{GM1,C}}(\psi)$ is the deformation-based DS threshold associated with structural collapse (or the lowest value of θ_{GM1} that results in $P(C|DS_{GM1}, IM_{GM2}, \psi)=1$), as a function of ψ . When the C thresholds are deterministic, the $P(C|DS_{GM1}, IM_{GM2}, \psi)$ in the $P(C|DS_{GM1}, IM_{GM2}, \psi)$ - θ_{GM1} space corresponds to a step function. Figure 6-11 illustrates the fitted median CGLM for the case-study building frame in pristine conditions.

$$P(C|DS_{GM1}, IM_{GM2}, \psi) = P(C|DS_{GM1}, IM_{GM2} = 0, \psi) + \frac{1 - P(C|DS_{GM1}, IM_{GM2} = 0, \psi)}{1 + \sqrt{1 - \frac{\theta_{GM1}}{\overline{\theta_{GM1,C}}(\psi)} e^{-[\beta_0+\beta_1 \ln(IM_{GM2})+\beta_2 \psi]}}} \quad (25)$$

6.2.3.1 Time- and state-dependent fragility relationships

The proposed vector-valued PSDM and CGLM are used to derive state-dependent fragility relationships given no collapse (i.e., NC). As shown in Figure 6-10, after selecting the $\overline{\theta_{GM1,DS}}(\psi)$ for each DS (depicted as coloured lines), the PSDM directly provides the corresponding median dissipated hysteretic energy-based DS thresholds, $\overline{E_{H,DS}}(\psi)$, at the horizontal plane projected by intersecting $\overline{\theta_{GM1,DS}}(\psi)$ when IM_{GM2} equals zero. Thereby, (energy-based) state-dependent fragility relationships given NC, can be derived for different combinations of the DS in both the GM1 and GM2 as per Equation (26).

$$F(DS_{GM2}|DS_{GM1}, IM_{GM2}, \psi, NC) = P(E_H \geq \overline{E_{H,DS}}(\psi)|DS_{GM1}, IM_{GM2}, \psi, NC) = 1 - F\left[\frac{\ln\left(\frac{\overline{E_{H,DS}}(\psi)}{\overline{E_H}}\right)}{\sigma_{\ln(E_H)}}\right] \quad (26)$$

Practically, $F(DS_{GM2}|DS_0, IM_{GM2}, \psi, NC)$ are the GM1 fragility relationships of a structure pre-damaged exclusively by corrosion (if present), while $F(DS_{GM2}|DS_{GM1}, IM_{GM2}, \psi, NC)$ represent the GM2 fragility relationship conditioned on a given DS attained during GM1 and corrosion (if present). Therefore, $P(DS_{GM2}|DS_0, IM_{GM2}, \psi, NC)$ is equal to $P(DS_{GM1}|IM_{GM1}, \psi, NC)$. Using $\overline{\theta_{GM1,DS}}(\psi)$ for GM1 and the

computed $\overline{E_{H,DS}}(\psi)$ for GM2, and by inverting Equation (26), the median values of such state-dependent fragility relationships can be computed as per Equation (27).

$$\mu_{DS_{GM2}|DS_{GM1},IM_{GM2},\psi,NC} = \left[\frac{\overline{E_{H,DS}}(\psi) - a_0 \theta_{GM1}^{b_0} (1 + \psi)^{c_0}}{d(1 + \psi)^{f_0}} \right]^{\frac{1}{e_0}} \quad (27)$$

The model dispersion, $\beta_{DS_{GM2}|DS_{GM1},IM_{GM2},\psi,NC}$, related to the record-to-record variability is computed using Equation (28) starting from the PSDM log-normal standard deviation, as defined above (i.e., corresponding to the root-mean-squared error), and it is constant following the adopted modelling assumptions. This is not deemed an issue since the relative variation between the dispersion in pristine conditions and at the highest corrosion deterioration level is found to be less than 5%. Such a dispersion is further augmented (by the square root of the sum of the squares) to propagate the uncertainty related to the strength of the structural materials (i.e., β_c) and the modelling of the structural components (i.e., β_m) with values of 0.25 and 0.39, respectively, as per customary practice in performance-based earthquake engineering (e.g., FEMA-P58, 2012).

$$\beta_{DS_{GM2}|DS_{GM1},IM_{GM2},\psi,NC} = \frac{\sigma_{\ln(E_H)}}{e_0} \quad (28)$$

The total probability theorem is used to derive state-dependent fragility relationships combining the $P(C|DS_{GM1},IM_{GM2},\psi)$ (as directly obtained from the CGLM) and $F(DS_{GM2}|DS_{GM1},IM_{GM2},\psi,NC)$, as per Equation (29) (e.g., Jalayer & Cornell, 2009). Such an equation estimates the conditional probability of exceeding a DS conditioned on a DS_{GM1} , an IM_{GM2} , and a value of ψ . The probability of no collapse, $P(NC|DS_{GM1},IM_{GM2},\psi)$, is the complement of $P(C|DS_{GM1},IM_{GM2},\psi)$; i.e., $1 - P(C|DS_{GM1},IM_{GM2},\psi)$. Figure 6-12 shows the obtained state-dependent fragility median values, $\mu_{DS_{GM2}|DS_{GM1},IM_{GM2},\psi}$, as a function of ψ . It is worth recalling that such median values correspond to the 50th percentile in the developed models.

$$F(DS_{GM2}|DS_{GM1},IM_{GM2},\psi) = P(C|DS_{GM1},IM_{GM2},\psi) + F(DS_{GM2}|DS_{GM1},IM_{GM2},\psi,NC)P(NC|DS_{GM1},IM_{GM2},\psi) \quad (29)$$

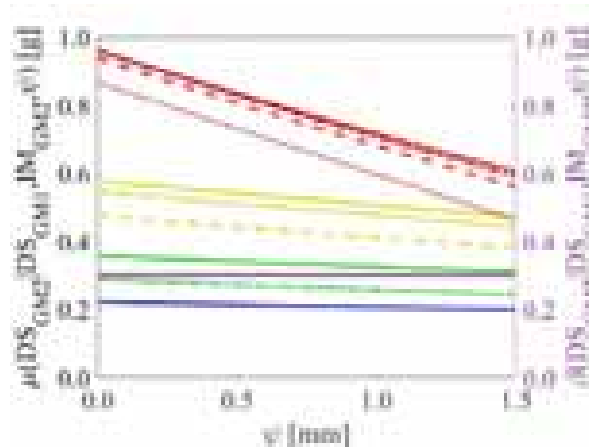


Figure 6-12: Evolution of the fragility median values and dispersion for the case-study building frame as a function ψ .

6.2.3.2 Time- and state-dependent vulnerability relationships

Estimating damage-to-loss ratios (DLRs) has conventionally relied on empirical methods involving post-earthquake reconnaissance or expert judgment. Nevertheless, more recently, simulation-based approaches have been increasingly adopted for their derivation. Such DLRs should be site- and building-specific and must be carefully selected while developing vulnerability relationships. Particularly, this study considers the simulation-based DLRs suggested by Aljawhari et al., 2023 for Italian buildings: a) 0.00 for DS0; b) 0.13 for DS1; c) 0.36 for DS2; 0.68 for DS3; and 1.00 for DS4. Vulnerability relationships are expressed in terms of mean loss ratio (LR) or the mean repair-to-replacement cost ratio of a building conditional on $avgSA$. The

relationships are derived through the total expectation law as in Equation (30). In such an equation, DLR_i is the DLR for the i^{th} DS_{GM2} , $F(DS_{GM2,i}|DS_{GM1,q})$ is the probability of exceeding the i^{th} DS_{GM2} given a prior q^{th} DS_{GM1} , and $F(DS_{GM2,i+1}|DS_{GM1,q})$ is the probability of exceeding the $(i + 1)^{th}$ DS_{GM2} given a prior q^{th} DS_{GM1} ; for $q = 1, \dots, i$ (where q is the index of the respective conditioning DS_{GM1}). Figure 6-13 presents state-dependent vulnerability relationships in pristine and deteriorated conditions for the case-study building frame.

$$LR(DS_{GM1,q}, IM_{GM2}, \psi) = \sum_{i=q}^4 DLR_i [F(DS_{GM2,i}|DS_{GM1,q}) - F(DS_{GM2,i+1}|DS_{GM1,q})] \quad (30)$$

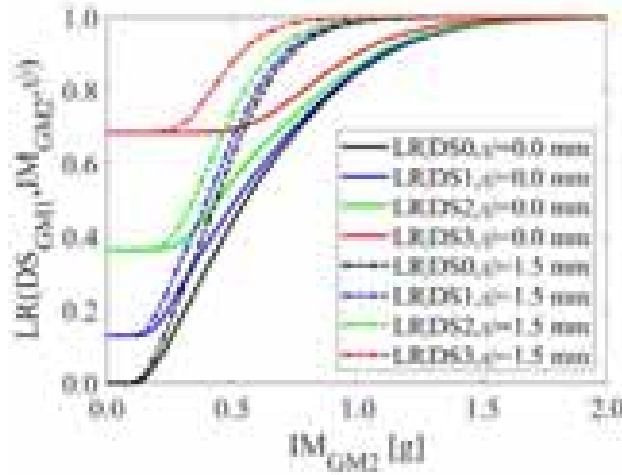


Figure 6-13: Evolution of the vulnerability relationships for the case-study building frame evaluated at $\psi = 0$ mm; 1.5 mm.

6.2.3.3 Stochastic event set assembly

Stochastic event sets comprising mainshock-mainshock, mainshock-aftershock, and aftershock-aftershock sequences are assembled through homogeneous and non-homogeneous Poisson processes employing the procedure for simulating interacting multiple natural hazard events for life-cycle consequence analysis developed by Iannacone et al., 2023. In this study, the rate curve for mainshocks and aftershocks is obtained from Iervolino et al., 2018. Namely, the exceedance curve for Zone 923 (e.g., Barani et al., 2009), corresponding to the Aquila region in Italy, is used. The minimum moment magnitude for both mainshocks and aftershocks is assumed as $m_{m,min} = m_{a,min} = 4.45$, which is slightly higher than the one in the original reference (i.e., 4.15), avoiding generating events with no engineering significance (i.e., unable to cause structural damage). The ground-motion and correlation models developed by Huang & Galasso, 2019 are used, and no correlation between the mainshock and aftershock IMs is considered (e.g., Papadopoulos et al., 2020). All earthquakes are assumed to occur on the same normal fault, which is considered to rupture completely after each event. Thus, the source-to-site distance is set constant, and it is assumed to be equal to 10 km in this case study. The shear wave velocity in the first 30 m of soil is assumed to be equal to 400 m/s. Figure 6-14 illustrates an example stochastic event set assembled with the suggested procedure. More advanced mainshock/aftershock occurrence models are available in the literature (e.g., epidemic-type aftershock sequence models; e.g., Iacopetti et al., 2022), which can be utilised within this study's framework; nevertheless, the proposed procedure is used for illustrative purposes and due to its practicality.

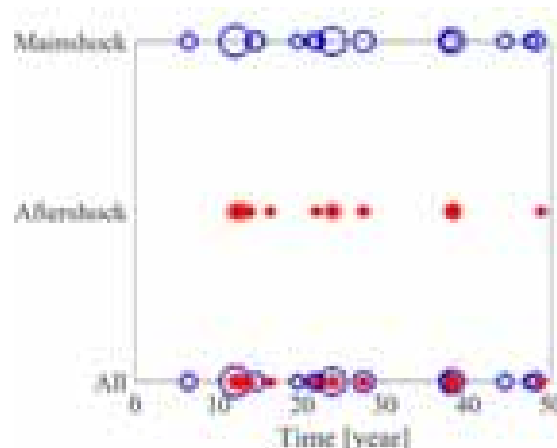


Figure 6-14: Stochastic event set with mainshock-mainshock, mainshock-aftershock, aftershock-aftershock sequences (i.e., seismic sequences; the marker size is proportional to the magnitude of the seismic events).

6.2.3.4 Life-cycle consequence analysis

A Monte-Carlo approach using Halton sequences (e.g., Halton, 1964) is proposed to assemble life-cycle scenarios in the presence of sudden and gradual deterioration for assessing life-cycle consequences (i.e., the approach leverages the inverse transform sampling technique using Halton deterministic, low-discrepancy numbers that can be related to diverse sources of aleatory uncertainty, similar to Latin-Hypercube sampling concepts for experiment design). Such sequences offer improved coverage of the sample space compared to purely random sequences, leading to more accurate estimates and faster convergence, avoiding the “curse of dimensionality” (e.g., Page & Bellman, 1962). An aspect that is particularly advantageous when a large number of simulations are required, as per the proposed application, which includes the aleatory uncertainties coming from the: 1) earthquake occurrences; 2) resulting (local) seismic intensities; 3) corrosion-induced deterioration; 4) state of damage after a seismic event; and 5) state of damage after repair actions. Such an approach includes the interplay between damage (from the multi-hazard threat) and recovery (from potential repair actions between seismic events). The recovery models used correspond to those presented in HAZUS-MH 5.1, 2022. A total of 100,000 Life-cycle scenarios are assembled by sampling a value for each of the aforementioned random variables. Such a number is selected to achieve invariant results based on a sensitivity analysis performed. Figure 6-15 presents a flowchart summarising the proposed Monte-Carlo approach to calculate the expected life-cycle consequences in terms of the life-cycle expected LR ($E[LR]_{LC}$). To account for the time value of money (if utilised), the estimated $E[LR]_e$ (i.e., expected loss ratio for the event e) are actualised at the time of construction (Net Present Value, NPV), with an assumed discount rate (δ) equal to 0.05 for the case-study building frame. The suffix NPV is disregarded in Figure 6-15 but can be included. Figure 6-16 illustrates the life-cycle consequence distribution (which follows a zero-inflated exponential distribution at a point in time) given earthquake- and environment-induced damage accumulation.

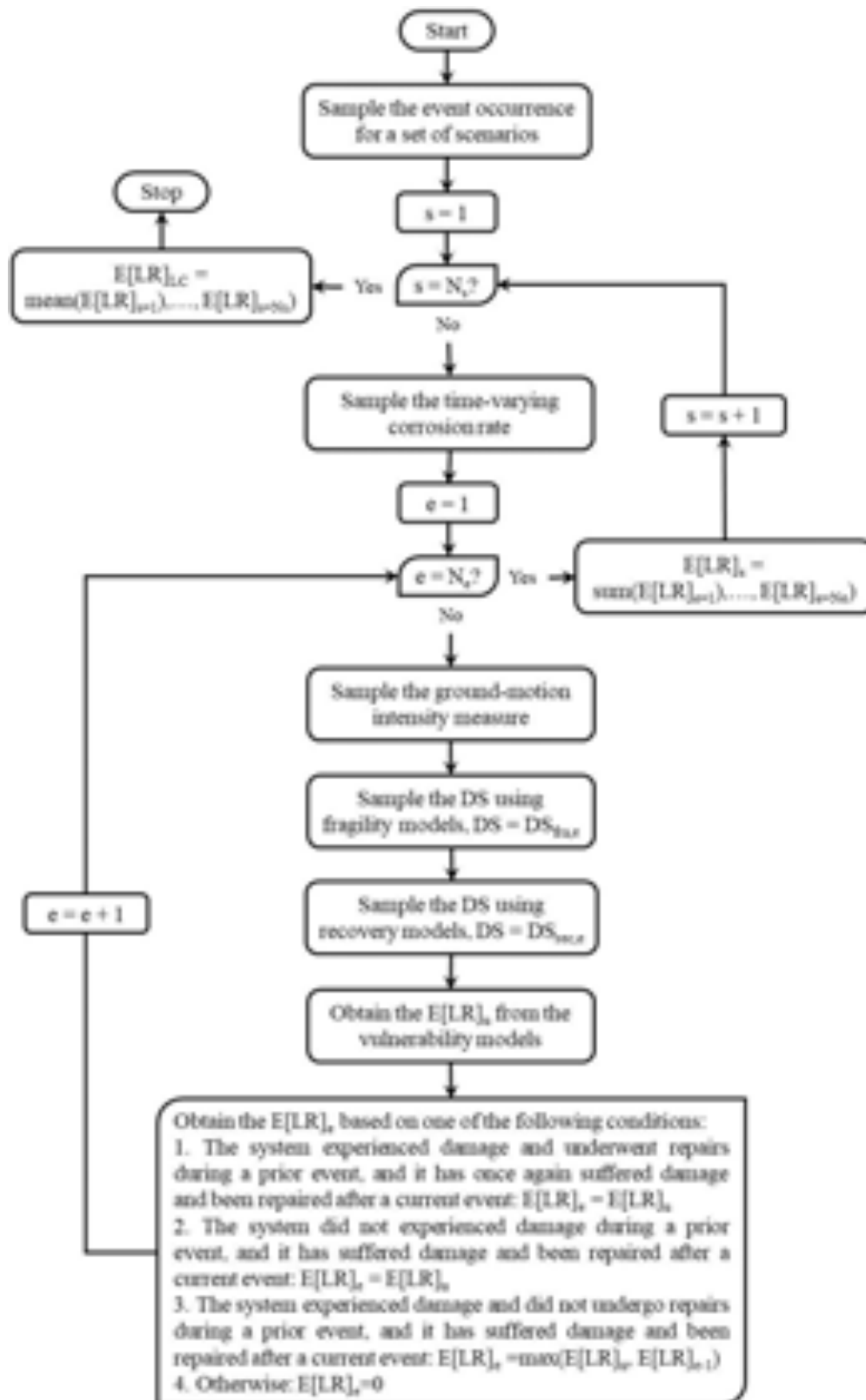


Figure 6-15: Simulation-based approach to assess the life-cycle consequences of deteriorating engineering systems.

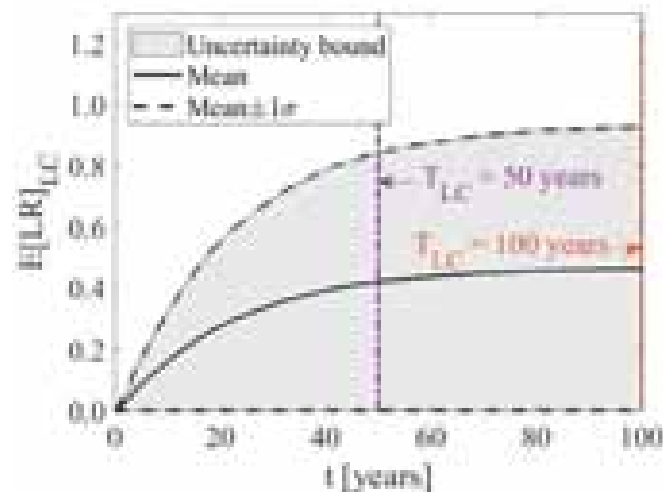


Figure 6-16: Life-cycle consequence distribution given earthquake- and environment-induced damage accumulation.

The expected life-cycle consequences are assessed for four different cases, namely: 1) MS+AS+DE: ground-motion sequences and environment-induced damage accumulation is included; 2) MS+DE: mainshocks and environment-induced damage accumulation is included; 3) MS+AS: ground-motion sequences damage accumulation is included; 4) MS: mainshocks damage accumulation is included. The $E[LR]_{LC}$ for a nominal service life of 50 years are equal to 0.422, 0.192, 0.413, and 0.187 for MS+AS+DE, MS+DE, MS+AS, and MS; respectively (Figure 6-17a). The corresponding relative variations using MS as a benchmark case are 130%, 4%, 123%, and 0% for MS+AS+DE, MS+DE, MS+AS, and MS; respectively (Figure 6-17b). Such differences are statistically significant, corroborated through the Kolmogorov-Smirnov and Wilcoxon rank sum test using the expected consequence realisations associated with the onset of the nominal service life at 50 and 100 years. While the relative variations when considering or excluding ground-motion sequence effects are highly apparent with differences above 100%, the relative variations when including or excluding corrosion-induced deteriorating effects are not that evident (mainly when low seismic events occurred). This is because the expected life-cycle consequences estimation is primarily controlled by the lower (i.e., left) tail of the vulnerability models; in other words, the ground-shaking intensities for the location in analysis tend to be from low to moderate. Therefore, the effects of corrosion on seismic structural performance are expected to be more evident in locations presenting high seismicity and high-intensity earthquake events. Indeed, the median ground-motion intensity across all realisations is equal to 0.06g, a threshold where the vulnerability curves at various levels of deterioration exhibit negligible differences. At the 84th percentile ground-motion intensity, which stands at 0.20g, subtle discrepancies begin to emerge. Consequently, the relative differences in the $E[LR]_{LC}$ primarily stem from the few high-intensity events within the diverse stochastic event sets. Naturally, more significant disparities in outcomes are expected as the ground-motion intensity increases.

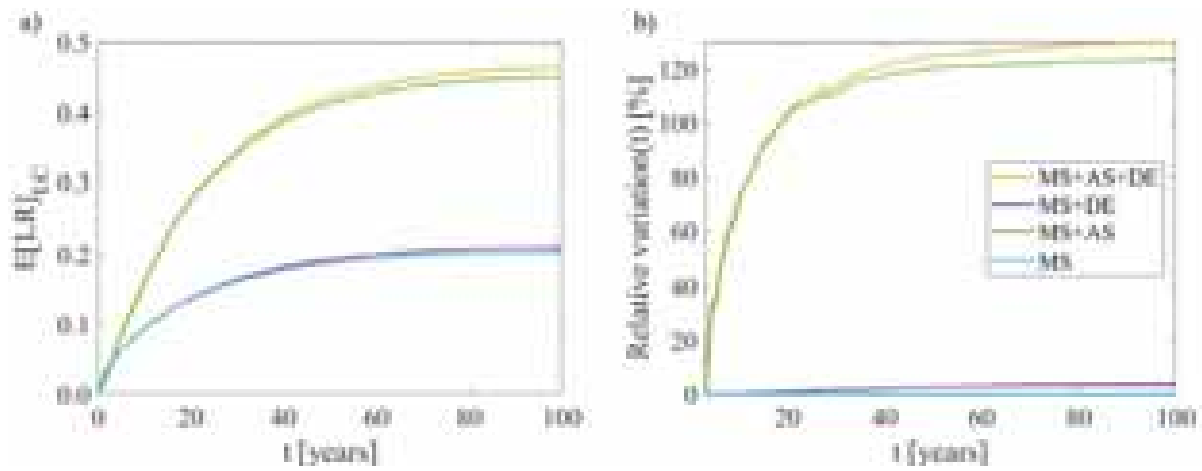


Figure 6-17: a) Life-cycle expected LR of the selected cases, as a function of time; b) relative variation (i.e., $1 - E[LR]_{LC,MS}/E[LR]_{LC,[MS+AS+DE,MS+DE,MS+AS]}$) between the life-cycle expected LR of the selected cases.

7 CONCLUSIONS

This report first presents a review of available sources and repositories for vulnerability and fragility models related to various hazard types (i.e., earthquake, flood and mass movement). It has been found that some of the models for flood include a damage scale that has been developed on the basis of the ESM-98 damage scale for earthquake damage. Because of this fact, it has similarities with the ESM-98 scale, nevertheless it is not identical. This should be noted, as it is relevant to the development of multi-hazard fragility models and their use in Markovian frameworks. The available flood vulnerability models cover a wide range of different types of elements (buildings, infrastructures, etc.) making flood risk calculations feasible in many cases. It should be noted that the available seismic fragility curves are more relevant to the characteristics of the buildings than physical vulnerability models for other hazards. Moreover, to the best of our knowledge, it is only in the literature of seismic fragility curves that the *efficiency* and *sufficiency* of intensity measures are discussed. As far as multi-hazard physical vulnerability models are concerned, the review builds upon the work by Gehl et al. (2019), underlining the available types of hazard interactions and the reasons for the lack of more models, e.g. the lack of harmonized damage scales across different hazards.

Regarding the scoring and ranking of available models for each of the testbeds, most of the models we collected from the literature have an equal level of relevance to all testbeds, and we consider that it is not very likely that a more extensive search would lead to more geographically relevant models. As far as buildings are concerned, the scored empirical models for a major hazard such as flooding have a low level of relevance with respect to the asset characteristics, another scoring criterion. For example, the models correspond either to masonry or to reinforced concrete buildings without any further specification with respect to the building characteristics. This observation is also related to another issue, i.e. the taxonomy for the buildings and the taxonomies for other elements. The only hazard for which the available models have a high relevance with respect to the asset characteristics is earthquake, which is not among the primarily considered hazards at the testbeds. The existence of highly relevant seismic fragility models has been made possible by developments in the 2020 European Seismic Risk Model (ESRM20), which includes fragility curves for a wide range of building classes. Despite the relative abundance of seismic fragility models, there is a scarcity of state-dependent seismic fragility models. State-dependent physical vulnerability models, which are required for multi-hazard risk analysis under successive hazard actions, are even more scarce for the other natural hazards.

This report also includes an application of the PARNASSUS v.3 methodology for the development of flood vulnerability models with a high geographical relevance and a fair level of relevance with respect to the characteristics of a building class. The application uses a virtual survey of 50 buildings, based on open source map resources for districts of the city of Nice with flood risk. The data collected by the survey are used to estimate vulnerability indices based on a scoring according to thirteen parameters related to building and curtilage characteristics. Subsequently, the vulnerability indices are used to calculate curves for the replacement cost as a function of the water depth at the locations of 500 simulated buildings. Note that field surveys could lead to check and/or better determine the building parameters used in the calculations.

The development of analytical state-dependent fragility models for reinforced-concrete buildings that are representative of the Nice testbed provides a methodological framework that may be applied to other hazard combinations and other exposed elements from other testbeds. A few take-aways points from this modelling task are detailed below:

- Despite the fact that we used a large number of simulations (10,000 simulations per building model), in some cases it was either impossible to calculate some parameters of the fragility models, or the responses leading to realizations of the damage states were too few. This was due to two reasons: the randomization of the seismic ground motion selection, and the behaviour of the building models with an existing damage state under flood loads.

- Flood fragility models (surfaces) are developed for a vector of two intensity measures, inundation depth and flow velocity. The fragility models concern the undamaged building models, and the building model with an existing damage state caused by flood. In the case of the simulations with the CR_LFINF_CDM_11_HEX_2 type building models and flood loads in both loading steps, we observe transitions from the existing damage state, caused by the loading in the first step, directly to the highest damage state, as observed by Petrone et al. (2020). This phenomenon is not observed in the case of the CR_LWAL_CDN_HEX_4 type model. A possible explanation for this may be the fact that the capacity curve of the CR_LWAL_CDN_HEX_4 type model shows a hardening effect (i.e., it has a positive slope), while the capacity curves of the CR_LFINF_CDM_11_HEX_2 type building models practically have no hardening (i.e., they are almost horizontal) after a value of the interstory drift in the range of the damage state DS2. Therefore, in the case of the CR_LFINF_CDM_11_HEX_2 type building models, it was not possible to calculate using the selected approach the parameters for the state-dependent fragility curves corresponding to the damage states between the existing damage state and the ultimate damage state (DS4). In such cases, Bayesian approaches for the calculation of the parameters of the fragility models in combination with informative priors might be more useful.
- As far as the randomization of the seismic ground motion selection in the simulations is concerned, the fact that it led to few responses in the higher damage states was expected for two reasons. The first reason is the composition of the used dataset of seismic ground motions. It was extracted from the Engineering Strong Motion Database (Luzi et al., 2020) using the following criteria, which are consistent with the characteristics of damaging earthquakes that may be expected in the Nice tesbed area: Magnitude ≥ 6.0 , PGA $\geq 1.0 \text{ cm/s}^2$, epicentral distance $\leq 30.0 \text{ km}$. Given that the distribution of the PGA of the ground motions corresponding to the flatfile is skewed towards the lower end, in addition to the fact that the simulations use ground motions selected at random from this dataset, it is unsurprising that the simulations led less often to responses in the range of the higher damage states than in the states of less damage. Potentially, a more informed ground motion selection strategy could lead to proportionally more responses in the higher damage states and reduce the computational cost required for developing multi-hazard synthetic fragility models based on multi-part simulations, where sequential hazard actions are applied.

State-based fragility models are one of the elements that may be used to model time-variable fragility based on a Markovian approach in the context of a life-cycle consequence analysis. Such approaches may also incorporate models for the gradual degradation of structures (e.g. due to reinforcement steel corrosion), and for structural rehabilitation. In the state-based seismic fragility curves developed for this deliverable, we observe differences between the curves depending on whether it was earthquake or flood that caused the existing damage stage. If further investigations confirm this finding, then the type of hazard causing the initial damage in state based fragilities may be a factor that should be taken into account. In that case, modelling time-variable fragility with Markovian approaches would have to take into account the probabilities of damage states due to each hazard.

Finally, as far as the gradual degradation of structures over time is concerned, in the studied cases, the effects of earthquake-induced ground motion sequences and steel corrosion phenomena have been modelled using state-dependent fragility relationships in the context of a Markovian life-cycle consequence analysis. Both lead to an increase of the loss ratio with respect to the case that ignores them; however, the effect of earthquake-induced ground motion sequences is more pronounced than the effect for reinforcement steel corrosion. Apart from the conclusions with respect to the specific case studies, the usefulness of the prososed Markovian life-cycle analysis lies in its capability to be applied to estimate time-dependent multi-hazard consequences.

8 REFERENCES

- Afsar Dizaj, E., Salami, M. R., & Kashani, M. M. (2022). Seismic vulnerability assessment of ageing reinforced concrete structures under real mainshock-aftershock ground motions. *Structure and Infrastructure Engineering*, 18(12), 1674–1690. <https://doi.org/10.1080/15732479.2021.1919148>
- Akaike, H. (1974). A new look at the statistical model identification. *IEEE Transactions on Automatic Control*, 19(6), 716–723. <https://doi.org/10.1109/TAC.1974.1100705>
- Alipour, A., & Shafei, B. (2012). Performance assessment of highway bridges under earthquake and scour effects. In Proceedings of the 15th world conference on earthquake engineering, Lisbon, Portugal.
- Aljawhari, K., Gentile, R., & Galasso, C. (2023). Simulation-based consequence models of seismic direct loss and repair time for archetype reinforced concrete frames. *Soil Dynamics and Earthquake Engineering*, 172, 107979. <https://doi.org/https://doi.org/10.1016/j.soildyn.2023.107979>
- Anagnos T (1999) Development of an Electrical Substation Equipment Performance Database for Evaluation of Equipment Fragilities. PEER Report 2001-06. Pacific Earthquake Engineering Research Center College of Engineering, University of California, Berkeley
- Ancheta, T. D., Darragh, R. B., Stewart, J. P., Seyhan, E., Silva, W. J., Chiou, B. S.-J., Wooddell, K. E., Graves, R. W., Kottke, A. R., Boore, D. M., Kishida, T., & Donahue, J. L. (2014). NGA-West2 Database. *Earthquake Spectra*, 30(3), 989–1005. <https://doi.org/10.1193/070913EQS197M>
- Applied Technology Council (ATC). (2012). Seismic Performance Assessment of Buildings Volume 1 – Methodology. FEMA P-58-1. *Federal Emergency Management Agency*, 1(August), 278.
- Argyroudis, S., Kaynia, A. M. (2014). Fragility Functions of Highway and Railway Infrastructure. In: Pitilakis, K., Crowley, H., Kaynia, A. (eds) SYNER-G: Typology Definition and Fragility Functions for Physical Elements at Seismic Risk. Geotechnical, Geological and Earthquake Engineering, vol 27. Springer, Dordrecht.
- Argyroudis SA, Mitoulis SA (2021) Vulnerability of bridges to individual and multiple hazards- floods and earthquakes. *Reliability Engineering & System Safety* 210:107564. <https://doi.org/10.1016/j.res.2021.107564>
- Asprone, D., Jalayer, F., Prota, A., & Manfredi, G. (2010). Proposal of a probabilistic model for multi-hazard risk assessment of structures in seismic zones subjected to blast for the limit state of collapse. *Structural Safety*, 32(1), 25-34.
- Babeyko A, Lorito S, Hernandez F, et al (2022) Towards the new Thematic Core Service Tsunami within the EPOS Research Infrastructure. *Annals of Geophysics* 65:DM215. <https://doi.org/10.4401/ag-8762>
- Badal, P. S., & Tesfamariam, S. (2023). Seismic resilience of typical code-conforming RC moment frame buildings in Canada. *Earthquake Spectra*, 39(2), 748–771. <https://doi.org/10.1177/87552930221145455>
- Baiguera M, Rossetto T, Robertson IN, Petrone C (2022) A Procedure for Performing Nonlinear Pushover Analysis for Tsunami Loading to ASCE 7. *J Struct Eng* 148:04021270. [https://doi.org/10.1061/\(ASCE\)ST.1943-541X.0003256](https://doi.org/10.1061/(ASCE)ST.1943-541X.0003256)
- Barani, S., Spallarossa, D., & Bazzurro, P. (2009). Disaggregation of probabilistic ground-motion Hazard in Italy. *Bulletin of the Seismological Society of America*, 99(5). <https://doi.org/10.1785/0120080348>

- Bodda, S.S., Sandhu, H.K., & Gupta, A. (2016). Fragility of a Flood Defense Structure Subjected to Multi-Hazard Scenario. In 24th International Conference on Nuclear Engineering (pp. V004T14A015-V004T14A015), American Society of Mechanical Engineers.
- Bonamente, M. (2017). Statistics and Analysis of Scientific Data. In *Springer*.
- Borzi B, Ceresa P, Franchin P, et al (2015) Seismic Vulnerability of the Italian Roadway Bridge Stock. *Earthquake Spectra* 31:2137–2161. <https://doi.org/10.1193/070413EQS190M>
- Bruneau, M., Barbato, M., Padgett, J. E., Zaghi, A. E., Mitrani-Reiser, J., & Li, Y. (2017). State of the art of multihazard design. *Journal of Structural Engineering*, 143(10), 03117002.
- Brzev S, Scawthorn C, Charleson AW, Allen L, Greene M, Jaiswal K, Silva V (2013). GEM building taxonomy version 2.0. GEM technical report 2013-02, June. Pavia: GEM Foundation.
- Burton, H. V., Deierlein, G., Lallemant, D., & Lin, T. (2016). Framework for Incorporating Probabilistic Building Performance in the Assessment of Community Seismic Resilience. *Journal of Structural Engineering*, 142(8). [https://doi.org/10.1061/\(asce\)st.1943-541x.0001321](https://doi.org/10.1061/(asce)st.1943-541x.0001321)
- Caltrans. (2019). *Seismic Design Criteria. Version 2.0*. California Department of Transportation, Sacramento, CA.
- Calvi, G. M., Pinho, R., Magenes, G., Bommer, J. J., Restrepo-Vélez, L. F., & Crowley, H. (2006). Development of seismic vulnerability assessment methodologies over the past 30 years. *ISSET journal of Earthquake Technology*, 43(3), 75-104.
- Cardinali M, Reichenbach P, Guzzetti F, et al (2002) A geomorphological approach to the estimation of landslide hazards and risks in Umbria, Central Italy. *Nat Hazards Earth Syst Sci* 2:57–72. <https://doi.org/10.5194/nhess-2-57-2002>
- Cardone D, Perrone G, Sofia S (2011). A performance-based adaptive methodology for the seismic evaluation of multi-span simply supported deck bridges. *Bull. Earthq. Eng.*, 9(5):1463–1498.
- Cardone, D., & Perrone, G. (2017). Damage and Loss Assessment of Pre-70 RC Frame Buildings with FEMA P-58. *Journal of Earthquake Engineering*, 21(1), 23–61. <https://doi.org/10.1080/13632469.2016.1149893>
- Cavalieri, F., Franchin, P., Pinto, P. E. (2014). Fragility Functions of Electric Power Stations. In: Pitilakis, K., Crowley, H., Kaynia, A. (eds) SYNER-G: Typology Definition and Fragility Functions for Physical Elements at Seismic Risk. Geotechnical, Geological and Earthquake Engineering, vol 27. Springer, Dordrecht.
- Cavalieri, F., Franchin, P., & Giovinazzi, S. (2016). Earthquake-altered flooding hazard induced by damage to storm water systems. *Sustainable and Resilient Infrastructure*, 1(1-2), 14-31.
- Cragg, J. G. (1971). Some Statistical Models for Limited Dependent Variables with Application to the Demand for Durable Goods. *Econometrica*, 39(5), 829–844. <https://doi.org/10.2307/1909582>
- Cremen, G., Galasso, C., & McCloskey, J. (2022). Modelling and quantifying tomorrow's risks from natural hazards. *Science of The Total Environment*, 817, 152552. <https://doi.org/https://doi.org/10.1016/j.scitotenv.2021.152552>

Charvet I, Macabuag J, Rossetto T (2017) Estimating Tsunami-Induced Building Damage through Fragility Functions: Critical Review and Research Needs. *Front Built Environ* 3:36. <https://doi.org/10.3389/fbuil.2017.00036>

Charvet, I., Suppasri, A., Kimura, H., Sugawara, D., & Imamura, F. (2015). Fragility estimations for Kesennuma City following the 2011 Great East Japan Tsunami based on maximum flow depths, velocities and debris impact, with evaluation of the ordinal model's predictive accuracy. *Natural Hazards*, 79(3), 2073-2099.

Chen X, Xiang N, Guan Z, Li J (2022) Seismic vulnerability assessment of tall pier bridges under mainshock-aftershock-like earthquake sequences using vector-valued intensity measure. *Engineering Structures* 253:113732. <https://doi.org/10.1016/j.engstruct.2021.113732>

Chiodi, R., Asprone, D., Maimone, F., Prota, A., & Ricciardelli, F. (2011). Multi-hazard assessment of steel hangar structures subjected to seismic and wind loads. In *Applied Mechanics and Materials* (Vol. 82, pp. 778-783), Trans Tech Publications.

Crawford PS, Mitrani-Reiser J, Sutley EJ, et al (2022) Measurement Approach to Develop Flood-Based Damage Fragilities for Residential Buildings Following Repeat Inundation Events. *ASCE-ASME J Risk Uncertainty Eng Syst, Part A: Civ Eng* 8:04022019. <https://doi.org/10.1061/AJRUA6.0001219>

Crowley, H., M. Colombi, V. Silva, N. Ahmad, M. Fardis, G. Tsionis, A. Papailia, F. Taucer, et al. (2011a). D3.1 Fragility functions for common RC building types in Europe. SYNER-G Deliverable 3.1. <http://www.vce.at/SYNER-G/files/dissemination/deliverables.html>. Accessed 29 June 2023.

Crowley, H., M. Colombi, V. Silva, N. Ahmad, M. Fardis, G. Tsionis, T. Karantoni, F. Lyrantzaki, F. Taucer, et al. (2011b). D3.1 Fragility functions for common masonry building types in Europe. SYNER-G Deliverable 3.2. <http://www.vce.at/SYNER-G/files/dissemination/deliverables.html>. Accessed 29 June 2023.

Crowley, H., M. Colombi, V. Silva, R. Monteiro, S. Ozcebe, M. Fardis, G. Tsionis, & P. Askouni (2011c). D3.6 Fragility functions for roadway bridges. SYNER-G Deliverable 3.6. <http://www.vce.at/SYNER-G/files/dissemination/deliverables.html>. Accessed 29 June 2023.

Crowley H., Dabbeek J., Despotaki V., Rodrigues D., Martins L., Silva V., Romão X., Pereira N., Weatherill G., Danciu L. (2021) European Seismic Risk Model (ESRM20). EFEHR Technical Report 002 V1.0.0, <https://doi.org/10.7414/EUC-EFEHR-TR002-ESRM20>

Crowley, H., V. Despotaki, D. Rodrigues, V. Silva, D. Toma-Danila, E. Riga, A. Karatzetzou, Z. Zugic, et al. 2021a. Exposure model for European seismic risk assessment. *Earthquake Spectra* 36(1). <https://doi.org/10.1177/8755293020919429>.

Crowley, H., V. Despotaki, D. Rodrigues, V. Silva, C. Costa, D. Toma-Danila, E. Riga, A. Karatzetzou, et al. 2021b. European exposure model data repository (v0.9). Zenodo. <https://doi.org/10.5281/zenodo.4402820>. Accessed 29 June 2023.

D'Ayala D, Copping A, Wang H (2006) A conceptual model for multi-hazard assessment of the vulnerability of historic buildings. In: Lourenco PB, Roca P, Modena C, Agrawal S (Eds.) *Structural analysis of historical constructions: possibilities of numerical and experimental techniques*. In: *Proceedings of the fifth international conference* (pp. 121–140). New Delhi, India

D'Ayala, D., Meslem, A., Vamvatsikos, D., Porter, K., Rossetto, T., Silva, V. (2015) *Guidelines for Analytical Vulnerability Assessment of Low/Mid-Ris Buildings*, Vulnerability Global Component Project. DOI 10.13117/GEM.VULN-MOD.TR2014.12

- D'Ayala, D., et al.: Assessment of the Multi-Hazard Vulnerability of Priority Cultural Heritage Structures in the Philippines, in: 1st International Conference on Natural Hazards & Infrastructure, Chania, Greece, 2016
- D'Ayala, D., Gehl, P., Martinovic, K., Gavin, K., Clarke, J., Tucker, M., Corbally, R., Avdeeva, Y. V., van Gelder, P., Salceda Page M. T., Segarra Martinez, M. J. (2015). Fragility Functions Matrix. INFRARISK Report D3.2.
- D'Ayala D, Wang K, Yan Y, et al (2020) Flood Vulnerability Assessment of Urban Traditional Buildings in Kuala Lumpur, Malaysia. *Natural Hazards and Earth System Sciences*, (April), pp. 1–30. <https://doi.org/10.5194/nhess-2020-96>
- Dabbeek J, Silva V (2020) Modeling the residential building stock in the Middle East for multi-hazard risk assessment. *Nat Hazards* 100:781–810. <https://doi.org/10.1007/s11069-019-03842-7>
- De Angeli, S., Malamud, B. D., Rossi, L., Taylor, F. E., Trasforini, E., & Rudari, R. (2022). A multi-hazard framework for spatial-temporal impact analysis. *International Journal of Disaster Risk Reduction*, 73, 102829.
- De Risi, R., Goda, K., Yasuda, T., & Mori, N. (2017a). Is flow velocity important in tsunami empirical fragility modeling?. *Earth-science reviews*, 166, 64-82.
- De Risi R, Goda K, Mori N, Yasuda T (2017b) Bayesian tsunami fragility modeling considering input data uncertainty. *Stoch Environ Res Risk Assess* 31:1253–1269. <https://doi.org/10.1007/s00477-016-1230-x>
- Dehghani, N. L., Fereshtehnejad, E., & Shafieezadeh, A. (2021). A Markovian approach to infrastructure life-cycle analysis: Modeling the interplay of hazard effects and recovery. *Earthquake Engineering and Structural Dynamics*, 50(3). <https://doi.org/10.1002/eqe.3359>
- Dijkstra, E. W. (1959). A note on two problems in connexion with graphs. *Numerische Mathematik*, 1(1), 269–271. <https://doi.org/10.1007/BF01386390>
- Douglas, J. (2007). Physical vulnerability modelling in natural hazard risk assessment. *Natural Hazards and Earth System Sciences*, 7(2), 283-288.
- Drakes, O., & Tate, E. (2022). Social vulnerability in a multi-hazard context: a systematic review. *Environmental research letters*, 17(3), 033001.
- Du, Y. G., Clark, L. A., & Chan, A. H. C. (2005). Residual capacity of corroded reinforcing bars. *Magazine of Concrete Research*, 57(3). <https://doi.org/10.1680/macr.2005.57.3.135>
- Du, Y. G., Clark, L. A., & Chan, A. H. C. (2005). Effect of corrosion on ductility of reinforcing bars. *Magazine of Concrete Research*, 57(7). <https://doi.org/10.1680/macr.2005.57.7.407>
- Duracrete. (2000). DuraCrete: Probabilistic Performance based Durability Design of Concrete Structures - Final Technical Report: General guidelines for durability design and redesign. In *Concrete*.
- Dunant, A. (2019). Quantification of multi-hazard risk from natural disasters. PhD dissertation, University of Canterbury, New Zealand.
- Eads L, Miranda E, Lignos DG (2015) Average spectral acceleration as an intensity measure for collapse risk assessment: Average Spectral Acceleration as an IM for Collapse Risk Assessment. *Earthquake Engng Struct Dyn* 44:2057–2073. <https://doi.org/10.1002/eqe.2575>

- Eidsvig UMK, Papathoma-Köhle M, Du J, et al (2014) Quantification of model uncertainty in debris flow vulnerability assessment. *Engineering Geology* 181:15–26. <https://doi.org/10.1016/j.enggeo.2014.08.006>
- Eurocode 8. (2005). European Standard EN 1998-3:2005: Design of structures for earthquake resistance - Part 3: Assessment and retrofitting of buildings. *Comite Europeen de Normalisation, Brussels*, 3(2005).
- European Commission. Joint Research Centre. (2013) Institute for the Protection and the Security of the Citizen.: Guidelines for deriving seismic fragility functions of elements at risk: buildings, lifelines, transportation networks and critical facilities. Publications Office, LU. <https://doi.org/10.2788/19605>
- European Commission. Joint Research Centre. (2016) Global flood depth-damage functions: methodology and the database with guidelines. Publications Office, LU. <https://dx.doi.org/10.2760/16510>
- Fardis, M., Tsionis, G. (2014). Fragility Functions of Road and Railway Bridges. In: Pitilakis, K., Crowley, H., Kaynia, A. (eds) SYNER-G: Typology Definition and Fragility Functions for Physical Elements at Seismic Risk. Geotechnical, Geological and Earthquake Engineering, vol 27. Springer, Dordrecht.
- FEMA (2020). Hazus Earthquake Model Technical Manual.
- FEMA (2022). Hazus Flood Technical Manual - Hazus 5.1.
- Fereshtehnejad, E., & Shafieezadeh, A. (2018). A multi-type multi-occurrence hazard lifecycle cost analysis framework for infrastructure management decision making. *Engineering Structures*, 167. <https://doi.org/10.1016/j.engstruct.2018.04.049>
- Fu X, Li H-N, Li G (2016) Fragility analysis and estimation of collapse status for transmission tower subjected to wind and rain loads. *Structural Safety* 58:1–10. <https://doi.org/10.1016/j.strusafe.2015.08.002>.
- Fuchs, S., Heiss, K., & Hübl, J. (2007). Towards an empirical vulnerability function for use in debris flow risk assessment. *Natural Hazards and Earth System Sciences*, 7(5), 495-506.
- Galasso, C., McCloskey, J., Pelling, M., Hope, M., Bean, C. J., Cremen, G., Guragain, R., Hancilar, U., Menoscal, J., Mwang'a, K., Phillips, J., Rush, D., & Sinclair, H. (2021). Editorial. Risk-based, Pro-poor Urban Design and Planning for Tomorrow's Cities. *International Journal of Disaster Risk Reduction*, 58, 102158. <https://doi.org/https://doi.org/10.1016/j.ijdr.2021.102158>
- Galasso C, Pregnotato M, Parisi F (2021). A model taxonomy for flood fragility and vulnerability assessment of buildings. *International Journal of Disaster Risk Reduction* 53:101985. <https://doi.org/10.1016/j.ijdr.2020.101985>
- Gasparini, P., & Garcia, A. (2014). *Seismic Risk Assessment, Cascading Effects* (pp. 1–20). https://doi.org/10.1007/978-3-642-36197-5_260-1
- Gehl P, Seyedi DM, Douglas J (2013) Vector-valued fragility functions for seismic risk evaluation. *Bull Earthquake Eng* 11:365–384. <https://doi.org/10.1007/s10518-012-9402-7>
- Gehl, P. (2017). Bayesian networks for the multi-risk assessment of road infrastructure. PhD dissertation, University College London, United Kingdom.
- Gehl, P., & D'Ayala, D. (2016). Development of Bayesian Networks for the multi-hazard fragility assessment of bridge systems. *Structural Safety*, 60, 37-46.

Gehl, P., Desramaut, N., Réveillère, A., Modaressi, H. (2014). Fragility Functions of Gas and Oil Networks. In: Pitilakis, K., Crowley, H., Kaynia, A. (eds) SYNER-G: Typology Definition and Fragility Functions for Physical Elements at Seismic Risk. Geotechnical, Geological and Earthquake Engineering, vol 27. Springer, Dordrecht.

Gehl, P., Rohmer, J., Zentner, I., Kowal, K., Potemski, S., Feau, C., Marcilhac-Fradin, M., Guigueno, Y., Pellissetti, M., & Daniell, J. (2019). Methodology to derive vector-based fragility functions. NARSIS Deliverable 2.6. <http://www.narsis.eu/page/deliverables>. Accessed 29 June 2023.

Gentile R, Galasso C (2021). Hysteretic energy-based state-dependent fragility for ground-motion sequences. *Earthquake Engng Struct Dyn* 50:1187–1203. <https://doi.org/10.1002/eqe.3387>

Gentile, R., Cremen, G., Galasso, C., Jenkins, L. T., Manandhar, V., Mentese, E. Y., ... & McCloskey, J. (2022). Scoring, selecting, and developing physical impact models for multi-hazard risk assessment. *International Journal of Disaster Risk Reduction*, 82, 103365.

Gill, J. C., & Malamud, B. D. (2014). Reviewing and visualizing the interactions of natural hazards. *Reviews of Geophysics*, 52(4), 680-722.

Giovinazzi, S., & King, A. (2009). Estimating seismic impacts on lifelines: an international review for RiskScape. In 2009 NZSEE Conference, Christchurch, New Zealand.

Goda, K., & De Risi, R. (2018). Multi-hazard loss estimation for shaking and tsunami using stochastic rupture sources. *International journal of disaster risk reduction*, 28, 539-554.

Gómez Zapata JC, Pittore M, Brinckmann N, et al (2023) Scenario-based multi-risk assessment from existing single-hazard vulnerability models. An application to consecutive earthquakes and tsunamis in Lima, Peru. *Nat Hazards Earth Syst Sci* 23:2203–2228. <https://doi.org/10.5194/nhess-23-2203-2023>

Ghosh, J., & Sood, P. (2016). Consideration of time-evolving capacity distributions and improved degradation models for seismic fragility assessment of aging highway bridges. *Reliability Engineering and System Safety*, 154. <https://doi.org/10.1016/j.ress.2016.06.001>

Grünthal, G. (1998). European macroseismic scale 1998. European Seismological Commission (ESC).

Guardiola-Víllora, A., Molina, S. & D'Ayala, D. Performance based probabilistic seismic risk assessment for urban heritage. An example in Pla del Remei Area (Valencia). *Bull Earthquake Eng* 21, 4951–4991 (2023). <https://doi.org/10.1007/s10518-023-01721-y>

HAZUS (2003). “HAZUS-MH MR3-Technical Manual.” Federal Emergency Management Agency, Washington, D.C.

Halton, J. H. (1964). Algorithm 247: Radical-Inverse Quasi-Random Point Sequence. *Commun. ACM*, 7(12), 701–702. <https://doi.org/10.1145/355588.365104>

Hill M, Rossetto T (2008) Comparison of building damage scales and damage descriptions for use in earthquake loss modelling in Europe. *Bulletin of Earthquake Engineering* 6: 335–365. [Crossref](#).

Huang, C., & Galasso, C. (2019). Ground-motion intensity measure correlations observed in Italian strong-motion records. *Earthquake Engineering and Structural Dynamics*, 48(15). <https://doi.org/10.1002/eqe.3216>

- Huizinga, J., De Moel, H., & Szewczyk, W. (2017). Global flood depth-damage functions: Methodology and the database with guidelines (No. JRC105688). Joint Research Centre (Seville site).
- Hwang, H., Liu, J. B., & Chiu, Y. H. (2001). Seismic Fragility Analysis of Highway Bridges. *9th ASCE Specialty Conference on Probabilistic Mechanics and Structural Reliability*, July.
- Iacometti, S., Cremen, G., & Galasso, C. (2022). Validation of the Epidemic-Type Aftershock Sequence (ETAS) Models for Simulation-Based Seismic Hazard Assessments. *Seismological Research Letters*.
- Iacometti, S., Cremen, G., & Galasso, C. (2023). Accounting for damage and loss accumulation during ground-motion sequences in building portfolio seismic loss assessment. *Earthquake Engineering & Structural Dynamics (under Review)*.
- Iannacone, L., Otárola, K., Gentile, R., & Galasso, C. (2023). Simulating Multi-hazard Event Sets for Life Cycle Consequence Analysis. *Natural Hazards and Earth System Sciences (under Review)*.
- Iervolino, I., Chioccarelli, E., & Giorgio, M. (2018). Aftershocks' Effect on Structural Design Actions in Italy. *Bulletin of the Seismological Society of America*, 108(4), 2209–2220. <https://doi.org/10.1785/0120170339>
- Iervolino, I., Chioccarelli, E., & Suzuki, A. (2020). Seismic damage accumulation in multiple mainshock–aftershock sequences. *Earthquake Engineering and Structural Dynamics*, 49(10). <https://doi.org/10.1002/eqe.3275>
- Iervolino, I., & Giorgio, M. (2022). Holistic Modelling of Loss and Recovery for the Resilience Assessment to Seismic Sequences. *Findings*. <https://doi.org/10.32866/001c.37210>
- Iervolino I, Giorgio M, Chioccarelli E (2016) Markovian modeling of seismic damage accumulation. *Earthq Engng Struct Dyn* 45:441–461. <https://doi.org/10.1002/eqe.2668>
- IPSEAU (1999), Plan de prevention des risques naturels previsibles d'inondation du Paillon, Service Amenagement Urbanism Operationnelle, Commune de Nice.
- Jalayer, F., Asprone, D., Prota, A., & Manfredi, G. (2011). Multi-hazard upgrade decision making for critical infrastructure based on life-cycle cost criteria. *Earthquake Engineering and Structural Dynamics*, 40(10). <https://doi.org/10.1002/eqe.1081>
- Jalayer, F., & Cornell, C. A. (2009). Alternative non-linear demand estimation methods for probability-based seismic assessments. *Earthquake Engineering and Structural Dynamics*, 38(8). <https://doi.org/10.1002/eqe.876>
- Jalayer, F., Ebrahimian, H., Trevelopoulos, K., & Bradley, B. (2023). Empirical tsunami fragility modelling for hierarchical damage levels. *Natural Hazards and Earth System Sciences*, 23(2), 909-931.
- Kafali, C. (2008). System performance under multi-hazard environment. PhD Thesis, Cornell University, Ithaca, NY.
- Kakderi, K., Argyroudis, S. (2014). Fragility Functions of Water and Waste-Water Systems. In: Pitilakis, K., Crowley, H., Kaynia, A. (eds) SYNER-G: Typology Definition and Fragility Functions for Physical Elements at Seismic Risk. Geotechnical, Geological and Earthquake Engineering, vol 27. Springer, Dordrecht.

- Kakderi, K., Pitilakis, K. (2014). Fragility Functions of Harbor Elements. In: Pitilakis, K., Crowley, H., Kaynia, A. (eds) SYNER-G: Typology Definition and Fragility Functions for Physical Elements at Seismic Risk. Geotechnical, Geological and Earthquake Engineering, vol 27. Springer, Dordrecht.
- Kameshwar, S., & Padgett, J.E. (2014). Multi-hazard risk assessment of highway bridges subjected to earthquake and hurricane hazards. *Engineering Structures*, 78, 154-166.
- Kappos, A. (2013). Seismic vulnerability and loss assessment for buildings in Greece. In *Seismic vulnerability of structure*, Ed., P. Guéguen, p. 111-160. ISTE, Wiley, ISBN: 978-1-84821-524-5.
- Kappos AJ, Panagopoulos G, Panagiotopoulos C, Penelis G (2006) A hybrid method for the vulnerability assessment of R/C and URM buildings. *Bull Earthquake Eng* 4:391–413. <https://doi.org/10.1007/s10518-006-9023-0>
- Karafagka, S., Fotopoulou, S., & Pitilakis, K. (2018). Analytical tsunami fragility curves for seaport RC buildings and steel light frame warehouses. *Soil Dynamics and Earthquake Engineering*, 112, 118-137.
- Karapetrou S, Manakou M, Bindi D, et al (2016) “Time-building specific” seismic vulnerability assessment of a hospital RC building using field monitoring data. *Engineering Structures* 112:114–132. <https://doi.org/10.1016/j.engstruct.2016.01.009>
- Kashani, M. M., Crewe, A. J., & Alexander, N. A. (2013). Nonlinear stress-strain behaviour of corrosion-damaged reinforcing bars including inelastic buckling. *Engineering Structures*, 48. <https://doi.org/10.1016/j.engstruct.2012.09.034>
- Kaynia, A. M. (2013). *Guidelines for deriving seismic fragility functions of elements at risk: Buildings, lifelines, transportation networks and critical facilities*. SYNER-G Reference Report 4, JRC Scientific and Policy Reports. doi:10.2788/19605.
- Kazantzi, A. K., & Vamvatsikos, D. (2015). Intensity measure selection for vulnerability studies of building classes. *Earthquake Engineering and Structural Dynamics*, 44(15). <https://doi.org/10.1002/eqe.2603>
- Korswagen PA, Jonkman SN, Terwel KC (2019). Probabilistic assessment of structural damage from coupled multi-hazards. *Structural Safety* 76:135–148. <https://doi.org/10.1016/j.strusafe.2018.08.001>
- Kramer, M., Terheiden, K., & Wieprecht, S. (2016). Safety criteria for the trafficability of inundated roads in urban floodings. *International journal of disaster risk reduction*, 17, 77-84.
- Lan, M., Gardoni, P., Luo, R., Zhu, J., & Lo, S. (2022). Risk-driven statistical modeling for hurricane-induced compound events: Design event implementation for industrial areas subjected to coastal floods and winds. *Ocean Engineering*, 251, 111159. <https://doi.org/https://doi.org/10.1016/j.oceaneng.2022.111159>
- Lanzano G, Luzi L, Cauzzi C, et al (2021) Accessing European Strong-Motion Data: An Update on ORFEUS Coordinated Services. *Seismological Research Letters* 92:1642–1658. <https://doi.org/10.1785/0220200398>
- Lee KH, Rosowsky DV (2006) Fragility analysis of woodframe buildings considering combined snow and earthquake loading. *Structural Safety* 28:289–303. <https://doi.org/10.1016/j.strusafe.2005.08.002>
- Li, Y., & van de Lindt, J.W. (2012). Loss-based formulation for multiple hazards with application to residential buildings. *Engineering Structures*, 38, 123–133

- Luo, H. Y., Zhang, L. M., He, J., & Yin, K. S. (2022). Reliability-based formulation of building vulnerability to debris flow impacts. *Canadian Geotechnical Journal*, 59(1), 40-54.
- Luo HY, Zhang LM, Zhang LL, et al (2023) Vulnerability of buildings to landslides: The state of the art and future needs. *Earth-Science Reviews* 238:104329. <https://doi.org/10.1016/j.earscirev.2023.104329>
- Lupoi, A., Cavalieri, F., Franchin, P. (2014). Component Fragilities and System Performance of Health Care Facilities. In: Pitilakis, K., Crowley, H., Kaynia, A. (eds) SYNER-G: Typology Definition and Fragility Functions for Physical Elements at Seismic Risk. *Geotechnical, Geological and Earthquake Engineering*, vol 27. Springer, Dordrecht.
- Luzi L, Puglia R, Russo E, et al (2016) The Engineering Strong-Motion Database: A Platform to Access Pan-European Accelerometric Data. *Seismological Research Letters* 87:987–997. <https://doi.org/10.1785/0220150278>
- Luzi L., Lanzano G., Felicetta C., D'Amico M. C., Russo E., Sgobba S., Pacor, F., & ORFEUS Working Group 5 (2020). Engineering Strong Motion Database (ESM) (Version 2.0). Istituto Nazionale di Geofisica e Vulcanologia (INGV). <https://doi.org/10.13127/ESM.2>
- Maiwald H, Schwarz J (2019) Vereinheitlichte Schadensbeschreibung und Risikobewertung von Bauwerken unter extremen Naturgefahren. *Mauerwerk* 23:95–111. <https://doi.org/10.1002/dama.201910014>
- Mander, J. B., Priestley, M. J. N., & Park, R. (1988). Observed Stress-Strain Behavior of Confined Concrete. *Journal of Structural Engineering*, 114(8). [https://doi.org/10.1061/\(asce\)0733-9445\(1988\)114:8\(1827\)](https://doi.org/10.1061/(asce)0733-9445(1988)114:8(1827))
- Manfredi, V., Masi, A., Nicodemo, G., & Digrisolo, A. (2023). Seismic fragility curves for the Italian RC residential buildings based on non-linear dynamic analyses. *Bulletin of Earthquake Engineering*, 21(4), 2173-2214.
- Martínez-Gomariz E, Forero-Ortiz E, Guerrero-Hidalga M, et al (2020) Flood Depth–Damage Curves for Spanish Urban Areas. *Sustainability* 12:2666. <https://doi.org/10.3390/su12072666>
- Martins, L., & Silva, V. (2021). Development of a fragility and vulnerability model for global seismic risk analyses. *Bulletin of Earthquake Engineering*, 19(15), 6719-6745.
- Marzocchi, W., Garcia-Aristizabal, A., Gasparini, P., Mastellone, M. L., & Di Ruocco, A. (2012). Basic principles of multi-risk assessment: a case study in Italy. *Natural hazards*, 62, 551-573.
- Molina Hutt, C., Vahanvaty, T., & Kourehpaz, P. (2022). An analytical framework to assess earthquake-induced downtime and model recovery of buildings. *Earthquake Spectra*, 38(2), 1283–1320. <https://doi.org/10.1177/87552930211060856>
- Morandi P, Manzini CF, Borzi B, Mauro A, Vecchi A, Tisalvi M, Iacobini F (2019). Simplified seismic vulnerability assessment of railway masonry arch bridges. *E-Proceedings of the 10th New York City Bridge Conference*, 26 -27 August, New York City, USA.
- Negulescu, C., & Foerster, E. (2010). Parametric studies and quantitative assessment of the vulnerability of a RC frame building exposed to differential settlements. *Natural Hazards and Earth System Sciences*, 10(9), 1781-1792.
- Nofal, O. M., & van de Lindt, J. W. (2020). Minimal Building Flood Fragility and Loss Function Portfolio for Resilience Analysis at the Community Level. *Water*, 12(8). <https://doi.org/10.3390/w12082277>.

- Nofal, O. M., van de Lindt, J. W., & Do, T. Q. (2020). Multi-variate and single-variable flood fragility and loss approaches for buildings. *Reliability Engineering & System Safety*, 202, 106971. <https://doi.org/https://doi.org/10.1016/j.res.2020.106971>
- Otárola, K., Fayaz, J., & Galasso, C. (2022a). Fragility analysis of deteriorating bridge components subjected to simulated ground-motion sequences. *12th National Conference on Earthquake Engineering, 12NCEE*.
- Otárola, K., Fayaz, J., & Galasso, C. (2022b). Fragility and vulnerability analysis of deteriorating ordinary bridges using simulated ground-motion sequences. *Earthquake Engineering & Structural Dynamics*, 51(13), 3215–3240. <https://doi.org/10.1002/eqe.3720>
- Otárola, K., Gentile, R., Sousa, L., & Galasso, C. (2023). Accounting for earthquake-induced ground-motion duration in building-portfolio loss assessment. *Earthquake Engineering & Structural Dynamics*, 52(4), 887–909. <https://doi.org/https://doi.org/10.1002/eqe.3791>
- Otárola, K., Gentile, R., Sousa, L., & Galasso, C. (2023). Impact of ground-motion duration on nonlinear structural performance: Part I: spectrally equivalent records and inelastic single-degree-of-freedom systems. *Earthquake Spectra*, 39(2), 829–859. <https://doi.org/10.1177/87552930231155502>
- Otárola, K., Iannacone, L., Gentile, R., & Galasso, C. (2023a). A Markovian framework to model life-cycle consequences of infrastructure systems in a multi-hazard environment. *8th International Symposium on Life-Cycle Civil Engineering, IALCCE 2023*.
- Otárola, K., Iannacone, L., Gentile, R., & Galasso, C. (2023b). Seismic fragility analysis of deteriorating reinforced concrete buildings from a life-cycle perspective. In I. 14th International Conference on Applications of Statistics and Probability in Civil Engineering (Ed.), *14th International Conference on Applications of Statistics and Probability in Civil Engineering, ICASP14*. 14th International Conference on Applications of Statistics and Probability in Civil Engineering, ICASP14.
- Otárola, K., Sousa, L., Gentile, R., & Galasso, C. (2023). Impact of ground-motion duration on nonlinear structural performance: Part II: site- and building-specific analysis. *Earthquake Spectra*, 39(2), 860–888. <https://doi.org/10.1177/87552930231155506>
- Page, E. S., & Bellman, R. (1962). Adaptive Control Processes: A Guided Tour. *Journal of the Royal Statistical Society. Series A (General)*, 125(1). <https://doi.org/10.2307/2343225>
- Papadopoulos, A. N., Kohrangi, M., & Bazzurro, P. (2020). Mainshock-consistent ground motion record selection for aftershock sequences. *Earthquake Engineering and Structural Dynamics*, 49(8). <https://doi.org/10.1002/eqe.3263>
- Papathoma-Koehle, M., Keiler, M., Totschnig, R., & Glade, T. (2012). Improvement of vulnerability curves using data from extreme events: debris flow event in South Tyrol. *Natural Hazards*, 64, 2083–2105.
- Papathoma-Köhle M, Zischg A, Fuchs S, et al (2015) Loss estimation for landslides in mountain areas – An integrated toolbox for vulnerability assessment and damage documentation. *Environmental Modelling & Software* 63:156–169. <https://doi.org/10.1016/j.envsoft.2014.10.003>
- Parammal Vatteri, A., D'Ayala, D., & Gehl, P. (2022). Bayesian networks for assessment of disruption to school systems under combined hazards. *International Journal of Disaster Risk Reduction*, 74, 102924.

Parisi, F., & Sabella, G. (2017). Flow-type landslide fragility of reinforced concrete framed buildings. *Engineering Structures*, 131, 28-43.

Paulay, T., & Priestly, M. J. N. (1992). *Seismic Design of Reinforced Concrete and Masonry Buildings* (1st Ed.). In *Seismic Design of Reinforced Concrete and Masonry Buildings*. John Wiley & Sons, Inc. <https://doi.org/10.1002/9780470172841>

Peduto, D., Ferlisi, S., Nicodemo, G., Reale, D., Pisciotta, G., & Gullà, G. (2017). Empirical fragility and vulnerability curves for buildings exposed to slow-moving landslides at medium and large scales. *Landslides*, 14, 1993-2007.

Pelà L, Aprile A, Benedetti A (2009). Seismic assessment of masonry arch bridges. *Engineering Structures*, 31(8): 1777-1788. DOI: 10.1016/j.engstruct.2009.02.012.

Petrone C, Rossetto T, Goda K (2017). Fragility assessment of a RC structure under tsunami actions via nonlinear static and dynamic analyses. *Engineering Structures* 136:36–53. <https://doi.org/10.1016/j.engstruct.2017.01.013>

Petrone C, Rossetto T, Baiguera M, et al (2020) Fragility functions for a reinforced concrete structure subjected to earthquake and tsunami in sequence. *Engineering Structures* 205:110120. <https://doi.org/10.1016/j.engstruct.2019.110120>

Pinto, P. E., Cavalieri, F., Franchin, P., & Vanzi, I. (2010). Fragility functions for electric power system elements. SYNER-G Report D3.3.

Pita, G., Pinelli, J.P., Cocke, S., Gurley, K., Mitrani-Reiser, J., Weekes, J., & Hamid, S. (2012). Assessment of hurricane-induced internal damage to low-rise buildings in the Florida Public Hurricane Loss Model. *Journal of Wind Engineering and Industrial Aerodynamics*, 104, 76-87.

Pitilakis, K., et al. (2011). Physical vulnerability of elements at risk to landslides: Methodology for evaluation, fragility curves and damage states for buildings and lifelines. SAFELAND Report D2.5.

Poljanšek, K., Marin Ferrer, M., Clark, I., & De Groeve, T. (2017). Science for disaster risk management 2017: knowing better and losing less. *Publications Office of the European Union, Luxembourg, EUR 28034*. <https://doi.org/10.2788/842809>

Porter K., Farokhnia K., Vamvatsikos D., Cho I.H. Guidelines for component-based analytical vulnerability assessment of buildings and non-structural elements, 2014, Global Earthquake Model Foundation, Pavia, Italy: GEM Technical Report 2014-13.

Prasad, G., & Banerjee, S. (2013). The impact of flood-induced scour on seismic fragility characteristics of bridges. *Journal of Earthquake Engineering*, 17(6), 803-828.

Pregolato, M., Ford, A., Wilkinson, S. M., & Dawson, R. J. (2017). The impact of flooding on road transport: A depth-disruption function. *Transportation research part D: transport and environment*, 55, 67-81.

Priestley MJN, Calvi GM, Kowalsky MJ (2007). *Displacement-based seismic design of structures*, IUSS PRESS, Pavia, Italy.

Priestley, M. J. N., Seible, F., & Calvi, G. M. (1996). *Seismic Design and Retrofit of Bridges* (1st ed.). In *Seismic Design and Retrofit of Bridges*. John Wiley & Sons, Inc. <https://doi.org/10.1002/9780470172858>

- Raj SV, Bhatia U, Kumar M (2022) Cyclone preparedness strategies for regional power transmission systems in data-scarce coastal regions of India. *International Journal of Disaster Risk Reduction* 75:102957. <https://doi.org/10.1016/j.ijdr.2022.102957>
- Rasulo, A., Goretti, A., & Nuti, C. (2004). Performance of lifelines during the 2002 Molise, Italy, earthquake. *Earthquake Spectra*, 20(S1), S301-S314.
- Reed DA, Friedland CJ, Wang S, Massarra CC (2016) Multi-hazard system-level logit fragility functions. *Engineering Structures* 122:14–23. <https://doi.org/10.1016/j.engstruct.2016.05.006>
- Reese S, Bradley BA, Bind J, et al (2011) Empirical building fragilities from observed damage in the 2009 South Pacific tsunami. *Earth-Science Reviews* 107:156–173. <https://doi.org/10.1016/j.earscirev.2011.01.009>
- Ribeiro, F.L., Barbosa, A.R., & Neves, L.C. (2014). Application of reliability-based robustness assessment of steel moment resisting frame structures under post-mainshock cascading events. *Journal of Structural Engineering*, 140(8), A4014008.
- Richards, F. J. (1959). A flexible growth function for empirical use. *Journal of Experimental Botany*, 10(2). <https://doi.org/10.1093/jxb/10.2.290>
- Romao, X., Castro, J. M., Pereira, N., Crowley, H., Silva, V., Martins, L., & Rodrigues, D. (2019a). European physical vulnerability models. SERA Deliverable 26.5. http://eu-risk.eucentre.it/wp-content/uploads/2019/08/SERA_D26.5_Physical_Vulnerability.pdf. Accessed 29 June 2023.
- Romao, X., Pereira, N., Castro, J. M., De Maio, F., Crowley, H., Silva, V., & Martins, L. (2019b). European building vulnerability data repository. <http://zenodo.org/record/4062411>. Accessed 29 June 2023.
- Rossetto, T., I. Ioannou, D.N. Grant and T. Maqsood (2014), Guidelines for empirical vulnerability assessment, GEM Technical Report 2014-08 V1.0.0, 140 pp., GEM Foundation, Pavia, Italy, doi: 10.13117/GEM.VULN-MOD.TR2014.1
- Schwarz J, Maiwald H (2007) Prognose der Bauwerksschädigung unter Hochwassereinwirkung. *Bautechnik* 84:450–464. <https://doi.org/10.1002/bate.200710039>
- Selva, J. (2013). Long-term multi-risk assessment: statistical treatment of interaction among risks. *Natural hazards*, 67, 701–722.
- Shahnazaryan, D., O'Reilly, G. J., & Monteiro, R. (2021). Story loss functions for seismic design and assessment: Development of tools and application. *Earthquake Spectra*, 37(4), 2813–2839. <https://doi.org/10.1177/87552930211023523>
- Shokrabadi M, Burton HV (2018) Building service life economic loss assessment under sequential seismic events. *Earthq Engng Struct Dyn* 47:1864–1881. <https://doi.org/10.1002/eqe.3045>
- Silva V, Amo-Oduro D, Calderon A, et al (2020) Development of a global seismic risk model. *Earthquake Spectra* 36:372–394. <https://doi.org/10.1177/8755293019899953>
- Silva, V., H. Crowley, and M. Colombi. 2014. Fragility function manager tool. In SYNER-G: Typology definition and fragility functions for physical elements at seismic risk, ed. K. Pitilakis, H. Crowley, and A. Kaynia, 385–402. Dordrecht: Springer.

- Silva M, Pereira S (2014) Assessment of physical vulnerability and potential losses of buildings due to shallow slides. *Nat Hazards* 72:1029–1050. <https://doi.org/10.1007/s11069-014-1052-4>
- Silva V, Yepes-Estrada C, Dabbeek J, Martins L, Brzev S (2018). GED4ALL: Global exposure database for multi-hazard risk analysis —Multi-hazard exposure taxonomy. GEM technical report 2018-01. Pavia: GEM Foundation.
- Silva-Lopez, R., Bhattacharjee, G., Poulos, A., & Baker, J. W. (2022). Commuter welfare-based probabilistic seismic risk assessment of regional road networks. *Reliability Engineering & System Safety*, 227, 108730. <https://doi.org/https://doi.org/10.1016/j.ress.2022.108730>
- Song, R., Li, Y., & van de Lindt, J.W. (2016). Loss estimation of steel buildings to earthquake mainshock–aftershock sequences. *Structural Safety*, 61, 1-11.
- Stephenson, V. and D’Ayala, D.: A new approach to flood vulnerability assessment for historic buildings in England, *Nat. Hazards Earth Syst. Sci.*, 14, 1035–1048, <https://doi.org/10.5194/nhess14-1035-2014>, 2014.
- Sun L, D’Ayala D, Fayjaloun R, Gehl P. Agent-based model on resilience-oriented rapid responses of road networks under seismic hazard. *Reliab Eng Syst Saf* 2021; 216:108030. <https://doi.org/10.1016/j.ress.2021.108030>.
- Stewart, M. G. (2004). Spatial variability of pitting corrosion and its influence on structural fragility and reliability of RC beams in flexure. *Structural Safety*, 26(4). <https://doi.org/10.1016/j.strusafe.2004.03.002>
- Tao, W., Lin, P., & Wang, N. (2021). Optimum life-cycle maintenance strategies of deteriorating highway bridges subject to seismic hazard by a hybrid Markov decision process model. *Structural Safety*, 89, 102042. <https://doi.org/https://doi.org/10.1016/j.strusafe.2020.102042>
- Tecchio G, Donà M, Da Porto F (2016). Seismic fragility curves of as-built single-span masonry arch bridges. *Bull. Earthq. Eng.*, 14(11): 3099–3124, doi:10.1007/s10518-016-9931-6.
- Tiganescu, A., Ozcebe, A., Kharazian, A., Di Meo, A., Famà, A., Darzi, A., Borzi, B., Halldórsson, B., Bessason, B., Negulescu, C., D’Ayala, D., Toma-Danila, D., Bozzoni, F., ..., et al. (2022). Report on recommendations on fragility functions for buildings and infrastructure components to be used in rapid response context. TURNkey Deliverable 4.2. Zenodo. <https://doi.org/10.5281/zenodo.7442433>
- Trevlopoulos K, Guéguen P (2016) Period elongation-based framework for operative assessment of the variation of seismic vulnerability of reinforced concrete buildings during aftershock sequences. *Soil Dynamics and Earthquake Engineering* 84:224–237. <https://doi.org/10.1016/j.soildyn.2016.02.009>
- Trevlopoulos K, Guéguen P, Helmstetter A, Cotton F (2020) Earthquake risk in reinforced concrete buildings during aftershock sequences based on period elongation and operational earthquake forecasting. *Structural Safety* 84:101922. <https://doi.org/10.1016/j.strusafe.2020.101922>
- Tyagunov, S., Vorogushyn, S., Muñoz Jimenez, C., Parolai, S., & Fleming, K. (2018). Multi-hazard fragility analysis for fluvial dikes in earthquake-and flood-prone areas. *Natural Hazards and Earth System Sciences*, 18(9), 2345-2354.
- Venanzi, I., Lavan, O., Ierimonti, L., & Fabrizi, S. (2018). Multi-hazard loss analysis of tall buildings under wind and seismic loads. *Structure and Infrastructure Engineering*, 1-17.

Watson E (2018) Modeling Electrical Grid Resilience under Hurricane Wind Conditions with Increased Solar Photovoltaic and Wind Turbine Power Generation. George Washington University

Ward, P. J., Daniell, J., Duncan, M., Dunne, A., Hananel, C., Hochrainer-Stigler, S., Tijssen, A., Torresan, S., Ciurean, R., Gill, J. C., Sillmann, J., Couasnon, A., Koks, E., Padrón-Fumero, N., Tatman, S., Tronstad Lund, M., Adesiyun, A., Aerts, J. C. J. H., Alabaster, A., ... de Ruiter, M. C. (2022). Invited perspectives: A research agenda towards disaster risk management pathways in multi-(hazard-)risk assessment. *Natural Hazards and Earth System Sciences*, 22(4), 1487–1497. <https://doi.org/10.5194/nhess-22-1487-2022>

Winter, M. G., Smith, J. T., Fotopoulou, S., Pitilakis, K., Mavrouli, O., Corominas, J., & Argyroudis, S. (2014). An expert judgement approach to determining the physical vulnerability of roads to debris flow. *Bulletin of Engineering Geology and the Environment*, 73, 291-305.

Yepes-Estrada C, Silva V, Rossetto T, D'Ayala, D., Ioannou, I., Meslem A., Crowley, H. The Global Earthquake Model Physical Vulnerability Database. *Earthquake Spectra*. 2016;32(4):2567-2585. doi:10.1193/011816EQS015DP

Yilmaz, T. (2015). Risk assessment of highway bridges under multi-hazard effect of flood-induced scour and earthquake, PhD thesis, Pennsylvania State University, State College, PA.

Zaghi, A. E., Padgett, J. E., Bruneau, M., Barbato, M., Li, Y., Mitrani-Reiser, J., & McBride, A. (2016). Establishing common nomenclature, characterizing the problem, and identifying future opportunities in multihazard design. *Journal of Structural Engineering*, 142(12), H2516001.

Zampieri P, Zanini MA, Faleschini F (2016). Derivation of analytical seismic fragility functions for common masonry bridge types: methodology and application to real cases. *Engineering Failure Analysis*, 68: 275-291.

Zhu M, McKenna F, Scott MH (2018) OpenSeesPy: Python library for the OpenSees finite element framework. *SoftwareX* 7:6–11. <https://doi.org/10.1016/j.softx.2017.10.009>

Zuccaro, G., Cacace, F., Spence, R.J.S., & Baxter, P.J. (2008). Impact of explosive eruption scenarios at Vesuvius. *Journal of Volcanology and Geothermal Research*, 178(3), 416-453.

9 APPENDIX I: SELECTED FRAGILITY AND VULNERABILITY MODELS

This Appendix details the fragility and vulnerability models that have been screened and selected before being ranked, as discussed in Chapter 3. Regarding fragility models, each table contains the following fields:

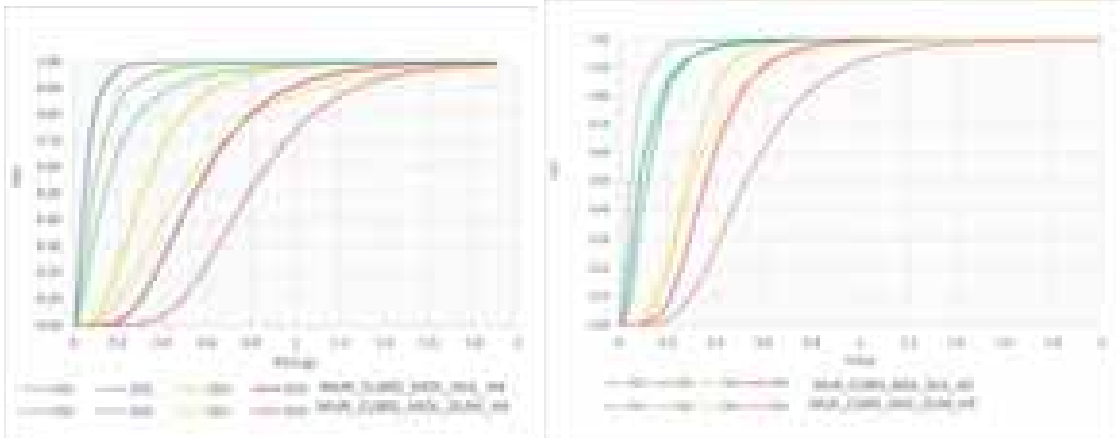
- *Reference* of the study related to the model;
- *Region of applicability*, if the model has been derived for a specific geographical area;
- *Class*, which details the structural typology of the asset(s) covered by the model;
- *Methodology* used in the derivation of the model (e.g., analytical, empirical, etc.);
- *Damage states*, with a qualitative description of the damage scaled used;
- *Intensity measure*, describing the physical variable that is used to represent the hazard loading;
- *Fragility parameters*, detailing the mean standard deviation of the fragility functions;
- *Figures*, which represent plots of the models (if available).

In the case of vulnerability models, the field *Damage states* is replaced by *Damage measure* (loss metric that is output by the model), and *Fragility parameters* by *Functional form* (equation of the vulnerability function, if available).

9.1 Seismic fragility models

9.1.1 Buildings

FRAG_EQ_BDG_Guardiola 2023									
<i>Reference</i>	Guardiola-Víllora, A., Molina, S. & D'Ayala, D. Performance based probabilistic seismic risk assessment for urban heritage. An example in Pla del Remei Area (Valencia). Bull Earthquake Eng 21, 4951–4991 (2023). https://doi.org/10.1007/s10518-023-01721-y								
<i>Region of applicability</i>	Europe (global model) South Europe: south France, Spain, Italy, Portugal, late nineteen century early twentieth century buildings.								
<i>Typology</i>	MUR_CLBRS_MOL_DUL_H4: unreinforced masonry brick with lime mortar/low ductility/4 storey with poor connection between orthogonal walls MUR_CLBRS_MOL_DUM_H4: unreinforced masonry brick with lime mortar/medium ductility/4 storey with good connection between orthogonal walls MUR_CLBRS_MOL_DUL_H5-6: unreinforced masonry brick with lime mortar/low ductility/5 storey with poor connection between orthogonal walls MUR_CLBRS_MOL_DUM_H5-6: unreinforced masonry brick with lime mortar/medium ductility/5 storey with good connection between orthogonal walls								
<i>Methodology</i>	Analytical, from capacity curves								
<i>Damage states</i>	ESRM20 limit states, based on the yield displacement and the ultimate (final) displacement in the capacity curve: DS1: slight DS2: moderate DS3: extensive DS4: complete								
<i>Intensity Measure</i>	PGA (g)								
<i>Fragility parameters</i>	Typology	DS1		DS2		DS3		DS4	
		α [m]	β	α [m]	β	α [m]	β	α [m]	β

	MUR_CLBRS_MOL_DUL_H4	0.0063	0.959 8	0.0250 5	0.882 9	0.0538	0.550 3	0.0962	0.286 4
	MUR_CLBRS_MOL_DUL_H5	0.0233	0.712 2	0.0290	0.761 0	0.0603	0.449 9	0.0776	0.492 6
	MUR_CLBRS_MOL_DUM_H4	0.0043 5	0.896 9	0.0242	0.969 1	0.0488 2	0.620 2	0.0828 5	0.369 9
	MUR_CLBRS_MOL_DUM_H5	0.0149	0.679 8	0.0264	0.773 8	0.0627	0.342 0	0.0968	0.283 7
Figures									

FRAG_EQ_BDG_Putрино&D'Ayala 2020

Putrino V, D'Ayala D (2020) Effectiveness of seismic strengthening to repeated earthquakes in historic urban contexts Norcia 2016. Disaster Prev Manag 29(1):47–64

The fragility functions are derived from in situ data exposure collected in Norcia post 2016 earthquake on about 100 buildings

Europe (global model) South Europe: South France, Spain, Italy, Portugal, Greece, stone buildings with different number of storeys and quality of connections between orthogonal walls. Curves are provided for low and medium rise.

MUR_ST_MOL_DUL_H2: unreinforced masonry stone with lime mortar/low ductility/2 storey with poor connection between orthogonal walls

MUR_ST_MOL_DUM_H2: unreinforced masonry stone with lime mortar/medium ductility/2 storey with good connection between orthogonal walls

MUR_ST_MOL_DUL_H3: unreinforced masonry stone with lime mortar/low ductility/3 storey with poor connection between orthogonal walls

MUR_ST_MOL_DUM_H3: unreinforced masonry stone with lime mortar/medium ductility/3 storey with good connection between orthogonal walls

Analytical, from capacity curves

ESRM20 limit states, based on the yield displacement and the ultimate (final) displacement in the capacity curve:

DS1: slight

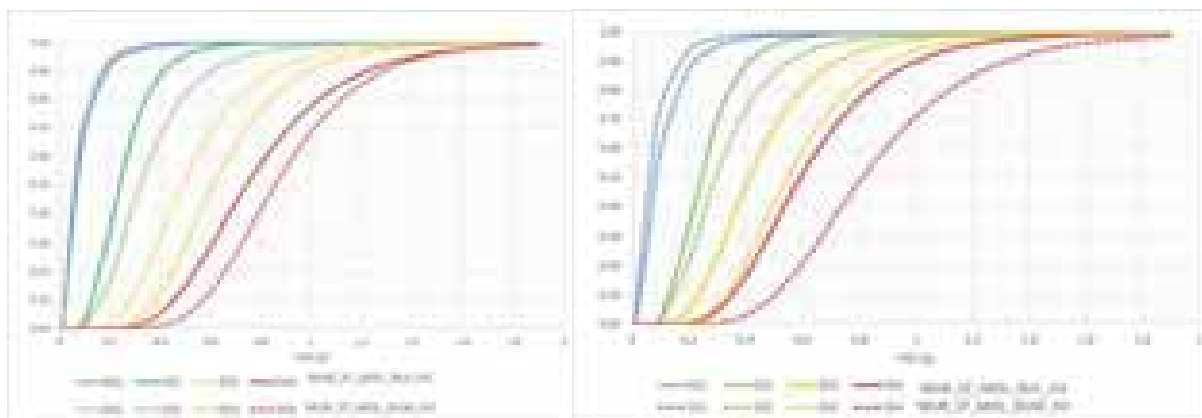
DS2: moderate

DS3: extensive

DS4: complete

PGA (g), functions are also available in displacement (m)

Typology	DS1		DS2		DS3		DS4	
	α [m]	β	α [m]	β	α [m]	β	α [m]	β
MUR_ST_MOL_DUL_H2	0.08691 8	0.77428 5	0.26019 9	0.433411	0.53532 8	0.42859 5	0.80042 7	0.38517
MUR_ST_MOL_DUM_H2	0.07686 9	0.77011 8	0.36249 8	0.491969	0.65766 6	0.37332 9	0.90115 9	0.31724 4
MUR_ST_MOL_DUL_H3	0.10686 6	0.77314 1	0.26122 7	0.424221	0.45121	0.43707 7	0.64119 4	0.40705 2
MUR_ST_MOL_DUM_H3	0.07645 1	0.79109 7	0.33171 3	0.495202	0.59119 6	0.39424 5	0.8723	0.37620 7

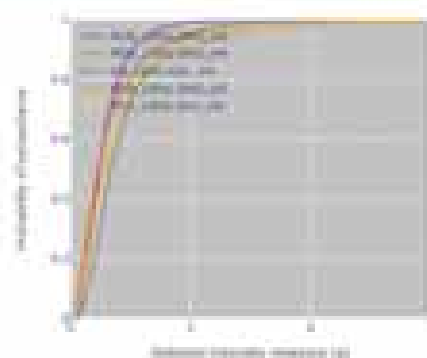


FRAG_EQ_BDG_Crowley2021

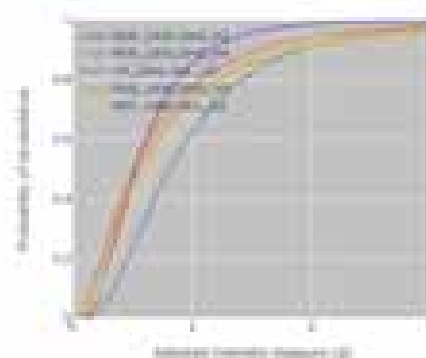
<i>References</i>	Crowley, H., V. Despotaki, D. Rodrigues, V. Silva, C. Costa, D. Toma-Danila, E. Riga, A. Karatzetzou, et al. (2021b). European exposure model data repository (v0.9). Zenodo. https://doi.org/10.5281/zenodo.4402820 .					
<i>Region of applicability</i>	Europe (global model)					
<i>Class</i>	<ul style="list-style-type: none"> • MUR_LWAL-DNO_H2: Unreinforced masonry / load-bearing wall / non-ductile / 2 storeys • MUR_LWAL-DNO_H4: Unreinforced masonry / load-bearing wall / non-ductile / 4 storeys • CR_LWAL-DUL_H4: Reinforced concrete / shear wall system / low ductility / 4 storeys • MUR_LWAL-DNO_H5: Unreinforced masonry / load-bearing wall / non-ductile / 5 storeys • MCF_LWAL-DUL_H4: Confined masonry / load-bearing wall / low ductility / 4 storeys 					
<i>Methodology</i>	Analytical, from capacity curves					
<i>Damage states</i>	ESRM20 limit states, based on the yield displacement and the ultimate (final) displacement in the capacity curve: <ul style="list-style-type: none"> • DS1: slight • DS2: moderate • DS3: extensive • DS4: complete 					
<i>Intensity Measure</i>	PGA [g]					
<i>Fragility parameters</i>	Class	Median [g]				β
		DS1	DS2	DS3	DS4	
	MUR_LWAL-DNO_H2	0.239	0.526	0.760	0.958	0.61
	MUR_LWAL-DNO_H4	0.230	0.514	0.780	1.023	0.86
	CR_LWAL-DUL_H4	0.340	0.810	1.214	1.566	0.66
	MUR_LWAL-DNO_H5	0.275	0.554	0.828	1.083	0.93
	MCF_LWAL-DUL_H4	0.291	0.659	0.997	1.300	0.79

Figures

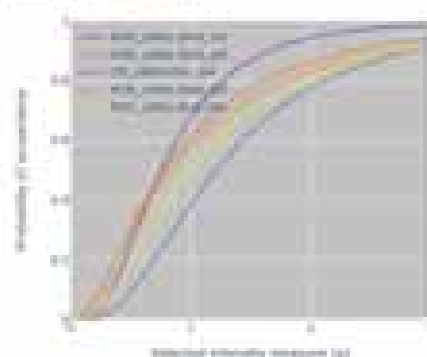
Fragility Functions (D1)



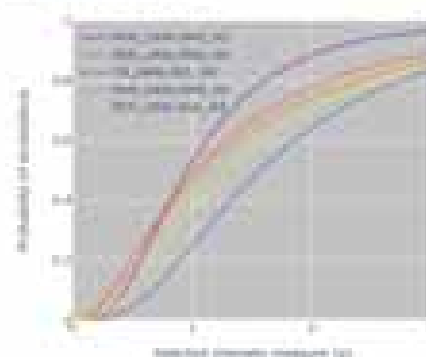
Fragility Functions (D2)



Fragility Functions (D3)

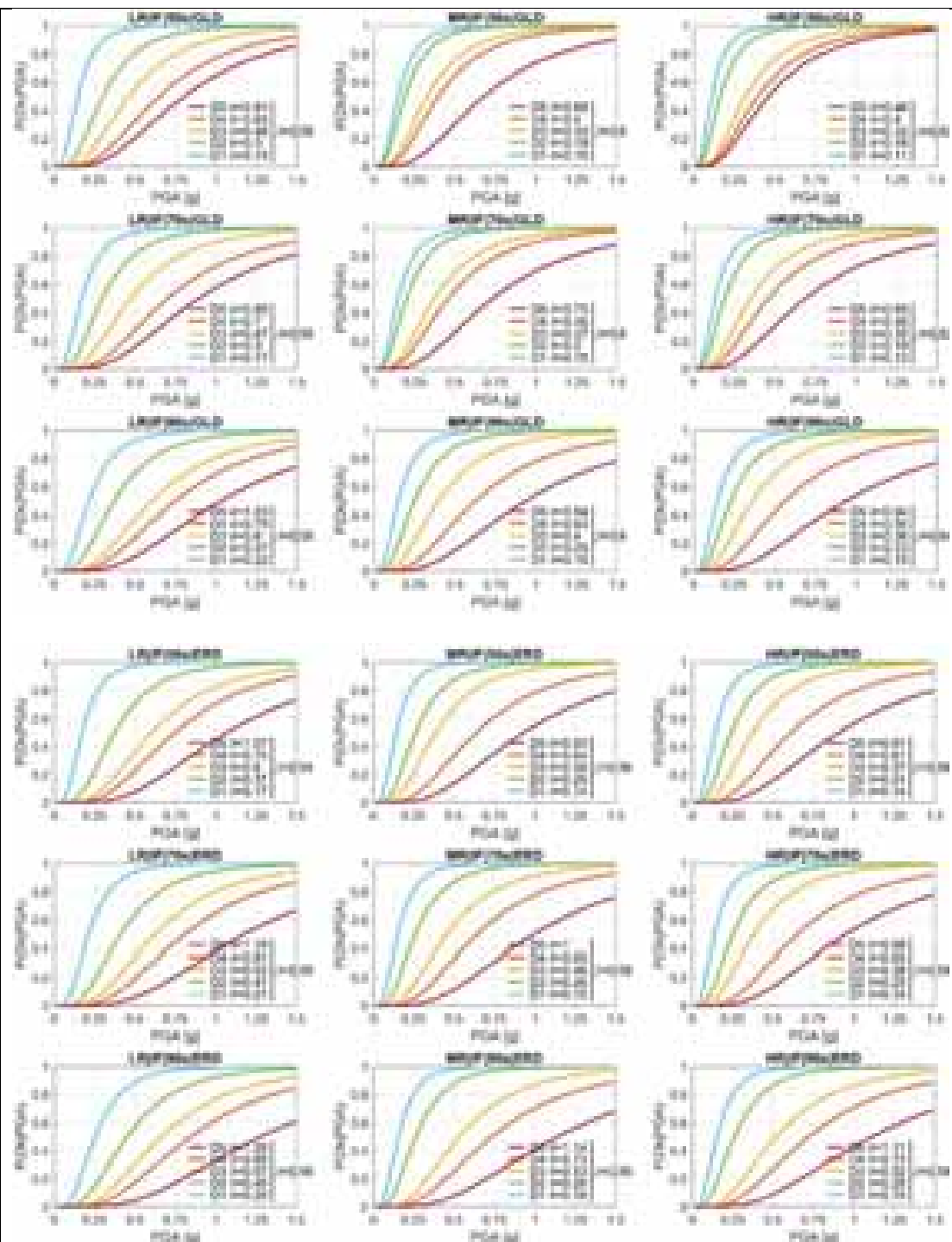


Fragility Functions (D4)



FRAG EQ BDG Manfredi2023																																																																																																																																																																																																																																						
References	Manfredi, V., Masi, A., Nicodemo, G., & Digrisolo, A. (2023). Seismic fragility curves for the Italian RC residential buildings based on non-linear dynamic analyses. Bulletin of Earthquake Engineering, 21(4), 2173-2214.																																																																																																																																																																																																																																					
Region of applicability	Italy																																																																																																																																																																																																																																					
Class	54 classes of RC residential buildings, with a combination of the following attributes: <ul style="list-style-type: none">• LR / MR / HR (height): low-rise (2 storeys), mid-rise (4 storeys), high-rise (6 storeys)• IF / BF / PF (arrangement in elevation of infills): infilled frame, bare frame, pilotis frame• 50s / 70s / 90s (age of construction): built around the 1950s, 1970s, 1990s• ERD / GLD (design level): earthquake design level, gravity load design																																																																																																																																																																																																																																					
Methodology	Analytical, based on non-linear dynamic analyses																																																																																																																																																																																																																																					
Damage states	EMS-98 damage grades: <ul style="list-style-type: none">• DS1: slight• DS2: moderate• DS3: heavy• DS4: very heavy• DS5: destruction																																																																																																																																																																																																																																					
Intensity Measure	PGA [g]																																																																																																																																																																																																																																					
Fragility parameters	Fragility parameters for the class of RC infilled frame buildings: <table><tr><th rowspan="2">Class</th><th colspan="2">DS1</th><th colspan="2">DS2</th><th colspan="2">DS3</th><th colspan="2">DS4</th><th colspan="2">DS</th></tr><tr><th>α [g]</th><th>β</th><th>α [g]</th><th>β</th><th>α [g]</th><th>β</th><th>α [g]</th><th>β</th><th>α [g]</th><th>β</th></tr><tr><td>LR IF 50s GLD</td><td>0.15</td><td>0.58</td><td>0.30</td><td>0.58</td><td>0.46</td><td>0.58</td><td>0.65</td><td>0.58</td><td>0.81</td><td>0.58</td></tr><tr><td>MR IF 50s GLD</td><td>0.15</td><td>0.60</td><td>0.19</td><td>0.60</td><td>0.33</td><td>0.60</td><td>0.40</td><td>0.60</td><td>0.68</td><td>0.60</td></tr><tr><td>HR IF 50s GLD</td><td>0.11</td><td>0.62</td><td>0.16</td><td>0.62</td><td>0.32</td><td>0.62</td><td>0.40</td><td>0.62</td><td>0.46</td><td>0.62</td></tr><tr><td>LR IF 70s GLD</td><td>0.17</td><td>0.58</td><td>0.30</td><td>0.58</td><td>0.47</td><td>0.58</td><td>0.70</td><td>0.58</td><td>0.89</td><td>0.58</td></tr><tr><td>MR IF 70s GLD</td><td>0.15</td><td>0.60</td><td>0.20</td><td>0.60</td><td>0.37</td><td>0.60</td><td>0.46</td><td>0.60</td><td>0.73</td><td>0.60</td></tr><tr><td>HR IF 70s GLD</td><td>0.13</td><td>0.62</td><td>0.19</td><td>0.62</td><td>0.35</td><td>0.62</td><td>0.46</td><td>0.62</td><td>0.69</td><td>0.62</td></tr><tr><td>LR IF 90s GLD</td><td>0.22</td><td>0.58</td><td>0.37</td><td>0.58</td><td>0.60</td><td>0.58</td><td>0.75</td><td>0.58</td><td>1.03</td><td>0.58</td></tr><tr><td>MR IF 90s GLD</td><td>0.15</td><td>0.60</td><td>0.25</td><td>0.60</td><td>0.40</td><td>0.60</td><td>0.63</td><td>0.60</td><td>0.94</td><td>0.60</td></tr><tr><td>HR IF 90s GLD</td><td>0.15</td><td>0.64</td><td>0.23</td><td>0.64</td><td>0.36</td><td>0.64</td><td>0.56</td><td>0.64</td><td>0.94</td><td>0.64</td></tr><tr><td>LR IF 50s ERD</td><td>0.17</td><td>0.54</td><td>0.37</td><td>0.54</td><td>0.60</td><td>0.54</td><td>0.75</td><td>0.54</td><td>1.07</td><td>0.54</td></tr><tr><td>MR IF 50s ERD</td><td>0.14</td><td>0.56</td><td>0.26</td><td>0.56</td><td>0.39</td><td>0.56</td><td>0.64</td><td>0.56</td><td>0.93</td><td>0.56</td></tr><tr><td>HR IF 50s ERD</td><td>0.14</td><td>0.58</td><td>0.24</td><td>0.58</td><td>0.37</td><td>0.58</td><td>0.61</td><td>0.58</td><td>0.91</td><td>0.58</td></tr><tr><td>LR IF 70s ERD</td><td>0.21</td><td>0.55</td><td>0.41</td><td>0.55</td><td>0.63</td><td>0.55</td><td>0.81</td><td>0.55</td><td>1.18</td><td>0.55</td></tr><tr><td>MR IF 70s ERD</td><td>0.15</td><td>0.58</td><td>0.26</td><td>0.58</td><td>0.46</td><td>0.58</td><td>0.65</td><td>0.58</td><td>1.00</td><td>0.58</td></tr><tr><td>HR IF 70s ERD</td><td>0.14</td><td>0.59</td><td>0.25</td><td>0.59</td><td>0.38</td><td>0.59</td><td>0.65</td><td>0.59</td><td>0.96</td><td>0.59</td></tr><tr><td>LR IF 90s ERD</td><td>0.25</td><td>0.56</td><td>0.45</td><td>0.56</td><td>0.67</td><td>0.56</td><td>0.85</td><td>0.56</td><td>1.28</td><td>0.56</td></tr><tr><td>MR IF 90s ERD</td><td>0.16</td><td>0.56</td><td>0.26</td><td>0.56</td><td>0.53</td><td>0.56</td><td>0.73</td><td>0.56</td><td>1.14</td><td>0.56</td></tr><tr><td>HR IF 90s ERD</td><td>0.15</td><td>0.59</td><td>0.26</td><td>0.59</td><td>0.52</td><td>0.59</td><td>0.72</td><td>0.59</td><td>1.11</td><td>0.59</td></tr></table>											Class	DS1		DS2		DS3		DS4		DS		α [g]	β	α [g]	β	α [g]	β	α [g]	β	α [g]	β	LR IF 50s GLD	0.15	0.58	0.30	0.58	0.46	0.58	0.65	0.58	0.81	0.58	MR IF 50s GLD	0.15	0.60	0.19	0.60	0.33	0.60	0.40	0.60	0.68	0.60	HR IF 50s GLD	0.11	0.62	0.16	0.62	0.32	0.62	0.40	0.62	0.46	0.62	LR IF 70s GLD	0.17	0.58	0.30	0.58	0.47	0.58	0.70	0.58	0.89	0.58	MR IF 70s GLD	0.15	0.60	0.20	0.60	0.37	0.60	0.46	0.60	0.73	0.60	HR IF 70s GLD	0.13	0.62	0.19	0.62	0.35	0.62	0.46	0.62	0.69	0.62	LR IF 90s GLD	0.22	0.58	0.37	0.58	0.60	0.58	0.75	0.58	1.03	0.58	MR IF 90s GLD	0.15	0.60	0.25	0.60	0.40	0.60	0.63	0.60	0.94	0.60	HR IF 90s GLD	0.15	0.64	0.23	0.64	0.36	0.64	0.56	0.64	0.94	0.64	LR IF 50s ERD	0.17	0.54	0.37	0.54	0.60	0.54	0.75	0.54	1.07	0.54	MR IF 50s ERD	0.14	0.56	0.26	0.56	0.39	0.56	0.64	0.56	0.93	0.56	HR IF 50s ERD	0.14	0.58	0.24	0.58	0.37	0.58	0.61	0.58	0.91	0.58	LR IF 70s ERD	0.21	0.55	0.41	0.55	0.63	0.55	0.81	0.55	1.18	0.55	MR IF 70s ERD	0.15	0.58	0.26	0.58	0.46	0.58	0.65	0.58	1.00	0.58	HR IF 70s ERD	0.14	0.59	0.25	0.59	0.38	0.59	0.65	0.59	0.96	0.59	LR IF 90s ERD	0.25	0.56	0.45	0.56	0.67	0.56	0.85	0.56	1.28	0.56	MR IF 90s ERD	0.16	0.56	0.26	0.56	0.53	0.56	0.73	0.56	1.14	0.56	HR IF 90s ERD	0.15	0.59	0.26	0.59	0.52	0.59	0.72	0.59	1.11	0.59
Class	DS1		DS2		DS3		DS4		DS																																																																																																																																																																																																																													
	α [g]	β	α [g]	β	α [g]	β	α [g]	β	α [g]	β																																																																																																																																																																																																																												
LR IF 50s GLD	0.15	0.58	0.30	0.58	0.46	0.58	0.65	0.58	0.81	0.58																																																																																																																																																																																																																												
MR IF 50s GLD	0.15	0.60	0.19	0.60	0.33	0.60	0.40	0.60	0.68	0.60																																																																																																																																																																																																																												
HR IF 50s GLD	0.11	0.62	0.16	0.62	0.32	0.62	0.40	0.62	0.46	0.62																																																																																																																																																																																																																												
LR IF 70s GLD	0.17	0.58	0.30	0.58	0.47	0.58	0.70	0.58	0.89	0.58																																																																																																																																																																																																																												
MR IF 70s GLD	0.15	0.60	0.20	0.60	0.37	0.60	0.46	0.60	0.73	0.60																																																																																																																																																																																																																												
HR IF 70s GLD	0.13	0.62	0.19	0.62	0.35	0.62	0.46	0.62	0.69	0.62																																																																																																																																																																																																																												
LR IF 90s GLD	0.22	0.58	0.37	0.58	0.60	0.58	0.75	0.58	1.03	0.58																																																																																																																																																																																																																												
MR IF 90s GLD	0.15	0.60	0.25	0.60	0.40	0.60	0.63	0.60	0.94	0.60																																																																																																																																																																																																																												
HR IF 90s GLD	0.15	0.64	0.23	0.64	0.36	0.64	0.56	0.64	0.94	0.64																																																																																																																																																																																																																												
LR IF 50s ERD	0.17	0.54	0.37	0.54	0.60	0.54	0.75	0.54	1.07	0.54																																																																																																																																																																																																																												
MR IF 50s ERD	0.14	0.56	0.26	0.56	0.39	0.56	0.64	0.56	0.93	0.56																																																																																																																																																																																																																												
HR IF 50s ERD	0.14	0.58	0.24	0.58	0.37	0.58	0.61	0.58	0.91	0.58																																																																																																																																																																																																																												
LR IF 70s ERD	0.21	0.55	0.41	0.55	0.63	0.55	0.81	0.55	1.18	0.55																																																																																																																																																																																																																												
MR IF 70s ERD	0.15	0.58	0.26	0.58	0.46	0.58	0.65	0.58	1.00	0.58																																																																																																																																																																																																																												
HR IF 70s ERD	0.14	0.59	0.25	0.59	0.38	0.59	0.65	0.59	0.96	0.59																																																																																																																																																																																																																												
LR IF 90s ERD	0.25	0.56	0.45	0.56	0.67	0.56	0.85	0.56	1.28	0.56																																																																																																																																																																																																																												
MR IF 90s ERD	0.16	0.56	0.26	0.56	0.53	0.56	0.73	0.56	1.14	0.56																																																																																																																																																																																																																												
HR IF 90s ERD	0.15	0.59	0.26	0.59	0.52	0.59	0.72	0.59	1.11	0.59																																																																																																																																																																																																																												

Figures

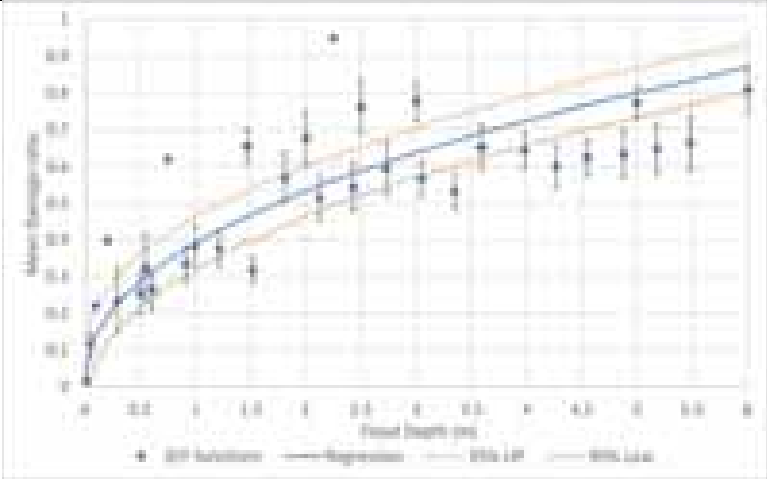


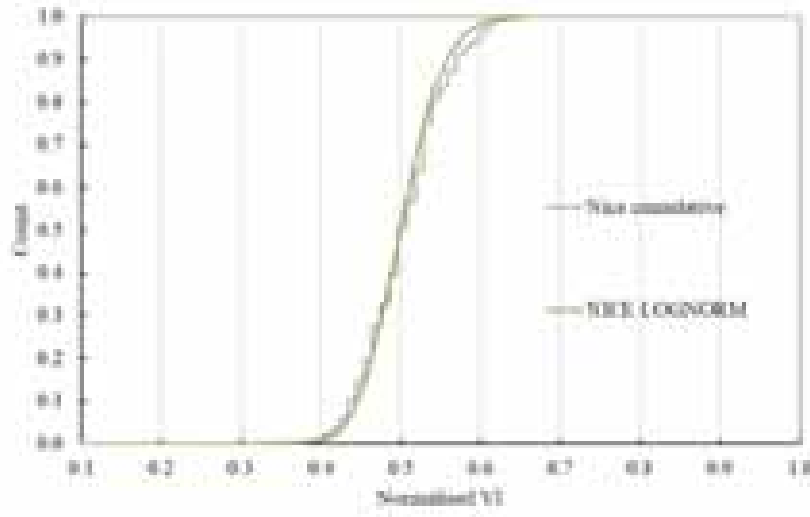
FRAG EQ BDG Kappos2013																																																																																																																																																																																																																																					
References	Kappos, A. (2013). Seismic vulnerability and loss assessment for buildings in Greece. In Seismic vulnerability of structure, Ed., P. Guéguen, p. 111-160. ISTE, Wiley, ISBN: 978-1-84821-524-5																																																																																																																																																																																																																																				
Region of applicability	Greece																																																																																																																																																																																																																																				
Class	18 classes of RC frame buildings, with a combination of the following attributes: <ul style="list-style-type: none"> • RC1 / RC3.1 / R3.2 (structural system): bare frame, regularly infilled frame, irregularly infilled frame • L / M / H (height): low-rise (2 storeys), mid-rise (4 storeys), high-rise (6 storeys) • L / M (design level): low code, moderate code 																																																																																																																																																																																																																																				
Methodology	“Hybrid” approach, combining empirical data with results from non-linear dynamic and static analyses																																																																																																																																																																																																																																				
Damage states	<ul style="list-style-type: none"> • DS1: slight • DS2: moderate • DS3: substantial to heavy • DS4: very heavy • DS5: collapse 																																																																																																																																																																																																																																				
Intensity Measure	PGA [g]																																																																																																																																																																																																																																				
Fragility parameters	<table border="1"> <thead> <tr> <th rowspan="2">Class</th><th colspan="2">DS1</th><th colspan="2">DS2</th><th colspan="2">DS3</th><th colspan="2">DS4</th><th colspan="2">DS</th></tr> <tr> <th>α [g]</th><th>β</th><th>α [g]</th><th>β</th><th>α [g]</th><th>β</th><th>α [g]</th><th>β</th><th>α [g]</th><th>β</th></tr> </thead> <tbody> <tr><td>RC1LL</td><td>0.001</td><td>0.733</td><td>0.012</td><td>0.733</td><td>0.096</td><td>0.733</td><td>0.157</td><td>0.733</td><td>0.219</td><td>0.733</td></tr> <tr><td>RC3.1LL</td><td>0.021</td><td>0.733</td><td>0.101</td><td>0.733</td><td>0.201</td><td>0.733</td><td>0.257</td><td>0.733</td><td>0.343</td><td>0.733</td></tr> <tr><td>RC3.2LL</td><td>0.005</td><td>0.733</td><td>0.049</td><td>0.733</td><td>0.116</td><td>0.733</td><td>0.181</td><td>0.733</td><td>0.230</td><td>0.733</td></tr> <tr><td>RC1ML</td><td>0.001</td><td>0.651</td><td>0.013</td><td>0.651</td><td>0.095</td><td>0.651</td><td>0.136</td><td>0.651</td><td>0.192</td><td>0.651</td></tr> <tr><td>RC3.1ML</td><td>0.005</td><td>0.651</td><td>0.055</td><td>0.651</td><td>0.190</td><td>0.651</td><td>0.216</td><td>0.651</td><td>0.254</td><td>0.651</td></tr> <tr><td>RC3.2ML</td><td>0.000</td><td>0.651</td><td>0.004</td><td>0.651</td><td>0.042</td><td>0.651</td><td>0.099</td><td>0.651</td><td>0.136</td><td>0.651</td></tr> <tr><td>RC1HL</td><td>0.006</td><td>0.629</td><td>0.061</td><td>0.629</td><td>0.149</td><td>0.629</td><td>0.276</td><td>0.629</td><td>0.545</td><td>0.629</td></tr> <tr><td>RC3.1HL</td><td>0.013</td><td>0.629</td><td>0.097</td><td>0.629</td><td>0.210</td><td>0.629</td><td>0.296</td><td>0.629</td><td>0.548</td><td>0.629</td></tr> <tr><td>RC3.2HL</td><td>0.044</td><td>0.629</td><td>0.101</td><td>0.629</td><td>0.209</td><td>0.629</td><td>0.353</td><td>0.629</td><td>0.673</td><td>0.629</td></tr> <tr><td>RC1LM</td><td>0.002</td><td>0.733</td><td>0.023</td><td>0.733</td><td>0.148</td><td>0.733</td><td>0.413</td><td>0.733</td><td>0.639</td><td>0.733</td></tr> <tr><td>RC3.1LM</td><td>0.090</td><td>0.733</td><td>0.123</td><td>0.733</td><td>0.298</td><td>0.733</td><td>0.730</td><td>0.733</td><td>1.391</td><td>0.733</td></tr> <tr><td>RC3.2LM</td><td>0.005</td><td>0.733</td><td>0.051</td><td>0.733</td><td>0.215</td><td>0.733</td><td>0.497</td><td>0.733</td><td>0.748</td><td>0.733</td></tr> <tr><td>RC1MM</td><td>0.001</td><td>0.651</td><td>0.014</td><td>0.651</td><td>0.115</td><td>0.651</td><td>0.297</td><td>0.651</td><td>0.844</td><td>0.651</td></tr> <tr><td>RC3.1MM</td><td>0.008</td><td>0.651</td><td>0.078</td><td>0.651</td><td>0.201</td><td>0.651</td><td>0.422</td><td>0.651</td><td>0.853</td><td>0.651</td></tr> <tr><td>RC3.2MM</td><td>0.001</td><td>0.651</td><td>0.011</td><td>0.651</td><td>0.116</td><td>0.651</td><td>0.476</td><td>0.651</td><td>0.795</td><td>0.651</td></tr> <tr><td>RC1HM</td><td>0.006</td><td>0.629</td><td>0.056</td><td>0.629</td><td>0.363</td><td>0.629</td><td>1.471</td><td>0.629</td><td>2.724</td><td>0.629</td></tr> <tr><td>RC3.1HM</td><td>0.017</td><td>0.629</td><td>0.109</td><td>0.629</td><td>0.419</td><td>0.629</td><td>0.923</td><td>0.629</td><td>3.471</td><td>0.629</td></tr> <tr><td>RC3.2HM</td><td>0.015</td><td>0.629</td><td>0.110</td><td>0.629</td><td>0.525</td><td>0.629</td><td>1.103</td><td>0.629</td><td>2.370</td><td>0.629</td></tr> </tbody> </table>										Class	DS1		DS2		DS3		DS4		DS		α [g]	β	α [g]	β	α [g]	β	α [g]	β	α [g]	β	RC1LL	0.001	0.733	0.012	0.733	0.096	0.733	0.157	0.733	0.219	0.733	RC3.1LL	0.021	0.733	0.101	0.733	0.201	0.733	0.257	0.733	0.343	0.733	RC3.2LL	0.005	0.733	0.049	0.733	0.116	0.733	0.181	0.733	0.230	0.733	RC1ML	0.001	0.651	0.013	0.651	0.095	0.651	0.136	0.651	0.192	0.651	RC3.1ML	0.005	0.651	0.055	0.651	0.190	0.651	0.216	0.651	0.254	0.651	RC3.2ML	0.000	0.651	0.004	0.651	0.042	0.651	0.099	0.651	0.136	0.651	RC1HL	0.006	0.629	0.061	0.629	0.149	0.629	0.276	0.629	0.545	0.629	RC3.1HL	0.013	0.629	0.097	0.629	0.210	0.629	0.296	0.629	0.548	0.629	RC3.2HL	0.044	0.629	0.101	0.629	0.209	0.629	0.353	0.629	0.673	0.629	RC1LM	0.002	0.733	0.023	0.733	0.148	0.733	0.413	0.733	0.639	0.733	RC3.1LM	0.090	0.733	0.123	0.733	0.298	0.733	0.730	0.733	1.391	0.733	RC3.2LM	0.005	0.733	0.051	0.733	0.215	0.733	0.497	0.733	0.748	0.733	RC1MM	0.001	0.651	0.014	0.651	0.115	0.651	0.297	0.651	0.844	0.651	RC3.1MM	0.008	0.651	0.078	0.651	0.201	0.651	0.422	0.651	0.853	0.651	RC3.2MM	0.001	0.651	0.011	0.651	0.116	0.651	0.476	0.651	0.795	0.651	RC1HM	0.006	0.629	0.056	0.629	0.363	0.629	1.471	0.629	2.724	0.629	RC3.1HM	0.017	0.629	0.109	0.629	0.419	0.629	0.923	0.629	3.471	0.629	RC3.2HM	0.015	0.629	0.110	0.629	0.525	0.629	1.103	0.629	2.370	0.629
Class	DS1		DS2		DS3		DS4		DS																																																																																																																																																																																																																												
	α [g]	β	α [g]	β	α [g]	β	α [g]	β	α [g]	β																																																																																																																																																																																																																											
RC1LL	0.001	0.733	0.012	0.733	0.096	0.733	0.157	0.733	0.219	0.733																																																																																																																																																																																																																											
RC3.1LL	0.021	0.733	0.101	0.733	0.201	0.733	0.257	0.733	0.343	0.733																																																																																																																																																																																																																											
RC3.2LL	0.005	0.733	0.049	0.733	0.116	0.733	0.181	0.733	0.230	0.733																																																																																																																																																																																																																											
RC1ML	0.001	0.651	0.013	0.651	0.095	0.651	0.136	0.651	0.192	0.651																																																																																																																																																																																																																											
RC3.1ML	0.005	0.651	0.055	0.651	0.190	0.651	0.216	0.651	0.254	0.651																																																																																																																																																																																																																											
RC3.2ML	0.000	0.651	0.004	0.651	0.042	0.651	0.099	0.651	0.136	0.651																																																																																																																																																																																																																											
RC1HL	0.006	0.629	0.061	0.629	0.149	0.629	0.276	0.629	0.545	0.629																																																																																																																																																																																																																											
RC3.1HL	0.013	0.629	0.097	0.629	0.210	0.629	0.296	0.629	0.548	0.629																																																																																																																																																																																																																											
RC3.2HL	0.044	0.629	0.101	0.629	0.209	0.629	0.353	0.629	0.673	0.629																																																																																																																																																																																																																											
RC1LM	0.002	0.733	0.023	0.733	0.148	0.733	0.413	0.733	0.639	0.733																																																																																																																																																																																																																											
RC3.1LM	0.090	0.733	0.123	0.733	0.298	0.733	0.730	0.733	1.391	0.733																																																																																																																																																																																																																											
RC3.2LM	0.005	0.733	0.051	0.733	0.215	0.733	0.497	0.733	0.748	0.733																																																																																																																																																																																																																											
RC1MM	0.001	0.651	0.014	0.651	0.115	0.651	0.297	0.651	0.844	0.651																																																																																																																																																																																																																											
RC3.1MM	0.008	0.651	0.078	0.651	0.201	0.651	0.422	0.651	0.853	0.651																																																																																																																																																																																																																											
RC3.2MM	0.001	0.651	0.011	0.651	0.116	0.651	0.476	0.651	0.795	0.651																																																																																																																																																																																																																											
RC1HM	0.006	0.629	0.056	0.629	0.363	0.629	1.471	0.629	2.724	0.629																																																																																																																																																																																																																											
RC3.1HM	0.017	0.629	0.109	0.629	0.419	0.629	0.923	0.629	3.471	0.629																																																																																																																																																																																																																											
RC3.2HM	0.015	0.629	0.110	0.629	0.525	0.629	1.103	0.629	2.370	0.629																																																																																																																																																																																																																											
Figures	-																																																																																																																																																																																																																																				

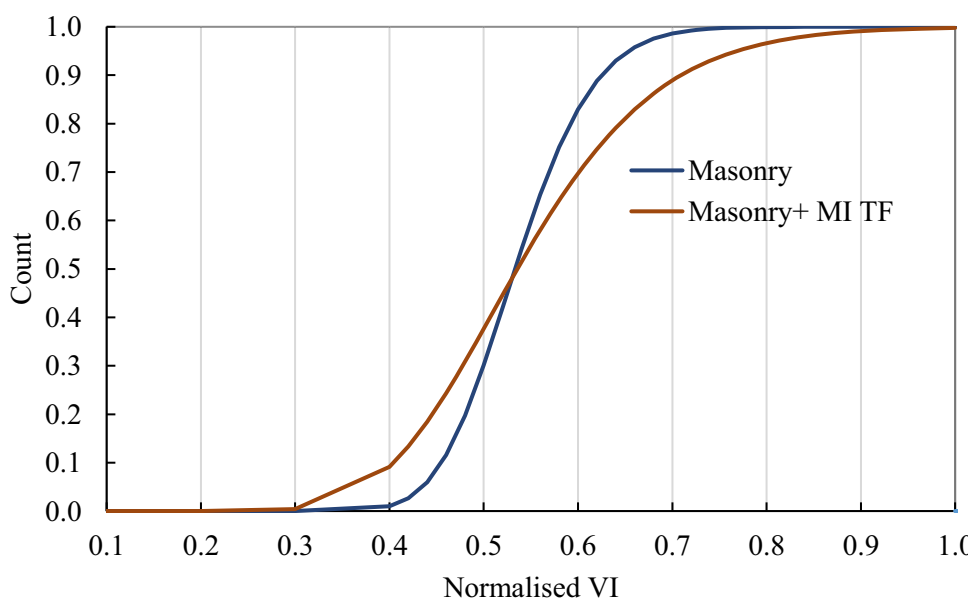
9.2 Flood vulnerability models

9.2.1 Buildings

VUL_FL_BDG_D'Ayala 2020. PARNASUSS V.3		
<i>References</i>	D. D'Ayala, K. Wang, Y. Yan, H. Smith, A. Massam, V. Filipova, J.J. Pereira, Flood vulnerability and risk assessment of urban traditional buildings in a heritage district of Kuala Lumpur Malaysia. Natural Hazards and Earth System Sciences, 20 (8) (2020), pp. 2221-2241, 10.5194/nhess-20-2221-2020	
<i>Region of applicability</i>	Worldwide, as obtained from regression of a large number of proposed flood depth/damage ratios used in different countries	
<i>Typology</i>	No typological classification – applicable to residential buildings	
<i>Methodology</i>	Empirical data and literature survey.	
<i>Damage Measure</i>	Damage factor between 0 and 1 (non-dimensional economic value of the buildings and its contents)	
<i>Intensity Measure</i>	Flood depth [m]	
<i>Functional form</i>	Generic function	
	Flood Dept (m)	Damage factor
	0	0
	0.005	0.03714702
	0.05	0.103377
	0.1	0.14067981
	0.2	0.19144305
	0.3	0.22925149
	0.5	0.28768945
	0.6	0.31197515
	0.7	0.33410105
	0.8	0.35453186
	0.9	0.37358769
	1	0.3915
	1.2	0.42454901
	1.5	0.46881806
	1.7	0.49563996
	2	0.5327698
	2.3	0.5669174
	2.5	0.58832337
	2.7	0.60879764
	3	0.63798749
	3.3	0.66559678
	3.5	0.68323485
	3.7	0.70032146

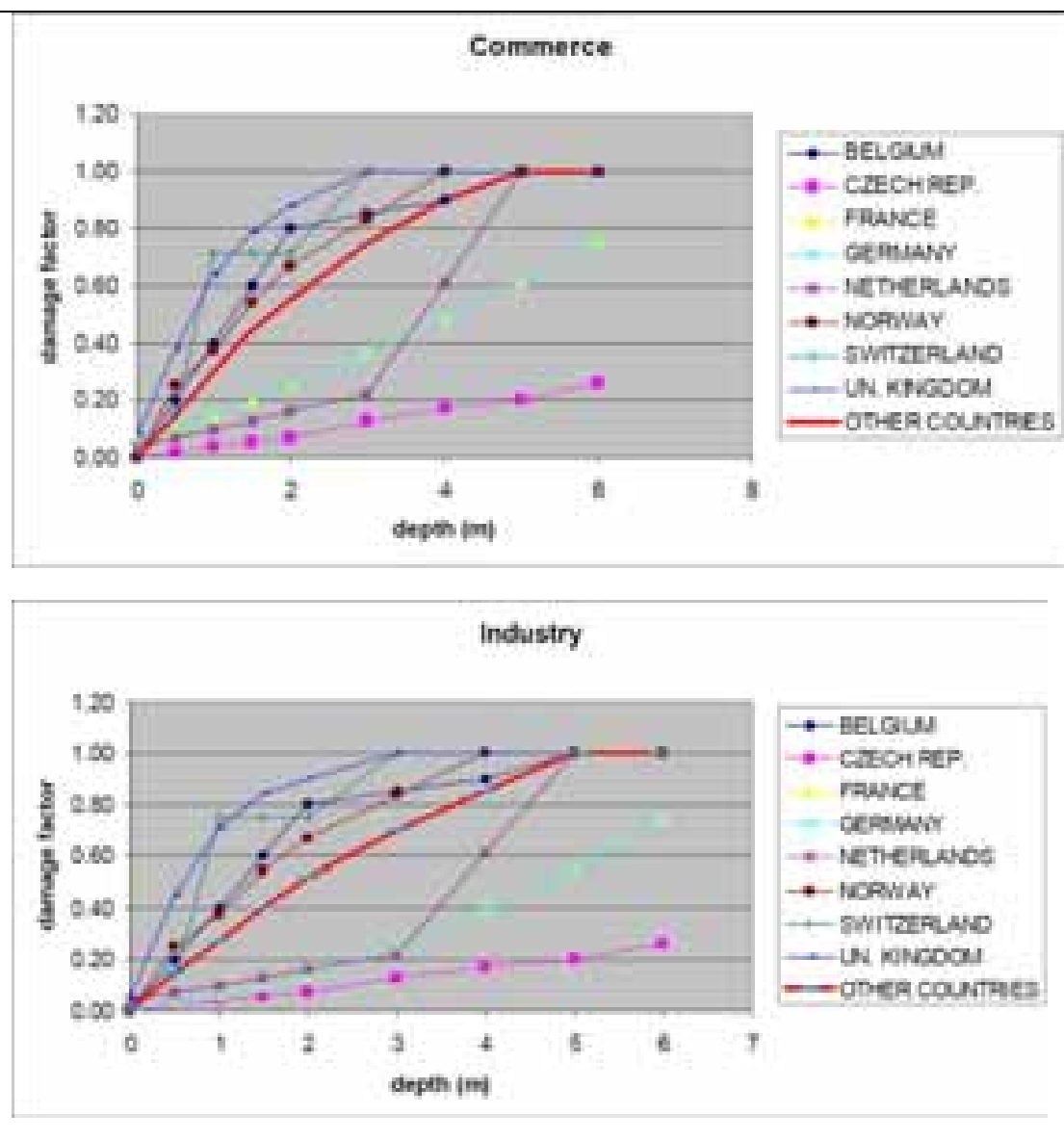
	4	0.72501574
	4.5	0.76398482
	5	0.80061539
	5.5	0.8352625
	6	0.86820043
Figures		

VUL INDEX FL BDG D'Ayala 2020. PARNASUSS V.3 for NICE testbed																		
References	D. D'Ayala, K. Wang, Y. Yan, H. Smith, A. Massam, V. Filipova, J.J. Pereira, Flood vulnerability and risk assessment of urban traditional buildings in a heritage district of Kuala Lumpur Malaysia. Natural Hazards and Earth System Sciences, 20 (8) (2020), pp. 2221-2241, 10.5194/nhess-20-2221-2020																	
Region of applicability	Nice and South France																	
Typology	Residential Masonry buildings																	
Methodology	Empirical data and virtual survey .																	
Damage Measure	Damage factor between 0 and 1 (value of the buildings and its contents)																	
Intensity Measure	Vulnerability index $VI_i = \sum_j VR_{ij}$ normalised $nVI_i = \frac{VI_i}{(VI_{i_{max}} + VI_{i_{min}})/2}$																	
Functional form	<p>Vulnerability index normalised curve and natural log</p> <table border="1"> <thead> <tr> <th rowspan="2">Typology</th><th colspan="2">VI</th><th colspan="2">Natural log</th></tr> <tr> <th>α</th><th>β</th><th>α</th><th>β</th></tr> </thead> <tbody> <tr> <td>Residential masonry buildings 1 to 4 storey high</td><td>0.496528</td><td>0.050741</td><td>-0.700116</td><td>0.402578</td></tr> </tbody> </table> <p>To be used in conjunction with the Flood depth to damage ratio curve in the previous table to compute losses for specific flood hazard scenario</p>				Typology	VI		Natural log		α	β	α	β	Residential masonry buildings 1 to 4 storey high	0.496528	0.050741	-0.700116	0.402578
Typology	VI		Natural log															
	α	β	α	β														
Residential masonry buildings 1 to 4 storey high	0.496528	0.050741	-0.700116	0.402578														
Figures																		

VUL INDEX FL BDG D'Ayala 2020. PARNASUSS V.3 for Essex Testbed																							
References	D. D'Ayala, K. Wang, Y. Yan, H. Smith, A. Massam, V. Filipova, J.J. Pereira, Flood vulnerability and risk assessment of urban traditional buildings in a heritage district of Kuala Lumpur Malaysia. Natural Hazards and Earth System Sciences, 20 (8) (2020), pp. 2221-2241, 10.5194/nhess-20-2221-2020																						
Region of applicability	Chelmsford and other historic centres in Essex and beyond in the UK																						
Typology	Residential Masonry buildings																						
Methodology	Empirical data collected on site in Bristol and Tewkesbury .																						
Damage Measure	Damage factor between 0 and 1 (value of the buildings and its contents)																						
Intensity Measure	Vulnerability index $VI_i = \sum_j VR_{ij}$ normalised $nVI_i = \frac{VI_i}{(VI_{i_{max}} + VI_{i_{min}})/2}$																						
Functional form	<p>Vulnerability index normalised curve and natural log</p> <table border="1"> <thead> <tr> <th rowspan="2">Typology</th><th colspan="2">VI</th><th colspan="2">Natural log</th></tr> <tr> <th>α</th><th>β</th><th>α</th><th>β</th></tr> </thead> <tbody> <tr> <td>Residential masonry buildings 1 to 4 storey high</td><td>0.533333</td><td>0.06259</td><td>-0.62862</td><td>0.123584</td></tr> <tr> <td>Residential masonry and masonry infilled timber frame buildings 1 to 3 storey high</td><td>0.536</td><td>0.114084</td><td>-0.62415</td><td>0.219131</td></tr> </tbody> </table> <p>To be used in conjunction with the Flood depth to damage ratio curve in the previous table to compute losses for specific flood hazard scenario</p>				Typology	VI		Natural log		α	β	α	β	Residential masonry buildings 1 to 4 storey high	0.533333	0.06259	-0.62862	0.123584	Residential masonry and masonry infilled timber frame buildings 1 to 3 storey high	0.536	0.114084	-0.62415	0.219131
Typology	VI		Natural log																				
	α	β	α	β																			
Residential masonry buildings 1 to 4 storey high	0.533333	0.06259	-0.62862	0.123584																			
Residential masonry and masonry infilled timber frame buildings 1 to 3 storey high	0.536	0.114084	-0.62415	0.219131																			
Figures																							

VUL FL BDG Huizinga2017

References	Huizinga, J., Moel, H. de, Szewczyk, W. (2017). Global flood depth-damage functions. Methodology and the database with guidelines. EUR 28552 EN. doi: 10.2760/16510																																																																																																
Region of applicability	Europe (Belgium, Czech Rep., Denmark, France, Germany, Hungary, Netherlands, Norway, Switzerland, UK)																																																																																																
Classs	No classification – Differences between Residential, Commerce and Industry																																																																																																
Methodology	Empirical data and literature survey																																																																																																
Damage Measure	Damage factor between 0 and 1 (value of the buildings and is contents)																																																																																																
Intensity Measure	Flood depth [m]																																																																																																
Functional form	Generic function for Europe: <table><tr><th rowspan="2">Flood depth [m]</th><th colspan="3">Damage factor</th></tr><tr><th>Residential</th><th>Commercial</th><th>Industrial</th></tr><tr><td>0.0</td><td>0.00</td><td>0.00</td><td>0.00</td></tr><tr><td>0.5</td><td>0.25</td><td>0.15</td><td>0.15</td></tr><tr><td>1.0</td><td>0.40</td><td>0.30</td><td>0.27</td></tr><tr><td>1.</td><td>0.50</td><td>0.45</td><td>0.40</td></tr><tr><td>2.0</td><td>0.60</td><td>0.55</td><td>0.52</td></tr><tr><td>3.0</td><td>0.75</td><td>0.75</td><td>0.70</td></tr><tr><td>4.0</td><td>0.85</td><td>0.90</td><td>0.85</td></tr><tr><td>5.0</td><td>0.95</td><td>1.00</td><td>1.00</td></tr><tr><td>6.0</td><td>1.00</td><td>1.00</td><td>1.00</td></tr></table>	Flood depth [m]	Damage factor			Residential	Commercial	Industrial	0.0	0.00	0.00	0.00	0.5	0.25	0.15	0.15	1.0	0.40	0.30	0.27	1.	0.50	0.45	0.40	2.0	0.60	0.55	0.52	3.0	0.75	0.75	0.70	4.0	0.85	0.90	0.85	5.0	0.95	1.00	1.00	6.0	1.00	1.00	1.00																																																					
Flood depth [m]	Damage factor																																																																																																
	Residential	Commercial	Industrial																																																																																														
0.0	0.00	0.00	0.00																																																																																														
0.5	0.25	0.15	0.15																																																																																														
1.0	0.40	0.30	0.27																																																																																														
1.	0.50	0.45	0.40																																																																																														
2.0	0.60	0.55	0.52																																																																																														
3.0	0.75	0.75	0.70																																																																																														
4.0	0.85	0.90	0.85																																																																																														
5.0	0.95	1.00	1.00																																																																																														
6.0	1.00	1.00	1.00																																																																																														
Figures	<div>Residential buildings & content</div> <table><caption>Estimated data from 'Residential buildings & content' graph</caption><thead><tr><th>Depth (m)</th><th>Belgium</th><th>Czech Rep.</th><th>Denmark</th><th>France</th><th>Germany</th><th>Hungary</th><th>Netherlands</th><th>Norway</th><th>Switzerland</th><th>LN. Kingdom</th><th>Other Countries</th></tr></thead><tbody><tr><td>0</td><td>0.00</td><td>0.00</td><td>0.00</td><td>0.00</td><td>0.00</td><td>0.00</td><td>0.00</td><td>0.00</td><td>0.00</td><td>0.00</td><td>0.00</td></tr><tr><td>1</td><td>0.20</td><td>0.10</td><td>1.00</td><td>0.40</td><td>0.30</td><td>0.05</td><td>0.15</td><td>0.25</td><td>0.10</td><td>0.05</td><td>0.40</td></tr><tr><td>2</td><td>0.25</td><td>0.15</td><td>1.00</td><td>0.45</td><td>0.35</td><td>0.05</td><td>0.20</td><td>0.30</td><td>0.15</td><td>0.10</td><td>0.55</td></tr><tr><td>3</td><td>0.35</td><td>0.20</td><td>1.00</td><td>0.50</td><td>0.40</td><td>0.05</td><td>0.25</td><td>0.40</td><td>0.20</td><td>0.15</td><td>0.70</td></tr><tr><td>4</td><td>0.45</td><td>0.30</td><td>1.00</td><td>0.55</td><td>0.45</td><td>0.05</td><td>0.30</td><td>0.50</td><td>0.25</td><td>0.20</td><td>0.80</td></tr><tr><td>5</td><td>0.70</td><td>0.35</td><td>1.00</td><td>0.60</td><td>0.50</td><td>0.05</td><td>0.35</td><td>0.60</td><td>0.30</td><td>0.25</td><td>0.90</td></tr><tr><td>6</td><td>0.85</td><td>0.40</td><td>1.00</td><td>0.65</td><td>0.55</td><td>0.05</td><td>0.40</td><td>0.70</td><td>0.35</td><td>0.30</td><td>1.00</td></tr></tbody></table>	Depth (m)	Belgium	Czech Rep.	Denmark	France	Germany	Hungary	Netherlands	Norway	Switzerland	LN. Kingdom	Other Countries	0	0.00	0.00	0.00	0.00	0.00	0.00	0.00	0.00	0.00	0.00	0.00	1	0.20	0.10	1.00	0.40	0.30	0.05	0.15	0.25	0.10	0.05	0.40	2	0.25	0.15	1.00	0.45	0.35	0.05	0.20	0.30	0.15	0.10	0.55	3	0.35	0.20	1.00	0.50	0.40	0.05	0.25	0.40	0.20	0.15	0.70	4	0.45	0.30	1.00	0.55	0.45	0.05	0.30	0.50	0.25	0.20	0.80	5	0.70	0.35	1.00	0.60	0.50	0.05	0.35	0.60	0.30	0.25	0.90	6	0.85	0.40	1.00	0.65	0.55	0.05	0.40	0.70	0.35	0.30	1.00
Depth (m)	Belgium	Czech Rep.	Denmark	France	Germany	Hungary	Netherlands	Norway	Switzerland	LN. Kingdom	Other Countries																																																																																						
0	0.00	0.00	0.00	0.00	0.00	0.00	0.00	0.00	0.00	0.00	0.00																																																																																						
1	0.20	0.10	1.00	0.40	0.30	0.05	0.15	0.25	0.10	0.05	0.40																																																																																						
2	0.25	0.15	1.00	0.45	0.35	0.05	0.20	0.30	0.15	0.10	0.55																																																																																						
3	0.35	0.20	1.00	0.50	0.40	0.05	0.25	0.40	0.20	0.15	0.70																																																																																						
4	0.45	0.30	1.00	0.55	0.45	0.05	0.30	0.50	0.25	0.20	0.80																																																																																						
5	0.70	0.35	1.00	0.60	0.50	0.05	0.35	0.60	0.30	0.25	0.90																																																																																						
6	0.85	0.40	1.00	0.65	0.55	0.05	0.40	0.70	0.35	0.30	1.00																																																																																						

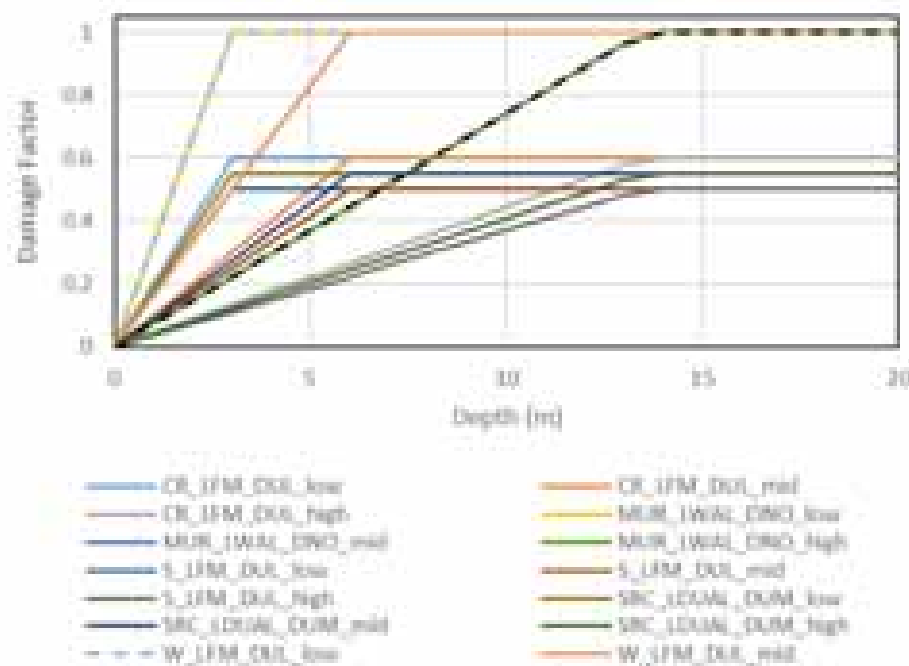


VUL_FL_BDG_Huizinga2017adaptedOsloResidential						
<i>References</i>	Huizinga, J., Moel, H. de, Szewczyk, W. (2017). Global flood depth-damage functions. Methodology and the database with guidelines. EUR 28552 EN. doi: 10.2760/16510					
<i>Class</i>	15 classes of residential buildings (5 structural types x 3 height ranges): <ul style="list-style-type: none"> • CR_LFM_DUL: • MUR_LWAL_DNO: • S_LFM_DUL: • SRC_LDUAL_DUM: • W_LFM_DUL: • low / mid / high: 2 / 4 / 9 storeys 					
<i>Methodology</i>	Adaptation of the baseline function by Huizinga et al. (2017) for Norway, with corrective factors based on building material and building height					
<i>Damage Measure</i>	Damage factor between 0 and 1 (value of the buildings and its contents)					
<i>Intensity Measure</i>	Flood depth [m]					
<i>Functional form</i>	Low-rise buildings					
	Flood depth [m]	CR_LFM_DUL	MUR_LWAL_DNO	S_LFM_DUL	SRC_LDUAL_DUM	W_LFM_DUL
	0.0	0.00	0.00	0.00	0.00	0.00
	1.0	0.20	0.33	0.17	0.18	0.33
	2.0	0.40	0.67	0.33	0.37	0.67
	3.0	0.60	1.00	0.50	0.55	1.00
	4.0	0.60	1.00	0.50	0.55	1.00
	5.0	0.60	1.00	0.50	0.55	1.00
	6.0	0.60	1.00	0.50	0.55	1.00
	7.0	0.60	1.00	0.50	0.55	1.00
	8.0	0.60	1.00	0.50	0.55	1.00
	9.0	0.60	1.00	0.50	0.55	1.00
	10.0	0.60	1.00	0.50	0.55	1.00
	11.0	0.60	1.00	0.50	0.55	1.00
	12.0	0.60	1.00	0.50	0.55	1.00
	13.0	0.60	1.00	0.50	0.55	1.00
	14.0	0.60	1.00	0.50	0.55	1.00
	15.0	0.60	1.00	0.50	0.55	1.00
	Mid-rise buildings					
	Flood depth [m]	CR_LFM_DUL	MUR_LWAL_DNO	S_LFM_DUL	SRC_LDUAL_DUM	W_LFM_DUL
	0.0	0.00	0.00	0.00	0.00	0.00
	1.0	0.10	0.17	0.08	0.09	0.17
	2.0	0.20	0.33	0.17	0.18	0.33
	3.0	0.30	0.50	0.25	0.28	0.50
	4.0	0.40	0.67	0.33	0.37	0.67
	5.0	0.50	0.83	0.42	0.46	0.83
	6.0	0.60	1.00	0.50	0.55	1.00
	7.0	0.60	1.00	0.50	0.55	1.00

8.0	0.60	1.00	0.50	0.55	1.00
9.0	0.60	1.00	0.50	0.55	1.00
10.0	0.60	1.00	0.50	0.55	1.00
11.0	0.60	1.00	0.50	0.55	1.00
12.0	0.60	1.00	0.50	0.55	1.00
13.0	0.60	1.00	0.50	0.55	1.00
14.0	0.60	1.00	0.50	0.55	1.00
15.0	0.60	1.00	0.50	0.55	1.00

High-rise buildings					
Flood depth [m]	CR_LFM_DU L	MUR_LWAL _DNO	S_LFM_DUL	SRC_LDUAL _DUM	W_LFM_DU L
0.0	0.00	0.00	0.00	0.00	0.00
1.0	0.20	0.33	0.17	0.18	0.33
2.0	0.40	0.67	0.33	0.37	0.67
3.0	0.60	1.00	0.50	0.55	1.00
4.0	0.60	1.00	0.50	0.55	1.00
5.0	0.60	1.00	0.50	0.55	1.00
6.0	0.60	1.00	0.50	0.55	1.00
7.0	0.60	1.00	0.50	0.55	1.00
8.0	0.60	1.00	0.50	0.55	1.00
9.0	0.60	1.00	0.50	0.55	1.00
10.0	0.60	1.00	0.50	0.55	1.00
11.0	0.60	1.00	0.50	0.55	1.00
12.0	0.60	1.00	0.50	0.55	1.00
13.0	0.60	1.00	0.50	0.55	1.00
14.0	0.60	1.00	0.50	0.55	1.00
15.0	0.60	1.00	0.50	0.55	1.00

Figures

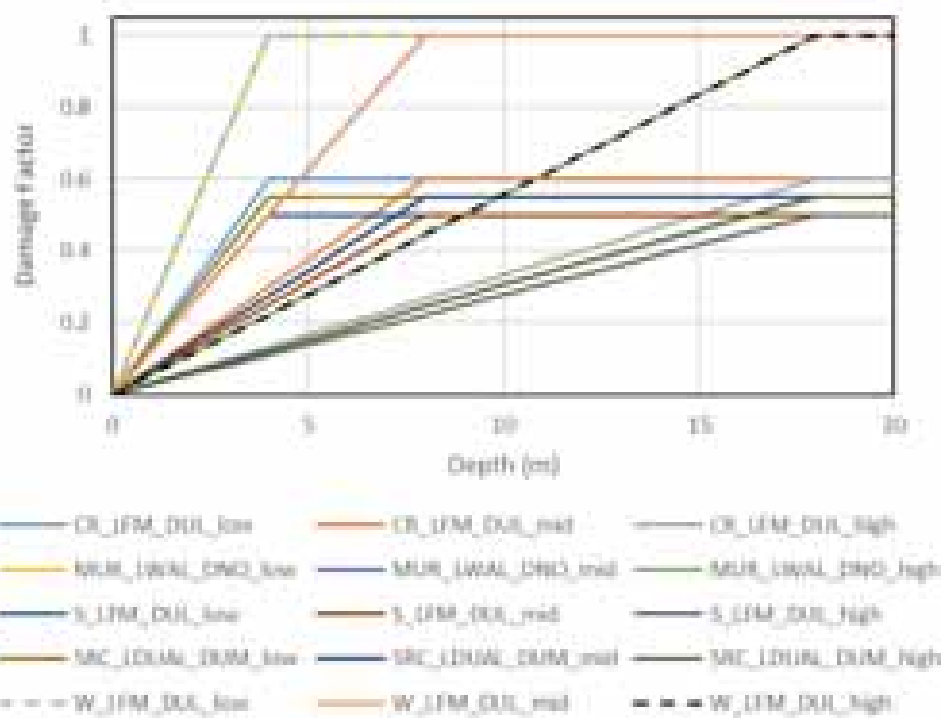


VUL FL BDG Huizinga2017adaptedOsloCommercial						
<i>References</i>	Huizinga, J., Moel, H. de, Szewczyk, W. (2017). Global flood depth-damage functions. Methodology and the database with guidelines. EUR 28552 EN. doi: 10.2760/16510					
<i>Class</i>	15 classes of residential buildings (5 structural types x 3 height ranges): <ul style="list-style-type: none"> • CR_LFM_DUL: • MUR_LWAL_DNO: • S_LFM_DUL: • SRC_LDUAL_DUM: • W_LFM_DUL: • low / mid / high: 2 / 4 / 9 storeys 					
<i>Methodology</i>	Adaptation of the baseline function by Huizinga et al. (2017) for Norway, with corrective factors based on building material and building height					
<i>Damage Measure</i>	Damage factor between 0 and 1 (value of the buildings and its contents)					
<i>Intensity Measure</i>	Flood depth [m]					
<i>Functional form</i>	Low-rise buildings					
	Flood depth [m]	CR_LFM_DUL	MUR_LWAL_DNO	S_LFM_DUL	SRC_LDUAL_DUM	W_LFM_DUL
	0.0	0.00	0.00	0.00	0.00	0.00
	1.0	0.15	0.25	0.13	0.14	0.25
	2.0	0.30	0.50	0.25	0.28	0.50
	3.0	0.45	0.75	0.38	0.41	0.75
	4.0	0.60	1.00	0.50	0.55	1.00
	5.0	0.60	1.00	0.50	0.55	1.00
	6.0	0.60	1.00	0.50	0.55	1.00
	7.0	0.60	1.00	0.50	0.55	1.00
	8.0	0.60	1.00	0.50	0.55	1.00
	9.0	0.60	1.00	0.50	0.55	1.00
	10.0	0.60	1.00	0.50	0.55	1.00
	11.0	0.60	1.00	0.50	0.55	1.00
	12.0	0.60	1.00	0.50	0.55	1.00
	13.0	0.60	1.00	0.50	0.55	1.00
	14.0	0.60	1.00	0.50	0.55	1.00
	15.0	0.60	1.00	0.50	0.55	1.00
	Mid-rise buildings					
	Flood depth [m]	CR_LFM_DUL	MUR_LWAL_DNO	S_LFM_DUL	SRC_LDUAL_DUM	W_LFM_DUL
	0.0	0.00	0.00	0.00	0.00	0.00
	1.0	0.08	0.13	0.06	0.07	0.13
	2.0	0.15	0.25	0.13	0.14	0.25
	3.0	0.23	0.38	0.19	0.21	0.38
	4.0	0.30	0.50	0.25	0.28	0.50
	5.0	0.38	0.63	0.31	0.34	0.63
	6.0	0.45	0.75	0.38	0.41	0.75
	7.0	0.53	0.88	0.44	0.48	0.88

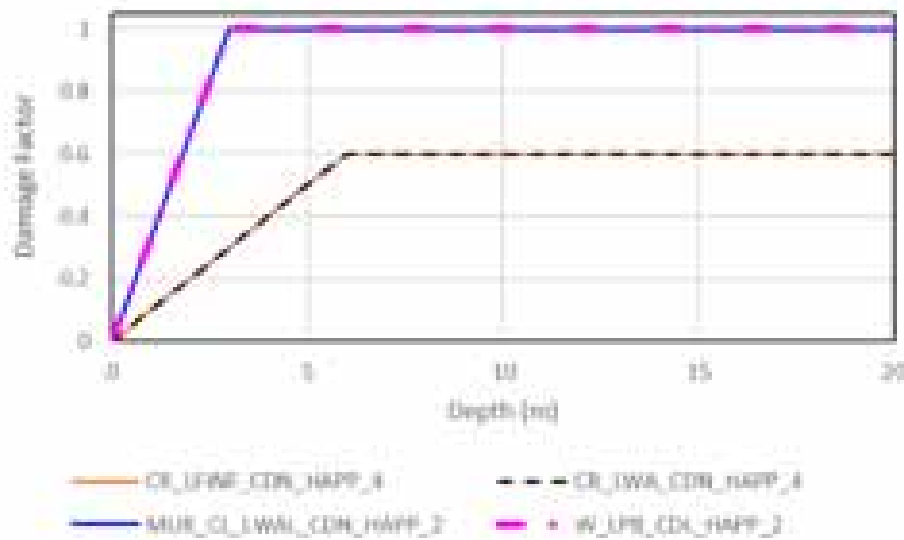
8.0	0.60	1.00	0.50	0.55	1.00
9.0	0.60	1.00	0.50	0.55	1.00
10.0	0.60	1.00	0.50	0.55	1.00
11.0	0.60	1.00	0.50	0.55	1.00
12.0	0.60	1.00	0.50	0.55	1.00
13.0	0.60	1.00	0.50	0.55	1.00
14.0	0.60	1.00	0.50	0.55	1.00
15.0	0.60	1.00	0.50	0.55	1.00

High-rise buildings					
Flood depth [m]	CR_LFM_DU L	MUR_LWAL _DNO	S_LFM_DUL	SRC_LDUAL _DUM	W_LFM_DU L
0.0	0.00	0.00	0.00	0.00	0.00
1.0	0.03	0.06	0.03	0.03	0.06
2.0	0.07	0.11	0.06	0.06	0.11
3.0	0.10	0.17	0.08	0.09	0.17
4.0	0.13	0.22	0.11	0.12	0.22
5.0	0.17	0.28	0.14	0.15	0.28
6.0	0.20	0.33	0.17	0.18	0.33
7.0	0.23	0.39	0.19	0.21	0.39
8.0	0.27	0.44	0.22	0.24	0.44
9.0	0.30	0.50	0.25	0.28	0.50
10.0	0.33	0.56	0.28	0.31	0.56
11.0	0.37	0.61	0.31	0.34	0.61
12.0	0.40	0.67	0.33	0.37	0.67
13.0	0.43	0.72	0.36	0.40	0.72
14.0	0.47	0.78	0.39	0.43	0.78
15.0	0.50	0.83	0.42	0.46	0.83

Figures

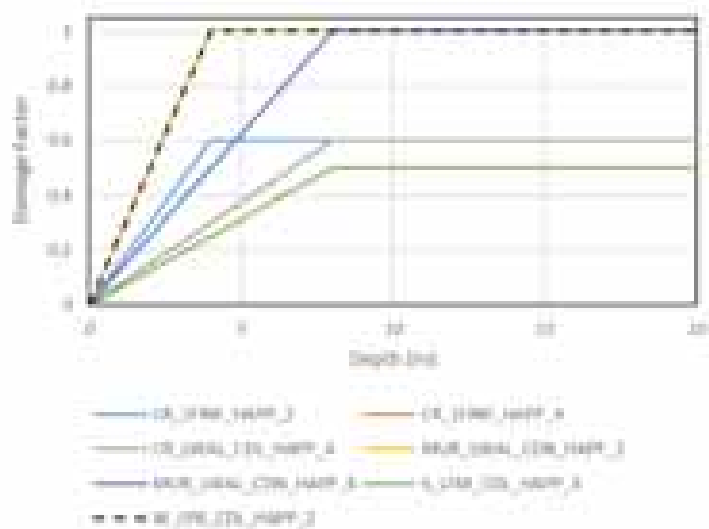


VUL FL BDG Huizinga2017adaptedEssexResidential

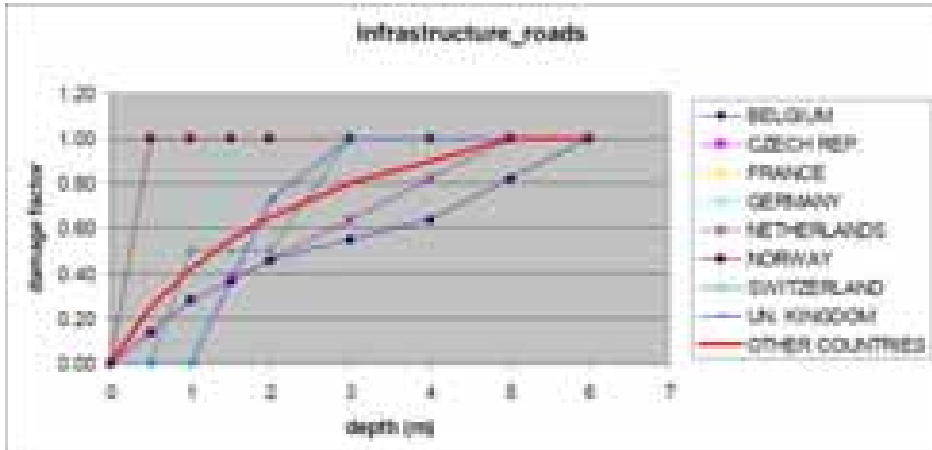
VUL_FL_BDG_Huizinga2017adaptedEssexResidential																																																																	
References	Huizinga, J., Moel, H. de, Szewczyk, W. (2017). Global flood depth-damage functions. Methodology and the database with guidelines. EUR 28552 EN. doi: 10.2760/16510																																																																
Class	Classes of residential buildings <ul style="list-style-type: none">• CR_LFINF_CDN_HAPP_4• CR_LWA_CDN_HAPP_4• MUR_CL_LWAL_CDN_HAPP_2• W_LPB_CDL_HAPP_2																																																																
Methodology	Adaptation of the baseline function by Huizinga et al. (2017) for Norway, with corrective factors based on building material and building height																																																																
Damage Measure	Damage factor between 0 and 1 (value of the buildings and is contents)																																																																
Intensity Measure	Flood depth [m]																																																																
Functional form	<table><tr><th>Flood depth [m]</th><th>CR_LFINF_CDN_HAPP_4</th><th>CR_LWA_CDN_HAPP_4</th><th>MUR_CL_LWAL_CDN_HAPP_2</th><th>W_LPB_CDL_HAPP_2</th></tr><tr><td>0.0</td><td>0.00</td><td>0.00</td><td>0.00</td><td>0.00</td></tr><tr><td>1.0</td><td>0.10</td><td>0.10</td><td>0.33</td><td>0.33</td></tr><tr><td>2.0</td><td>0.20</td><td>0.20</td><td>0.67</td><td>0.67</td></tr><tr><td>3.0</td><td>0.30</td><td>0.30</td><td>1.00</td><td>1.00</td></tr><tr><td>4.0</td><td>0.40</td><td>0.40</td><td>1.00</td><td>1.00</td></tr><tr><td>5.0</td><td>0.50</td><td>0.50</td><td>1.00</td><td>1.00</td></tr><tr><td>6.0</td><td>0.60</td><td>0.60</td><td>1.00</td><td>1.00</td></tr><tr><td>7.0</td><td>0.60</td><td>0.60</td><td>1.00</td><td>1.00</td></tr><tr><td>8.0</td><td>0.60</td><td>0.60</td><td>1.00</td><td>1.00</td></tr><tr><td>9.0</td><td>0.60</td><td>0.60</td><td>1.00</td><td>1.00</td></tr><tr><td>10.0</td><td>0.60</td><td>0.60</td><td>1.00</td><td>1.00</td></tr></table>					Flood depth [m]	CR_LFINF_CDN_HAPP_4	CR_LWA_CDN_HAPP_4	MUR_CL_LWAL_CDN_HAPP_2	W_LPB_CDL_HAPP_2	0.0	0.00	0.00	0.00	0.00	1.0	0.10	0.10	0.33	0.33	2.0	0.20	0.20	0.67	0.67	3.0	0.30	0.30	1.00	1.00	4.0	0.40	0.40	1.00	1.00	5.0	0.50	0.50	1.00	1.00	6.0	0.60	0.60	1.00	1.00	7.0	0.60	0.60	1.00	1.00	8.0	0.60	0.60	1.00	1.00	9.0	0.60	0.60	1.00	1.00	10.0	0.60	0.60	1.00	1.00
Flood depth [m]	CR_LFINF_CDN_HAPP_4	CR_LWA_CDN_HAPP_4	MUR_CL_LWAL_CDN_HAPP_2	W_LPB_CDL_HAPP_2																																																													
0.0	0.00	0.00	0.00	0.00																																																													
1.0	0.10	0.10	0.33	0.33																																																													
2.0	0.20	0.20	0.67	0.67																																																													
3.0	0.30	0.30	1.00	1.00																																																													
4.0	0.40	0.40	1.00	1.00																																																													
5.0	0.50	0.50	1.00	1.00																																																													
6.0	0.60	0.60	1.00	1.00																																																													
7.0	0.60	0.60	1.00	1.00																																																													
8.0	0.60	0.60	1.00	1.00																																																													
9.0	0.60	0.60	1.00	1.00																																																													
10.0	0.60	0.60	1.00	1.00																																																													
Figures																																																																	

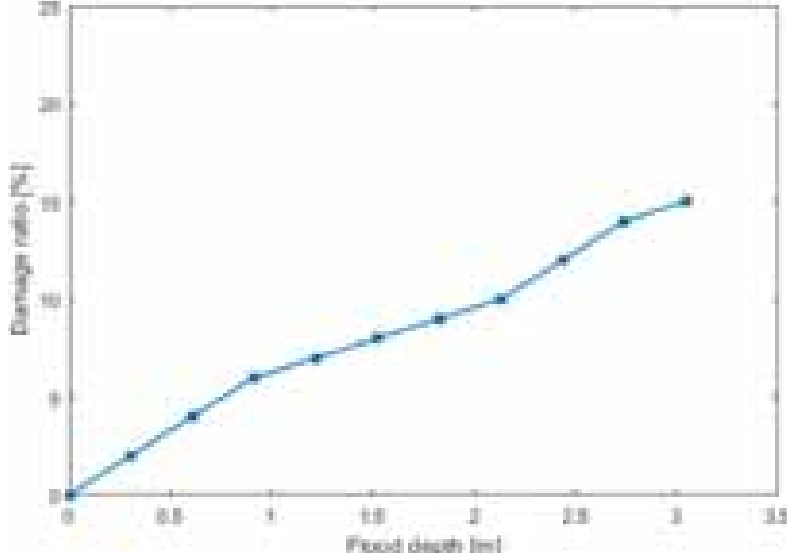
VUL_FL_BDG_Huizinga2017adaptedEssexCommercial																																																																	
References	Huizinga, J., Moel, H. de, Szewczyk, W. (2017). Global flood depth-damage functions. Methodology and the database with guidelines. EUR 28552 EN. doi: 10.2760/16510																																																																
Class	Classes of commercial buildings <ul style="list-style-type: none">• CR_LFINF_HAPP_2• CR_LFINF_HAPP_4• CR_LWAL_CDL_HAPP_4• MUR_LWAL_CDN_HAPP_2• MUR_LWAL_CDN_HAPP_4• S_LFM_CDL_HAPP_4• W_LPB_CDL_HAPP_2																																																																
Methodology	Adaptation of the baseline function by Huizinga et al. (2017) for Norway, with corrective factors based on building material and building height																																																																
Damage Measure	Damage factor between 0 and 1 (value of the buildings and is contents)																																																																
Intensity Measure	Flood depth [m]																																																																
Functional form	<table><tr><th>Flood depth [m]</th><th>CR_LFINF_HAPP_2</th><th>CR_LFINF_HAPP_4</th><th>CR_LWAL_CDL_HAPP_4</th><th>MUR_LWAL_CDN_HAPP_2</th></tr><tr><td>0.0</td><td>0.00</td><td>0.00</td><td>0.00</td><td>0.00</td></tr><tr><td>1.0</td><td>0.15</td><td>0.08</td><td>0.08</td><td>0.25</td></tr><tr><td>2.0</td><td>0.30</td><td>0.15</td><td>0.15</td><td>0.50</td></tr><tr><td>3.0</td><td>0.45</td><td>0.23</td><td>0.23</td><td>0.75</td></tr><tr><td>4.0</td><td>0.60</td><td>0.30</td><td>0.30</td><td>1.00</td></tr><tr><td>5.0</td><td>0.60</td><td>0.38</td><td>0.38</td><td>1.00</td></tr><tr><td>6.0</td><td>0.60</td><td>0.45</td><td>0.45</td><td>1.00</td></tr><tr><td>7.0</td><td>0.60</td><td>0.53</td><td>0.53</td><td>1.00</td></tr><tr><td>8.0</td><td>0.60</td><td>0.60</td><td>0.60</td><td>1.00</td></tr><tr><td>9.0</td><td>0.60</td><td>0.60</td><td>0.60</td><td>1.00</td></tr><tr><td>10.0</td><td>0.60</td><td>0.60</td><td>0.60</td><td>1.00</td></tr></table>					Flood depth [m]	CR_LFINF_HAPP_2	CR_LFINF_HAPP_4	CR_LWAL_CDL_HAPP_4	MUR_LWAL_CDN_HAPP_2	0.0	0.00	0.00	0.00	0.00	1.0	0.15	0.08	0.08	0.25	2.0	0.30	0.15	0.15	0.50	3.0	0.45	0.23	0.23	0.75	4.0	0.60	0.30	0.30	1.00	5.0	0.60	0.38	0.38	1.00	6.0	0.60	0.45	0.45	1.00	7.0	0.60	0.53	0.53	1.00	8.0	0.60	0.60	0.60	1.00	9.0	0.60	0.60	0.60	1.00	10.0	0.60	0.60	0.60	1.00
	Flood depth [m]	CR_LFINF_HAPP_2	CR_LFINF_HAPP_4	CR_LWAL_CDL_HAPP_4	MUR_LWAL_CDN_HAPP_2																																																												
	0.0	0.00	0.00	0.00	0.00																																																												
	1.0	0.15	0.08	0.08	0.25																																																												
	2.0	0.30	0.15	0.15	0.50																																																												
	3.0	0.45	0.23	0.23	0.75																																																												
	4.0	0.60	0.30	0.30	1.00																																																												
	5.0	0.60	0.38	0.38	1.00																																																												
	6.0	0.60	0.45	0.45	1.00																																																												
	7.0	0.60	0.53	0.53	1.00																																																												
	8.0	0.60	0.60	0.60	1.00																																																												
	9.0	0.60	0.60	0.60	1.00																																																												
	10.0	0.60	0.60	0.60	1.00																																																												
	<table><tr><th>Flood depth [m]</th><th>MUR_LWAL_CDN_HAPP_4</th><th>S_LFM_CDL_HAPP_4</th><th>W_LPB_CDL_HAPP_2</th></tr><tr><td>0.0</td><td>0.00</td><td>0.00</td><td>0.00</td></tr><tr><td>1.0</td><td>0.13</td><td>0.06</td><td>0.25</td></tr><tr><td>2.0</td><td>0.25</td><td>0.13</td><td>0.50</td></tr><tr><td>3.0</td><td>0.38</td><td>0.19</td><td>0.75</td></tr><tr><td>4.0</td><td>0.50</td><td>0.25</td><td>1.00</td></tr><tr><td>5.0</td><td>0.63</td><td>0.31</td><td>1.00</td></tr><tr><td>6.0</td><td>0.75</td><td>0.38</td><td>1.00</td></tr><tr><td>7.0</td><td>0.88</td><td>0.44</td><td>1.00</td></tr><tr><td>8.0</td><td>1.00</td><td>0.50</td><td>1.00</td></tr><tr><td>9.0</td><td>1.00</td><td>0.50</td><td>1.00</td></tr><tr><td>10.0</td><td>1.00</td><td>0.50</td><td>1.00</td></tr></table>					Flood depth [m]	MUR_LWAL_CDN_HAPP_4	S_LFM_CDL_HAPP_4	W_LPB_CDL_HAPP_2	0.0	0.00	0.00	0.00	1.0	0.13	0.06	0.25	2.0	0.25	0.13	0.50	3.0	0.38	0.19	0.75	4.0	0.50	0.25	1.00	5.0	0.63	0.31	1.00	6.0	0.75	0.38	1.00	7.0	0.88	0.44	1.00	8.0	1.00	0.50	1.00	9.0	1.00	0.50	1.00	10.0	1.00	0.50	1.00												
	Flood depth [m]	MUR_LWAL_CDN_HAPP_4	S_LFM_CDL_HAPP_4	W_LPB_CDL_HAPP_2																																																													
	0.0	0.00	0.00	0.00																																																													
	1.0	0.13	0.06	0.25																																																													
	2.0	0.25	0.13	0.50																																																													
	3.0	0.38	0.19	0.75																																																													
	4.0	0.50	0.25	1.00																																																													
	5.0	0.63	0.31	1.00																																																													
	6.0	0.75	0.38	1.00																																																													
	7.0	0.88	0.44	1.00																																																													
8.0	1.00	0.50	1.00																																																														
9.0	1.00	0.50	1.00																																																														
10.0	1.00	0.50	1.00																																																														

Figures



9.2.2 Infrastructure

VUL_FL_RDN_Huizinga2017																					
<i>References</i>	Huizinga, J., Moel, H. de, Szewczyk, W. (2017). Global flood depth-damage functions. Methodology and the database with guidelines. EUR 28552 EN. doi: 10.2760/16510																				
<i>Region of applicability</i>	Europe (Belgium, Czech Rep., France, Germany, Netherlands, Norway, Switzerland, UK)																				
<i>Class</i>	Road infrastructure - No classification																				
<i>Methodology</i>	Empirical data and literature survey																				
<i>Damage Measure</i>	Damage factor between 0 and 1 (value of the road infrastructure)																				
<i>Intensity Measure</i>	Flood depth [m]																				
<i>Functional form</i>	<p>Generic function for Europe:</p> <table border="1"> <thead> <tr> <th>Flood depth [m]</th><th>Damage factor Residential</th></tr> </thead> <tbody> <tr><td>0.0</td><td>0.00</td></tr> <tr><td>0.5</td><td>0.25</td></tr> <tr><td>1.0</td><td>0.42</td></tr> <tr><td>1.</td><td>0.55</td></tr> <tr><td>2.0</td><td>0.65</td></tr> <tr><td>3.0</td><td>0.80</td></tr> <tr><td>4.0</td><td>0.90</td></tr> <tr><td>5.0</td><td>1.00</td></tr> <tr><td>6.0</td><td>1.00</td></tr> </tbody> </table>	Flood depth [m]	Damage factor Residential	0.0	0.00	0.5	0.25	1.0	0.42	1.	0.55	2.0	0.65	3.0	0.80	4.0	0.90	5.0	1.00	6.0	1.00
Flood depth [m]	Damage factor Residential																				
0.0	0.00																				
0.5	0.25																				
1.0	0.42																				
1.	0.55																				
2.0	0.65																				
3.0	0.80																				
4.0	0.90																				
5.0	1.00																				
6.0	1.00																				
<i>Figures</i>																					

VUL FL EPN Hazus2003																																			
References	HAZUS (2003). “HAZUS-MH MR3-Technical Manual.” Federal Emergency Management Agency, Washington, D.C.																																		
Region of applicability	United States																																		
Class	Electric sub-station – 3 classes based on voltage level (ESSL: low voltage; ESSM; medium voltage; ESSH: high voltage) Damage function is the same for all three classes.																																		
Methodology	Empirical data and literature survey																																		
Damage Measure	Damage factor between 0 and 1 (value of the asset)																																		
Intensity Measure	Flood depth [m]																																		
Functional form	<table><tr><th>Flood depth [m]</th><th>Flood depth [ft]</th><th>Damage factor ESSL, ESSM, ESSH</th></tr><tr><td>0.3048</td><td>1.0</td><td>0.02</td></tr><tr><td>0.6096</td><td>2.0</td><td>0.04</td></tr><tr><td>0.9144</td><td>3.0</td><td>0.06</td></tr><tr><td>1.2192</td><td>4.0</td><td>0.07</td></tr><tr><td>1.5240</td><td>5.0</td><td>0.08</td></tr><tr><td>1.8288</td><td>6.0</td><td>0.09</td></tr><tr><td>2.1336</td><td>7.0</td><td>0.10</td></tr><tr><td>2.4384</td><td>8.0</td><td>0.12</td></tr><tr><td>2.7432</td><td>9.0</td><td>0.14</td></tr><tr><td>3.048</td><td>10.0</td><td>0.15</td></tr></table>		Flood depth [m]	Flood depth [ft]	Damage factor ESSL, ESSM, ESSH	0.3048	1.0	0.02	0.6096	2.0	0.04	0.9144	3.0	0.06	1.2192	4.0	0.07	1.5240	5.0	0.08	1.8288	6.0	0.09	2.1336	7.0	0.10	2.4384	8.0	0.12	2.7432	9.0	0.14	3.048	10.0	0.15
Flood depth [m]	Flood depth [ft]	Damage factor ESSL, ESSM, ESSH																																	
0.3048	1.0	0.02																																	
0.6096	2.0	0.04																																	
0.9144	3.0	0.06																																	
1.2192	4.0	0.07																																	
1.5240	5.0	0.08																																	
1.8288	6.0	0.09																																	
2.1336	7.0	0.10																																	
2.4384	8.0	0.12																																	
2.7432	9.0	0.14																																	
3.048	10.0	0.15																																	
Figures	 <p>The graph plots the Damage ratio (%) on the y-axis (ranging from 0 to 25) against Flood depth (m) on the x-axis (ranging from 0 to 3.5). The data points from the table are plotted and connected by a smooth curve, showing a non-linear increase in damage ratio with flood depth.</p> <table><caption>Data points for the Damage ratio vs Flood depth graph</caption><tr><th>Flood depth [m]</th><th>Damage ratio [%]</th></tr><tr><td>0.3048</td><td>2</td></tr><tr><td>0.6096</td><td>4</td></tr><tr><td>0.9144</td><td>6</td></tr><tr><td>1.2192</td><td>7</td></tr><tr><td>1.5240</td><td>8</td></tr><tr><td>1.8288</td><td>9</td></tr><tr><td>2.1336</td><td>10</td></tr><tr><td>2.4384</td><td>12</td></tr><tr><td>2.7432</td><td>14</td></tr><tr><td>3.048</td><td>15</td></tr></table>		Flood depth [m]	Damage ratio [%]	0.3048	2	0.6096	4	0.9144	6	1.2192	7	1.5240	8	1.8288	9	2.1336	10	2.4384	12	2.7432	14	3.048	15											
Flood depth [m]	Damage ratio [%]																																		
0.3048	2																																		
0.6096	4																																		
0.9144	6																																		
1.2192	7																																		
1.5240	8																																		
1.8288	9																																		
2.1336	10																																		
2.4384	12																																		
2.7432	14																																		
3.048	15																																		

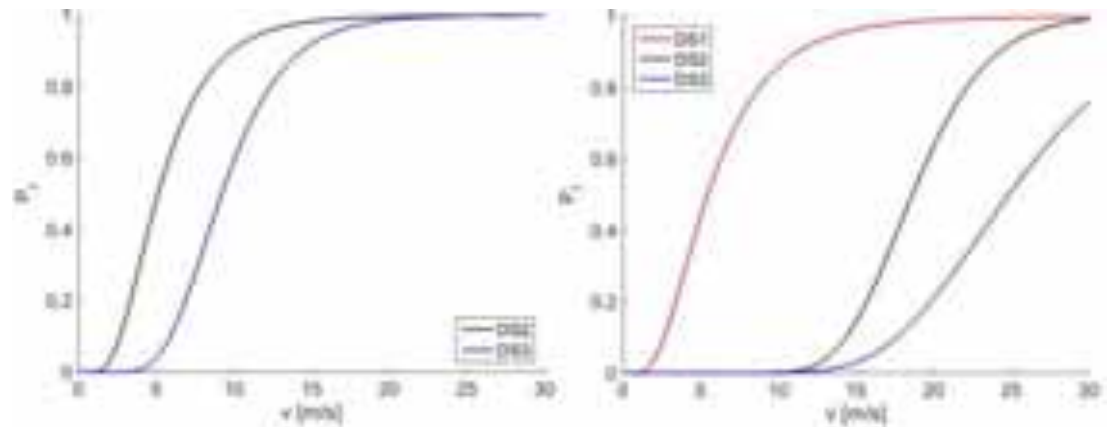
9.3 Debris flow fragility models

9.3.1 Buildings

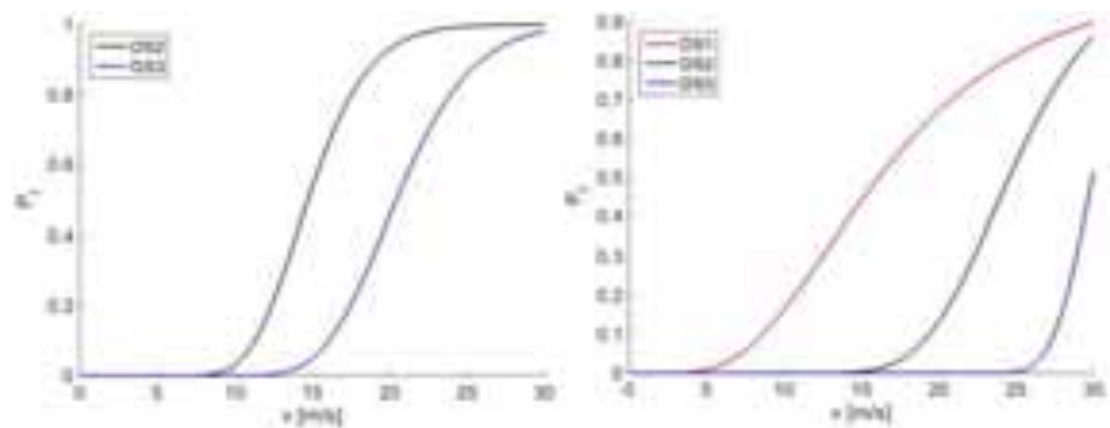
FRAG_DB_BDG_Parisi2017																																																											
References	Parisi, F., & Sabella, G. (2017). Flow-type landslide fragility of reinforced concrete framed buildings. Engineering Structures, 131, 28-43.																																																										
Region of applicability	Euro-Mediterranean regions																																																										
Class	Low-rise RC frame buildings. Classes for in-plane damage: <ul style="list-style-type: none">• Gravity-load designed, bare frame• Gravity-load designed, infilled frame• Earthquake resistant, bare frame• Earthquake resistant, infilled frame Classes of masonry infill walls for out-of-plane damage: <ul style="list-style-type: none">• Weak wall: two hollow clay block masonry leaves with 60% volumetric percentage of holes and an internal cavity for thermal isolation• Medium wall: single-leaf masonry made of perforated clay blocks with volumetric percentage of holes lower than 45% and dry vertical mortar joints• Strong wall: same geometry as medium walls, but with higher strength, stiffness and weight																																																										
Methodology	Analytical, methodology adapted to flow-type landslides.																																																										
Damage states	Damage states for in-plane damage: <ul style="list-style-type: none">• DS1: in-plane cracking of infill walls (slight damage)• DS2: formation of a plastic hinge in a column (moderate damage)• DS3: rupture of a plastic hinge in a column (severe damage) Damage states for out-of-plane damage: <ul style="list-style-type: none">• Single damage state for out-of-plane collapse (three-hinge flexural mechanism or shear sliding at the wall-column and/or wall-beam interfaces)																																																										
Intensity Measure	Flow velocity [m/s]																																																										
Fragility parameters	Fragility curves for in-plane damage: <table><tr><th rowspan="2">Class</th><th colspan="2">DS1</th><th colspan="2">DS2</th><th colspan="2">DS3</th></tr><tr><th>α [m/s]</th><th>β</th><th>α [m/s]</th><th>β</th><th>α [m/s]</th><th>β</th></tr><tr><td>Gravity-load designed, bare frame</td><td>-</td><td>-</td><td>5.13</td><td>0.51</td><td>9.22</td><td>0.35</td></tr><tr><td>Gravity-load designed, infilled frame</td><td>5.45</td><td>0.57</td><td>18.63</td><td>0.20</td><td>24.84</td><td>0.27</td></tr><tr><td>Earthquake resistant, bare frame</td><td>-</td><td>-</td><td>14.74</td><td>0.21</td><td>20.46</td><td>0.19</td></tr><tr><td>Earthquake resistant, infilled frame</td><td>10.09</td><td>1.07</td><td>24.56</td><td>0.18</td><td>29.94</td><td>0.07</td></tr></table> Fragility curves for out-of-plane collapse: <table><tr><th>Infill wall type</th><th>α [m/s]</th><th>β</th></tr><tr><td>Weak</td><td>0.00</td><td>4.54</td></tr><tr><td>Medium</td><td>4.86</td><td>0.33</td></tr><tr><td>Strong</td><td>8.82</td><td>0.35</td></tr></table>						Class	DS1		DS2		DS3		α [m/s]	β	α [m/s]	β	α [m/s]	β	Gravity-load designed, bare frame	-	-	5.13	0.51	9.22	0.35	Gravity-load designed, infilled frame	5.45	0.57	18.63	0.20	24.84	0.27	Earthquake resistant, bare frame	-	-	14.74	0.21	20.46	0.19	Earthquake resistant, infilled frame	10.09	1.07	24.56	0.18	29.94	0.07	Infill wall type	α [m/s]	β	Weak	0.00	4.54	Medium	4.86	0.33	Strong	8.82	0.35
Class	DS1		DS2		DS3																																																						
	α [m/s]	β	α [m/s]	β	α [m/s]	β																																																					
Gravity-load designed, bare frame	-	-	5.13	0.51	9.22	0.35																																																					
Gravity-load designed, infilled frame	5.45	0.57	18.63	0.20	24.84	0.27																																																					
Earthquake resistant, bare frame	-	-	14.74	0.21	20.46	0.19																																																					
Earthquake resistant, infilled frame	10.09	1.07	24.56	0.18	29.94	0.07																																																					
Infill wall type	α [m/s]	β																																																									
Weak	0.00	4.54																																																									
Medium	4.86	0.33																																																									
Strong	8.82	0.35																																																									

Figures

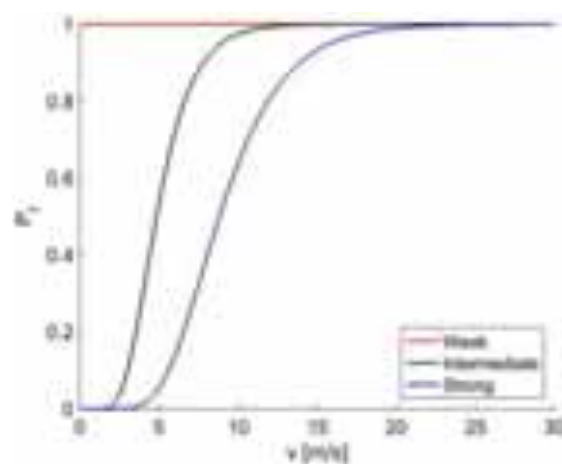
Fragility curves for in-plane damage in gravity-load designed buildings (Left: bare frame; Right: infilled frame):

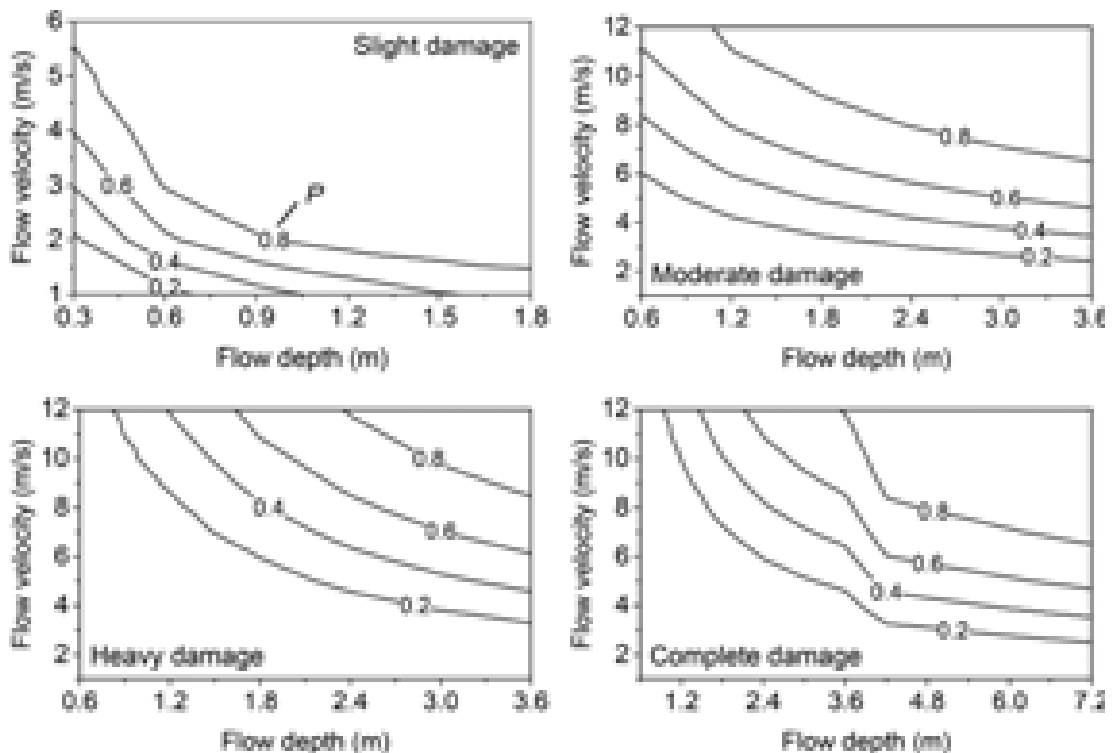


Fragility curves for in-plane damage in earthquake resistant buildings (Left: bare frame; Right: infilled frame):



Fragility curves for out-of-plane collapse of infill walls:



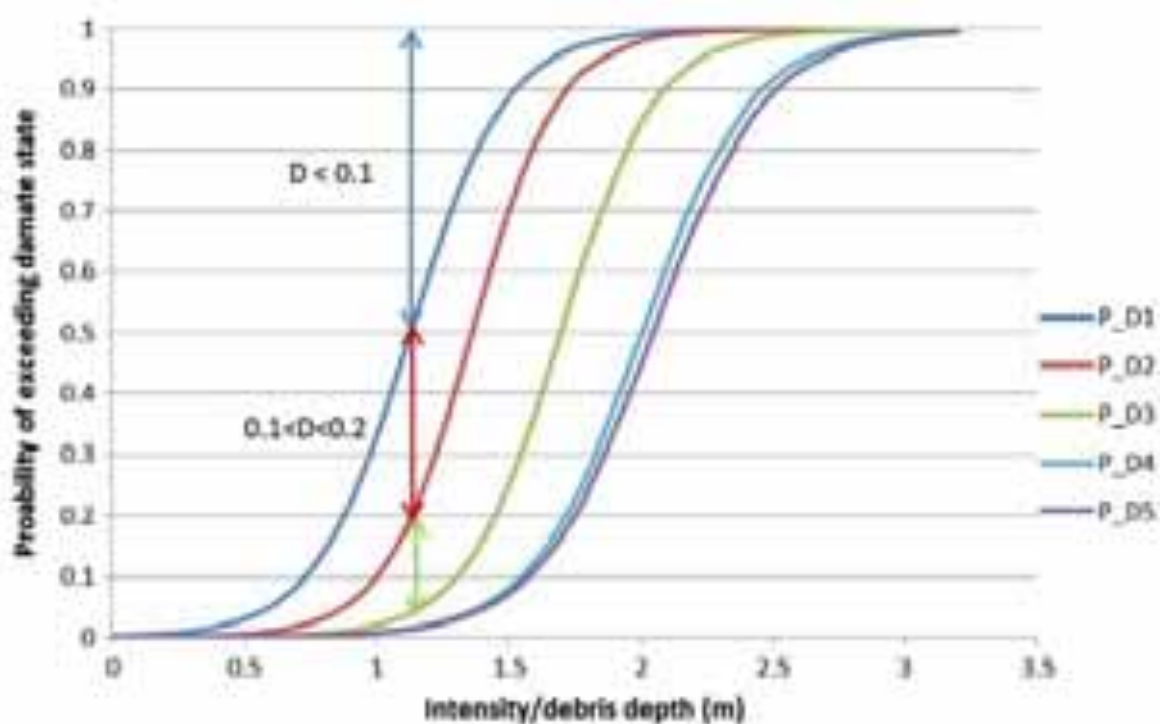
FRAG DB BDG Luo2022	
References	Luo, H. Y., Zhang, L. M., He, J., & Yin, K. S. (2022). Reliability-based formulation of building vulnerability to debris flow impacts. Canadian Geotechnical Journal, 59(1), 40-54.
Region of applicability	-
Class	Three-storey RC frame building.
Methodology	Analytical, using a hydrodynamic model
Damage states	Damage states: <ul style="list-style-type: none"> • Slight: frontal wall out-of-plane flexural failure • Moderate: side wall cracking shear failure • Heavy: column bending failure • Complete: frame pushover failure
Intensity Measure	Flow depth [m] and Flow velocity [m/s]
Fragility parameters	No functional form available.
Figures	Fragility surfaces: 

FRAG DB BDG Eidsvig2014																																																																																																																								
References	Eidsvig UMK, Papathoma-Köhle M, Du J, et al (2014) Quantification of model uncertainty in debris flow vulnerability assessment. Engineering Geology 181:15–26. https://doi.org/10.1016/j.enggeo.2014.08.006																																																																																																																							
Region of applicability	South Tyrol, Italy																																																																																																																							
Class	Rural area buildings																																																																																																																							
Methodology	Emprirical																																																																																																																							
Damage states	<table><tr><td>Damage state</td><td>Degree of loss</td></tr><tr><td>1 (DS1)</td><td>≤ 0.1</td></tr><tr><td>2 (DS2)</td><td>0.1 – 0.2</td></tr><tr><td>3 (DS3)</td><td>0.2 – 0.3</td></tr><tr><td>4 (DS4)</td><td>0.3 – 0.5</td></tr><tr><td>5 (DS5)</td><td>0.5 – 0.8</td></tr><tr><td>6 (DS6)</td><td>> 0.8</td></tr></table>						Damage state	Degree of loss	1 (DS1)	≤ 0.1	2 (DS2)	0.1 – 0.2	3 (DS3)	0.2 – 0.3	4 (DS4)	0.3 – 0.5	5 (DS5)	0.5 – 0.8	6 (DS6)	> 0.8																																																																																																				
Damage state	Degree of loss																																																																																																																							
1 (DS1)	≤ 0.1																																																																																																																							
2 (DS2)	0.1 – 0.2																																																																																																																							
3 (DS3)	0.2 – 0.3																																																																																																																							
4 (DS4)	0.3 – 0.5																																																																																																																							
5 (DS5)	0.5 – 0.8																																																																																																																							
6 (DS6)	> 0.8																																																																																																																							
Intensity Measure	Flow depth [m] and Flow velocity [m/s]																																																																																																																							
Fragility parameters	The parameters for the logistic fragility curves are not made available in the publication. The could be calculated based on the digitized curves. Functional form of the fragility curves: $P = 1 / [1 + e^{(aI+b)}]$ <table><tr><td>Debris depth (m)</td><td>P(DS>DS1)</td><td>Debris depth (m)</td><td>P(DS>DS2)</td><td>Debris depth (m)</td><td>P(DS>DS3)</td></tr><tr><td>0.000</td><td>0.000</td><td>0.000</td><td>0.000</td><td>0.000</td><td>0.000</td></tr><tr><td>0.326</td><td>0.010</td><td>0.421</td><td>0.000</td><td>0.635</td><td>0.000</td></tr><tr><td>0.455</td><td>0.020</td><td>0.596</td><td>0.007</td><td>0.874</td><td>0.008</td></tr><tr><td>0.569</td><td>0.041</td><td>0.755</td><td>0.022</td><td>1.059</td><td>0.024</td></tr><tr><td>0.679</td><td>0.073</td><td>0.879</td><td>0.046</td><td>1.181</td><td>0.051</td></tr><tr><td>0.757</td><td>0.111</td><td>0.979</td><td>0.086</td><td>1.298</td><td>0.094</td></tr><tr><td>0.843</td><td>0.166</td><td>1.074</td><td>0.145</td><td>1.421</td><td>0.171</td></tr><tr><td>0.953</td><td>0.269</td><td>1.202</td><td>0.266</td><td>1.541</td><td>0.291</td></tr><tr><td>1.128</td><td>0.498</td><td>1.288</td><td>0.380</td><td>1.617</td><td>0.385</td></tr><tr><td>1.253</td><td>0.656</td><td>1.391</td><td>0.535</td><td>1.737</td><td>0.546</td></tr><tr><td>1.324</td><td>0.738</td><td>1.467</td><td>0.650</td><td>1.835</td><td>0.677</td></tr><tr><td>1.393</td><td>0.809</td><td>1.570</td><td>0.769</td><td>1.951</td><td>0.796</td></tr><tr><td>1.488</td><td>0.874</td><td>1.654</td><td>0.852</td><td>2.078</td><td>0.888</td></tr><tr><td>1.586</td><td>0.924</td><td>1.751</td><td>0.913</td><td>2.229</td><td>0.949</td></tr><tr><td>1.713</td><td>0.958</td><td>1.900</td><td>0.957</td><td>2.424</td><td>0.981</td></tr><tr><td>1.864</td><td>0.981</td><td>2.110</td><td>0.989</td><td>2.629</td><td>0.992</td></tr><tr><td>2.008</td><td>0.990</td><td>2.454</td><td>0.996</td><td>2.822</td><td>0.996</td></tr><tr><td>2.269</td><td>0.997</td><td>3.500</td><td>1.000</td><td>3.500</td><td>1.000</td></tr></table>						Debris depth (m)	P(DS>DS1)	Debris depth (m)	P(DS>DS2)	Debris depth (m)	P(DS>DS3)	0.000	0.000	0.000	0.000	0.000	0.000	0.326	0.010	0.421	0.000	0.635	0.000	0.455	0.020	0.596	0.007	0.874	0.008	0.569	0.041	0.755	0.022	1.059	0.024	0.679	0.073	0.879	0.046	1.181	0.051	0.757	0.111	0.979	0.086	1.298	0.094	0.843	0.166	1.074	0.145	1.421	0.171	0.953	0.269	1.202	0.266	1.541	0.291	1.128	0.498	1.288	0.380	1.617	0.385	1.253	0.656	1.391	0.535	1.737	0.546	1.324	0.738	1.467	0.650	1.835	0.677	1.393	0.809	1.570	0.769	1.951	0.796	1.488	0.874	1.654	0.852	2.078	0.888	1.586	0.924	1.751	0.913	2.229	0.949	1.713	0.958	1.900	0.957	2.424	0.981	1.864	0.981	2.110	0.989	2.629	0.992	2.008	0.990	2.454	0.996	2.822	0.996	2.269	0.997	3.500	1.000	3.500	1.000
Debris depth (m)	P(DS>DS1)	Debris depth (m)	P(DS>DS2)	Debris depth (m)	P(DS>DS3)																																																																																																																			
0.000	0.000	0.000	0.000	0.000	0.000																																																																																																																			
0.326	0.010	0.421	0.000	0.635	0.000																																																																																																																			
0.455	0.020	0.596	0.007	0.874	0.008																																																																																																																			
0.569	0.041	0.755	0.022	1.059	0.024																																																																																																																			
0.679	0.073	0.879	0.046	1.181	0.051																																																																																																																			
0.757	0.111	0.979	0.086	1.298	0.094																																																																																																																			
0.843	0.166	1.074	0.145	1.421	0.171																																																																																																																			
0.953	0.269	1.202	0.266	1.541	0.291																																																																																																																			
1.128	0.498	1.288	0.380	1.617	0.385																																																																																																																			
1.253	0.656	1.391	0.535	1.737	0.546																																																																																																																			
1.324	0.738	1.467	0.650	1.835	0.677																																																																																																																			
1.393	0.809	1.570	0.769	1.951	0.796																																																																																																																			
1.488	0.874	1.654	0.852	2.078	0.888																																																																																																																			
1.586	0.924	1.751	0.913	2.229	0.949																																																																																																																			
1.713	0.958	1.900	0.957	2.424	0.981																																																																																																																			
1.864	0.981	2.110	0.989	2.629	0.992																																																																																																																			
2.008	0.990	2.454	0.996	2.822	0.996																																																																																																																			
2.269	0.997	3.500	1.000	3.500	1.000																																																																																																																			

Debris depth (m)	P(DS>DS4)	Debris depth (m)	P(DS>DS5)
0.000	0.000	0.000	0.000
0.715	0.000	0.520	0.000
0.947	0.004	1.001	0.006
1.137	0.010	1.183	0.015
1.278	0.027	1.356	0.037
1.444	0.061	1.535	0.079
1.584	0.115	1.674	0.143
1.706	0.189	1.821	0.253
1.806	0.273	1.963	0.400
1.907	0.383	2.103	0.561
2.074	0.571	2.240	0.698
2.204	0.719	2.384	0.828
2.360	0.839	2.548	0.910
2.475	0.905	2.748	0.959
2.639	0.952	2.970	0.983
2.870	0.984	3.119	0.989
3.097	0.996	3.207	0.992
3.211	0.998	3.500	1.000

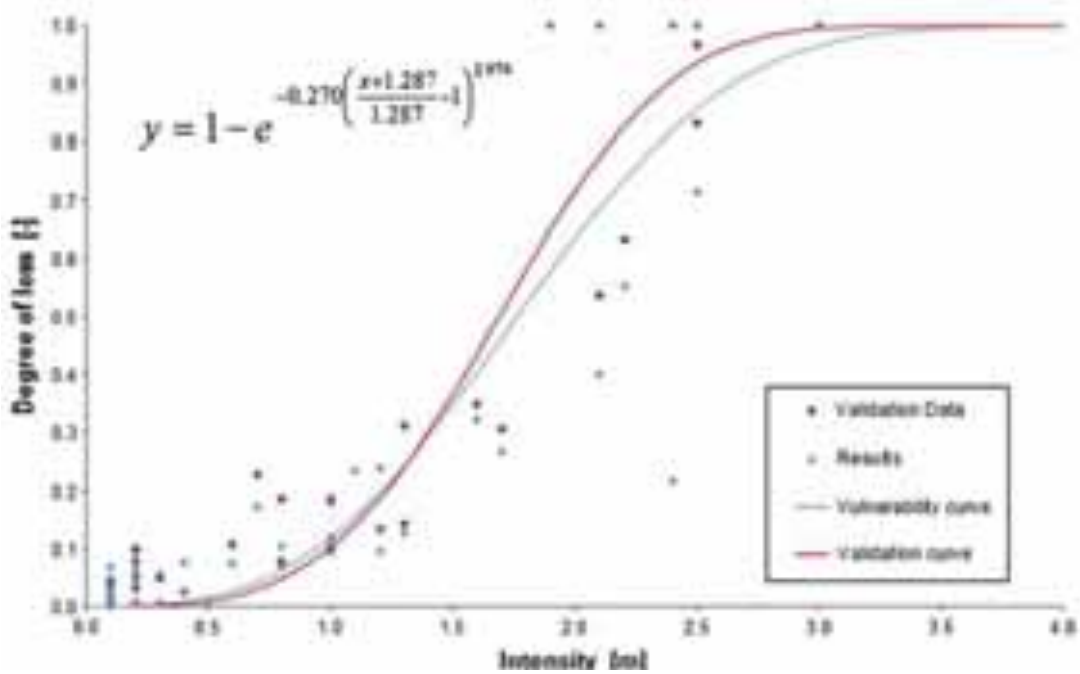
Figures

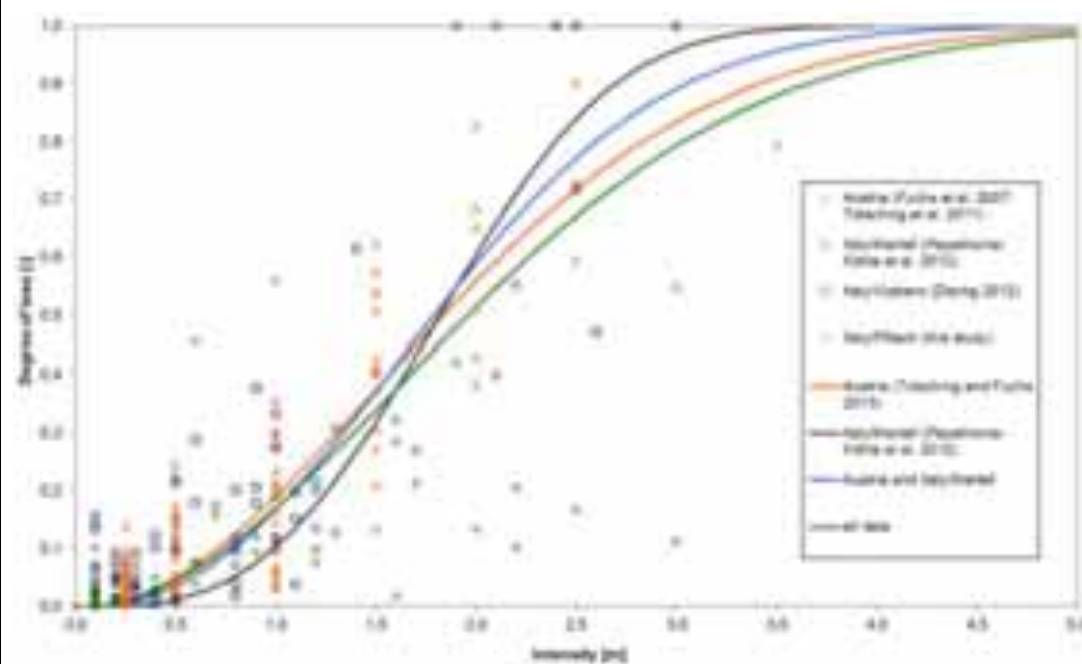
Fragility curves.

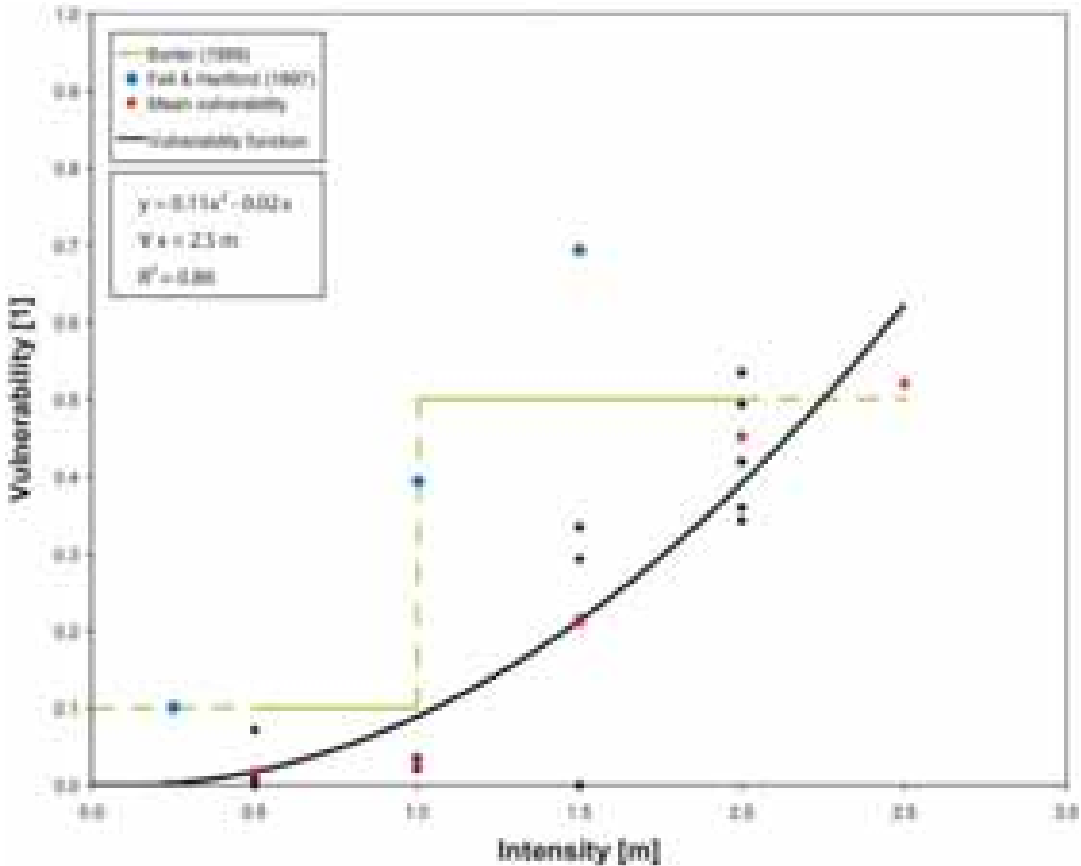


9.4 Debris flow vulnerability models

9.4.1 Buildings

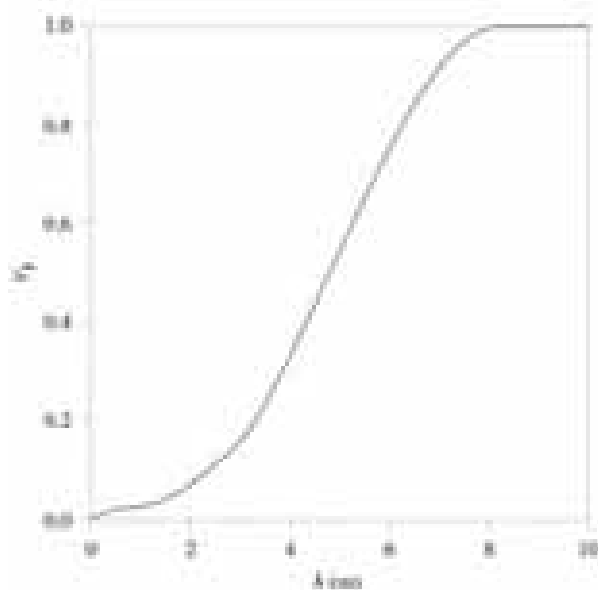
VUL_DB_BDG_PK2012	
References	Papathoma-Koehle, M., Keiler, M., Totschnig, R., & Glade, T. (2012). Improvement of vulnerability curves using data from extreme events: debris flow event in South Tyrol. Natural Hazards, 64, 2083-2105.
Region of applicability	South Tyrol (Italy)
Class	Low-rise rural area masonry buildings
Methodology	Empirical data
Damage Measure	Damage factor between 0 and 1 (value of the asset)
Intensity Measure	Deposit height [m]
Functional form	$y = 1 - \exp \left[-0.270 \left(\frac{x + 1.287}{1.287} - 1 \right)^{2.974} \right]$
Figures	

VUL DB BDG PK2015																								
References	Papathoma-Köhle, M., Zischg, A., Fuchs, S., Glade, T., & Keiler, M. (2015). Loss estimation for landslides in mountain areas–An integrated toolbox for vulnerability assessment and damage documentation. Environmental Modelling & Software, 63, 156-169.																							
Region of applicability	Austria, Italy																							
Class	Low-rise rural area masonry buildings																							
Methodology	Empirical data, update of Papathoma-Koehle et al; (2012) with larger datasets																							
Damage Measure	Damage factor between 0 and 1 (value of the asset)																							
Intensity Measure	Deposit height [m]																							
Functional form	<div>Weibull function:<div>$y = 1 - \exp \left[a \left(\frac{x + b}{b} - 1 \right)^c \right]$</div><table><tr><th>Parameter</th><th>Austria</th><th>Austria & Italy/Martell</th><th>Italy/Martell</th><th>All data</th></tr><tr><td><i>a</i></td><td>-1.253</td><td>-1.138</td><td>-0.27</td><td>-1.671</td></tr><tr><td><i>b</i></td><td>2.438</td><td>2.177</td><td>1.287</td><td>3.189</td></tr><tr><td><i>c</i></td><td>1.892</td><td>2.202</td><td>2.974</td><td>1.746</td></tr></table></div>				Parameter	Austria	Austria & Italy/Martell	Italy/Martell	All data	<i>a</i>	-1.253	-1.138	-0.27	-1.671	<i>b</i>	2.438	2.177	1.287	3.189	<i>c</i>	1.892	2.202	2.974	1.746
Parameter	Austria	Austria & Italy/Martell	Italy/Martell	All data																				
<i>a</i>	-1.253	-1.138	-0.27	-1.671																				
<i>b</i>	2.438	2.177	1.287	3.189																				
<i>c</i>	1.892	2.202	2.974	1.746																				
Figures																								

VUL DB BDG Fuchs2007	
References	Fuchs, S., Heiss, K., & Hübl, J. (2007). Towards an empirical vulnerability function for use in debris flow risk assessment. Natural Hazards and Earth System Sciences, 7(5), 495-506.
Region of applicability	Austria
Class	Low-rise rural area masonry buildings
Methodology	Empirical data
Damage Measure	Damage factor between 0 and 1 (value of the asset)
Intensity Measure	Deposit height [m]
Functional form	Quadratic function: $y = 0.11x^2 - 0.02x$
Figures	

VUL DB BDG Calvo2009		
References	Calvo B, Savi F (2009) A real-world application of Monte Carlo procedure for debris flow risk assessment. Computers & Geosciences 35:967–977. https://doi.org/10.1016/j.cageo.2008.04.002	
Region of applicability		
Class	Low-rise rural area masonry buildings	
Methodology	Empirical data	
Damage Measure	Damage factor between 0 and 1 (value of the asset)	
Intensity Measure	Deposit height [m]	
Functional form	Non-parametric curve	
	h (m)	V _i
	0.00	0.000
	0.50	0.023
	0.95	0.024
	1.38	0.036
	1.79	0.060
	2.22	0.089
	2.76	0.135
	3.11	0.175
	3.30	0.200
	3.55	0.244
	3.95	0.328
	4.31	0.399
	4.65	0.470
	4.98	0.545
	5.34	0.622
	5.75	0.704
	6.15	0.780
	6.55	0.855
	6.95	0.913
	7.34	0.955
	7.65	0.984
7.99	1.000	
10.00	1.000	

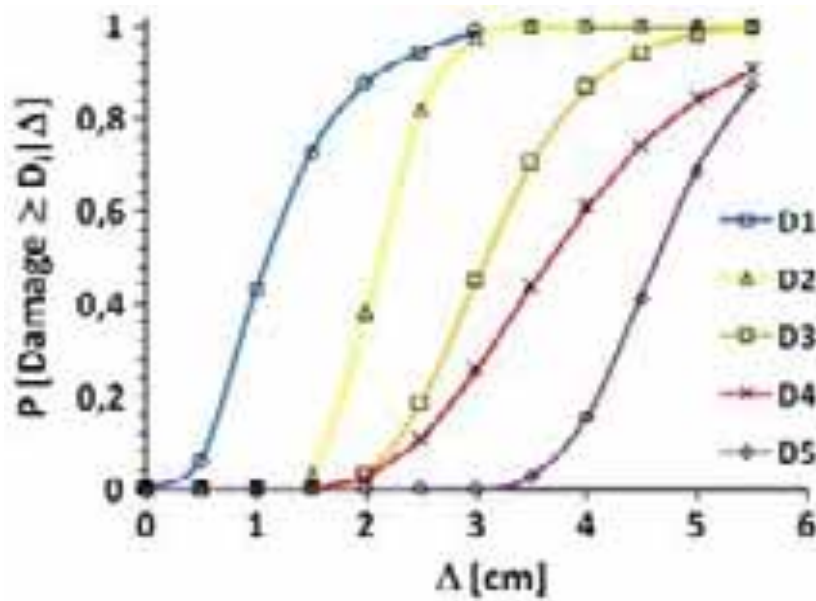
Figures

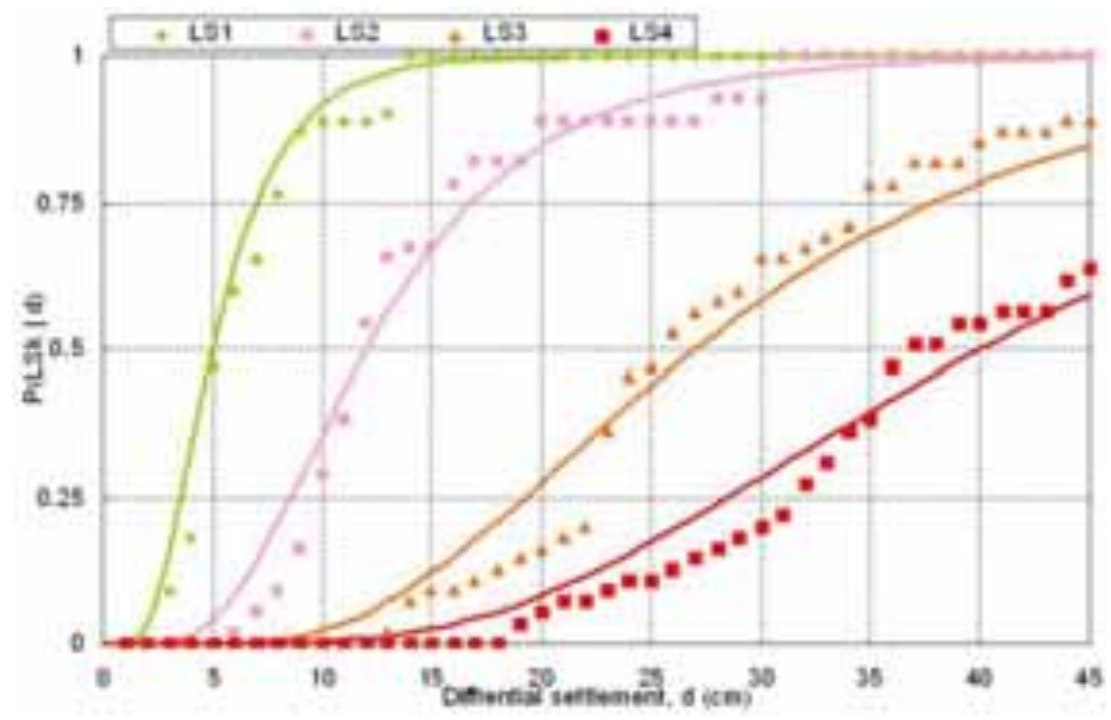


Vulnerability function: loss ratio [V1] as a function of debris flow depth [h] (Calvo and Salvi, 2009).

9.5 Landslide fragility models

9.5.1 Buildings

FRAG_LA_BDG_Peduto2017																																								
References	Peduto, D., Ferlisi, S., Nicodemo, G., Reale, D., Pisciotta, G., & Gullà, G. (2017). Empirical fragility and vulnerability curves for buildings exposed to slow-moving landslides at medium and large scales. Landslides, 14, 1993-2007.																																							
Region of applicability	Italy																																							
Class	Low-rise masonry buildings from Campania Region (Southern Italy)																																							
Methodology	Empirical, from DInSAR data and damage surveys																																							
Damage states	Damage states: <ul style="list-style-type: none">• D1: Very slight• D2: Slight• D3: Moderate• D4: Severe• D5: Very severe																																							
Intensity Measure	DInSAR-derived differential settlement Δ [cm]																																							
Fragility parameters	<table><tr><th colspan="2">D1</th><th colspan="2">D2</th><th colspan="2">D3</th><th colspan="2">D4</th><th colspan="2">D5</th></tr><tr><th>α [cm]</th><th>β</th><th>α [cm]</th><th>β</th><th>α [cm]</th><th>β</th><th>α [cm]</th><th>β</th><th>α [cm]</th><th>β</th></tr><tr><td>1.10</td><td>0.50</td><td>2.11</td><td>0.18</td><td>3.08</td><td>0.24</td><td>3.67</td><td>0.31</td><td>4.65</td><td>0.15</td></tr></table>										D1		D2		D3		D4		D5		α [cm]	β	α [cm]	β	α [cm]	β	α [cm]	β	α [cm]	β	1.10	0.50	2.11	0.18	3.08	0.24	3.67	0.31	4.65	0.15
D1		D2		D3		D4		D5																																
α [cm]	β	α [cm]	β	α [cm]	β	α [cm]	β	α [cm]	β																															
1.10	0.50	2.11	0.18	3.08	0.24	3.67	0.31	4.65	0.15																															
Figures																																								

FRAG LA BDG Negulescu2010																									
References	Negulescu, C., & Foerster, E. (2010). Parametric studies and quantitative assessment of the vulnerability of a RC frame building exposed to differential settlements. Natural Hazards and Earth System Sciences, 10(9), 1781-1792.																								
Region of applicability	-																								
Class	One-bay One-storey RC frame structure																								
Methodology	Analytical																								
Damage states	Damage states, based on allowable values of material strains on steel and concrete: <ul style="list-style-type: none">• LS1: Slight• LS2: Moderate• LS3: Extensive• LS4: Complete																								
Intensity Measure	Differential settlement d [cm]																								
Fragility parameters	<table><tr><th colspan="2">LS1</th><th colspan="2">LS2</th><th colspan="2">LS3</th><th colspan="2">LS4</th></tr><tr><th>α [cm]</th><th>β</th><th>α [cm]</th><th>β</th><th>α [cm]</th><th>β</th><th>α [cm]</th><th>β</th></tr><tr><td>5.0</td><td>0.5</td><td>12.0</td><td>0.5</td><td>27.0</td><td>0.5</td><td>40.0</td><td>0.5</td></tr></table>	LS1		LS2		LS3		LS4		α [cm]	β	α [cm]	β	α [cm]	β	α [cm]	β	5.0	0.5	12.0	0.5	27.0	0.5	40.0	0.5
LS1		LS2		LS3		LS4																			
α [cm]	β	α [cm]	β	α [cm]	β	α [cm]	β																		
5.0	0.5	12.0	0.5	27.0	0.5	40.0	0.5																		
Figures																									

9.6 Wind fragility models

FRAG WI BDG Abdelhady2021																																																																																																																																																																																																												
References	Abdelhady AU, Spence SMJ, McCormick J (2022) Risk and fragility assessment of residential wooden buildings subject to hurricane winds. Structural Safety 94:102137. https://doi.org/10.1016/j.strusafe.2021.102137																																																																																																																																																																																																											
Region of applicability	Brisbane, Australia; Sydney/Melbourne, Australia																																																																																																																																																																																																											
Class	<ul style="list-style-type: none"> W/HAPP:2: Wood, low-rise; Residential 																																																																																																																																																																																																											
Methodology	Analytical, from capacity curves																																																																																																																																																																																																											
Damage states	<ul style="list-style-type: none"> DS0: No damage DS1: Minor damage DS2: Moderate damage DS3: Severe damage DS4: Destruction 																																																																																																																																																																																																											
Intensity Measure	Maximum 3-sec gust wind speed [m/s]																																																																																																																																																																																																											
Fragility parameters	<p>lognormal curves; λ_1: the logarithmic median, ζ_1: the log-normal standard deviation.</p> <ul style="list-style-type: none"> The Floor Area Ratio is the ratio of the surface covered by the floor of buildings to the surface of the the given are. Higher Floor Area ratios lead to reduced fragilities due to the shielding effect by the surrounding buildings. The construction cases 1-10 are in order of increasing resistance / decreasing fragility. The parameters selected for the calculations for the testbeds are highlighted. <p>Floor Area Ratio = 0.1, Debris</p> <table> <tr> <th rowspan="2">Construction case</th><th colspan="2">DS1</th><th colspan="2">DS2</th><th colspan="2">DS3</th><th colspan="2">DS4</th></tr> <tr> <th>λ_1</th><th>ζ_1</th><th>λ_1</th><th>ζ_1</th><th>λ_1</th><th>ζ_1</th><th>λ_1</th><th>ζ_1</th></tr> <tr><td>1</td><td>3.13</td><td>0.09</td><td>3.13</td><td>0.09</td><td>3.45</td><td>0.05</td><td>3.72</td><td>0.04</td></tr> <tr><td>2</td><td>3.38</td><td>0.12</td><td>3.38</td><td>0.12</td><td>3.72</td><td>0.07</td><td>3.95</td><td>0.04</td></tr> <tr><td>3</td><td>3.57</td><td>0.11</td><td>3.57</td><td>0.11</td><td>3.89</td><td>0.07</td><td>4.14</td><td>0.05</td></tr> <tr><td>4</td><td>3.70</td><td>0.13</td><td>3.70</td><td>0.13</td><td>4.01</td><td>0.05</td><td>4.26</td><td>0.06</td></tr> <tr><td>5</td><td>3.80</td><td>0.11</td><td>3.80</td><td>0.12</td><td>4.11</td><td>0.08</td><td>4.37</td><td>0.06</td></tr> <tr><td>6</td><td>3.88</td><td>0.12</td><td>3.89</td><td>0.13</td><td>4.21</td><td>0.05</td><td>4.46</td><td>0.05</td></tr> <tr><td>7</td><td>3.94</td><td>0.14</td><td>3.96</td><td>0.15</td><td>4.27</td><td>0.06</td><td>4.52</td><td>0.07</td></tr> <tr><td>8</td><td>4.02</td><td>0.10</td><td>4.04</td><td>0.12</td><td>4.33</td><td>0.07</td><td>4.58</td><td>0.07</td></tr> <tr><td>9</td><td>4.06</td><td>0.10</td><td>4.09</td><td>0.11</td><td>4.39</td><td>0.07</td><td>4.63</td><td>0.08</td></tr> <tr><td>10</td><td>4.11</td><td>0.10</td><td>4.14</td><td>0.11</td><td>4.44</td><td>0.06</td><td>4.68</td><td>0.08</td></tr> </table> <p>Floor Area Ratio = 0.1, No debris</p> <table> <tr> <th rowspan="2">Construction case</th><th colspan="2">DS1</th><th colspan="2">DS2</th><th colspan="2">DS3</th><th colspan="2">DS4</th></tr> <tr> <th>λ_1</th><th>ζ_1</th><th>λ_1</th><th>ζ_1</th><th>λ_1</th><th>ζ_1</th><th>λ_1</th><th>ζ_1</th></tr> <tr><td>1</td><td>3.13</td><td>0.09</td><td>3.13</td><td>0.09</td><td>3.45</td><td>0.05</td><td>3.72</td><td>0.04</td></tr> <tr><td>2</td><td>3.38</td><td>0.12</td><td>3.38</td><td>0.12</td><td>3.72</td><td>0.07</td><td>4.00</td><td>0.05</td></tr> <tr><td>3</td><td>3.57</td><td>0.11</td><td>3.57</td><td>0.11</td><td>3.91</td><td>0.07</td><td>4.17</td><td>0.04</td></tr> <tr><td>4</td><td>3.70</td><td>0.13</td><td>3.70</td><td>0.13</td><td>4.02</td><td>0.04</td><td>4.28</td><td>0.06</td></tr> <tr><td>5</td><td>3.80</td><td>0.11</td><td>3.80</td><td>0.12</td><td>4.13</td><td>0.08</td><td>4.38</td><td>0.06</td></tr> <tr><td>6</td><td>3.88</td><td>0.12</td><td>3.89</td><td>0.13</td><td>4.22</td><td>0.05</td><td>4.47</td><td>0.05</td></tr> <tr><td>7</td><td>3.95</td><td>0.14</td><td>3.96</td><td>0.15</td><td>4.29</td><td>0.06</td><td>4.53</td><td>0.07</td></tr> <tr><td>8</td><td>4.02</td><td>0.10</td><td>4.05</td><td>0.12</td><td>4.36</td><td>0.08</td><td>4.59</td><td>0.07</td></tr> </table>								Construction case	DS1		DS2		DS3		DS4		λ_1	ζ_1	λ_1	ζ_1	λ_1	ζ_1	λ_1	ζ_1	1	3.13	0.09	3.13	0.09	3.45	0.05	3.72	0.04	2	3.38	0.12	3.38	0.12	3.72	0.07	3.95	0.04	3	3.57	0.11	3.57	0.11	3.89	0.07	4.14	0.05	4	3.70	0.13	3.70	0.13	4.01	0.05	4.26	0.06	5	3.80	0.11	3.80	0.12	4.11	0.08	4.37	0.06	6	3.88	0.12	3.89	0.13	4.21	0.05	4.46	0.05	7	3.94	0.14	3.96	0.15	4.27	0.06	4.52	0.07	8	4.02	0.10	4.04	0.12	4.33	0.07	4.58	0.07	9	4.06	0.10	4.09	0.11	4.39	0.07	4.63	0.08	10	4.11	0.10	4.14	0.11	4.44	0.06	4.68	0.08	Construction case	DS1		DS2		DS3		DS4		λ_1	ζ_1	λ_1	ζ_1	λ_1	ζ_1	λ_1	ζ_1	1	3.13	0.09	3.13	0.09	3.45	0.05	3.72	0.04	2	3.38	0.12	3.38	0.12	3.72	0.07	4.00	0.05	3	3.57	0.11	3.57	0.11	3.91	0.07	4.17	0.04	4	3.70	0.13	3.70	0.13	4.02	0.04	4.28	0.06	5	3.80	0.11	3.80	0.12	4.13	0.08	4.38	0.06	6	3.88	0.12	3.89	0.13	4.22	0.05	4.47	0.05	7	3.95	0.14	3.96	0.15	4.29	0.06	4.53	0.07	8	4.02	0.10	4.05	0.12	4.36	0.08	4.59	0.07
Construction case	DS1		DS2		DS3		DS4																																																																																																																																																																																																					
	λ_1	ζ_1	λ_1	ζ_1	λ_1	ζ_1	λ_1	ζ_1																																																																																																																																																																																																				
1	3.13	0.09	3.13	0.09	3.45	0.05	3.72	0.04																																																																																																																																																																																																				
2	3.38	0.12	3.38	0.12	3.72	0.07	3.95	0.04																																																																																																																																																																																																				
3	3.57	0.11	3.57	0.11	3.89	0.07	4.14	0.05																																																																																																																																																																																																				
4	3.70	0.13	3.70	0.13	4.01	0.05	4.26	0.06																																																																																																																																																																																																				
5	3.80	0.11	3.80	0.12	4.11	0.08	4.37	0.06																																																																																																																																																																																																				
6	3.88	0.12	3.89	0.13	4.21	0.05	4.46	0.05																																																																																																																																																																																																				
7	3.94	0.14	3.96	0.15	4.27	0.06	4.52	0.07																																																																																																																																																																																																				
8	4.02	0.10	4.04	0.12	4.33	0.07	4.58	0.07																																																																																																																																																																																																				
9	4.06	0.10	4.09	0.11	4.39	0.07	4.63	0.08																																																																																																																																																																																																				
10	4.11	0.10	4.14	0.11	4.44	0.06	4.68	0.08																																																																																																																																																																																																				
Construction case	DS1		DS2		DS3		DS4																																																																																																																																																																																																					
	λ_1	ζ_1	λ_1	ζ_1	λ_1	ζ_1	λ_1	ζ_1																																																																																																																																																																																																				
1	3.13	0.09	3.13	0.09	3.45	0.05	3.72	0.04																																																																																																																																																																																																				
2	3.38	0.12	3.38	0.12	3.72	0.07	4.00	0.05																																																																																																																																																																																																				
3	3.57	0.11	3.57	0.11	3.91	0.07	4.17	0.04																																																																																																																																																																																																				
4	3.70	0.13	3.70	0.13	4.02	0.04	4.28	0.06																																																																																																																																																																																																				
5	3.80	0.11	3.80	0.12	4.13	0.08	4.38	0.06																																																																																																																																																																																																				
6	3.88	0.12	3.89	0.13	4.22	0.05	4.47	0.05																																																																																																																																																																																																				
7	3.95	0.14	3.96	0.15	4.29	0.06	4.53	0.07																																																																																																																																																																																																				
8	4.02	0.10	4.05	0.12	4.36	0.08	4.59	0.07																																																																																																																																																																																																				

9	4.07	0.10	4.09	0.11	4.41	0.07	4.64	0.08
10	4.11	0.10	4.14	0.11	4.46	0.07	4.69	0.08

Floor Area Ratio = 0.3, Debris

Construction case	DS1		DS2		DS3		DS4	
	λ_1	ζ_1	λ_1	ζ_1	λ_1	ζ_1	λ_1	ζ_1
1	3.21	0.09	3.21	0.10	3.51	0.08	3.81	0.06
2	3.49	0.13	3.49	0.13	3.82	0.05	4.06	0.05
3	3.68	0.12	3.68	0.12	3.98	0.07	4.24	0.05
4	3.81	0.10	3.81	0.11	4.10	0.07	4.36	0.06
5	3.89	0.12	3.90	0.13	4.21	0.06	4.46	0.06
6	4.00	0.12	4.00	0.12	4.29	0.07	4.54	0.07
7	4.06	0.11	4.07	0.12	4.36	0.07	4.61	0.08
8	4.11	0.11	4.12	0.12	4.41	0.07	4.67	0.09
9	4.16	0.10	4.18	0.11	4.47	0.07	4.72	0.08
10	4.20	0.10	4.22	0.11	4.52	0.07	-	-

Floor Area Ratio = 0.3, No debris

Construction case	DS1		DS2		DS3		DS4	
	λ_1	ζ_1	λ_1	ζ_1	λ_1	ζ_1	λ_1	ζ_1
1	3.21	0.09	3.21	0.10	3.51	0.08	3.81	0.06
2	3.49	0.13	3.49	0.13	3.82	0.05	4.10	0.05
3	3.68	0.12	3.68	0.12	3.98	0.07	4.25	0.06
4	3.81	0.10	3.81	0.11	4.10	0.07	4.37	0.06
5	3.89	0.12	3.90	0.13	4.21	0.06	4.48	0.06
6	4.00	0.12	4.00	0.12	4.29	0.07	4.56	0.08
7	4.06	0.11	4.07	0.12	4.36	0.07	4.63	0.08
8	4.11	0.11	4.12	0.12	4.41	0.07	4.70	0.09
9	4.16	0.10	4.18	0.11	4.47	0.07	4.73	0.08
10	4.20	0.10	4.22	0.11	4.52	0.07	-	-

Floor Area Ratio = 0.6, Debris

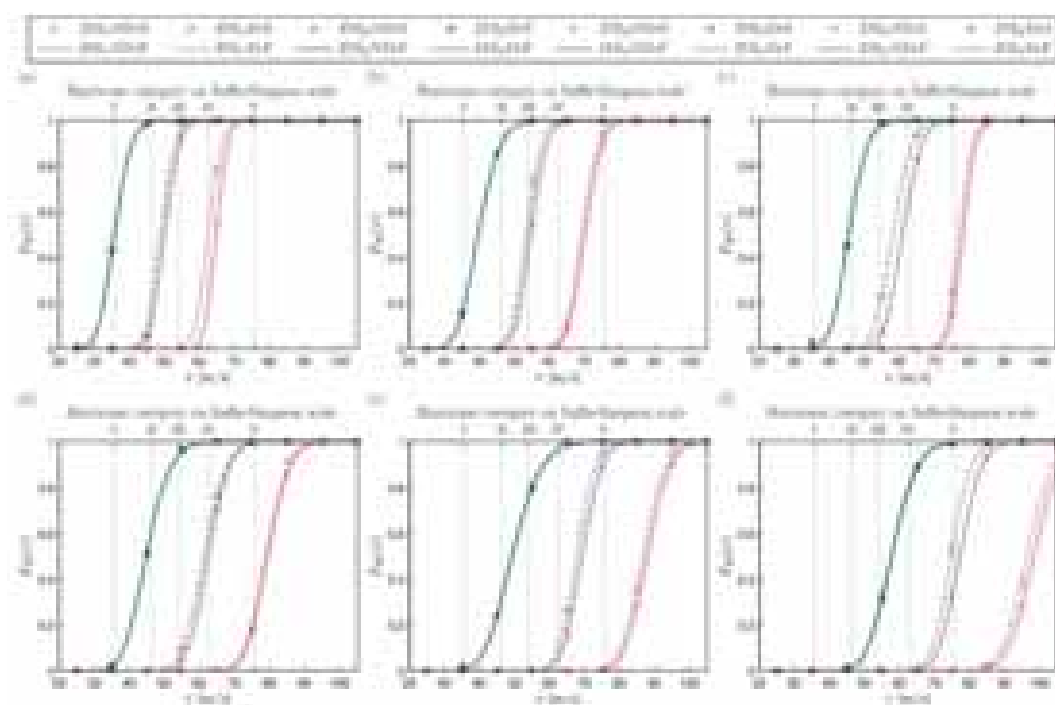
Construction case	DS1		DS2		DS3		DS4	
	λ_1	ζ_1	λ_1	ζ_1	λ_1	ζ_1	λ_1	ζ_1
1	3.31	0.10	3.31	0.10	3.51	0.08	3.92	0.03
2	3.63	0.10	3.63	0.10	3.82	0.05	4.17	0.04
3	3.82	0.09	3.82	0.09	4.00	0.07	4.34	0.04
4	3.94	0.11	3.94	0.11	4.13	0.07	4.46	0.05
5	4.05	0.10	4.05	0.10	4.24	0.06	4.57	0.06
6	4.11	0.09	4.12	0.09	4.31	0.07	4.65	0.08
7	4.18	0.09	4.18	0.10	4.39	0.07	4.72	0.07
8	4.23	0.09	4.24	0.10	4.45	0.08	-	-
9	4.28	0.10	4.29	0.11	4.52	0.07	-	-
10	4.33	0.09	4.34	0.10	4.56	0.07	-	-

Floor Area Ratio = 0.6, No debris

Construction case	DS1		DS2		DS3		DS4	
	λ_1	ζ_1	λ_1	ζ_1	λ_1	ζ_1	λ_1	ζ_1
1	3.31	0.10	3.31	0.10	3.62	0.05	3.93	0.03
2	3.63	0.10	3.63	0.10	3.91	0.06	4.20	0.03

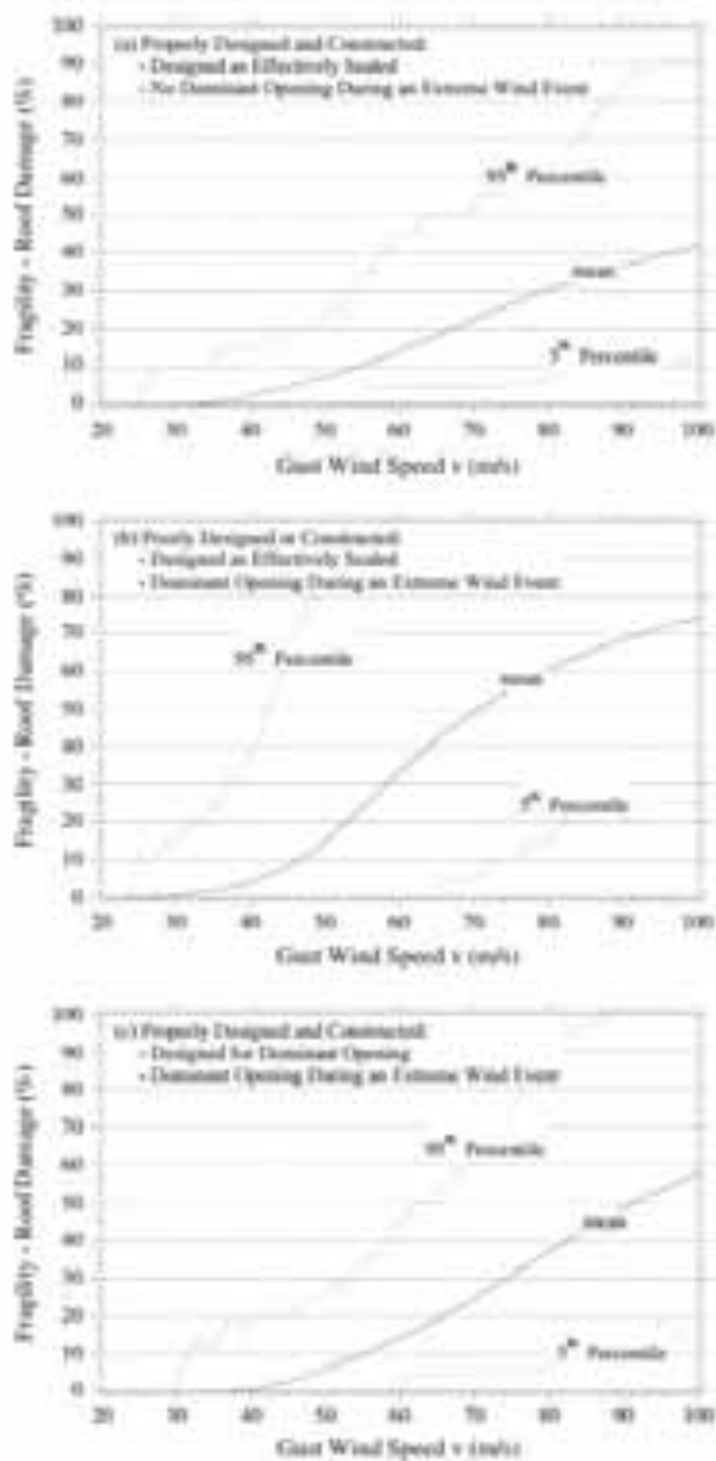
3	3.82	0.09	3.82	0.09	4.06	0.07	4.36	0.04
4	3.94	0.11	3.94	0.11	4.22	0.06	4.48	0.05
5	4.05	0.10	4.06	0.10	4.31	0.06	4.59	0.06
6	4.12	0.09	4.12	0.10	4.39	0.06	4.68	0.08
7	4.19	0.09	4.19	0.10	4.46	0.06	4.73	0.07
8	4.25	0.09	4.25	0.10	4.52	0.07	-	-
9	4.30	0.10	4.31	0.11	4.57	0.07	-	-
10	4.36	0.09	4.37	0.10	4.61	0.06	-	-

Figures



FRAG WI BDG Stewart2016																																																												
References	Stewart MG, Ryan PC, Henderson DJ, Ginger JD (2016) Fragility analysis of roof damage to industrial buildings subject to extreme wind loading in non-cyclonic regions. Engineering Structures 128:333–343. https://doi.org/10.1016/j.engstruct.2016.09.053																																																											
Region of applicability	NA																																																											
Class	<ul style="list-style-type: none"> S/HAPP:2: Steel, low-rise; Industrial 																																																											
Methodology	Analytical, from capacity curves																																																											
Damage states	<ul style="list-style-type: none"> DS0: No damage DS1: Roof damage 																																																											
Intensity Measure	Maximum 3-sec gust wind speed [m/s]																																																											
Fragility parameters	<p>Weibul curve:</p> $P_1(DSH) = \gamma \left(1 - \exp \left[- \left(\frac{v}{a} \right)^\gamma \right] \right) \quad v \leq 80 \text{ m/s}, P_1(DSH) \leq 100\%$ <table border="1"> <thead> <tr> <th rowspan="2">Building Designed as Effectively Sealed</th><th rowspan="2">Dominant Opening During Extreme Winds</th><th colspan="3">Brisbane</th></tr> <tr> <th>γ</th><th>a</th><th>b</th></tr> </thead> <tbody> <tr> <td>Yes</td><td>No</td><td>18.97</td><td>0.1678</td><td>4.271</td></tr> <tr> <td>Yes</td><td>Yes</td><td>46.16</td><td>0.1503</td><td>4.278</td></tr> <tr> <td>No</td><td>No</td><td>10.28</td><td>0.1177</td><td>4.333</td></tr> <tr> <td>No</td><td>Yes</td><td>24.80</td><td>0.1102</td><td>4.347</td></tr> </tbody> </table> <table border="1"> <thead> <tr> <th rowspan="2">Building Designed as Effectively Sealed</th><th rowspan="2">Dominant Opening During Extreme Winds</th><th colspan="3">Sydney/Melbourne</th></tr> <tr> <th>γ</th><th>a</th><th>b</th></tr> </thead> <tbody> <tr> <td>Yes</td><td>No</td><td>34.69</td><td>0.2137</td><td>4.234</td></tr> <tr> <td>Yes</td><td>Yes</td><td>60.08</td><td>0.1820</td><td>4.140</td></tr> <tr> <td>No</td><td>No</td><td>18.53</td><td>0.1317</td><td>4.227</td></tr> <tr> <td>No</td><td>Yes</td><td>36.93</td><td>0.1263</td><td>4.280</td></tr> </tbody> </table>				Building Designed as Effectively Sealed	Dominant Opening During Extreme Winds	Brisbane			γ	a	b	Yes	No	18.97	0.1678	4.271	Yes	Yes	46.16	0.1503	4.278	No	No	10.28	0.1177	4.333	No	Yes	24.80	0.1102	4.347	Building Designed as Effectively Sealed	Dominant Opening During Extreme Winds	Sydney/Melbourne			γ	a	b	Yes	No	34.69	0.2137	4.234	Yes	Yes	60.08	0.1820	4.140	No	No	18.53	0.1317	4.227	No	Yes	36.93	0.1263	4.280
Building Designed as Effectively Sealed	Dominant Opening During Extreme Winds	Brisbane																																																										
		γ	a	b																																																								
Yes	No	18.97	0.1678	4.271																																																								
Yes	Yes	46.16	0.1503	4.278																																																								
No	No	10.28	0.1177	4.333																																																								
No	Yes	24.80	0.1102	4.347																																																								
Building Designed as Effectively Sealed	Dominant Opening During Extreme Winds	Sydney/Melbourne																																																										
		γ	a	b																																																								
Yes	No	34.69	0.2137	4.234																																																								
Yes	Yes	60.08	0.1820	4.140																																																								
No	No	18.53	0.1317	4.227																																																								
No	Yes	36.93	0.1263	4.280																																																								

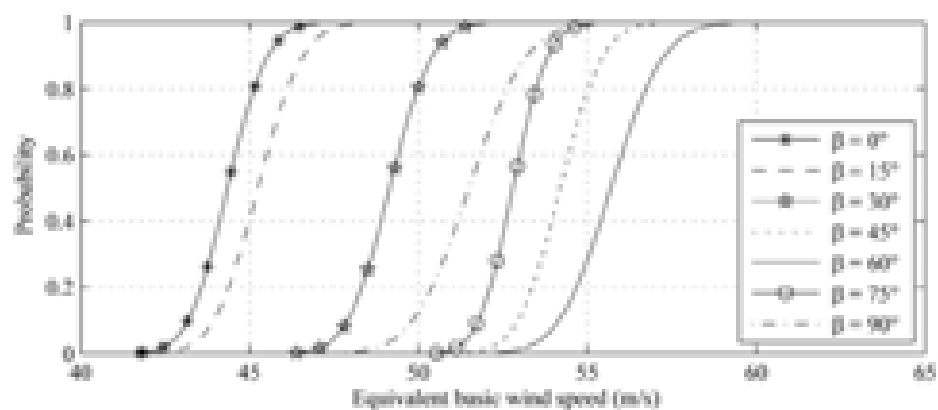
Figures



FRAG WI NETW ELEC TOW Fu2016																																																																																																							
References	Fu X, Li H-N, Li G (2016) Fragility analysis and estimation of collapse status for transmission tower subjected to wind and rain loads. Structural Safety 58:1–10. https://doi.org/10.1016/j.strusafe.2015.08.002																																																																																																						
Region of applicability	NA																																																																																																						
Class	<ul style="list-style-type: none"> NA (Transmission line tower) 																																																																																																						
Methodology	Analytical, from capacity curves																																																																																																						
Damage states	<ul style="list-style-type: none"> DS0: No damage DS1: Collapse 																																																																																																						
Intensity Measure	Equivalent basic wind speed (under wind and rain)																																																																																																						
Fragility parameters	<p>Fragility curves for different attack angles (β)</p> <table border="1"> <thead> <tr> <th colspan="2">$\beta = 0$ degrees</th><th colspan="2">$\beta = 15$ degrees</th></tr> <tr> <th>Equivalent basic wind speed (m/s)</th><th>Probability</th><th>Equivalent basic wind speed (m/s)</th><th>Probability</th></tr> </thead> <tbody> <tr><td>41.80</td><td>0.0000</td><td>42.45</td><td>0.0000</td></tr> <tr><td>42.45</td><td>0.0183</td><td>43.08</td><td>0.0157</td></tr> <tr><td>43.15</td><td>0.0968</td><td>43.69</td><td>0.0648</td></tr> <tr><td>43.77</td><td>0.2609</td><td>44.43</td><td>0.2082</td></tr> <tr><td>44.48</td><td>0.5475</td><td>45.97</td><td>0.7532</td></tr> <tr><td>45.19</td><td>0.8078</td><td>46.64</td><td>0.9022</td></tr> <tr><td>45.88</td><td>0.9455</td><td>47.18</td><td>0.9607</td></tr> <tr><td>46.47</td><td>0.9870</td><td>47.90</td><td>0.9928</td></tr> <tr><td>47.25</td><td>1.0000</td><td>48.00</td><td>1.0000</td></tr> </tbody> </table> <table border="1"> <thead> <tr> <th colspan="2">$\beta = 30$ degrees</th><th colspan="2">$\beta = 45$ degrees</th></tr> <tr> <th>Equivalent basic wind speed (m/s)</th><th>Probability</th><th>Equivalent basic wind speed (m/s)</th><th>Probability</th></tr> </thead> <tbody> <tr><td>46.41</td><td>0.0000</td><td>47.62</td><td>0.0000</td></tr> <tr><td>47.10</td><td>0.0161</td><td>48.51</td><td>0.0125</td></tr> <tr><td>47.81</td><td>0.0859</td><td>49.32</td><td>0.0465</td></tr> <tr><td>48.49</td><td>0.2557</td><td>49.90</td><td>0.1125</td></tr> <tr><td>49.32</td><td>0.5631</td><td>50.76</td><td>0.2860</td></tr> <tr><td>50.01</td><td>0.8045</td><td>52.75</td><td>0.8254</td></tr> <tr><td>50.72</td><td>0.9384</td><td>53.27</td><td>0.9047</td></tr> <tr><td>51.44</td><td>0.9856</td><td>54.16</td><td>0.9745</td></tr> <tr><td>52.55</td><td>1.0000</td><td>55.30</td><td>1.0000</td></tr> </tbody> </table> <table border="1"> <thead> <tr> <th colspan="2">$\beta = 60$ degrees</th><th colspan="2">$\beta = 75$ degrees</th></tr> <tr> <th>Equivalent basic wind speed (m/s)</th><th>Probability</th><th>Equivalent basic wind speed (m/s)</th><th>Probability</th></tr> </thead> <tbody> <tr><td></td><td></td><td></td><td></td></tr> </tbody> </table>			$\beta = 0$ degrees		$\beta = 15$ degrees		Equivalent basic wind speed (m/s)	Probability	Equivalent basic wind speed (m/s)	Probability	41.80	0.0000	42.45	0.0000	42.45	0.0183	43.08	0.0157	43.15	0.0968	43.69	0.0648	43.77	0.2609	44.43	0.2082	44.48	0.5475	45.97	0.7532	45.19	0.8078	46.64	0.9022	45.88	0.9455	47.18	0.9607	46.47	0.9870	47.90	0.9928	47.25	1.0000	48.00	1.0000	$\beta = 30$ degrees		$\beta = 45$ degrees		Equivalent basic wind speed (m/s)	Probability	Equivalent basic wind speed (m/s)	Probability	46.41	0.0000	47.62	0.0000	47.10	0.0161	48.51	0.0125	47.81	0.0859	49.32	0.0465	48.49	0.2557	49.90	0.1125	49.32	0.5631	50.76	0.2860	50.01	0.8045	52.75	0.8254	50.72	0.9384	53.27	0.9047	51.44	0.9856	54.16	0.9745	52.55	1.0000	55.30	1.0000	$\beta = 60$ degrees		$\beta = 75$ degrees		Equivalent basic wind speed (m/s)	Probability	Equivalent basic wind speed (m/s)	Probability				
$\beta = 0$ degrees		$\beta = 15$ degrees																																																																																																					
Equivalent basic wind speed (m/s)	Probability	Equivalent basic wind speed (m/s)	Probability																																																																																																				
41.80	0.0000	42.45	0.0000																																																																																																				
42.45	0.0183	43.08	0.0157																																																																																																				
43.15	0.0968	43.69	0.0648																																																																																																				
43.77	0.2609	44.43	0.2082																																																																																																				
44.48	0.5475	45.97	0.7532																																																																																																				
45.19	0.8078	46.64	0.9022																																																																																																				
45.88	0.9455	47.18	0.9607																																																																																																				
46.47	0.9870	47.90	0.9928																																																																																																				
47.25	1.0000	48.00	1.0000																																																																																																				
$\beta = 30$ degrees		$\beta = 45$ degrees																																																																																																					
Equivalent basic wind speed (m/s)	Probability	Equivalent basic wind speed (m/s)	Probability																																																																																																				
46.41	0.0000	47.62	0.0000																																																																																																				
47.10	0.0161	48.51	0.0125																																																																																																				
47.81	0.0859	49.32	0.0465																																																																																																				
48.49	0.2557	49.90	0.1125																																																																																																				
49.32	0.5631	50.76	0.2860																																																																																																				
50.01	0.8045	52.75	0.8254																																																																																																				
50.72	0.9384	53.27	0.9047																																																																																																				
51.44	0.9856	54.16	0.9745																																																																																																				
52.55	1.0000	55.30	1.0000																																																																																																				
$\beta = 60$ degrees		$\beta = 75$ degrees																																																																																																					
Equivalent basic wind speed (m/s)	Probability	Equivalent basic wind speed (m/s)	Probability																																																																																																				

	50.51	0.0000	51.32	0.0000
	51.12	0.0184	52.21	0.0203
	51.73	0.0919	52.81	0.0807
	52.33	0.2786	53.20	0.1543
	52.93	0.5672	53.91	0.3844
	53.46	0.7821	55.05	0.8087
	54.03	0.9349	55.63	0.9200
	54.65	0.9878	56.59	0.9898
	55.83	1.0000	57.67	1.0000
	β = 90 degrees			
	Equivalent basic wind speed (m/s)	Probability		
	51.96	0.0000		
	53.22	0.0185		
	54.01	0.0846		
	54.59	0.1808		
	55.32	0.3826		
	56.85	0.8164		
	57.39	0.9088		
	58.22	0.9768		
	59.69	1.0000		

Figures



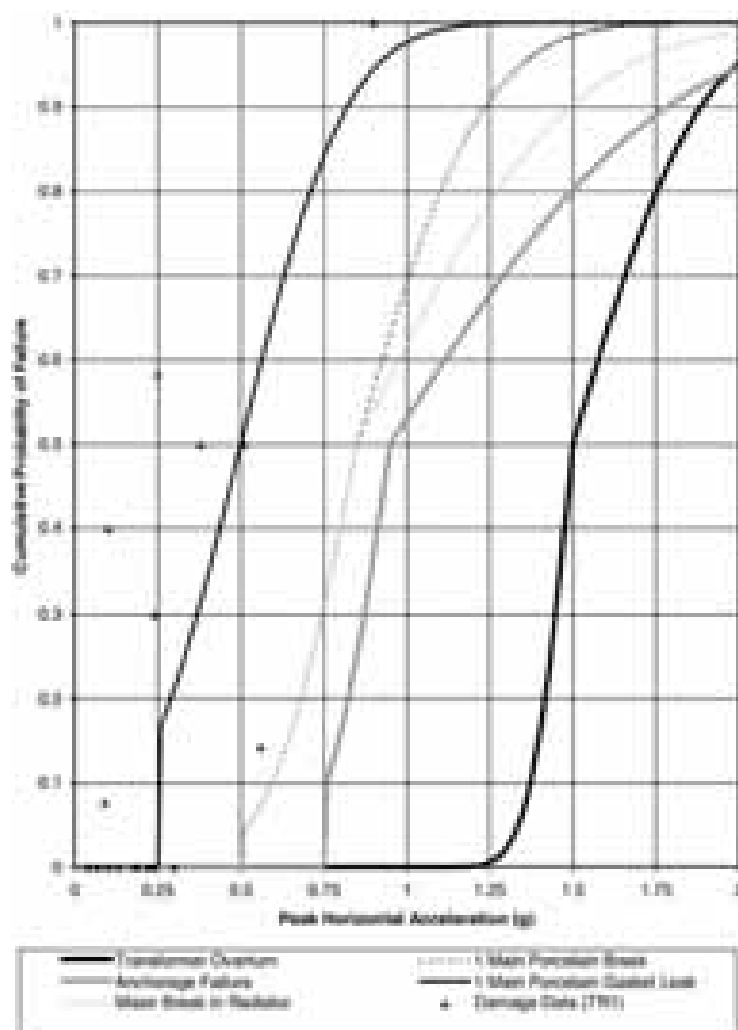
FRAG WI NETW ELEC SUB Anagnos1999																																																																																																				
References	Anagnos T (1999) Development of an Electrical Substation Equipment Performance Database for Evaluation of Equipment Fragilities. PEER Report 2001-06. Pacific Earthquake Engineering Research Center College of Engineering, University of California, Berkeley																																																																																																			
Region of applicability	California, United States of America																																																																																																			
Classes	• NA (Electric power network substation)																																																																																																			
Methodology	Empirical																																																																																																			
Damage states	Fragility curves for different modes of failure (not to be considered as mutually exclusive and collectively exhaustive)																																																																																																			
Intensity Measure	Peak Horizontal Acceleration [g]																																																																																																			
Fragility parameters	<div>Non-parametric fragility curves</div> <table><tr><th colspan="2">Main Porcelain Gasket Leak</th><th colspan="2">Main Pcelain Break</th></tr><tr><th>Peak Horizontal Acceleration [g]</th><th>Cummulative Probability of Failure</th><th>Peak Horizontal Acceleration [g]]</th><th>Cummulative Probability of Failure</th></tr><tr><td>0.000</td><td>0.000</td><td>0.000</td><td>0.000</td></tr><tr><td>0.249</td><td>0.001</td><td>0.499</td><td>0.001</td></tr><tr><td>0.249</td><td>0.053</td><td>0.509</td><td>0.044</td></tr><tr><td>0.249</td><td>0.099</td><td>0.591</td><td>0.098</td></tr><tr><td>0.260</td><td>0.169</td><td>0.640</td><td>0.148</td></tr><tr><td>0.289</td><td>0.200</td><td>0.680</td><td>0.200</td></tr><tr><td>0.333</td><td>0.252</td><td>0.714</td><td>0.252</td></tr><tr><td>0.367</td><td>0.301</td><td>0.745</td><td>0.300</td></tr><tr><td>0.404</td><td>0.352</td><td>0.774</td><td>0.355</td></tr><tr><td>0.436</td><td>0.400</td><td>0.798</td><td>0.400</td></tr><tr><td>0.467</td><td>0.447</td><td>0.824</td><td>0.448</td></tr><tr><td>0.504</td><td>0.500</td><td>0.848</td><td>0.499</td></tr><tr><td>0.535</td><td>0.554</td><td>0.898</td><td>0.565</td></tr><tr><td>0.562</td><td>0.599</td><td>0.927</td><td>0.600</td></tr><tr><td>0.598</td><td>0.653</td><td>0.971</td><td>0.656</td></tr><tr><td>0.630</td><td>0.699</td><td>1.003</td><td>0.701</td></tr><tr><td>0.672</td><td>0.752</td><td>1.060</td><td>0.758</td></tr><tr><td>0.709</td><td>0.799</td><td>1.102</td><td>0.799</td></tr><tr><td>0.761</td><td>0.854</td><td>1.171</td><td>0.857</td></tr><tr><td>0.822</td><td>0.899</td><td>1.239</td><td>0.900</td></tr><tr><td>0.919</td><td>0.953</td><td>1.365</td><td>0.957</td></tr><tr><td>1.241</td><td>0.999</td><td>1.701</td><td>0.998</td></tr></table>				Main Porcelain Gasket Leak		Main Pcelain Break		Peak Horizontal Acceleration [g]	Cummulative Probability of Failure	Peak Horizontal Acceleration [g]]	Cummulative Probability of Failure	0.000	0.000	0.000	0.000	0.249	0.001	0.499	0.001	0.249	0.053	0.509	0.044	0.249	0.099	0.591	0.098	0.260	0.169	0.640	0.148	0.289	0.200	0.680	0.200	0.333	0.252	0.714	0.252	0.367	0.301	0.745	0.300	0.404	0.352	0.774	0.355	0.436	0.400	0.798	0.400	0.467	0.447	0.824	0.448	0.504	0.500	0.848	0.499	0.535	0.554	0.898	0.565	0.562	0.599	0.927	0.600	0.598	0.653	0.971	0.656	0.630	0.699	1.003	0.701	0.672	0.752	1.060	0.758	0.709	0.799	1.102	0.799	0.761	0.854	1.171	0.857	0.822	0.899	1.239	0.900	0.919	0.953	1.365	0.957	1.241	0.999	1.701	0.998
Main Porcelain Gasket Leak		Main Pcelain Break																																																																																																		
Peak Horizontal Acceleration [g]	Cummulative Probability of Failure	Peak Horizontal Acceleration [g]]	Cummulative Probability of Failure																																																																																																	
0.000	0.000	0.000	0.000																																																																																																	
0.249	0.001	0.499	0.001																																																																																																	
0.249	0.053	0.509	0.044																																																																																																	
0.249	0.099	0.591	0.098																																																																																																	
0.260	0.169	0.640	0.148																																																																																																	
0.289	0.200	0.680	0.200																																																																																																	
0.333	0.252	0.714	0.252																																																																																																	
0.367	0.301	0.745	0.300																																																																																																	
0.404	0.352	0.774	0.355																																																																																																	
0.436	0.400	0.798	0.400																																																																																																	
0.467	0.447	0.824	0.448																																																																																																	
0.504	0.500	0.848	0.499																																																																																																	
0.535	0.554	0.898	0.565																																																																																																	
0.562	0.599	0.927	0.600																																																																																																	
0.598	0.653	0.971	0.656																																																																																																	
0.630	0.699	1.003	0.701																																																																																																	
0.672	0.752	1.060	0.758																																																																																																	
0.709	0.799	1.102	0.799																																																																																																	
0.761	0.854	1.171	0.857																																																																																																	
0.822	0.899	1.239	0.900																																																																																																	
0.919	0.953	1.365	0.957																																																																																																	
1.241	0.999	1.701	0.998																																																																																																	

	Major Break in Radiator		Anchorage Failure	
	Peak Horizontal Acceleration [g]	Cummulative Probability of Failure	Peak Horizontal Acceleration [g]	Cummulative Probability of Failure
	0.000	0.000	0.000	0.000
	0.504	0.001	0.300	0.000
	0.512	0.046	0.748	0.000
	0.596	0.101	0.759	0.100
	0.643	0.150	0.795	0.152
	0.680	0.198	0.824	0.200
	0.719	0.250	0.848	0.251
	0.745	0.298	0.871	0.299
	0.774	0.353	0.892	0.352
	0.801	0.398	0.911	0.400
	0.824	0.450	0.929	0.447
	0.850	0.500	0.950	0.500
	0.929	0.563	1.045	0.557
	0.976	0.600	1.115	0.599
	1.047	0.653	1.202	0.653
	1.113	0.700	1.289	0.700
	1.184	0.749	1.386	0.749
	1.270	0.799	1.496	0.799
	1.375	0.852	1.635	0.854
	1.491	0.899	1.782	0.899
	1.685	0.952	1.892	0.925
	1.997	0.988	2.000	0.945
	Transformer Overturn			
	Peak Horizontal Acceleration [g]	Cummulative Probability of Failure		
	0.000	0.000		
	1.186	0.000		
	1.294	0.019		
	1.373	0.099		
	1.396	0.153		
	1.415	0.201		
	1.436	0.255		
	1.444	0.299		
	1.465	0.356		
	1.472	0.400		

1.491	0.452
1.499	0.499
1.541	0.556
1.577	0.599
1.617	0.654
1.656	0.699
1.703	0.753
1.753	0.799
1.819	0.855
1.885	0.898
1.934	0.927
2.000	0.951

Figures

Seismic fragility curves for single-phase 230 kV transformers Anagnos (1999).



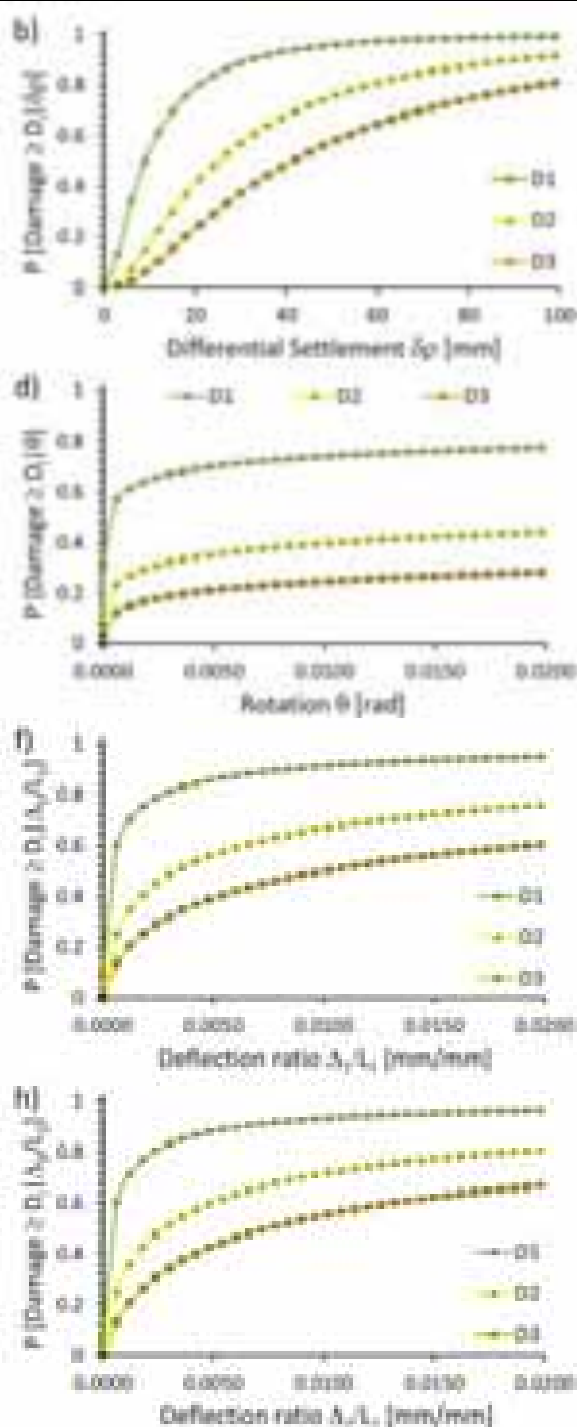
9.7 Ground settlement fragility models

9.7.1 Buildings

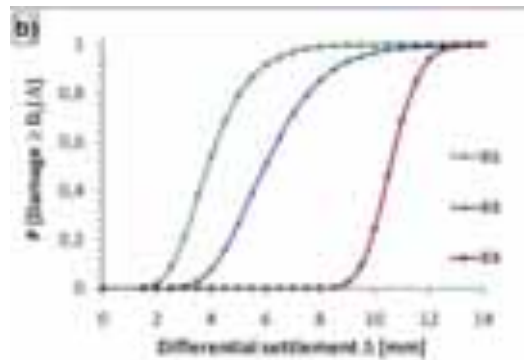
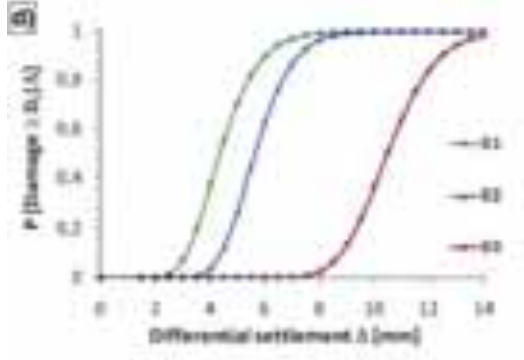
FRAG_SET_BDG_Peduto2019																																																																																		
References	Peduto D, Korff M, Nicodemo G, et al (2019) Empirical fragility curves for settlement-affected buildings: Analysis of different intensity parameters for seven hundred masonry buildings in The Netherlands. Soils and Foundations 59:380–397. https://doi.org/10.1016/j.sandf.2018.12.009																																																																																	
Region of applicability	Dordrecht; Rotterdam; Schiedam; Zaanstad, Netherlands																																																																																	
Class	<ul style="list-style-type: none"> MUR/HAPP:2: Masonry; Low-rise 																																																																																	
Methodology	Analytical, from capacity curves																																																																																	
Damage states	<ul style="list-style-type: none"> DS0: negligible DS1: very slight (aesthetical damage) DS2: slight (aesthetical damage) DS3: moderate (loss of functionality) DS4: severe (loss of functionality) DS5: very severe (compromise of building's stability) <p>The damage scale is based on the Limit Tensile Strain Method (LTSM) by Burland et al. (1977).</p>																																																																																	
Intensity Measure	<ul style="list-style-type: none"> Differential settlement ($\delta\rho$) [mm] Rotation (θ) [rad] Deflection ratio (Δ_1/L_1) [mm/mm] Deflection ratio (Δ_2/L_2) [mm/mm] 																																																																																	
Fragility parameters	<p>Lognormal curves</p> <p>The parameters selected for application in the calculations for the testbeds are highlighted.</p> <table> <tr> <th rowspan="3">SRI parameter</th><th rowspan="3">Damage level</th><th colspan="4">Foundation type</th></tr> <tr> <th colspan="2">Shallow</th><th colspan="2">Piled</th></tr> <tr> <th>Median SRI</th><th>Standard deviation β</th><th>Median SRI</th><th>Standard deviation β</th></tr> <tr> <td rowspan="4">$\delta\rho$ [mm]</td><td>DS1</td><td>9.04</td><td>0.99</td><td>12.57</td><td>0.57</td></tr> <tr> <td>DS2</td><td>25.06</td><td>0.99</td><td>23.26</td><td>0.57</td></tr> <tr> <td>DS3</td><td>41.53</td><td>0.99</td><td>36.81</td><td>0.57</td></tr> <tr> <td>DS4/DS5</td><td>-</td><td>-</td><td>48.6</td><td>0.57</td></tr> <tr> <td rowspan="4">θ [rad]</td><td>DS1</td><td>2.16E-04</td><td>6.04</td><td>3.10E-04</td><td>4.14</td></tr> <tr> <td>DS2</td><td>4.67E-02</td><td>6.04</td><td>8.69E-03</td><td>4.14</td></tr> <tr> <td>DS3</td><td>6.38E-01</td><td>6.04</td><td>9.08E-02</td><td>4.14</td></tr> <tr> <td>DS4/DS5</td><td>-</td><td>-</td><td>1.69E-01</td><td>4.14</td></tr> <tr> <td rowspan="4">D1/L1 [mm/mm]</td><td>D1</td><td>3.16E-04</td><td>2.56</td><td>5.00E-04</td><td>1.76</td></tr> <tr> <td>DS2</td><td>3.26E-03</td><td>2.56</td><td>2.21E-03</td><td>1.76</td></tr> <tr> <td>DS3</td><td>1.01E-02</td><td>2.56</td><td>6.45E-03</td><td>1.76</td></tr> <tr> <td>DS4/DS5</td><td>-</td><td>-</td><td>1.26E-02</td><td>1.76</td></tr> </table>					SRI parameter	Damage level	Foundation type				Shallow		Piled		Median SRI	Standard deviation β	Median SRI	Standard deviation β	$\delta\rho$ [mm]	DS1	9.04	0.99	12.57	0.57	DS2	25.06	0.99	23.26	0.57	DS3	41.53	0.99	36.81	0.57	DS4/DS5	-	-	48.6	0.57	θ [rad]	DS1	2.16E-04	6.04	3.10E-04	4.14	DS2	4.67E-02	6.04	8.69E-03	4.14	DS3	6.38E-01	6.04	9.08E-02	4.14	DS4/DS5	-	-	1.69E-01	4.14	D1/L1 [mm/mm]	D1	3.16E-04	2.56	5.00E-04	1.76	DS2	3.26E-03	2.56	2.21E-03	1.76	DS3	1.01E-02	2.56	6.45E-03	1.76	DS4/DS5	-	-	1.26E-02	1.76
SRI parameter	Damage level	Foundation type																																																																																
		Shallow		Piled																																																																														
		Median SRI	Standard deviation β	Median SRI	Standard deviation β																																																																													
$\delta\rho$ [mm]	DS1	9.04	0.99	12.57	0.57																																																																													
	DS2	25.06	0.99	23.26	0.57																																																																													
	DS3	41.53	0.99	36.81	0.57																																																																													
	DS4/DS5	-	-	48.6	0.57																																																																													
θ [rad]	DS1	2.16E-04	6.04	3.10E-04	4.14																																																																													
	DS2	4.67E-02	6.04	8.69E-03	4.14																																																																													
	DS3	6.38E-01	6.04	9.08E-02	4.14																																																																													
	DS4/DS5	-	-	1.69E-01	4.14																																																																													
D1/L1 [mm/mm]	D1	3.16E-04	2.56	5.00E-04	1.76																																																																													
	DS2	3.26E-03	2.56	2.21E-03	1.76																																																																													
	DS3	1.01E-02	2.56	6.45E-03	1.76																																																																													
	DS4/DS5	-	-	1.26E-02	1.76																																																																													

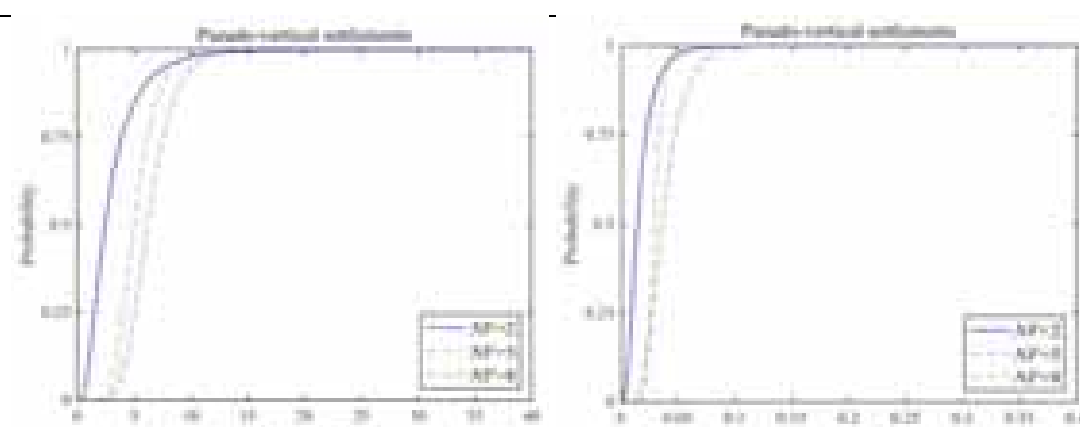
	D2/L2	DS1	3.46E-04	2.25	5.32E-04	1.50
	[mm/mm]	DS2	2.74E-03	2.25	1.95E-03	1.50
		DS3	7.45E-03	2.25	5.01E-03	1.50
		DS4/DS5	-	-	9.00E-03	1.50

Figures



Fragility curves for shallow foundations

FRAG SET BDG Peduto2017																															
References	Peduto D, Nicodemo G, Maccabiani J, Ferlisi S (2017) Multi-scale analysis of settlement-induced building damage using damage surveys and DInSAR data: A case study in The Netherlands. Engineering Geology 218:117–133. https://doi.org/10.1016/j.enggeo.2016.12.018																														
Region of applicability	Rotterdam; Schiedam, Netherlands																														
Class	<ul style="list-style-type: none">Buildings in densely urbanized area																														
Methodology	Analytical, from capacity curves																														
Damage states	<ul style="list-style-type: none">DS0: negligibleDS1: very slight (aesthetical damage)DS2: slight (aesthetical damage)DS3: moderate (loss of functionality)DS4: severe (loss of functionality)DS5: very severe (compromise of building’s stability) <p>The damage scale is based on the Limit Tensile Strain Method (LTSM) by Burland et al. (1977).</p>																														
Intensity Measure	<ul style="list-style-type: none">Differential settlement ($\delta\rho$) [mm]Rotation (θ) [rad]Deflection ratio (Δ_1/L_1) [mm/mm]Deflection ratio (Δ_2/L_2) [mm/mm]																														
Fragility parameters	<p>Lognormal curves</p> <p>The parameters selected for application in the calculations for the testbeds are highlighted.</p> <table><tr><th rowspan="3">Intensity Measure</th><th rowspan="3">Damage level</th><th colspan="4">Foundation type</th></tr><tr><th colspan="2">Shallow</th><th colspan="2">Piled</th></tr><tr><th>Median [mm]</th><th>Stand. dev. [mm]</th><th>Median [mm]</th><th>Stand. dev. [mm]</th></tr><tr><td rowspan="3">Differential settlement [mm]</td><td>DS1</td><td>3.86</td><td>0.32</td><td>4.35</td><td>0.26</td></tr><tr><td>DS2</td><td>5.94</td><td>0.28</td><td>5.64</td><td>0.19</td></tr><tr><td>DS3</td><td>10.58</td><td>0.08</td><td>10.47</td><td>0.14</td></tr></table>	Intensity Measure	Damage level	Foundation type				Shallow		Piled		Median [mm]	Stand. dev. [mm]	Median [mm]	Stand. dev. [mm]	Differential settlement [mm]	DS1	3.86	0.32	4.35	0.26	DS2	5.94	0.28	5.64	0.19	DS3	10.58	0.08	10.47	0.14
Intensity Measure	Damage level			Foundation type																											
				Shallow		Piled																									
		Median [mm]	Stand. dev. [mm]	Median [mm]	Stand. dev. [mm]																										
Differential settlement [mm]	DS1	3.86	0.32	4.35	0.26																										
	DS2	5.94	0.28	5.64	0.19																										
	DS3	10.58	0.08	10.47	0.14																										
Figures	<div></div> <div></div> <p>Fragility curves for (left) shallow and (right) piled foundations</p>																														

FRAG SET BDG Miano2022																																		
References	Miano A, Mele A, Prota A (2022) Fragility curves for different classes of existing RC buildings under ground differential settlements. Engineering Structures 257:114077. https://doi.org/10.1016/j.engstruct.2022.114077																																	
Region of applicability	Italy																																	
Class	CR_LFINF_CDL_0_HEX_2 CR_LFINF_CDL_0_HEX_5 CR_LFINF_CDL_0_HEX_8																																	
Methodology	Analytical, from capacity curves																																	
Damage states	<ul style="list-style-type: none">Limit state of Significant Damage (Eurocode 8)																																	
Intensity Measure	<ul style="list-style-type: none">Deflection ratio (chord rotation) [%]Differential Settlement [mm]																																	
Fragility parameters	Lognormal curves <table><tr><th rowspan="2">Intensity Measure</th><th colspan="2">Number of storeys: 2</th><th colspan="2">Number of storeys: 5</th><th colspan="2">Number of storeys: 8</th></tr><tr><th>Median</th><th>Log. stand. dev. β</th><th>Median</th><th>Log. stand. dev. β</th><th>Median</th><th>Log. stand. dev. β</th></tr><tr><td>Differential settlement $\delta\rho_{\max}$ [mm]</td><td>0.01</td><td>0.62</td><td>0.02</td><td>0.20</td><td>0.03</td><td>0.23</td></tr><tr><td>Deflection ratio γ [%]</td><td>1.55</td><td>0.67</td><td>3.34</td><td>0.37</td><td>5.45</td><td>0.35</td></tr></table>							Intensity Measure	Number of storeys: 2		Number of storeys: 5		Number of storeys: 8		Median	Log. stand. dev. β	Median	Log. stand. dev. β	Median	Log. stand. dev. β	Differential settlement $\delta\rho_{\max}$ [mm]	0.01	0.62	0.02	0.20	0.03	0.23	Deflection ratio γ [%]	1.55	0.67	3.34	0.37	5.45	0.35
Intensity Measure	Number of storeys: 2		Number of storeys: 5		Number of storeys: 8																													
	Median	Log. stand. dev. β	Median	Log. stand. dev. β	Median	Log. stand. dev. β																												
Differential settlement $\delta\rho_{\max}$ [mm]	0.01	0.62	0.02	0.20	0.03	0.23																												
Deflection ratio γ [%]	1.55	0.67	3.34	0.37	5.45	0.35																												
Figures	<div></div> <p>NF = Number of floors</p>																																	

10 APPENDIX II: RANKING OF SELECTED FRAGILITY AND VULNERABILITY MODELS

10.1 Oslo Testbed

Table AII-1 Detailed Scoring for the vulnerability models for Flood (NA: Not Applicable)

Criterion	Apel et al. 2004	Buechele et al. 2006	D'Ayala et al. 2020 PARNASSUS v3
Relevance: Geographical area	Low	Low	Low
Relevance: Asset characteristics	W_LFM_DUL_LOW: Low CR_LFM_DUL_MID: Low MUR_LWAL_DNO_MID: Low CR_LFM_DUL_LOW: Low	W_LFM_DUL_LOW: Low CR_LFM_DUL_MID: Low MUR_LWAL_DNO_MID: Low CR_LFM_DUL_LOW: Low	W_LFM_DUL_LOW: NA CR_LFM_DUL_MID: NA MUR_LWAL_DNO_MID: High CR_LFM_DUL_LOW: NA
Relevance: IM	Low	Low	High
Statistical refinement: Uncertainties	Low	Low	High
Statistical refinement: First principles	Low	High	High
Model quality (emp.): Impact observations	NA	Low	Low
Model quality (emp.): IM observations	NA	Low	High
Model quality (emp.): Constrained asset class	NA	Low	High
Model quality (emp.): Data quantity	NA	Low	Medium
Model quality (synt.): Fidelity to mechanics	Low	NA	NA
Model quality (synt.): Aggregation level	Low	NA	NA
Score (0-100)	W_LFM_DUL_LOW: 26 CR_LFM_DUL_MID: 26 MUR_LWAL_DNO_MID: 26 CR_LFM_DUL_LOW: 26	W_LFM_DUL_LOW: 37 CR_LFM_DUL_MID: 37 MUR_LWAL_DNO_MID: 37 CR_LFM_DUL_LOW: 37	W_LFM_DUL_LOW: - CR_LFM_DUL_MID: - MUR_LWAL_DNO_MID: 70 CR_LFM_DUL_LOW: -

Table AII-1(continued) Detailed Scoring for the vulnerability models for Flood

Criterion	Gersonius et al. 2008	Huizinga et al. 2017
Relevance: Geographical area	Low	Low
Relevance: Asset characteristics	W_LFM_DUL_LOW: Low CR_LFM_DUL_MID: Low MUR_LWAL_DNO_MID: Low CR_LFM_DUL_LOW: Low	W_LFM_DUL_LOW: Low CR_LFM_DUL_MID: Low MUR_LWAL_DNO_MID: Low CR_LFM_DUL_LOW: Low
Relevance: IM	High	High
Statistical refinement: Uncertainties	Low	Medium
Statistical refinement: First principles	Low	Medium
Model quality (emp.): Impact observations	Low	Low
Model quality (emp.): IM observations	Low	Low
Model quality (emp.): Constrained asset class	Low	Low
Model quality (emp.): Data quantity	Low	Low
Model quality (synt.): Fidelity to mechanics	NA	NA
Model quality (synt.): Aggregation level	NA	NA
Score (0-100)	W_LFM_DUL_LOW: 37 CR_LFM_DUL_MID: 37 MUR_LWAL_DNO_MID: 37 CR_LFM_DUL_LOW: 37	W_LFM_DUL_LOW: 44 CR_LFM_DUL_MID: 44 MUR_LWAL_DNO_MID: 44 CR_LFM_DUL_LOW: 44

Table AII-2 Detailed Scoring for the vulnerability models for Landslide / Debris Flow (NA: Not Applicable)

Criterion	Calvo and Savi (2009)	Fuchs et al. 2007
Relevance: Geographical area	Low	Low
Relevance: Asset characteristics	W_LFM_DUL_LOW: NA CR_LFM_DUL_MID: Low MUR_LWAL_DNO_MID: NA CR_LFM_DUL_LOW: Low	W_LFM_DUL_LOW: NA CR_LFM_DUL_MID: NA MUR_LWAL_DNO_MID: Medium CR_LFM_DUL_LOW: NA
Relevance: IM	High	High
Statistical refinement: Uncertainties	High	Low
Statistical refinement: First principles	High	High
Model quality (emp.): Impact observations	High	Medium
Model quality (emp.): IM observations	High	Low
Model quality (emp.): Constrained asset class	Medium	Low
Model quality (emp.): Data quantity	Medium	Medium
Model quality (synt.): Fidelity to mechanics	NA	NA
Model quality (synt.): Aggregation level	NA	NA
Score (0-100)	W_LFM_DUL_LOW: - CR_LFM_DUL_MID: 70 MUR_LWAL_DNO_MID: - CR_LFM_DUL_LOW: 70	W_LFM_DUL_LOW: - CR_LFM_DUL_MID: - MUR_LWAL_DNO_MID: 56 CR_LFM_DUL_LOW: -

Table AII-2(continued) Detailed Scoring for the vulnerability models for Landslide / Debris Flow (NA: Not Applicable)

Criterion	Papathoma-Köhle et al. 2012	Papathoma-Köhle et al. 2015
Relevance: Geographical area	Low	Low
Relevance: Asset characteristics	W_LFM_DUL_LOW: Low CR_LFM_DUL_MID: Low MUR_LWAL_DNO_MID: Low CR_LFM_DUL_LOW: Low	W_LFM_DUL_LOW: Low CR_LFM_DUL_MID: Low MUR_LWAL_DNO_MID: Low CR_LFM_DUL_LOW: Low
Relevance: IM	High	High
Statistical refinement: Uncertainties	High	High
Statistical refinement: First principles	High	High
Model quality (emp.): Impact observations	Medium	Medium
Model quality (emp.): IM observations	Medium	Medium
Model quality (emp.): Constrained asset class	Low	Low
Model quality (emp.): Data quantity	Low	Low
Model quality (synt.): Fidelity to mechanics	NA	NA
Model quality (synt.): Aggregation level	NA	NA
Score (0-100)	W_LFM_DUL_LOW: 56 CR_LFM_DUL_MID: 56 MUR_LWAL_DNO_MID: 56 CR_LFM_DUL_LOW: 56	W_LFM_DUL_LOW: 56 CR_LFM_DUL_MID: 56 MUR_LWAL_DNO_MID: 56 CR_LFM_DUL_LOW: 56

Table AII-3 Detailed Scoring for the fragility models for Earthquake (NA: Not Applicable)

Criterion	Crowley et al. 2021	Jeon et al. 2015
Relevance: Geographical area	Low	Low
Relevance: Asset characteristics	W_LFM_DUL_LOW: Medium CR_LFM_DUL_MID: Medium MUR_LWAL_DNO_MID: Medium CR_LFM_DUL_LOW: Medium	W_LFM_DUL_LOW: NA CR_LFM_DUL_MID: Low MUR_LWAL_DNO_MID: NA CR_LFM_DUL_LOW: Low
Relevance: IM	High	High
Statistical refinement: Uncertainties	High	High
Statistical refinement: First principles	High	High
Model quality (emp.): Impact observations	NA	NA
Model quality (emp.): IM observations	NA	NA
Model quality (emp.): Constrained asset class	NA	NA
Model quality (emp.): Data quantity	NA	NA
Model quality (synt.): Fidelity to mechanics	High	High
Model quality (synt.): Aggregation level	High	High
Score (0-100)	W_LFM_DUL_LOW: 67 CR_LFM_DUL_MID: 67 MUR_LWAL_DNO_MID: 67 CR_LFM_DUL_LOW: 67	W_LFM_DUL_LOW: - CR_LFM_DUL_MID: 63 MUR_LWAL_DNO_MID: - CR_LFM_DUL_LOW: 63

Table AII-3(continued) Detailed Scoring for the fragility models for Earthquake (NA: Not Applicable)

Criterion	Kappos 2013	Manfredi et al. 2023
Relevance: Geographical area	Low	Low
Relevance: Asset characteristics	W_LFM_DUL_LOW: NA CR_LFM_DUL_MID: Low MUR_LWAL_DNO_MID: Low CR_LFM_DUL_LOW: Low	W_LFM_DUL_LOW: NA CR_LFM_DUL_MID: Low MUR_LWAL_DNO_MID: BA CR_LFM_DUL_LOW: Low
Relevance: IM	High	High
Statistical refinement: Uncertainties	Medium	High
Statistical refinement: First principles	High	High
Model quality (emp.): Impact observations	NA	NA
Model quality (emp.): IM observations	NA	NA
Model quality (emp.): Constrained asset class	NA	NA
Model quality (emp.): Data quantity	NA	NA
Model quality (synt.): Fidelity to mechanics	High	High
Model quality (synt.): Aggregation level	High	High
Score (0-100)	W_LFM_DUL_LOW: - CR_LFM_DUL_MID: 59 MUR_LWAL_DNO_MID: 59 CR_LFM_DUL_LOW: 59	W_LFM_DUL_LOW: 63 CR_LFM_DUL_MID: 63 MUR_LWAL_DNO_MID: 63 CR_LFM_DUL_LOW: 63

Table AII-4 Detailed Scoring for the fragility models for Landslide / Ground Settlement (NA: Not Applicable)

Criterion	Miano et al., 2022. [Number of storeys: 2; IM: Deflection ratio]	Miano et al., 2022. [Number of storeys: 5; IM: Deflection ratio]	Negulescu and Foerster 2010
Relevance: Geographical area	Low	Low	Low
Relevance: Asset characteristics	W_LFM_DUL_LOW: NA CR_LFM_DUL_MID: Low MUR_LWAL_DNO_MID: NA CR_LFM_DUL_LOW: Medium	W_LFM_DUL_LOW: NA CR_LFM_DUL_MID: Medium MUR_LWAL_DNO_MID: NA CR_LFM_DUL_LOW: Low	W_LFM_DUL_LOW: NA CR_LFM_DUL_MID: High MUR_LWAL_DNO_MID: NA CR_LFM_DUL_LOW: High
Relevance: IM	High	High	High
Statistical refinement: Uncertainties	High	High	High
Statistical refinement: First principles	High	High	High
Model quality (emp.): Impact observations	NA	NA	NA
Model quality (emp.): IM observations	NA	NA	NA
Model quality (emp.): Constrained asset class	NA	NA	NA
Model quality (emp.): Data quantity	NA	NA	NA
Model quality (synt.): Fidelity to mechanics	High	High	High
Model quality (synt.): Aggregation level	High	High	High
Score (0-100)	W_LFM_DUL_LOW: - CR_LFM_DUL_MID: 60 MUR_LWAL_DNO_MID: - CR_LFM_DUL_LOW: 63	W_LFM_DUL_LOW: - CR_LFM_DUL_MID: 63 MUR_LWAL_DNO_MID: - CR_LFM_DUL_LOW: 60	W_LFM_DUL_LOW: - CR_LFM_DUL_MID: 70 MUR_LWAL_DNO_MID: - CR_LFM_DUL_LOW: 70

Table AII-4(continued) Detailed Scoring for the fragility models for Landslide / Ground Settlement (NA: Not Applicable)

Criterion	Peduto et al. 2017	Peduto et al. 2019
Relevance: Geographical area	Low	Low
Relevance: Asset characteristics	W_LFM_DUL_LOW: Low CR_LFM_DUL_MID: Low MUR_LWAL_DNO_MID: Low CR_LFM_DUL_LOW: Low	W_LFM_DUL_LOW: NA CR_LFM_DUL_MID: NA MUR_LWAL_DNO_MID: Low CR_LFM_DUL_LOW: NA
Relevance: IM	Low	High
Statistical refinement: Uncertainties	High	High
Statistical refinement: First principles	High	High
Model quality (emp.): Impact observations	Low	Low
Model quality (emp.): IM observations	Low	Low
Model quality (emp.): Constrained asset class	Low	Low
Model quality (emp.): Data quantity	Low	Low
Model quality (synt.): Fidelity to mechanics	NA	NA
Model quality (synt.): Aggregation level	NA	NA
Score (0-100)	W_LFM_DUL_LOW: 44 CR_LFM_DUL_MID: 44 MUR_LWAL_DNO_MID: 44 CR_LFM_DUL_LOW: 44	W_LFM_DUL_LOW: - CR_LFM_DUL_MID: - MUR_LWAL_DNO_MID: 52 CR_LFM_DUL_LOW: -

10.2 Nice Testbed

Table AII-5 Detailed Scoring for the vulnerability models for Flood (NA: Not Applicable)

Criterion	Apel et al. 2004	Buechele et al. 2006	D'Ayala et al. 2020 PARNASSUS v3 Model specifically adapted to the Nice testbed
Relevance: Geographical area	Low	Low	Low
Relevance: Asset characteristics	MUR_LWAL_CDN_LOW: Low MUR_LWAL_CDN_MID: Low CR_LWAL_DUL_MID: Low MUR_LWAL_CDN_HIG: Low MCF_LWAL_MID: Low	UR_LWAL_CDN_LOW: Low MUR_LWAL_CDN_MID: Low CR_LWAL_DUL_MID: Low MUR_LWAL_CDN_HIG: Low MCF_LWAL_MID: Low	MUR_LWAL_CDN_LOW: High MUR_LWAL_CDN_MID: High CR_LWAL_DUL_MID: NA MUR_LWAL_CDN_HIG: High MCF_LWAL_MID: High
Relevance: IM	High	High	High
Statistical refinement: Uncertainties	Low	Medium	High
Statistical refinement: First principles	Low	Medium	High
Model quality (emp.): Impact observations	Low	Low	Low
Model quality (emp.): IM observations	Low	Low	High
Model quality (emp.): Constrained asset class	Low	Low	High
Model quality (emp.): Data quantity	Low	Low	Medium
Model quality (synt.): Fidelity to mechanics	NA	NA	NA
Model quality (synt.): Aggregation level	NA	NA	NA
Score (0-100)	MUR_LWAL_CDN_LOW: 26 MUR_LWAL_CDN_MID: 26 CR_LWAL_DUL_MID: 26 MUR_LWAL_CDN_HIG: 26 MCF_LWAL_MID: 26	MUR_LWAL_CDN_LOW: 37 MUR_LWAL_CDN_MID: 37 CR_LWAL_DUL_MID: 37 MUR_LWAL_CDN_HIG: 37 MCF_LWAL_MID: 37	MUR_LWAL_CDN_LOW: 78 MUR_LWAL_CDN_MID: 78 CR_LWAL_DUL_MID: - MUR_LWAL_CDN_HIG: 78 MCF_LWAL_MID: 78

Table AII-5(continued) Detailed Scoring for the vulnerability models for Flood (NA: Not Applicable)

Criterion	Gersonius et al. 2008	Huizinga et al. 2017
Relevance: Geographical area	MUR_LWAL_CDN_LOW: Low MUR_LWAL_CDN_MID: Low CR_LWAL_DUL_MID: Low MUR_LWAL_CDN_HIG: Low MCF_LWAL_MID: Low	MUR_LWAL_CDN_LOW: Low MUR_LWAL_CDN_MID: Low CR_LWAL_DUL_MID: Low MUR_LWAL_CDN_HIG: Low MCF_LWAL_MID: Low
Relevance: Asset characteristics	Low	Low
Relevance: IM	High	High
Statistical refinement: Uncertainties	Low	Medium
Statistical refinement: First principles	Low	Medium
Model quality (emp.): Impact observations	Low	Low
Model quality (emp.): IM observations	Low	Low
Model quality (emp.): Constrained asset class	Low	Low
Model quality (emp.): Data quantity	Low	Low
Model quality (synt.): Fidelity to mechanics	NA	NA
Model quality (synt.): Aggregation level	NA	NA
Score (0-100)	MUR_LWAL_CDN_LOW: 37 MUR_LWAL_CDN_MID: 37 CR_LWAL_DUL_MID: 37 MUR_LWAL_CDN_HIG: 37 MCF_LWAL_MID: 37	MUR_LWAL_CDN_LOW: 44 MUR_LWAL_CDN_MID: 44 CR_LWAL_DUL_MID: 44 MUR_LWAL_CDN_HIG: 44 MCF_LWAL_MID: 44

Table AII-6 Detailed Scoring for the vulnerability models for Landslide / Debris Flow (NA: Not Applicable)

Criterion	Calvo and Savi (2009)	Fuchs et al. 2007
Relevance: Geographical area	Low	Low
Relevance: Asset characteristics	MUR_LWAL_CDN_LOW: NA MUR_LWAL_CDN_MID: NA CR_LWAL_DUL_MID: Medium MUR_LWAL_CDN_HIG: NA MCF_LWAL_MID: NA	MUR_LWAL_CDN_LOW: Medium MUR_LWAL_CDN_MID: Medium CR_LWAL_DUL_MID: NA MUR_LWAL_CDN_HIG: Medium MCF_LWAL_MID: Medium
Relevance: IM	High	High
Statistical refinement: Uncertainties	High	Low
Statistical refinement: First principles	High	High
Model quality (emp.): Impact observations	High	Medium
Model quality (emp.): IM observations	High	Low
Model quality (emp.): Constrained asset class	Medium	Low
Model quality (emp.): Data quantity	Medium	Medium
Model quality (synt.): Fidelity to mechanics	NA	NA
Model quality (synt.): Aggregation level	NA	NA
Score (0-100)	MUR_LWAL_CDN_LOW: - MUR_LWAL_CDN_MID: - CR_LWAL_DUL_MID: 60 MUR_LWAL_CDN_HIG: - MCF_LWAL_MID: -	MUR_LWAL_CDN_LOW: 46 MUR_LWAL_CDN_MID: 46 CR_LWAL_DUL_MID: - MUR_LWAL_CDN_HIG: 46 MCF_LWAL_MID: 46

Table AII-6(continued) Detailed Scoring for the vulnerability models for Landslide / Debris Flow (NA: Not Applicable)

Criterion	Papathoma-Köhle et al. 2012	Papathoma-Köhle et al. 2015
Relevance: Geographical area	Low	Low
Relevance: Asset characteristics	MUR_LWAL_CDN_LOW: Low MUR_LWAL_CDN_MID: Low CR_LWAL_DUL_MID: Low MUR_LWAL_CDN_HIG: Low MCF_LWAL_MID: Low	MUR_LWAL_CDN_LOW: Low MUR_LWAL_CDN_MID: Low CR_LWAL_DUL_MID: Low MUR_LWAL_CDN_HIG: Low MCF_LWAL_MID: Low
Relevance: IM	High	High
Statistical refinement: Uncertainties	High	High
Statistical refinement: First principles	High	High
Model quality (emp.): Impact observations	Medium	Medium
Model quality (emp.): IM observations	Medium	Medium
Model quality (emp.): Constrained asset class	Low	Low
Model quality (emp.): Data quantity	Low	Low
Model quality (synt.): Fidelity to mechanics	NA	NA
Model quality (synt.): Aggregation level	NA	NA
Score (0-100)	MUR_LWAL_CDN_LOW: 56 MUR_LWAL_CDN_MID: 56 CR_LWAL_DUL_MID: 56 MUR_LWAL_CDN_HIG: 56 MCF_LWAL_MID: 56	MUR_LWAL_CDN_LOW: 56 MUR_LWAL_CDN_MID: 56 CR_LWAL_DUL_MID: 56 MUR_LWAL_CDN_HIG: 56 MCF_LWAL_MID: 56

Table AII-7 Detailed Scoring for the fragility models for Earthquake (NA: Not Applicable)

Criterion	Crowley et al. 2021	Jeon et al. 2015
Relevance: Geographical area	Low	Low
Relevance: Asset characteristics	MUR_LWAL_CDN_LOW: Medium MUR_LWAL_CDN_MID: Medium CR_LWAL_DUL_MID: Medium MUR_LWAL_CDN_HIG: Medium MCF_LWAL_MID: Medium	MUR_LWAL_CDN_LOW: NA MUR_LWAL_CDN_MID: NA CR_LWAL_DUL_MID: Low MUR_LWAL_CDN_HIG: NA MCF_LWAL_MID: NA
Relevance: IM	High	High
Statistical refinement: Uncertainties	High	High
Statistical refinement: First principles	High	High
Model quality (emp.): Impact observations	NA	NA
Model quality (emp.): IM observations	NA	NA
Model quality (emp.): Constrained asset class	NA	NA
Model quality (emp.): Data quantity	NA	NA
Model quality (synt.): Fidelity to mechanics	High	High
Model quality (synt.): Aggregation level	High	High
Score (0-100)	MUR_LWAL_CDN_LOW: 67 MUR_LWAL_CDN_MID: 67 CR_LWAL_DUL_MID: 67 MUR_LWAL_CDN_HIG: 67 MCF_LWAL_MID: 67	MUR_LWAL_CDN_LOW: - MUR_LWAL_CDN_MID: - CR_LWAL_DUL_MID: 63 MUR_LWAL_CDN_HIG: - MCF_LWAL_MID: -

Table AII-7(continued) Detailed Scoring for the fragility models for Earthquake (NA: Not Applicable)

Criterion	Kappos 2013	Manfredi et al. 2023
Relevance: Geographical area	Low	Low
Relevance: Asset characteristics	MUR_LWAL_CDN_LOW: Low MUR_LWAL_CDN_MID: Low CR_LWAL_DUL_MID: Low MUR_LWAL_CDN_HIG: Low MCF_LWAL_MID: Low	MUR_LWAL_CDN_LOW: NA MUR_LWAL_CDN_MID: NA CR_LWAL_DUL_MID: Low MUR_LWAL_CDN_HIG: NA MCF_LWAL_MID: NA
Relevance: IM	High	High
Statistical refinement: Uncertainties	Medium	High
Statistical refinement: First principles	High	High
Model quality (emp.): Impact observations	NA	NA
Model quality (emp.): IM observations	NA	NA
Model quality (emp.): Constrained asset class	NA	NA
Model quality (emp.): Data quantity	NA	NA
Model quality (synt.): Fidelity to mechanics	High	High
Model quality (synt.): Aggregation level	High	High
Score (0-100)	MUR_LWAL_CDN_LOW: 59 MUR_LWAL_CDN_MID: 59 CR_LWAL_DUL_MID: 59 MUR_LWAL_CDN_HIG: 59 MCF_LWAL_MID: 59	MUR_LWAL_CDN_LOW: - MUR_LWAL_CDN_MID: - CR_LWAL_DUL_MID: 63 MUR_LWAL_CDN_HIG: - MCF_LWAL_MID: -

Table AII-8 Detailed Scoring for the fragility models for Landslide / Ground Settlement (NA: Not Applicable)

Criterion	Miano et al., 2022. [Number of storeys: 2; IM: Deflection ratio]	Miano et al., 2022. [Number of storeys: 5; IM: Deflection ratio]	Negulescu and Foerster 2010
Relevance: Geographical area	Low	Low	Low
Relevance: Asset characteristics	MUR_LWAL_CDN_LOW: NA MUR_LWAL_CDN_MID: NA CR_LWAL_DUL_MID: Low MUR_LWAL_CDN_HIG: NA MCF_LWAL_MID: NA	MUR_LWAL_CDN_LOW: NA MUR_LWAL_CDN_MID: NA CR_LWAL_DUL_MID: Low MUR_LWAL_CDN_HIG: NA MCF_LWAL_MID: NA	MUR_LWAL_CDN_LOW: NA MUR_LWAL_CDN_MID: NA CR_LWAL_DUL_MID: High MUR_LWAL_CDN_HIG: NA MCF_LWAL_MID: NA
Relevance: IM	High	High	High
Statistical refinement: Uncertainties	High	High	High
Statistical refinement: First principles	High	High	High
Model quality (emp.): Impact observations	NA	NA	NA
Model quality (emp.): IM observations	NA	NA	NA
Model quality (emp.): Constrained asset class	NA	NA	NA
Model quality (emp.): Data quantity	NA	NA	NA
Model quality (synt.): Fidelity to mechanics	High	High	High
Model quality (synt.): Aggregation level	High	High	High
Score (0-100)	MUR_LWAL_CDN_LOW: - MUR_LWAL_CDN_MID: - CR_LWAL_DUL_MID: 60 MUR_LWAL_CDN_HIG: - MCF_LWAL_MID: -	MUR_LWAL_CDN_LOW: - MUR_LWAL_CDN_MID: - CR_LWAL_DUL_MID: 63 MUR_LWAL_CDN_HIG: - MCF_LWAL_MID: -	MUR_LWAL_CDN_LOW: - MUR_LWAL_CDN_MID: - CR_LWAL_DUL_MID: 70 MUR_LWAL_CDN_HIG: - MCF_LWAL_MID: -

Table AII-8(continued) Detailed Scoring for the fragility models for Landslide / Ground Settlement (NA: Not Applicable)

Criterion	Peduto et al. 2017	Peduto et al. 2019
Relevance: Geographical area	Low	Low
Relevance: Asset characteristics	MUR_LWAL_CDN_LOW: Low MUR_LWAL_CDN_MID: Low CR_LWAL_DUL_MID: Low MUR_LWAL_CDN_HIG: Low MCF_LWAL_MID: Low	MUR_LWAL_CDN_LOW: Low MUR_LWAL_CDN_MID: Low CR_LWAL_DUL_MID: NA MUR_LWAL_CDN_HIG: Low MCF_LWAL_MID: Low
Relevance: IM	Low	High
Statistical refinement: Uncertainties	High	High
Statistical refinement: First principles	High	High
Model quality (emp.): Impact observations	Low	Low
Model quality (emp.): IM observations	Low	Low
Model quality (emp.): Constrained asset class	Low	Low
Model quality (emp.): Data quantity	Low	Low
Model quality (synt.): Fidelity to mechanics	NA	NA
Model quality (synt.): Aggregation level	NA	NA
Score (0-100)	MUR_LWAL_CDN_LOW: 44 MUR_LWAL_CDN_MID: 44 CR_LWAL_DUL_MID: 44 MUR_LWAL_CDN_HIG: 44 MCF_LWAL_MID: 44	MUR_LWAL_CDN_LOW: 52 MUR_LWAL_CDN_MID: 52 CR_LWAL_DUL_MID: - MUR_LWAL_CDN_HIG: 52 MCF_LWAL_MID: 52

10.3 Essex Testbed

Table AII-9 Detailed Scoring for the vulnerability models for Flood (NA: Not Applicable)

Criterion	Apel et al. 2004	Buechele et al. 2006	D'Ayala et al. 2020 PARNASSUS v3 Model specifically adapted to the Essex testbed
Relevance: Geographical area	Low	Low	Low
Relevance: Asset characteristics	MUR_CL_LWAL_CDN_LOW: Low CR_LFINF_CDN_MID: Low W_LPB_CDL_LOW: Low CR_LFM_CDN_LOW: Low	MUR_CL_LWAL_CDN_LOW: Low CR_LFINF_CDN_MID: Low W_LPB_CDL_LOW: Low CR_LFM_CDN_LOW: Low	MUR_CL_LWAL_CDN_LOW: Medium CR_LFINF_CDN_MID: NA W_LPB_CDL_LOW: NA CR_LFM_CDN_LOW: NA
Relevance: IM	High	High	High
Statistical refinement: Uncertainties	Low	Medium	High
Statistical refinement: First principles	Low	Medium	High
Model quality (emp.): Impact observations	Low	Low	Low
Model quality (emp.): IM observations	Low	Low	High
Model quality (emp.): Constrained asset class	Low	Low	High
Model quality (emp.): Data quantity	Low	Low	Medium
Model quality (synt.): Fidelity to mechanics	NA	NA	NA
Model quality (synt.): Aggregation level	NA	NA	NA
Score (0-100)	MUR_CL_LWAL_CDN_LOW: 26 CR_LFINF_CDN_MID: 26 W_LPB_CDL_LOW: 26 CR_LFM_CDN_LOW: 26	MUR_CL_LWAL_CDN_LOW: 37 CR_LFINF_CDN_MID: 37 W_LPB_CDL_LOW: 37 CR_LFM_CDN_LOW: 37	MUR_CL_LWAL_CDN_LOW: 74 CR_LFINF_CDN_MID: - W_LPB_CDL_LOW: - CR_LFM_CDN_LOW: -

Table AII-9(continued) Detailed Scoring for the vulnerability models for Flood (NA: Not Applicable)

Criterion	Gersonius et al. 2008	Huizinga et al. 2017
Relevance: Geographical area	MUR_CL_LWAL_CDN_LOW: Low CR_LFINF_CDN_MID: Low W_LPB_CDL_LOW: Low CR_LFM_CDN_LOW: Low	MUR_CL_LWAL_CDN_LOW: Low CR_LFINF_CDN_MID: Low W_LPB_CDL_LOW: Low CR_LFM_CDN_LOW: Low
Relevance: Asset characteristics	Low	Low
Relevance: IM	High	High
Statistical refinement: Uncertainties	Low	Medium
Statistical refinement: First principles	Low	Medium
Model quality (emp.): Impact observations	Low	Low
Model quality (emp.): IM observations	Low	Low
Model quality (emp.): Constrained asset class	Low	Low
Model quality (emp.): Data quantity	Low	Low
Model quality (synt.): Fidelity to mechanics	NA	NA
Model quality (synt.): Aggregation level	NA	NA
Score (0-100)	MUR_CL_LWAL_CDN_LOW: 37 CR_LFINF_CDN_MID: 37 W_LPB_CDL_LOW: 37 CR_LFM_CDN_LOW: 37	MUR_CL_LWAL_CDN_LOW: 44 CR_LFINF_CDN_MID: 44 W_LPB_CDL_LOW: 44 CR_LFM_CDN_LOW: 44

Table AII-10 Detailed Scoring for the vulnerability models for Landslide / Debris Flow (NA: Not Applicable)

Criterion	Calvo and Savi (2009)	Fuchs et al. 2007
Relevance: Geographical area	Low	Low
Relevance: Asset characteristics	MUR_CL_LWAL_CDN_LOW: NA CR_LFINF_CDN_MID: Medium W_LPB_CDL_LOW: NA CR_LFM_CDN_LOW: Medium	MUR_CL_LWAL_CDN_LOW: Medium CR_LFINF_CDN_MID: NA W_LPB_CDL_LOW: NA CR_LFM_CDN_LOW: NA
Relevance: IM	High	High
Statistical refinement: Uncertainties	High	Low
Statistical refinement: First principles	High	High
Model quality (emp.): Impact observations	High	Medium
Model quality (emp.): IM observations	High	Low
Model quality (emp.): Constrained asset class	Medium	Low
Model quality (emp.): Data quantity	Medium	Medium
Model quality (synt.): Fidelity to mechanics	NA	NA
Model quality (synt.): Aggregation level	NA	NA
Score (0-100)	MUR_CL_LWAL_CDN_LOW: - CR_LFINF_CDN_MID: 70 W_LPB_CDL_LOW: - CR_LFM_CDN_LOW: 70	MUR_CL_LWAL_CDN_LOW: 56 CR_LFINF_CDN_MID: - W_LPB_CDL_LOW: - CR_LFM_CDN_LOW: -

Table AII-10(continued) Detailed Scoring for the vulnerability models for Landslide / Debris Flow (NA: Not Applicable)

Criterion	Papathoma-Köhle et al. 2012	Papathoma-Köhle et al. 2015
Relevance: Geographical area	Low	Low
Relevance: Asset characteristics	MUR_CL_LWAL_CDN_LOW: Low CR_LFINF_CDN_MID: Low W_LPB_CDL_LOW: Low CR_LFM_CDN_LOW: Low	MUR_CL_LWAL_CDN_LOW: Low CR_LFINF_CDN_MID: Low W_LPB_CDL_LOW: Low CR_LFM_CDN_LOW: Low
Relevance: IM	High	High
Statistical refinement: Uncertainties	High	High
Statistical refinement: First principles	High	High
Model quality (emp.): Impact observations	Medium	Medium
Model quality (emp.): IM observations	Medium	Medium
Model quality (emp.): Constrained asset class	Low	Low
Model quality (emp.): Data quantity	Low	Low
Model quality (synt.): Fidelity to mechanics	NA	NA
Model quality (synt.): Aggregation level	NA	NA
Score (0-100)	MUR_CL_LWAL_CDN_LOW: 56 CR_LFINF_CDN_MID: 56 W_LPB_CDL_LOW: 56 CR_LFM_CDN_LOW: 56	MUR_CL_LWAL_CDN_LOW: 56 CR_LFINF_CDN_MID: 56 W_LPB_CDL_LOW: 56 CR_LFM_CDN_LOW: 56

Table AII-11 Detailed Scoring for the fragility models for Earthquake (NA: Not Applicable)

Criterion	Crowley et al. 2021	Jeon et al. 2015
Relevance: Geographical area	Low	Low
Relevance: Asset characteristics	MUR_CL_LWAL_CDN_LOW: Medium CR_LFINF_CDN_MID: Medium W_LPB_CDL_LOW: Medium CR_LFM_CDN_LOW: Medium	MUR_CL_LWAL_CDN_LOW: NA CR_LFINF_CDN_MID: Low W_LPB_CDL_LOW: NA CR_LFM_CDN_LOW: Low
Relevance: IM	High	High
Statistical refinement: Uncertainties	High	High
Statistical refinement: First principles	High	High
Model quality (emp.): Impact observations	NA	NA
Model quality (emp.): IM observations	NA	NA
Model quality (emp.): Constrained asset class	NA	NA
Model quality (emp.): Data quantity	NA	NA
Model quality (synt.): Fidelity to mechanics	High	High
Model quality (synt.): Aggregation level	High	High
Score (0-100)	MUR_CL_LWAL_CDN_LOW: 67 CR_LFINF_CDN_MID: 67 W_LPB_CDL_LOW: 67 CR_LFM_CDN_LOW: 67	MUR_CL_LWAL_CDN_LOW: - CR_LFINF_CDN_MID: 63 W_LPB_CDL_LOW: - CR_LFM_CDN_LOW: 63

Table AII-11(continued) Detailed Scoring for the fragility models for Earthquake (NA: Not Applicable)

Criterion	Kappos 2013	Manfredi et al. 2023
Relevance: Geographical area	Low	Low
Relevance: Asset characteristics	MUR_CL_LWAL_CDN_LOW: Low CR_LFINF_CDN_MID: Low W_LPB_CDL_LOW: Low CR_LFM_CDN_LOW: Low	MUR_CL_LWAL_CDN_LOW: NA CR_LFINF_CDN_MID: Low W_LPB_CDL_LOW: NA CR_LFM_CDN_LOW: Low
Relevance: IM	High	High
Statistical refinement: Uncertainties	Medium	High
Statistical refinement: First principles	High	High
Model quality (emp.): Impact observations	NA	NA
Model quality (emp.): IM observations	NA	NA
Model quality (emp.): Constrained asset class	NA	NA
Model quality (emp.): Data quantity	NA	NA
Model quality (synt.): Fidelity to mechanics	High	High
Model quality (synt.): Aggregation level	High	High
Score (0-100)	MUR_CL_LWAL_CDN_LOW: 59 CR_LFINF_CDN_MID: 59 W_LPB_CDL_LOW: 59 CR_LFM_CDN_LOW: 59	MUR_CL_LWAL_CDN_LOW: - CR_LFINF_CDN_MID: 63 W_LPB_CDL_LOW: - CR_LFM_CDN_LOW: 63

Table AII-12 Detailed Scoring for the fragility models for Landslide / Ground Settlement (NA: Not Applicable)

Criterion	Miano et al., 2022. [Number of storeys: 2; IM: Deflection ratio]	Miano et al., 2022. [Number of storeys: 5; IM: Deflection ratio]	Negulescu and Foerster 2010
Relevance: Geographical area	Low	Low	Low
Relevance: Asset characteristics	MUR_CL_LWAL_CDN_LOW: NA CR_LFINF_CDN_MID: Low W_LPB_CDL_LOW: NA CR_LFM_CDN_LOW: Medium	MUR_CL_LWAL_CDN_LOW: NA CR_LFINF_CDN_MID: Medium W_LPB_CDL_LOW: NA CR_LFM_CDN_LOW: Low	MUR_CL_LWAL_CDN_LOW: NA CR_LFINF_CDN_MID: High W_LPB_CDL_LOW: NA CR_LFM_CDN_LOW: High
Relevance: IM	High	High	High
Statistical refinement: Uncertainties	High	High	High
Statistical refinement: First principles	High	High	High
Model quality (emp.): Impact observations	NA	NA	NA
Model quality (emp.): IM observations	NA	NA	NA
Model quality (emp.): Constrained asset class	NA	NA	NA
Model quality (emp.): Data quantity	NA	NA	NA
Model quality (synt.): Fidelity to mechanics	High	High	High
Model quality (synt.): Aggregation level	High	High	High
Score (0-100)	MUR_CL_LWAL_CDN_LOW: - CR_LFINF_CDN_MID: 60 W_LPB_CDL_LOW: - CR_LFM_CDN_LOW: 63	MUR_CL_LWAL_CDN_LOW: - CR_LFINF_CDN_MID: 63 W_LPB_CDL_LOW: - CR_LFM_CDN_LOW: 60	MUR_CL_LWAL_CDN_LOW: - CR_LFINF_CDN_MID: 70 W_LPB_CDL_LOW: - CR_LFM_CDN_LOW: 70

Table AII-12(continued) Detailed Scoring for the fragility models for Landslide / Ground Settlement (NA: Not Applicable)

Criterion	Peduto et al. 2017	Peduto et al. 2019
Relevance: Geographical area	Low	Low
Relevance: Asset characteristics	MUR_CL_LWAL_CDN_LOW: Low CR_LFINF_CDN_MID: Low W_LPB_CDL_LOW: Low CR_LFM_CDN_LOW: Low	MUR_CL_LWAL_CDN_LOW: Low CR_LFINF_CDN_MID: NA W_LPB_CDL_LOW: NA CR_LFM_CDN_LOW: NA
Relevance: IM	Low	High
Statistical refinement: Uncertainties	High	High
Statistical refinement: First principles	High	High
Model quality (emp.): Impact observations	Low	Low
Model quality (emp.): IM observations	Low	Low
Model quality (emp.): Constrained asset class	Low	Low
Model quality (emp.): Data quantity	Low	Low
Model quality (synt.): Fidelity to mechanics	NA	NA
Model quality (synt.): Aggregation level	NA	NA
Score (0-100)	MUR_CL_LWAL_CDN_LOW: 44 CR_LFINF_CDN_MID: 44 W_LPB_CDL_LOW: 44 CR_LFM_CDN_LOW: 44	MUR_CL_LWAL_CDN_LOW: 52 CR_LFINF_CDN_MID: - W_LPB_CDL_LOW: - CR_LFM_CDN_LOW: -

10.4 Mulathing Testbed

Table AII-13 Detailed Scoring for the vulnerability models for Flood (NA: Not Applicable)

Criterion	Apel et al. 2004	Buechele et al. 2006	D'Ayala et al. 2020 PARNASSUS v3
Relevance: Geographical area	Low	Low	Low
Relevance: Asset characteristics	CR_LWAL_CDL_LOW: Low W_LWAL_LOW: Low CR_LWAL_CDN_LOW: Low CR_LDUAL_CDH_LOW: Low	CR_LWAL_CDL_LOW: Low W_LWAL_LOW: Low CR_LWAL_CDN_LOW: Low CR_LDUAL_CDH_LOW: Low	CR_LWAL_CDL_LOW: NA W_LWAL_LOW: NA CR_LWAL_CDN_LOW: NA CR_LDUAL_CDH_LOW: NA
Relevance: IM	High	High	High
Statistical refinement: Uncertainties	Low	Medium	High
Statistical refinement: First principles	Low	Medium	High
Model quality (emp.): Impact observations	Low	Low	Low
Model quality (emp.): IM observations	Low	Low	High
Model quality (emp.): Constrained asset class	Low	Low	High
Model quality (emp.): Data quantity	Low	Low	Medium
Model quality (synt.): Fidelity to mechanics	NA	NA	NA
Model quality (synt.): Aggregation level	NA	NA	NA
Score (0-100)	CR_LWAL_CDL_LOW: 26 W_LWAL_LOW: 26 CR_LWAL_CDN_LOW: 26 CR_LDUAL_CDH_LOW: 26	CR_LWAL_CDL_LOW: 37 W_LWAL_LOW: 37 CR_LWAL_CDN_LOW: 37 CR_LDUAL_CDH_LOW: 37	MUR_CL_LWAL_CDN_LOW: - CR_LFINF_CDN_MID: - W_LPB_CDL_LOW: - CR_LFM_CDN_LOW: -

Table AII-13(continued) Detailed Scoring for the vulnerability models for Flood (NA: Not Applicable)

Criterion	Gersonius et al. 2008	Huizinga et al. 2017
Relevance: Geographical area	CR_LWAL_CDL_LOW: Low W_LWAL_LOW: Low CR_LWAL_CDN_LOW: Low CR_LDUAL_CDH_LOW: Low	CR_LWAL_CDL_LOW: Low W_LWAL_LOW: Low CR_LWAL_CDN_LOW: Low CR_LDUAL_CDH_LOW: Low
Relevance: Asset characteristics	Low	Low
Relevance: IM	High	High
Statistical refinement: Uncertainties	Low	Medium
Statistical refinement: First principles	Low	Medium
Model quality (emp.): Impact observations	Low	Low
Model quality (emp.): IM observations	Low	Low
Model quality (emp.): Constrained asset class	Low	Low
Model quality (emp.): Data quantity	Low	Low
Model quality (synt.): Fidelity to mechanics	NA	NA
Model quality (synt.): Aggregation level	NA	NA
Score (0-100)	CR_LWAL_CDL_LOW: 37 W_LWAL_LOW: 37 CR_LWAL_CDN_LOW: 37 CR_LDUAL_CDH_LOW: 37	CR_LWAL_CDL_LOW: 44 W_LWAL_LOW: 44 CR_LWAL_CDN_LOW: 44 CR_LDUAL_CDH_LOW: 44

Table AII-14 Detailed Scoring for the vulnerability models for Landslide / Debris Flow (NA: Not Applicable)

Criterion	Calvo and Savi (2009)	Fuchs et al. 2007
Relevance: Geographical area	Low	Low
Relevance: Asset characteristics	CR_LWAL_CDL_LOW: Medium W_LWAL_LOW: NA CR_LWAL_CDN_LOW: Medium CR_LDUAL_CDH_LOW: Medium	CR_LWAL_CDL_LOW: NA W_LWAL_LOW: NA CR_LWAL_CDN_LOW: NA CR_LDUAL_CDH_LOW: NA
Relevance: IM	High	High
Statistical refinement: Uncertainties	High	Low
Statistical refinement: First principles	High	High
Model quality (emp.): Impact observations	High	Medium
Model quality (emp.): IM observations	High	Low
Model quality (emp.): Constrained asset class	Medium	Low
Model quality (emp.): Data quantity	Medium	Medium
Model quality (synt.): Fidelity to mechanics	NA	NA
Model quality (synt.): Aggregation level	NA	NA
Score (0-100)	CR_LWAL_CDL_LOW: 70 W_LWAL_LOW: - CR_LWAL_CDN_LOW: 70 CR_LDUAL_CDH_LOW: 70	CR_LWAL_CDL_LOW: - W_LWAL_LOW: - CR_LWAL_CDN_LOW: - CR_LDUAL_CDH_LOW: -

Table AII-14(continued) Detailed Scoring for the vulnerability models for Landslide / Debris Flow (NA: Not Applicable)

Criterion	Papathoma-Köhle et al. 2012	Papathoma-Köhle et al. 2015
Relevance: Geographical area	Low	Low
Relevance: Asset characteristics	CR_LWAL_CDL_LOW: Low W_LWAL_LOW: Low CR_LWAL_CDN_LOW: Low CR_LDUAL_CDH_LOW: Low	CR_LWAL_CDL_LOW: Low W_LWAL_LOW: Low CR_LWAL_CDN_LOW: Low CR_LDUAL_CDH_LOW: Low
Relevance: IM	High	High
Statistical refinement: Uncertainties	High	High
Statistical refinement: First principles	High	High
Model quality (emp.): Impact observations	Medium	Medium
Model quality (emp.): IM observations	Medium	Medium
Model quality (emp.): Constrained asset class	Low	Low
Model quality (emp.): Data quantity	Low	Low
Model quality (synt.): Fidelity to mechanics	NA	NA
Model quality (synt.): Aggregation level	NA	NA
Score (0-100)	CR_LWAL_CDL_LOW: 56 W_LWAL_LOW: 56 CR_LWAL_CDN_LOW: 56 CR_LDUAL_CDH_LOW: 56	CR_LWAL_CDL_LOW: 56 W_LWAL_LOW: 56 CR_LWAL_CDN_LOW: 56 CR_LDUAL_CDH_LOW: 56

Table AII-15 Detailed Scoring for the fragility models for Earthquake (NA: Not Applicable)

Criterion	Crowley et al. 2021	Jeon et al. 2015
Relevance: Geographical area	Low	Low
Relevance: Asset characteristics	CR_LWAL_CDL_LOW: Medium W_LWAL_LOW: Medium CR_LWAL_CDN_LOW: Medium CR_LDUAL_CDH_LOW: Medium	CR_LWAL_CDL_LOW: Low W_LWAL_LOW: NA CR_LWAL_CDN_LOW: Low CR_LDUAL_CDH_LOW: Low
Relevance: IM	High	High
Statistical refinement: Uncertainties	High	High
Statistical refinement: First principles	High	High
Model quality (emp.): Impact observations	NA	NA
Model quality (emp.): IM observations	NA	NA
Model quality (emp.): Constrained asset class	NA	NA
Model quality (emp.): Data quantity	NA	NA
Model quality (synt.): Fidelity to mechanics	High	High
Model quality (synt.): Aggregation level	High	High
Score (0-100)	CR_LWAL_CDL_LOW: 67 W_LWAL_LOW: 67 CR_LWAL_CDN_LOW: 67 CR_LDUAL_CDH_LOW: 67	CR_LWAL_CDL_LOW: 63 W_LWAL_LOW: - CR_LWAL_CDN_LOW: 63 CR_LDUAL_CDH_LOW: 63

Table AII-15(continued) Detailed Scoring for the fragility models for Earthquake (NA: Not Applicable)

Criterion	Kappos 2013	Manfredi et al. 2023
Relevance: Geographical area	Low	Low
Relevance: Asset characteristics	CR_LWAL_CDL_LOW: Low W_LWAL_LOW: NA CR_LWAL_CDN_LOW: Low CR_LDUAL_CDH_LOW: Low	CR_LWAL_CDL_LOW: Low W_LWAL_LOW: NA CR_LWAL_CDN_LOW: Low CR_LDUAL_CDH_LOW: Low
Relevance: IM	High	High
Statistical refinement: Uncertainties	Medium	High
Statistical refinement: First principles	High	High
Model quality (emp.): Impact observations	NA	NA
Model quality (emp.): IM observations	NA	NA
Model quality (emp.): Constrained asset class	NA	NA
Model quality (emp.): Data quantity	NA	NA
Model quality (synt.): Fidelity to mechanics	High	High
Model quality (synt.): Aggregation level	High	High
Score (0-100)	CR_LWAL_CDL_LOW: 59 W_LWAL_LOW: - CR_LWAL_CDN_LOW: 59 CR_LDUAL_CDH_LOW: 59	CR_LWAL_CDL_LOW: 63 W_LWAL_LOW: - CR_LWAL_CDN_LOW: 63 CR_LDUAL_CDH_LOW: 63

Table AII-16 Detailed Scoring for the fragility models for Landslide / Ground Settlement (NA: Not Applicable)

Criterion	Miano et al., 2022. [Number of storeys: 2; IM: Deflection ratio]	Miano et al., 2022. [Number of storeys: 5; IM: Deflection ratio]	Negulescu and Foerster 2010
Relevance: Geographical area	Low	Low	Low
Relevance: Asset characteristics	CR_LWAL_CDL_LOW: Low W_LWAL_LOW: NA CR_LWAL_CDN_LOW: Low CR_LDUAL_CDH_LOW: Low	CR_LWAL_CDL_LOW: Low W_LWAL_LOW: NA CR_LWAL_CDN_LOW: Low CR_LDUAL_CDH_LOW: Low	CR_LWAL_CDL_LOW: High W_LWAL_LOW: NA CR_LWAL_CDN_LOW: High CR_LDUAL_CDH_LOW: High
Relevance: IM	High	High	High
Statistical refinement: Uncertainties	High	High	High
Statistical refinement: First principles	High	High	High
Model quality (emp.): Impact observations	NA	NA	NA
Model quality (emp.): IM observations	NA	NA	NA
Model quality (emp.): Constrained asset class	NA	NA	NA
Model quality (emp.): Data quantity	NA	NA	NA
Model quality (synt.): Fidelity to mechanics	High	High	High
Model quality (synt.): Aggregation level	High	High	High
Score (0-100)	CR_LWAL_CDL_LOW: 63 W_LWAL_LOW: - CR_LWAL_CDN_LOW: 63 CR_LDUAL_CDH_LOW: 63	CR_LWAL_CDL_LOW: 60 W_LWAL_LOW: - CR_LWAL_CDN_LOW: 60 CR_LDUAL_CDH_LOW: 60	CR_LWAL_CDL_LOW: 70 W_LWAL_LOW: - CR_LWAL_CDN_LOW: 70 CR_LDUAL_CDH_LOW: 70

Table AII-16(continued) Detailed Scoring for the fragility models for Landslide / Ground Settlement (NA: Not Applicable)

Criterion	Peduto et al. 2017	Peduto et al. 2019
Relevance: Geographical area	Low	Low
Relevance: Asset characteristics	CR_LWAL_CDL_LOW: NA W_LWAL_LOW: Low CR_LWAL_CDN_LOW: Low CR_LDUAL_CDH_LOW: Low	CR_LWAL_CDL_LOW: NA W_LWAL_LOW: NA CR_LWAL_CDN_LOW: NA CR_LDUAL_CDH_LOW: NA(
Relevance: IM	Low	High
Statistical refinement: Uncertainties	High	High
Statistical refinement: First principles	High	High
Model quality (emp.): Impact observations	Low	Low
Model quality (emp.): IM observations	Low	Low
Model quality (emp.): Constrained asset class	Low	Low
Model quality (emp.): Data quantity	Low	Low
Model quality (synt.): Fidelity to mechanics	NA	NA
Model quality (synt.): Aggregation level	NA	NA
Score (0-100)	CR_LWAL_CDL_LOW: 44 W_LWAL_LOW: 44 CR_LWAL_CDN_LOW: 44 CR_LDUAL_CDH_LOW: 44	CR_LWAL_CDL_LOW: - W_LWAL_LOW: - CR_LWAL_CDN_LOW: - CR_LDUAL_CDH_LOW: -